UNIVERSIDAD COMPLUTENSE DE MADRID
FACULTAD DE CIENCIAS QUÍMICAS

TESIS DOCTORAL

Searching for new cannabinoid CB1 receptor-interacting proteins
(En busca de nuevas proteínas interactoras del receptor CB1 cannabinoide)

MEMORIA PARA OPTAR AL GRADO DE DOCTOR

PRESENTADA POR

Carlos Costas Insua

Directores

Manuel Guzmán Pastor
José Ignacio Rodríguez Crespo

Madrid

Universidad Complutense de Madrid

Facultad de Ciencias Químicas

TESIS DOCTORAL

Searching for new cannabinoid CB_1 receptor-interacting proteins

(En busca de nuevas proteínas interactoras del receptor CB_1 cannabinoide)

MEMORIA PARA OPTAR AL GRADO DE DOCTOR

PRESENTADA POR

Carlos Costas Insua

DIRECTORES

Manuel Guzmán Pastor

José Ignacio Rodríguez Crespo

MADRID

Febrero, 2022

TABLE OF CONTENTS

LIST OF FIGURES

Introduction

Materials and Methods

Results – Aim 1

Results – Aim 2

Discussion

LIST OF TABLES

Materials and Methods

Results – Aim 1

Results – Aim 2

Abbreviations

2-AG: 2-arachidonoylglycerol.
3D: Three-dimensional.
3-AT: 3-amino-triazole.
5-IAF: 5-(Iodoacetamido)fluorescein.
5-HT$_{2C}$: Type 2C serotonin receptor.
A: Amygdalar formation.
A$_{2A}$R: Type 2A Adenosine Receptor.
ABHD4/6/12: α/β-Hydrolase Domain-containing 4/6/12.
AEA: *N*-arachidonoylethanolamine.
AHA1: Activator of 90 kDa heat shock protein ATPase 1.
AIDS: Acquired Immune Deficiency Syndrome.
AP-3: Adaptor Protein 3.
AP/MS: Affinity Purification/Mass spectrometry.
ARNSMR: Autosomal Recessive Non-Syndromic Mental Retardation.
ATF6: Activating Transcription Factor 6.
BCE: Before Common Era.
BiP: Binding Immunoglobulin Protein.
BiP-IR: Binding Immunoglobulin Protein Interacting Region.
BRET: Bioluminiscence Resonance Energy Transfer.
BSA: Bovine Serum Albumin.
CA: *Cornu Ammonis*.
CamKII2α: Calcium/calmodulin-dependent protein Kinase type 2 subunit α.
cAMP: Cyclic Adenosine Monophosphate.
Cb: Cerebellum.
CB$_1$R: Type 1 Cannabinoid Receptor.
CB$_2$R: Type 2 Cannabinoid Receptor.
CBD: Cannabidiol.
cDNA: Complementary DNA.
CE: Common Era.
CLAHE: Contrast Limited Adaptive Histogram Equalization.
CNS: Central Nervous System.
CP-55,940: (-)-cis-3-[2-Hydroxy-4-(1,1-dimethylheptyl)phenyl]-trans-4-(3-hydroxypropyl)cyclohexanol.
CRBN: Cereblon.
CREB: cAMP response Element-binding.
CRIP1a/b: Cannabinoid Receptor Interacting Protein 1 a/b.
CTD: *C*-terminus Domain.
CUL4A: Cullin 4A.
Cx: Cortex.
D$_1$R: Type 1 Dopamine Receptor.
D$_2$R: Type 2 Dopamine Receptor.
DAG: Diacylglycerol.
DAGLα/β: Diacylglicerol Lipase α/β.
DAPI: 4′,6-diamidino-2-phenylindole.
DDB1: DNA-damage Binding protein 1.
DDM: n-Dodecyl-β-D-maltoside.
DG: Dentate gyrus.
DI: Discrimination Index.
DIO: Double-inverse Oriented.
DMEM: Dulbecco's Modified Eagle's Medium.
DMR: Dynamic Mass Redistribution.
DMSO: Dimethyl sulfoxide.

DSE: Depolarization-induced Supression of Excitation.
DSI: Depolarization-induced Supression of Inhibition.
DTT: Dithiotreitol.
ECL: Extracellular Loop.
ECS: Endocannabinoid System.
EDTA: Ethylenediaminetetraacetic acid.
EGTA: Ethylene glycol-bis(2-aminoethylether)-N,N,N',N'-tetraacetic acid.
Epac: Exchange Protein Activated by cAMP.
EPM: Elevated Plus Maze test.
ER: Endoplasmic Reticulum.
ERK: Extracellular Regulated Kinase.
FAAH: Fatty Acid Amide Hydrolase.
FAN: Factor Associated with Neutral sphingomyelinase.
FDA: Food and Drug Administration.
FP: Fluorescence Polarization.
FST: Forced Swimming Test.
GAD65/67: Glutamic Acid Decarboxylase 65/67.
GAP43: Growth Axonal Protein of 43 kDa.
GASP1: GPCR-associated Sorting Protein 1.
GFP: Green Fluorescent Protein.
GPCR: G-protein-coupled receptor.
GPR18/55/119: G-protein-coupled Receptor 18/55/119.
GRK: GPCR-related Kinase.
GRP78: Glucose-Regulated Protein of 78 kDa.
GST: Glutathione S-tranferase.
HBD: Helical Bundle Domain.
HBM: Hepes Buffered Medium.
HBSS: Hank's Balanced Salt Solution.
Hc: Hippocampal formation.
HET: Heterozygous.
His_6: 6x His tag**.**
HPRT: Hypoxanthine-guanine Phosphoribosyltransferase.
HSL: Hormone Sensitive Lipase
Hsp70: Heat Shock Protein of 70 kDa.
HTRF: Homologous Time Resolved Fluorescence.
HU-210: (6aR)-trans-3-(1,1-Dimethylheptyl)-6a,7,10,10a-tetrahydro-1-hydroxy-6,6-dimethyl-6H-dibenzo[b,d]pyran-9-methanol.
ICL: Intracellular Loop.
IMiD: Immunomodulatory Drug.
IRE1: Inositol Requiring Enzyme 1.
ISHH: *In Situ* Hybridization Histochemistry.
K_d: Dissociation constant.
KO: Knock-out.
LB: Lysogeny broth.
LTD: Long-term Depression.
LTP: Long-term Potentiation.
MAGL: Monoacylglycerol Lipase.
MC4: Melanocortin 4.
MEK1: Mitogen-activated protein Kinase Kinase 1.
mTORC1: Mechanistic Target Of Rapamycin Complex 1.
NAAA: *N*-Acylethanolamine-hydrolyzing Acid Amidase.
NAPE-PLD: *N*-acylphosphatidylethanolamine-phospholipase D.
NAT: *N*-acetyltransferase.
NBD: Nucleotide Binding Domain.

NCS-1: Neuronal Calcium Sensor 1.
NMDAR: *N*-methyl-D-aspartate Receptor.
NOR: Novel Object Recognition test.
NTD: *N*-terminus Domain.
OD_{580}: Optical density at 580 nanometers.
ORF: Open Reading Frame.
PCR: Polymerase Chain Reaction.
PERK: PKR-like endoplasmic reticulum kinase.
PI3K: Phosphatidylinositol 4,5-bisphosphate 3-kinase.
PLA: Proximity Ligation Assay.
PLA2: Phospholipase A2.
PLA2G4E: Phospholipase A2 group IV member E.
PLCβ/γ: Phospolipase C β/γ.
PPARα/γ: Peroxisome Proliferator-Activated Receptor α/γ.
PPI: Protein-protein Interaction.
PSD-95: Post-synaptic Density Protein of 95 kDa.
PVDF: Polyvinylidene fluoride.
Pyr: Pyriform cortex.
Q-PCR: Quantiative (real-time) Polymerase Chain Reaction.
RGS: Regulator of G-protein Signaling.
RIPA: Radioimmunoprecipitation Assay.
Rluc: Renilla Luciferase.
ROI: Region Of Interest.
SBD: Substrate Binding Domain.
SDS-PAGE: Sodium Dodecyl Sulfate – Polyacrylamide Gel Electrophoresis.
SGIP1: SH3-containing GRB2-like protein 3-interacting protein 1.
SR141716 (SR1): *N*-(Piperidin-1-yl)-5-(4-chlorophenyl)-1-(2,4-dichlorophenyl)-4-methyl-1H-pyrazole-3-carboxamide hydrochloride. Also rimonabant.
SR144528: 5-(4-Chloro-3-methylphenyl)-1-[(4-methylphenyl)methyl]-N-[(1S,2S,4R)-1,3,3-trimethylbicyclo[2.2.1]hept-2-yl]-1H-pyrazole-3-carboxamide.
SSC: Standard Saline Citrate.
Str: Striatum.
Syn: Synaptophysin 1.
TBP: TATA-binding Protein.
TBS: Tris Buffered Saline.
THC: Δ^9-tetrahydrocannabinol.
TM: Transmembrane Domain.
TRPV1: Transient Receptor Potential cation channel subfamily V member 1.
VANGL2: Vang-like Protein 2.
vGAT: Vesicular GABA Transporter.
vGluT1: Vesicular Glutamate Transporter 1.
WAVE1: Wiskott-Aldrich syndrome protein family Verprolin homologous protein 1.
WIN55,212-2: (R)-(+)-[2,3-Dihydro-5-methyl-3-(4-morpholinylmethyl)pyrrolo[1,2,3-de]-1,4-benzoxazin-6-yl]-1-naphthalenylmethanone mesylate.
WT: Wild Type.
Y2H: Yeast two-hybrid.
X-Gal: 5-Bromo-4-Chloro-3-Indolyl β-D-Galactopyranoside.

Resumen

Extractos de la planta *Cannabis sativa* se han utilizado durante milenios con fines medicinales, religiosos o recreativos, entre otros. El principal componente psicoactivo de la planta, el Δ^9-tetrahidrocannabinol (THC), ejerce sus acciones mayoritariamente por la activación del receptor cannabinoide 1 (CB_1R), un receptor acoplado a proteínas G (GPCR) muy abundante en el sistema nervioso central (SNC). En los últimos años, se ha estudiado intensamente el potencial terapéutico del THC y otros compuestos de la planta, lo que ha llevado a la regulación del uso del cannabis para fines medicinales, y también recreativos, en numerosos países, así como la aparición de fármacos basados en compuestos cannabinoides para tratar diversas patologías, como la espasticidad asociada a esclerosis múltiple, epilepsias refractarias infantiles, dolor neuropático, o como antiemético y modulador del apetito en pacientes de SIDA o de cáncer tratados con quimioterapia. Sin embargo, uno de los principales impedimentos al uso de estos compuestos es la aparición de efectos secundarios no deseados. Hoy en día, todavía no se conocen en detalle los mecanismos moleculares que subyacen a la activación de CB_1R, a partir de los cuales emergen estos efectos beneficiosos y perjudiciales. La señalización de este GPCR es enormemente pleiotrópica, y depende tanto del tipo celular y del estado fisiopatológico del tejido u organismo dónde se encuentra el receptor, como de la naturaleza química del ligando activante. En esta tesis doctoral hemos propuesto como hipótesis que proteínas intracelulares, a través de su unión física al receptor, constituyen un factor molecular que contribuye a modular de manera precisa la señalización del receptor en diferentes tipos celulares. Las bases fundamentales donde se inicia esta tesis son dos ensayos a gran escala, un doble híbrido en levadura, y una cromatografía de afinidad proseguida de espectrometría de masas, utilizando el dominio carboxilo-terminal del receptor, la superficie más grande de éste expuesta al interior celular. Esto nos permitió identificar dos nuevas proteínas que presumiblemente interaccionan con el receptor, la chaperona molecular BiP (Binding Immunoglobulin Protein), y el receptor de sustrato de un complejo E3 ubiquitina ligasa, Cereblon (CRBN). A partir de éste primer experimento, se derivaron los dos objetivos principales de esta tesis doctoral:

- Objetivo 1: Validación y caracterización, *in vitro* e *in vivo*, de la interacción entre BiP y CB_1R, así como de su significación fisiológica.
- Objetivo 2: Validación y caracterización, *in vitro* e *in vivo*, de la interacción entre CRBN y CB_1R, así como de su significación fisiológica.

En el Objetivo 1, inicialmente se validó la unión de BiP y CB_1R utilizando técnicas bioquímicas y de biología celular clásicas, que incluyeron doble híbrido en levadura, experimentos de polarización de fluorescencia con proteínas recombinantes purificadas, y ensayos de co-sedimentación y de transferencia de energía mediada por luminiscencia. Posteriormente, se caracterizó el efecto de BiP sobre la señalización inducida por CB_1R. Combinando técnicas vanguardistas, como la redistribución dinámica de masas, con aproximaciones más habituales, como la detección de proteínas fosforiladas, en sistemas heterólogos *in vitro*, se descubrió que BiP previene la unión de proteínas G del subtipo $G\alpha_{q/11}$ a CB_1R, lo que en último término atenúa la activación de las vías de Akt/mTORC1 y de ERK por parte del GPCR. A continuación, se estudió la presencia de complejos CB_1R-BiP en diferentes regiones del SNC (corteza, hipocampo y estriado) utilizando ensayos de ligación por proximidad en cortes de cerebro de ratones modificados genéticamente, que carecen de, o presentan, el receptor CB_1 exclusivamente en neuronas telencefálicas excitadoras dorsales, o, alternativamente, en neuronas prosencefálicas inhibidoras. Esto permitió delimitar la presencia de complejos CB_1R-BiP en neuronas inhibidoras del cerebro. Por

último, se realizaron estudios comportamentales en ratones que carecen de un alelo del gen de BiP (BiP-HET). La activación farmacológica aguda del receptor CB_1R en estos ratones indujo los efectos tradicionales adscritos al THC, como son la hipocinesia, la analgesia, la catalepsia y la hipotermia, en un grado similar a ratones control. No obstante, estas alteraciones dependen de la activación del receptor CB_1 en neuronas de proyección, dónde no están presentes los complejos. Por el contrario, un efecto secundario no deseado del consumo de THC, la aparición de ansiedad, que requiere moléculas de CB_1R presentes en neuronas inhibidoras, se encontró exacerbado en los ratones BiP-HET en comparación a ratones control. En resumen, este objetivo ha definido la proteína BiP como una nueva proteína que interacciona el receptor CB_1, contribuyendo a regular los efectos pro-ansiogénicos de su activación, gracias a disminuir la activación de las vías de señalización de Akt/mTORC1 y de ERK.

En el Objetivo 2, inicialmente se validó la unión de CB_1R y CRBN utilizando técnicas bioquímicas y de biología celular clásicas, que incluyeron experimentos de polarización de fluorescencia con proteínas recombinantes purificadas, y ensayos de co-inmunoprecipitación y de ligación por proximidad. Posteriormente, se caracterizó el efecto de CRBN sobre la señalización inducida por el receptor CB_1 con técnicas similares a las del Objetivo 1. En este caso, CRBN resultó ser un inhibidor selectivo de la vía canónica del receptor CB_1R, que involucra la inhibición de la adenilil ciclasa, y la reducción de los niveles de AMP cíclico intracelulares. Dado que una mutación en el gen *Crbn* causa una forma suave de retraso mental no sindrómico de herencia autosómica recesiva en humanos (ARNSMR), decidimos generar ratones carentes del gen *Crbn* en diferentes poblaciones neuronales, para estudiar, por un lado, las características neuroquímicas de las neuronas que podrían subyacer a esta patología, así como la potencial implicación de CB_1R en el proceso. Una extensa caracterización fenotípica demostró que ratones carentes de CRBN en la línea germinal, o selectivamente en neuronas telencefálicas excitadoras dorsales, presentan problemas de memoria a largo plazo, constituyendo, por tanto, una herramienta para estudiar la ARNSMR. Finalmente, hemos comenzado a analizar el papel que CB_1R desempeña en esta enfermedad, partiendo de la hipótesis de que éste podría encontrarse sobreactivado en ausencia de CRBN. En resumen, en el Objetivo 2 se ha caracterizado la proteína CRBN como una nueva proteína que interacciona con CB_1R, ha definido qué poblaciones neuronales originan déficits cognitivos cuando carecen de CRBN, y ha comenzado a estudiar la implicación de CB_1R en la patología de la ARNSMR.

Como conclusión general, esta tesis doctoral demuestra cómo dos proteínas intracelulares, BiP y CRBN, participan en la transducción de señales de CB_1R. Dilucidar los fenómenos moleculares que subyacen a la activación de CB_1R es de vital importancia para desarrollar terapias más seguras y eficaces dirigidas a dicho receptor.

Abstract

Extracts from the plant *Cannabis sativa* have been used for millennia for medicinal, religious or recreative purposes, among others. The plant's main psychoactive component, Δ^9-tetrahydrocannabinol (THC), exerts its actions through the activation of the CB_1 receptor (CB_1R), a G-protein coupled receptor very abundant in the central nervous system (CNS). The therapeutic potential of THC, and other plant molecules, has been extensively studied in the last years, which has led to the regulation of medicinal and recreational cannabis in numerous countries, as well as the generation of drugs based on cannabinoids to treat various pathologies, such as spasticity associated to multiple sclerosis, childhood refractory epilepsy, neuropathic pain, or as antiemetic and appetite modulator in AIDS and chemotherapy-treated cancer patients. However, one of the major setbacks that withdraw the use of these compounds is the onset of side-effects. Nowadays, the molecular mechanisms underlying CB_1R that give rise to beneficial and deleterious effects have not been elucidated in detail. CB_1R-induced signal transduction is highly pleiotropic and relies on both the cell type and physiopathological state of the tissue or organism where CB_1R molecules are located, as well as the chemical nature of the activating ligand. In this doctoral thesis, we propose the hypothesis that intracellular proteins, by physically interacting with CB_1R, constitute a molecular factor that contributes to precisely fine-tuning receptor action in different cellular settings. The founding grounds where this thesis resides on are two high-throughput experiments, based on yeast two-hybrid and affinity chromatography followed by mass spectrometry, employing the carboxy-terminal domain of the receptor, which is its largest surface exposed to the cytoplasm. This allowed us to identify two new proteins that presumably interact with the receptor, the molecular chaperone BiP, and the substrate recognition component of an E3-ubiquitin ligase complex, Cereblon (CRBN). From this starting point, we defined two main objectives for this doctoral thesis:

- Aim 1: Validation and characterization, *in vitro* and *in vivo*, of the interaction between BiP and CB_1R and assessment of its physiological significance.
- Aim 2: Validation and characterization, *in vitro* and *in vivo*, of the interaction between CRBN and CB_1R, and assessment of its physiological significance.

To address Aim 1, we initially validated the binding of BiP to CB_1R by using classical biochemistry and cellular biology approaches, which included yeast two-hybrid, fluorescence polarization experiments with recombinant purified proteins, and co-immunoprecipitation and bioluminescence energy transfer assays. Next, we characterized the effect of BiP in CB_1R-induced signaling pathways. By combining state-of-the-art techniques, such as dynamic mass redistribution assays, with classical approaches, like detection of phosphorylated proteins, in heterologous systems, we unveiled that BiP selectively prevents the binding of $G\alpha_{q/11}$ protein subunits to CB_1R, which ultimately diminishes the activation of Akt/mTORC1 and ERK triggered by the activated GPCR. Subsequently, we analyzed the presence of CB_1R-BiP complexes in different regions of the CNS (cortex, hippocampus, and striatum), by using proximity ligation assays in brain slices of genetically modified mice that lack, or solely display, CB_1R exclusively in dorsal telencephalic glutamatergic neurons or forebrain inhibitory neurons. This allowed us to delimitate the complexes to inhibitory neurons throughout the brain. Finally, we conducted behavioral experiments in mice lacking one allele of BiP (BiP-HET). Acute pharmacological activation of CB_1R in these mice induced classical effects ascribed to THC, such as hypokinesia, analgesia, catalepsy, or hypothermia to the same extent as control mice. Nonetheless, these alterations are evoked by CB_1R present in projection neurons, which do not host CB_1R-BiP complexes. On the contrary, a prominent side-effect of THC consumption,

the induction of anxiety, which requires CB_1R molecules located in inhibitory neurons, was exacerbated in BiP-HET mice compared to control mice. Taken together, our findings in this aim have defined BiP as a new protein that interacts with CB_1R, and by doing so, contributes to regulating anxiogenic outcomes elicited after receptor activation, by attenuating the activation of the Akt/mTORC1 and the ERK pathways.

To address Aim 2, we initially validated the binding of CRBN to CB_1R by using classical biochemistry and cellular biology approaches, which included fluorescence polarization experiments with recombinant purified proteins, and co-immunoprecipitation and proximity ligation assays. Next, we characterized the effect of CRBN on CB_1R-induced signaling pathways by using a similar strategy to that of Aim 1. In this case, CRBN turned out to be a selective inhibitor of the canonical CB_1R pathway, that involves adenylyl cyclase inhibition and reduction of intracellular cAMP levels. Since a mutation in the *Crbn* gene causes a mild form of autosomal recessive non-syndromic mental retardation (ARNSMR), we decided to generate mice devoid of the *Crbn* gene in different neuronal cell-type populations, to study not only the neurochemical identity of neurons that might underlie the pathology but also the potential implication of CB_1R in the disease. An extensive phenotypic characterization showed that mice lacking CRBN, either in the germline, or in dorsal telencephalic glutamatergic neurons, display long-term memory shortfalls, thus, constituting a tool to model ARNSMR. Finally, we have started to analyze the role that CB_1R might play in the pathology, based on the hypothesis that it could be overactivated when CRBN is absent. In summary, Aim 2 has defined CRBN as a new protein that interacts with CB_1R, and has unveiled which neuronal cell-type population causes memory deficits when CRBN is genetically inactivated, which represents a starting point to study the potential implication of CB_1R in ARNSMR.

As a general conclusion, this doctoral thesis demonstrates how two intracellular proteins, namely BiP and CRBN, participate in CB_1R-induced signal transduction. Elucidating molecular events that underlie the activation of CB_1R is of utmost importance to develop safer and more efficacious therapies aimed at targeting this receptor.

INTRODUCTION

AIMS

MATERIALS AND METHODS

RESULTS

DISCUSSION

CONCLUSIONS

REFERENCES

Introduction

Cannabis *(Cannabis sativa L.)*, also known **as marijuana, ganja, pot, or hemp**, is one of the plants most anciently cultivated by humankind (at least 50 centuries), for purposes ranging from medicinal to spiritual use, and even to clothe manufacturing or as food supply (Crocq, 2020). Paleobotanical analysis have dated Cannabis back to the Holocene, almost 11,700 years ago, near the Altai Mountains (Pisanti & Bifulco, 2019), from where it spread to the entire planet thanks to human domestication and its adaptability to a wide range of habitats, which represents a clear example of symbiosis. Several evidence attest for the use of cannabis across human history; for example, in the Xinjiang-Uighur autonomous region of China, a grave of a 45-year-old male buried around year 750 BCE was found to contain almost 800 grams of cultivated cannabis. Besides archaeological and paleobotanic data, linguistics also supports an ancient use of cannabis, since most of the words used to denominate the plant share a common radix, and many written records have documented its use throughout centuries until our days (Fig I1.).

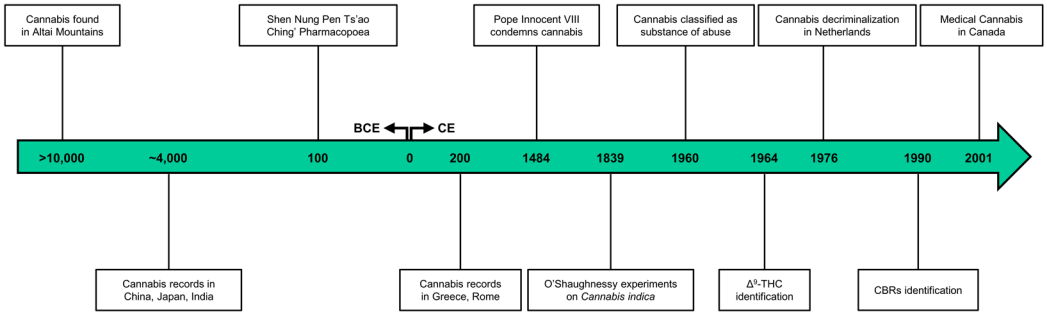

Figure I1. Timeline of Cannabis history. Abbreviations: Δ^9-THC (Δ9-tetrahydrocannabinol), CBRs (Cannabinoid receptors), BCE (Before common era), CE (common era).

This plant species, that has fascinated human beings for millennia, is to date the only one in the vascular plant kingdom that can produce significant amounts of **phytocannabinoids**, lipidic molecules, eicosanoid in nature, that exert pharmacological actions in our body. Even though more than a hundred different cannabinoids are present in *Cannabis sativa* extracts (Mechoulam *et al*, 2014), two molecules clearly stand out because of both their abundance and pharmacological profile: **Δ^9-tetrahydrocannabinol (THC) and cannabidiol (CBD)**. These molecules were discovered thanks to the fundamental work of Raphael Mechoulam and others in the past century, which converged in the isolation and structural elucidation of CBD in 1963 (Mechoulam & Shvo, 1963) and THC in 1964 (Gaoni & Mechoulam, 1964). Further studies identified THC as the molecule underlying psychoactive effects that follow cannabis consumption (Mechoulam *et al*, 1970), which laid the foundations to identify its mechanism of action. Nonetheless, only after 20 years of intense research, a first cannabinoid-binding receptor, namely the CB_1 receptor (CB_1R), very abundant in the brain, was identified (Devane *et al*, 1988; Matsuda *et al*, 1990). Soon enough, a second cannabinoid-binding receptor, namely, the CB_2 receptor (CB_2R) was cloned (Munro *et al*, 1993). The existence of specific cannabinoid receptors clearly suggested that THC resembled an endogenous ligand yet to be identified. Following this logic, a first cannabinoid-like substance was isolated from porcine brain in 1992 (Devane *et al*, 1992). This molecule was an arachidonic acid derivative, the lipid ***N*-arachidonoylethanolamine (AEA)**, and was named anandamide resulting from the combination of the Sanskrit word *ananda*, which means "joy, bliss, delight" and the amide bond present in the molecule. Three years later, a second molecule that bound cannabinoid receptors, the lipid **2-arachidonoyl glycerol (2-AG)**, was identified in extracts of canine gut (Mechoulam *et al*, 1995; Sugiura *et al*, 1995). In agreement with the plant's name, these compounds were termed

endocannabinoids. In accordance, synthetic compounds that target cannabinoid receptors have also been named **'synthocannabinoids'.**

The next milestone in cannabinoid research was the identification of synthesizing and degrading pathways that finely control 2-AG and AEA levels. Although alternative pathways account for residual production, it is well accepted that **sn1-diacylglycerol lipases α and β** (**DAGLα/β**) oversee 2-AG production (Bisogno *et al*, 2003), while an ***N*-acyl phosphatidylethanolamine-specific phospholipase D** (**NAPE-PLD**), with the aid of other enzymes, produces AEA (Okamoto *et al*, 2004). Catabolism of these lipids is mediated by a **monoacylglycerol lipase** (**MAGL**) in the case of 2-AG (Goparaju *et al*, 1999; Dinh *et al*, 2002), and **fatty acid amide hydrolase** (**FAAH**) in the case of AEA (Cravatt *et al*, 1996; Giang & Cravatt, 1997).

Taken together, cannabinoid receptors, endocannabinoid ligands, as well as synthetic and degradative enzymes constitute an intercellular communication system known as **the endocannabinoid system (ECS).**

Parallel to this basic science, many laboratories focused on the molecular mechanisms underlying THC and/or cannabis intake-mediated outcomes in our organism, unveiling an innumerable quantity of physiological processes where the ECS participates in, with a special focus on CB_1R. Thus, cannabis consumption can elicit memory and cognitive impairment, feelings of well-being, antinociception, psychosis, antiemesis, antispasticity, sedation, hyperphagia or motor discoordination (Pertwee *et al*, 2010). Cannabinoid-based therapies have been approved by regulatory agencies for the treatment of spasticity in multiple sclerosis (Novotna *et al*, 2011), as anticonvulsants in children with refractory forms of epilepsy (Devinsky *et al*, 2017), for the treatment of neuropathic pain, and as antiemetic and appetite stimulants in AIDS or chemotherapy-treated cancer patients (National Institute for Health and Care Excellence, UK, 2019). In fact, several countries (*e.g.,* Uruguay, Canada, Germany, The Netherlands, Italy, Israel) as well as many states of the US have already regulated the use of marijuana for medicinal purposes, and some even for recreational ends (Kumar *et al*, 2021). Since CB_1R triggers most psychoactive consequences of THC consumption but presumably also most of its therapeutic actions, it represents the most appealing pharmacological target within the ECS. Nonetheless, there are some crucial questions that need to be solved to exploit the therapeutic potential of CB_1R in a safer manner. The aim of any given therapy should be to tip the balance of desired *vs*. undesired effects towards the former, hence, understanding how the benefits and the risks of cannabis use arise upon CB_1R activation from a molecular point of view is of utmost importance to reduce detrimental side-effects. Recent evidence suggests that CB_1R function is highly regionalized and variable depending on cell-type, subcellular localization, physiopathological state, ligand used, receptor's post-translational modifications, and other molecular factors such as interacting proteins (Busquets-Garcia *et al*, 2018). Hence, we have continued to seek for explanations of how cannabis, through CB_1R, precisely exerts actions in our body.

1.1 The endocannabinoid system

Classically, the ECS is an intercellular signaling network that encompasses i) the G-protein coupled cannabinoid receptors CB_1R and CB_2R, ii) their endogenous ligands, 2-AG and AEA, and iii) the related anabolic enzymes (DAGLα/β and NAPE-PLD for 2-AG and AEA, respectively) and catabolic enzymes (MAGL and FAAH for 2-AG and AEA, respectively). Lately, some authors have proposed an expanded ECS, termed **endocannabinoidome**, that would include several other members, such as other long-chain N-acyl-amides (and their

own metabolic enzymes), non-classical receptors (*e.g.,* TRPV1, PPARα/γ), alternative enzymes for biosynthesis [*e.g.,* α, β hydrolase domain containing 4, (ABHD4) for AEA] or degradation [*e.g.,* α, β hydrolase domain containing 6/12, (ABHD6/12) for 2-AG] and endogenous allosteric modulators, such as pregnenolone, that counteracts CB_1R activation, or lipoxin A4, which enhances CB_1R receptor function (Cristino *et al*, 2020).

1.2 Cannabinoid receptors

1.2.1 Type 1 cannabinoid receptor (CB_1R)

CB_1R was first identified in 1988, using a radioactive-labeled synthetic agonist ([^{3}H]CP-55,940) whose binding to rat brain membranes was displaced by THC (Devane *et al*, 1988). Only two years later, the orphan G-protein coupled receptor, SKR6, cloned from rat brain, was identified as the aforementioned protein pharmacologically characterized by Howlett and colleagues, and renamed cannabinoid-binding receptor 1 or CB_1R (Matsuda *et al*, 1990; Munro *et al*, 1993). CB_1R is encoded at chromosome 6 in humans (chromosome 4 in mouse and 5 in rat) (Bouaboula *et al*, 1993). The coding region of the gene lacks introns, but possesses an intron upstream to the ATG starting codon and three additional exons (Zhang *et al*, 2004). This gives rise to several spliced versions of the receptor both in human, mouse and rat (Shire *et al*, 1995; Ruehle *et al*, 2017). To date, the contribution of splice variants to receptor action has not been explored in detail, but subtle differences in signaling properties have been reported (Straiker *et al*, 2012).

CB_1R is a protein of 472 amino acids (473 in mouse and rat) that belongs to the Class A GPCR superfamily. Like all GPCRs, CB_1R displays **seven transmembrane α-helices (TM1-7)** linked by **three intracellular (ICL1-3) and three extracellular (ECL1-3) loops** that face the cytoplasm and the extracellular matrix (or the lumen of the endoplasmic reticulum), respectively, in addition to an **extracellular *N*-terminal domain (NTD)** and a **cytoplasmic *C*-terminal domain (CTD).** Phylogenic analysis have found an ancestral gene in the urochordate *Ciona intestinalis* (Elphick *et al*, 2003) and the CB_1R protein can be found in mammals, birds, amphibians and fish with a high amino acidic conservation (*e.g.* the rat and mouse proteins share a 97% amino acid identity with human CB_1R). The wide distribution of CB_1R across the animal kingdom, and its high amino acid conservation suggests that some roles of the endocannabinoid system may be ancient and highly preserved (Elphick, 2012). Recent studies have determined a set of CB_1R structures bound to agonists (Hua *et al*, 2017), inverse agonists (Shao *et al*, 2016), antagonists (Hua *et al*, 2016) and even complexed with G-proteins (Krishna Kumar *et al*, 2019) (Fig. I2). As expected, the structure of CB_1R resembles those of other Class A GPCRs, and comparably to other lipid-binding GPCRs, its extended NTD occludes the ligand binding site (orthosteric site); that is composed of residues contributed by TM2, TM3, TM5, TM6 and ECL2 and situated within the membrane, from the outer side of the cell (Ramesh & Rosenbaum, 2021). Agonist binding occurs probably through the lipid bilayer and proceeds with a massive rearrangement of the transmembrane helices, that results in a ~50% reduction of the orthosteric pocket volume. Another important component for the activation of CB_1R is the movement of the so-called 'twin toggle switch', formed by residues F200 and W356. These two aromatic amino acids establish direct contacts in the inactive state. Upon agonist binding, this interaction is disrupted, with F200 forming a van der Waals contact with the ligand, and W356 moving away, thus allowing an outward movement of TM6 and G-protein binding (Ramesh & Rosenbaum, 2021). Interestingly, one recently solved structure (Shao *et al*, 2019) included a bound negative allosteric modulator of CB_1R, the compound Org27569 (Price *et al*, 2005), thus localizing one allosteric binding site embedded in the membrane, in-between the lipid-

facing sides of TM2 and TM4. Intriguingly, this region overlaps with a putative cholesterol binding site observed in one of the agonist-bound structures (Hua *et al*, 2017), which might diminish CB_1R activation (Bari *et al*, 2005). Despite their significant contributions, unfortunately, none of these studies was able to fully resolve the 3D structure of neither the *N*-terminus nor the *C*-terminus of the receptor. In addition to crystallographic data, previous nuclear magnetic resonance (NMR) analyses, using the CTD of CB_1R in solution with membrane mimics, reported two additional α-helices, the helix-8 (amino acids 401 to 412) and the helix-9 (amino acids 440 to 461) (Ahn *et al*, 2009). Since only helix-8 is present in the reported structures, a complete three-dimensional architecture of CB_1R remains an important missing tool in the cannabinoid field.

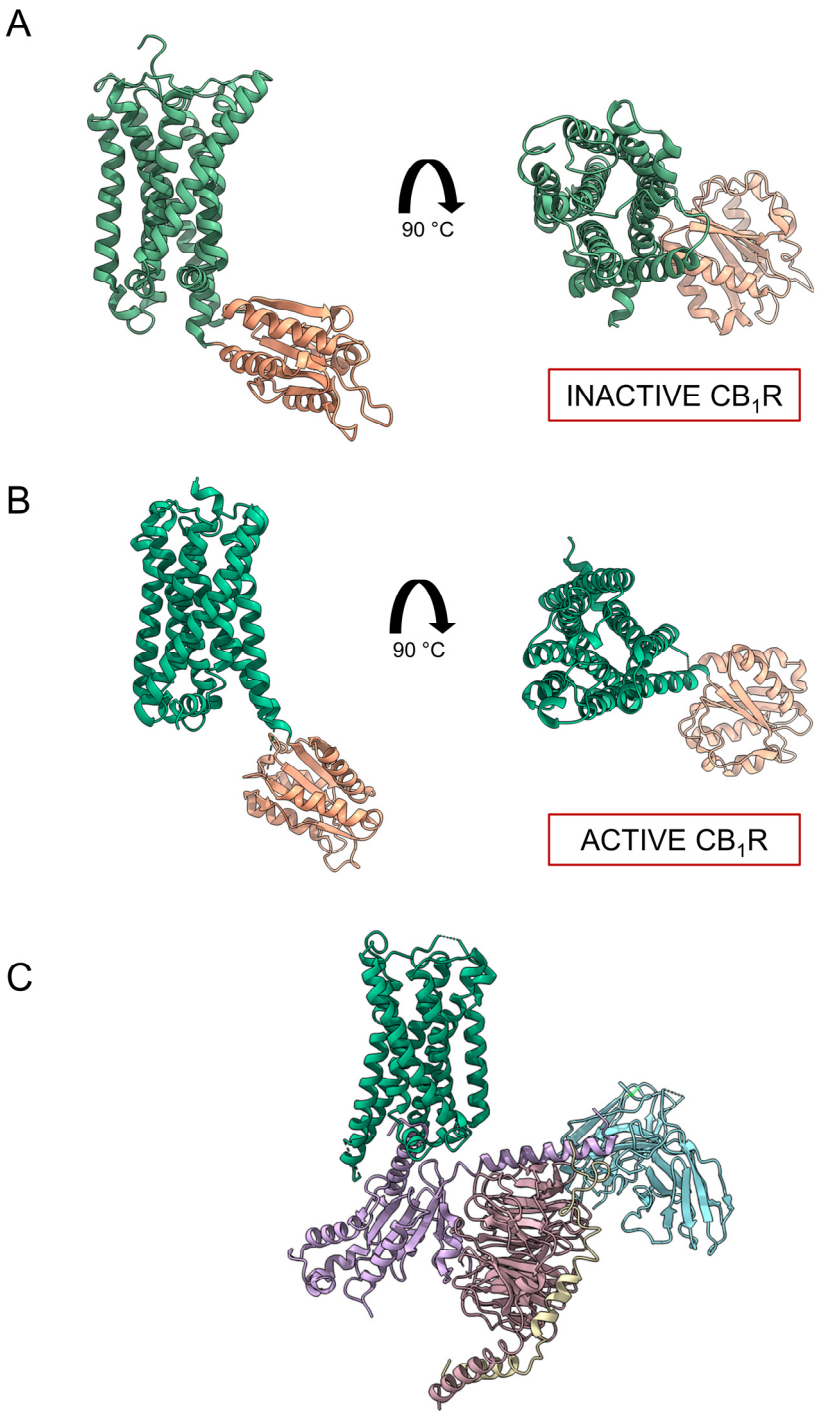

Figure I2. Three-dimensional structure of CB_1R. ***A,*** Structure of antagonist-bound CB_1R. Note the V-shaped loop formed by the NTD to occlude the interior from the extracellular milieu, and the loose conformation of the transmembrane helices. ***B,*** Structure of agonist-bound CB_1R. Note how the NTD forms a helix and the helices are compacted, diminishing the 3D volume. ***C,*** Structure of the CB_1R-G-protein complex. CB_1R is shown in green, $G_{\alpha i1}$ in pink, transducin β chain 1 in pale red, $G\gamma_1$ in gold, and the stabilizing antibody scFv16 in cyan. Images were created using ChimeraX (UCSF®) and Protein Data Bank accession numbers *5tgz* for panel A, *5xra* for panel B and *6n4b* for panel C.

CB_1R is one of the most abundant receptors in the mammalian central nervous system, with levels comparable to those of N-methyl-D-aspartate receptor (NMDAR) subunits (Herkenham *et al*, 1990; Marsicano & Lutz, 1999). Its expression is notably elevated in brain regions such as the basal ganglia nuclei, the cerebellum, the hippocampus, or the cortex (Fig. I3). This distribution pattern correlates well with known effects of THC such as motor discoordination, memory and cognition impairment or catalepsy. At the cellular level, CB_1R is primarily located to the axons of neurons, where they finely control neurotransmitter release (Piomelli, 2003), but receptors can also be found in the somatodendritic compartment (Leterrier *et al*, 2006), other cell types of the brain parenchyma such as astrocytes (Navarrete & Araque, 2008), oligodendroglial cells (Molina-Holgado *et al*, 2002) or neural stem cells (Aguado *et al*, 2005) and even at distinct subcellular localizations within the expressing-cell such as mitochondria (Bénard *et al*, 2012) or endosomes (Thibault *et al*, 2013). Besides this central distribution, CB_1R can be found in a variety or peripheral tissues such as the adrenal gland, the heart, the adipose tissue, the liver, the testis or the uterus, to quote but a few, from where it takes part virtually in most physiological processes (Galiègue *et al*, 1995; Piazza *et al*, 2017).

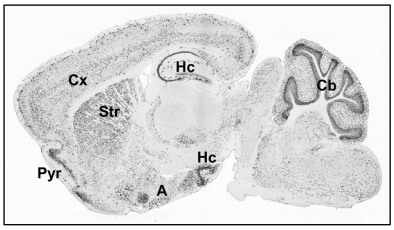

Figure I3. CB_1R distribution in the mouse brain. *In situ hybridization* (ISH) experiments show elevated CB_1R expression in several brain nuclei, such as cortex (Cx), pyriform cortex (Pyr), striatum (St), the hippocampal formation (Hc), the amygdala (A) or the cerebellum. Image credit: Allen Brain Atlas.

1.2.2 Type 2 cannabinoid receptor (CB_2R) and other receptors

CB_2R was identified in 1993 using the promyelocytic leukemia cell line HL60 (Munro *et al*, 1993). By using non-directed cloning and GPCR homology searching, the authors identified six cDNA clones that expressed functional GPCRs. One of them, the clone CX5, showed 44% amino acid identity to CB_1R (which raised to 68% when comparing transmembrane regions), and the resulting protein was found capable of binding synthetic cannabinoids as well as phytocannabinoids. With the aim of simplifying terminology, this receptor was renamed CB_2R. CB_2R is encoded in the genome at chromosome 1 in humans (chromosome 4 in mouse and 5 in rat). Similarly to CB_1R, it possesses a major coding exon, but some unprocessed exons can be found at the 5' untranslated region of the gene. In fact, two splice variants that differ either in the *N*-terminal or the *C*-terminal end have been identified both in human, mouse and rat but so far their contribution to receptor action has not been properly studied (Liu *et al*, 2009).

CB_2R is a protein of 360 amino acids that also belongs to the class A GPCR superfamily. It shares the common GPCR fold, with seven transmembrane α-helices (TM1-7) linked by three intracellular (ICL1-3) and three extracellular (ECL1-3) loops that face the cytoplasm and the cellular matrix, respectively, in addition to an extracellular *N*-terminal domain (NTD) and a cytoplasmic *C*-terminal domain (CTD). CB_2R is also widely distributed in nature, and clones have been isolated from rat, dog, mouse, zebrafish and other species (Howlett & Abood, 2017). However, amino acid conservation between species is lower than that observed for CB_1R; for instance, mouse and human CB_2Rs share 82% amino acid identity (Shire *et al*, 1996). Structural biologists have also focused their view on CB_2R. Recent works have unveiled agonist and antagonist-bound CB_2R structures, as well as CB_2R complexed with G-proteins (Li *et al*, 2019; Hua *et al*, 2020). Comparably to CB_1R, agonist binding causes an important rearrangement of TM2, TM3, TM5, TM6, TM7 and ECL2 that occludes the interaction between the 'twin toggle switch' formed by F117 and W258.

Intriguingly, the spatial distribution of antagonist-bound CB_2R reminds that of agonist-bound CB_1R, with the *N*-terminus adopting a very similar conformation on top of the orthosteric pocket, which is in turn practically identical between both proteins, a fact that could explain why it has been so difficult to develop selective agonists for each receptor (Li *et al*, 2020) (Fig. I4). The resemblance between inactive CB_2R and active CB_1R was so evident that the authors even demonstrated that a CB_2R-selective antagonist behaves as a CB_1R partial agonist (Li *et al*, 2019). This fact opens a new conceptual framework for the development of therapies aimed at targeting both receptors.

In contrast with CB_1R, CB_2R expression is almost undetectable in the central nervous **system, at least in 'basal' conditions** (Brown *et al*, 2002)**, but reports suggest that pathology** induces its expression in microglial cells (Benito *et al*, 2007). In addition, low levels of CB_2R have been found in astrocytes (Palazuelos *et al*, 2006) and neural progenitors (Stella, 2004). However, elevated CB_2R expression can be found in several immune tissues and cells, especially in macrophages, spleen, tonsils, thymus, and leukocytes (Galiègue *et al*, 1995), where it controls cytokine production, and immune-cell development and function (Malfitano *et al*, 2014).

Several other GPCRs and non-GPCRs have been suggested as a potential 'type 3 cannabinoid receptor', *e.g.,* GPR55, GPR119, GPR18, TRPV1 or PPAR family members. Even though CB_1R and CB_2R ligands can target many of these proteins, at least *in vitro*, there is still great controversy about whether these receptors should be included as full-fledged members under pathophysiologically-relevant conditions *in vivo* (Pertwee *et al*, 2010).

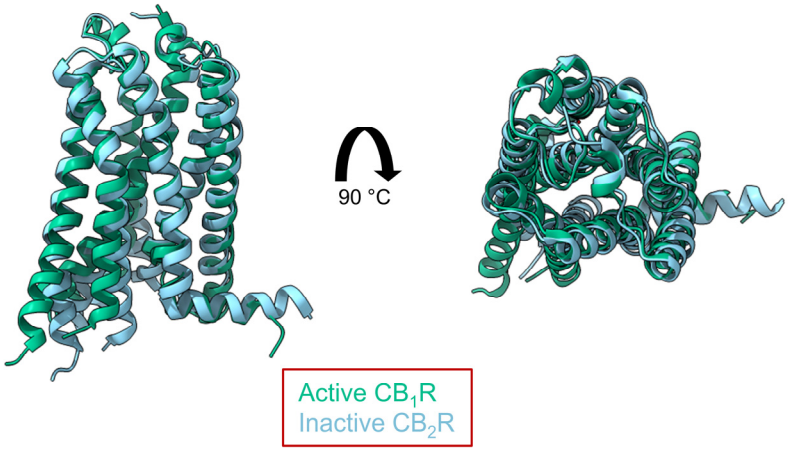

Figure I4 Structural similarities between active CB_1R and inactive CB_2R. Note the similarity between activated CB_1R (green) and antagonist-bound CB_2R (cyan), particularly at the helix formed by the extended NTD, as well as the compact formation of the helices. Images were created using ChimeraX (UCSF®) and Protein Data Bank accession numbers *5tgz* (CB_1R) and *5zty* (CB_2R).

1.3 Cannabinoids

Molecules that act through CB_1 and CB_2 receptors are considered cannabinoids from a pharmacodynamic standpoint. Depending on their source, they can be classified in endocannabinoids, those generated by animals; phytocannabinoids, that are generated by the plant *Cannabis sativa*; or synthocannabinoids, which are synthetic chemical compounds originated in medicinal-chemistry laboratories (Fig. I5). Generally, endocannabinoids and phytocannabinoids that act at both receptors, show enhanced activity at CB_1R compared with CB_2R (Pertwee *et al*, 2010).

Phytocannabinoids are the molecules that account for virtually all the effects elicited upon consumption of *Cannabis sativa* preparations and the founding members of the cannabinoid's family. The first isolated cannabinoid was cannabinol, at the end of the nineteenth century, which was followed by the discovery of more than a hundred different phytocannabinoids present in the plant (Mechoulam *et al*, 2014). Despite this plethora of molecules, two phytocannabinoids stand out from the rest, THC and CBD as they are the most studied compounds so far, both because of their abundance and their pharmacological properties. On the one hand, CBD acts as a negative allosteric modulator of CB_1R, among several other molecular targets (Laprairie *et al*, 2015). On the other hand, the dibenzopyran derivative, THC, displays a high affinity for CB_1 and CB_2 receptors, behaving as a partial agonist. When administered to animals, THC exerts the so-called 'cannabinoid tetrad', consisting of hypokinesia, analgesia, hypothermia, and catalepsy. Delivery of endocannabinoids or synthetic cannabinoids targeting CB_1R mimic these outcomes, so major THC actions are due to endocannabinoids impersonation.

Endocannabinoids are lipid molecules derived from arachidonic acid, hence, eicosanoids in nature. The two best studied are 2-AG and AEA. Several other *N*-acyl-ethanolamines (NAEs), long-chain *N*-acyl amides, that include *N*-acyl-taurine, *N*-acyl-dopamine, *N*-acyl-serotonin or *N*-acyl-amino acids have been proposed as endocannabinoid-like, structurally-related mediators, but they target receptors different from CB_1R and CB_2R (Cristino *et al*, 2020). As mentioned above, AEA is synthesized through the action of specific phospholipases from cellular membranes that contain *N*-acyl-phosphatidylethanolamine, a low abundant lipid generated by the enzymatically-mediated transfer of an acyl-chain to the free amine in the polar head by *N*-acyltransferases (NATs), a mechanism similar for other *N*-acyl-ethanolamines (Tsuboi *et al*, 2018). AEA acts as a partial agonist of CB_1R, but also exerts actions at TRPV1 or PPAR-γ receptors (Zygmunt *et al*, 1999; Bouaboula *et al*, 2005). On the other hand, 2-AG shows full agonism at CB_1R, and its abundance is hundreds to thousands of times higher than that of anandamide. Thus, it is believed to play a more prominent role as a CB_1R agonist than AEA physiologically (Tsuboi *et al*, 2018). As mentioned above, 2-AG is synthesized by DAGL-α or β from diacylglycerol, that originates either from phospholipids, after the action of phospholipases β or γ (PLCβ/γ) or from triglycerides, after the hydrolysis the hormone-sensitive lipase (HSL), carboxyl esterase or other lipases; (Baggelaar *et al*, 2018).

Synthocannabinoids are an ever-expanding group of molecules that target cannabinoid receptors. Initially developed as pharmacological tools, one of them (nabilone) having already reached the market (Mechoulam *et al*, 2014), they are becoming an important problem for public health, since recreational uses are increasing (Lobato-Freitas *et al*, 2021). Classically, they have been divided in three groups depending on their chemical nature.

- Classical or dibenzopyran derivatives group. They represent chemical analogues of THC. The most representative compound of this group is (6aR)-trans-3-(1,1-dimethylheptyl)-6a,7,10,10a-tetrahydro-1-hydroxy-6,6-dimethyl-6Hdibenzo[b,d]pyran-9-methanol, known as **HU-210**, a high affinity and potency CB_1R/CB_2R agonist.
- Nonclassical or cyclic derivatives group: They represent chemical analogues of THC that lack a pyran ring. The most used compound of this group is (-)-cis-3-[2-hydroxy-4-(1,1-dimethylheptyl)phenyl]-trans-4-(3-hydroxypropyl)cyclohexanol, known as **CP-55,940**, a CB_1R/CB_2R agonist with slightly less potency than HU-210.

- Aminoalkylindole group. They represent cannabinoids that have structures markedly different from classical and non-classical compounds. The best known member of this group is R-(+)-[2,3-dihydro-5-methyl-3-(4-morpholinylmethyl)pyrrolo[1,2,3-de]-1,4-benzoxazin-6-yl]-1-naphthalenyl-methanone mesylate, namely, **WIN55,212-2**, a CB_1R/CB_2R agonist with slightly less potency than HU-210.

Of note, several other chemicals apart from agonists are of relevance to study CB_1/CB_2 receptors. These include the inverse agonists SR141716, a diarylpyrazole also known as **rimonabant**, which is CB_1R-selective, and SR144528, another diarylpyrazole that is CB_2R-selective; as well as neutral antagonists, allosteric modulators and inhibitors of endocannabinoid anabolic and catabolic enzymes (Pertwee *et al*, 2010).

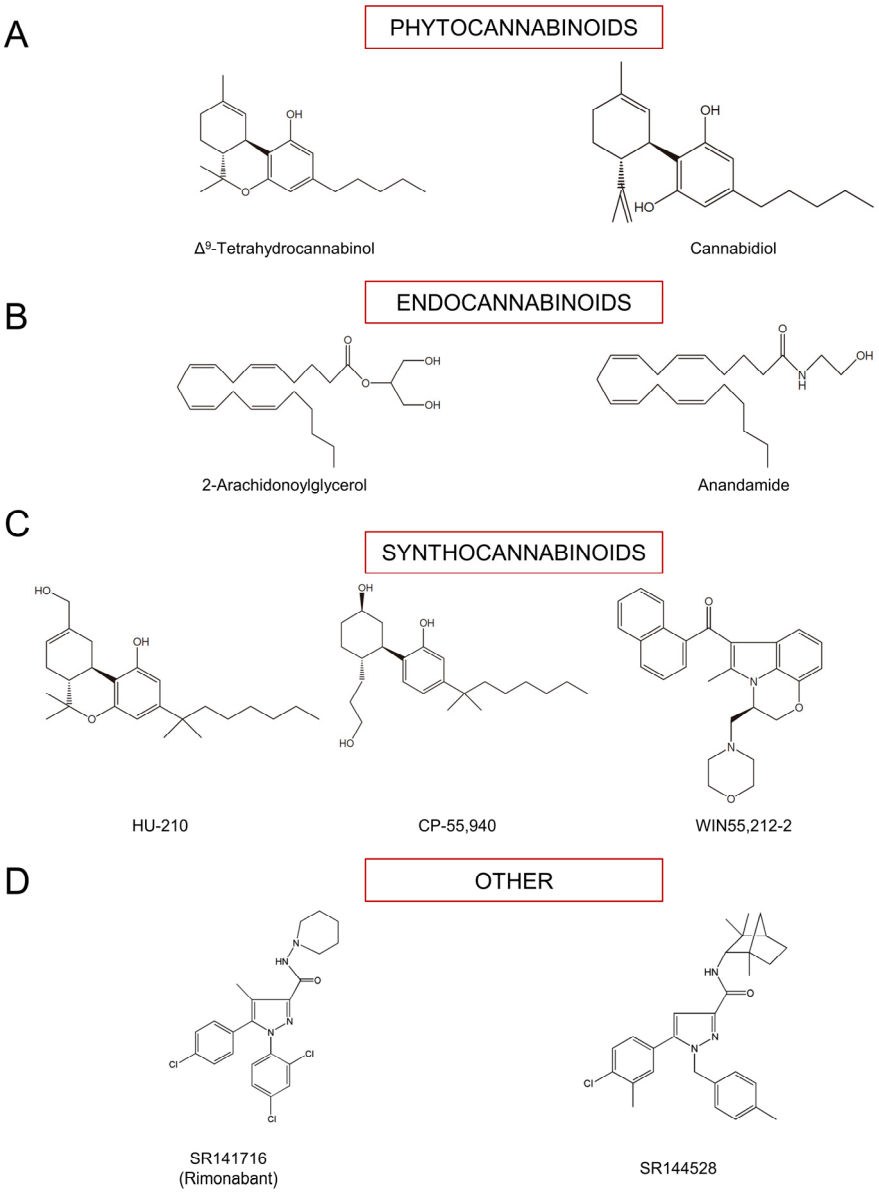

Figure I5. Major cannabinoids. ***A,*** Among > 100 phytocannabinoids, THC and CBD are by far the most abundant compounds. ***B,*** Two endocannabinoids, arachidonic acid derivatives, are *bona fide* CB_1R/CB_2R agonists. ***C,*** Many synthetic cannabinoids have been generated, including classical (HU-210), non-classical (CP-55,940) and aminoalkylindole derivatives (WIN55,212-2). ***D,*** Several other pharmacological tools, such as the inverse agonists SR141716 (CB_1R-selective) and SR144528 (CB_2R-selective) have also been discovered. Chemical structures were extracted from Pertwee *et al*, 2010.

1.4 Synthesis and degradation of endocannabinoids

The cellular levels of the endocannabinoids, 2-AG and AEA are tightly regulated owing to the balance between synthesis and degradation. Endocannabinoids are usually generated 'on demand' from cellular membranes of post-synaptic cells (although AEA may also come from the presynapse), where they are supposed to diffuse to reach CB_1R at the presynapse (Fig. I6). Hence, unlike classical neurotransmitters, they are not stored in vesicles, although this issue has been recently challenged (Albarran *et al*, 2021), and the possible existence of a putative AEA transporter is a recurrent topic in the field (Piomelli *et al*, 1999; Kaczocha & Haj-Dahmane, 2021).

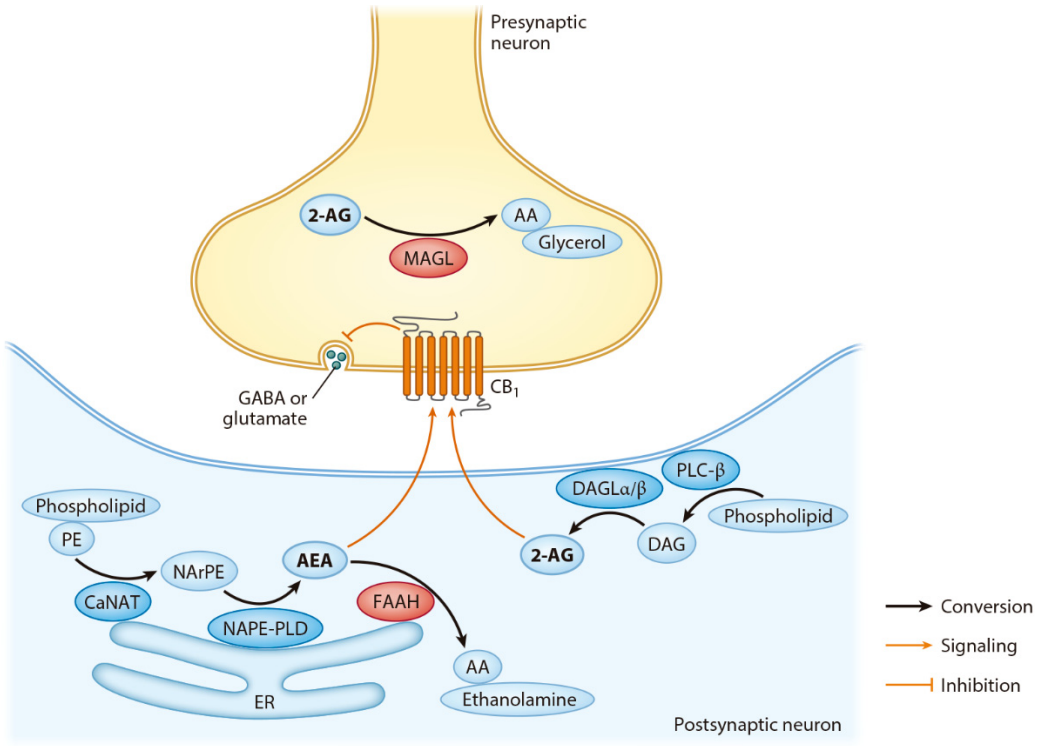

Figure I6. Endocannabinoid synthesis, degradation, and signaling function at the synapse. Concurrent activation of ionotropic and metabotropic receptors causes a raise in intracellular calcium that triggers endocannabinoid production from membrane phospholipids through the sequential action of PLCβ/DAGL in the case of DAG, or a calcium-dependent *N*-acyl transferase (CaNAT, probably the enzyme PLA2G4E) and NAPE-PLD in the case of AEA. Then, endocannabinoids traverse the synaptic cleft to activate CB_1R and block neurotransmission. 2-AG is then degraded in the presynapse, whereas FAAH, the AEA degrading enzyme is mostly localized in the post-synapse. Synthetic enzymes are shown in blue, while degradative enzymes are red-colored. Image source: Van Egmond *et al*, 2021.

2-AG is generated using arachidonate-containing diacylglycerols, which can arise from the hydrolysis of phosphatidylinositol-4,5-bisphosphate by PLCβ or PLCγ or through the various lipases on triglycerides (Stella *et al*, 1997) (Fig. I7). The first pathway is physiologically more relevant since variations in intracellular Ca^{2+} concentration due to the coincidental activation of $G\alpha_{q/11}$-coupled metabotropic receptors and calcium channels control PLC activity (Ohno-Shosaku *et al*, 2002). Once arachidonate-containing diacylglycerol is generated, both pathways converge, and 2-AG is generated by specific DAGLs. To date, two enzymes that display sn1-acyl hydrolytic activity from triglycerides have been identified: DAGL-α and -β; two membrane-bound serine hydrolases that differ by the absence of a large C-terminal tail in the β enzyme (Bisogno *et al*, 2003). Experiments with mice bearing germline deletions of either DAGL-α or DAGL-β have revealed tissue-specific contributions to 2-AG biosynthesis of each enzyme, and have also showed that

DAGL-α is the main source of 2-AG in neurons (Tanimura *et al*, 2010; Gao *et al*, 2010), and thus lays behind the neuromodulatory effects of 2-AG (see below). Of note, DAGL-α is highly enriched at post-synaptic sites, which is consistent with the notion that 2-AG is a retrograde neurotransmitter, while DAGL-β activity resides mainly in microglia (Yoshida *et al*, 2006; Viader *et al*, 2016). Decreases in 2-AG levels are mediated by multiple enzymes, but the 'canonical' pathway proceeds with hydrolysis of the ester bond into arachidonic acid and glycerol by the MAGL, which accounts for ~85% of 2-AG catabolism in the brain (Blankman *et al*, 2007). MAGL is a ubiquitously expressed serine hydrolase that associates with membranes and, in contrast to DAGL-α, it is positioned presynaptically, alike CB_1R (Hashimotodani *et al*, 2007). Several other enzymes, including, ABHD12, ABHD6, lipoxygenases, cyclooxygenases, and cytochrome P450 family members contribute to 2-AG bioconversion (Baggelaar *et al*, 2018).

The first step for anandamide biosynthesis proceeds with the formation of NAPE mediated by a calcium-dependent *N*-acyltransferase (proposed to be the enzyme PLA2G4E) (Cadas *et al*, 1996; Ogura *et al*, 2016). Next, NAPE-PLD, breaks down this lipid to generate anandamide (Okamoto *et al*, 2004) (Fig. I7). NAPE-PLD is a ubiquitously expressed, zinc-dependent cytosolic enzyme, member of the metallo-β-lactamase family that is particularly enriched in the brain, although in contrast with DAGLα, it is mainly regionalized in axons (Okamoto *et al*, 2004; Egertová *et al*, 2008; Magotti *et al*, 2015), which further strengthens the notion that 2-AG is the principal player behind the CB_1R-mediated neuromodulation. Early reports suggested NAPE-PLD activity could be enhanced by elevated Ca^{2+} concentrations, which was consistent with previous data that observed increased AEA synthesis after Ca^{2+} or cAMP mobilization (Cadas *et al*, 1996; Ueda *et al*, 2001; Wang *et al*, 2006a). Nonetheless, these experiments were performed with the purified enzyme and other divalent cations exerted similar actions. Recently, it has been found that NAPE-PLD is insensitive to Ca^{2+} when bound to membranes, but rather requires hydrophobic agents, such as bile acids, to enhance the reaction rate (Wang *et al*, 2008; Magotti *et al*, 2015). Other enzymes may contribute as well to the generation of AEA, such as PLA2, PLC and ABHD4, since a NAPE-PLD knockout mouse model did not show reduced levels of AEA (Leung *et al*, 2006; Hussain *et al*, 2017; Biringer, 2021). Inactivation of AEA can involve several enzymes, but the most relevant consists of serine hydrolase FAAH, which performs the hydrolysis to arachidonic acid and ethanolamine. This enzyme, opposite to MAGL, is an integral membrane protein that localizes to intracellular membranes of post-synaptic specializations and hydrolyzes not only AEA but also other NAEs (Egertova *et al*, 1998). However, experiments carried out with FAAH knockout mice show elevated AEA and phenotypes such as antinociception that can be reversed by CB_1R antagonism (Cravatt *et al*, 2001). Several other enzymes, including, *N*-acylethanolamine acid amidase (NAAA), lipoxygenases, cyclooxygenases, and cytochrome P450 family members contribute to AEA transformation (Scherma *et al*, 2019).

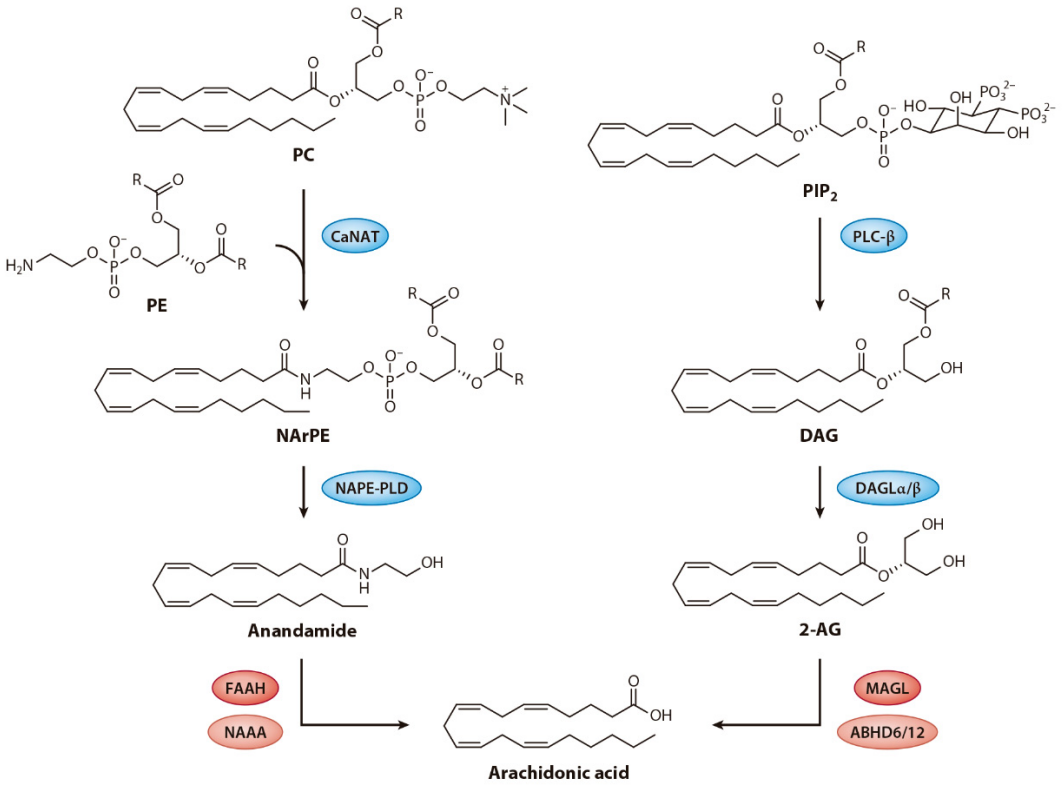

Figure I7. Metabolic pathways of AEA and 2-AG. AEA and 2-AG are synthesized from membrane phospholipids (PC: phosphatidylcholine, PIP2: phosphatidylinositol-4,5-bisphosphate, PE: phosphatidylethanolamine) through sequential actions of two pairs of enzymes: A calcium-dependent N-acyl transferase (CaNAT, probably the enzyme PLA2G4E) and NAPE-PLD in the case of AEA, or PLCβ followed by DAGLα/β in the case of 2-AG. Inactivation by the enzymes FAAH/NAAA (AEA) or MAGL/ABHD6/ABHD12 (2-AG) renders arachidonic acid. Synthetic enzymes are shown in blue, while degradative enzymes are red-colored. Image source: Van Egmond *et al*, 2021.

1.5 CB_1R function in the CNS

Despite the ever-increasing body of data, most of what is known regarding the elements of the ECS in the brain refers to CB_1R.

1.5.1 CB_1R signal transduction

CB_1R is a GPCR that engages G-proteins of the $\alpha_{i/o}$ subfamily, and thus, ligand-binding inhibits adenylyl cyclase activity and reduces cellular cAMP levels, which diminishes the activity of intracellular proteins that depend on this second messenger, such as protein kinase A, exchange protein directly activated by cAMP (Epac), and cyclic nucleotide-gated ion channels, which leads to fundamental changes in metabolism, gene expression, cell growth and differentiation, apoptosis, and neurotransmission (Cheng *et al*, 2008; Galve-Roperh *et al*, 2013). Under diverse experimental settings, CB_1R has been found associated with $G\alpha_{q/11}$, $G\alpha_{12/13}$ and even $G\alpha_s$ protein members, probably due to local changes in the availability of G-protein subunits and/or interactions with other proteins in particular cell environments (Glass & Felder, 1997; Lauckner *et al*, 2005; Chen *et al*, 2010; Diez-Alarcia *et al*, 2016). Hence, CB_1R activation can also trigger, for example, $G\alpha_s$-induced mobilization of cAMP, $G\alpha_q$-mediated Ca^{2+} and diacylglycerol (DAG) increases, or $G\alpha_{12/13}$-stimulated actin polymerization.

Aside from adenylyl cyclase inhibition, CB_1R regulates a large variety of signaling pathways, including, but not limited to, inhibition of L-, N- and P/Q-type Ca^{2+} channels (Howlett &

Abood, 2017), activation of G-protein-coupled inwardly rectifying K^+ channels (Mackie *et al*, 1995), as well as activation of the PI3K/Akt/mTORC1 pathway (Gómez Del Pulgar *et al*, 2000), the ERK pathway (Galve-Roperh *et al*, 2002), and several tyrosine kinases (Dalton & Howlett, 2012), among others. Many of these pathways are activated by the βγ dimers released after heterotrimeric G-protein dissociation (Fig. I8).

Finally, like many other class A GPCRs, activation of CB_1R triggers **β-arrestin1/2 binding** to induce **desensitization and internalization processes**. The general scheme, common to other GPCRs, proceeds with the phosphorylation of CB_1R-CTD by GPCR-related kinases (GRKs) and β-arrestin1/2 binding, which elicits both signaling and endocytic mechanisms (Nogueras-Ortiz & Yudowski, 2016). It has been proposed that for CB_1R, β-arrestin-1 and β-arrestin-2 have opposing roles, the former being responsible for ERK activation, and the latter in charge of internalization events (Ahn *et al*, 2013). Binding of each isoform probably occurs when particular conformations of the receptor are stabilized, presumably emanating from specific phosphorylation patterns in the CB_1R-CTD, that would depend on several factors, including the ligand used and the intracellular repertoire of GRKs and other kinases (Delgado-Peraza *et al*, 2016). To date, only two individual CB_1R phosphorylated residues have been linked to β-arrestin binding (S425/S429 in human, S426/S430 in mouse and rat), but several other phosphorylation-prone residues are important for CB_1R internalization, and high-throughput studies identified some of them phosphorylated in brain extracts (Daigle *et al*, 2008; Wiśniewski *et al*, 2010). Thus, which, how, and why carboxy-terminal amino acids in CB_1R are phosphorylated needs to be addressed in the future.

The molecular mechanisms described above empower CB_1R to fulfil one critical function of the endocannabinoid system: **the modulation of neurotransmission.**

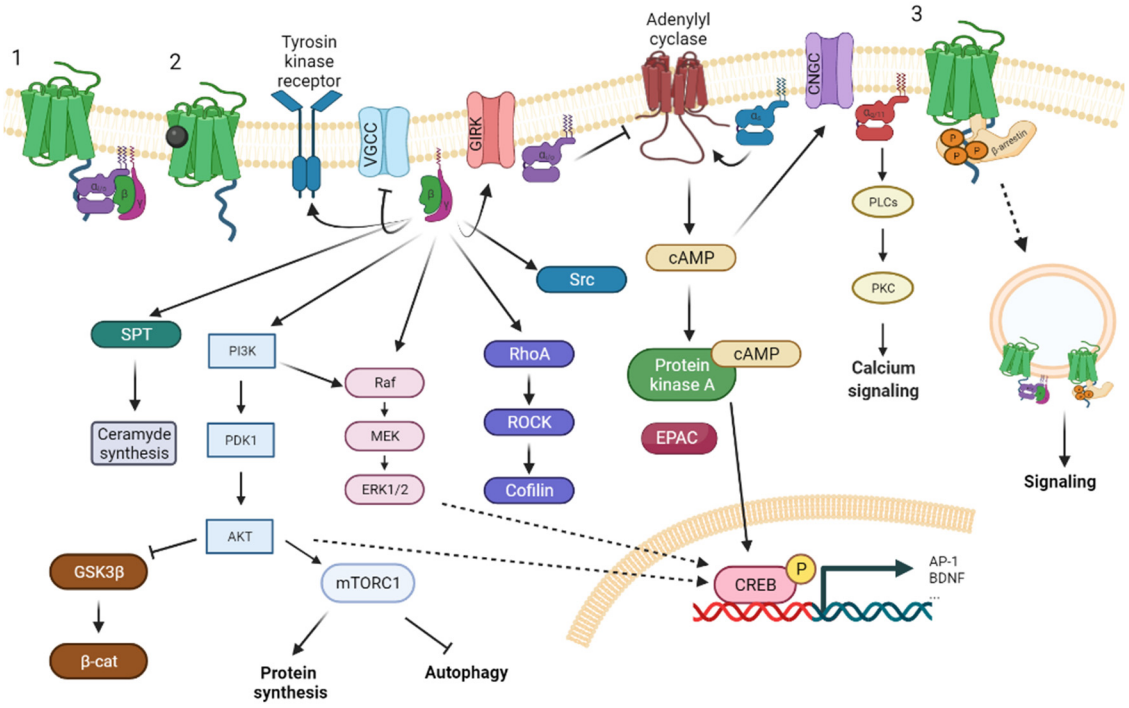

Figure I8. CB_1R-associated signaling pathways. CB_1R classically engages inhibitory G-proteins (1) that dissociate after agonist binding (2) and trigger several pathways, including PI3K-Akt-mTORC1, ERK or small G-proteins such as RhoA. Under different settings, CB_1R couples to $G\alpha_{q/11}$ or $G\alpha_s$ proteins and evokes Ca^{2+}- or cAMP-mediated pathways. Soon after activation, CB_1R is phosphorylated and β-arrestin desensitize G-proteins, causing internalization but also extending signaling events from endosomes (3). Image was created with BioRender®. VGCC: Voltage-gated calcium channel. GIRK: G-protein-coupled inwardly-rectifying potassium channel. CNGC: Cyclic nucleotide-gated channel.

1.5.2 CB_1R and synaptic transmission

CB_1R can be found across the mouse brain at the presynapse of almost every neuron subtype of the major neurotransmitter systems (glutamate, GABA, serotonin, noradrenaline, acetylcholine and dopamine) with varying degrees of expression, where it participates in the control of synaptic plasticity (Lutz *et al*, 2015).

Endocannabinoids act as retrograde regulators of neuronal activity. They constitute a feedback mechanism, whereby postsynaptic depolarization induces endocannabinoid production, that, in turn, diffuses to the adjacent cell and reduces presynaptic neurotransmitter release (Piomelli, 2003). Depending on the neurochemical identity of the presynaptic component, these mechanisms are termed **depolarization-induced suppression of inhibition (DSI) or excitation (DSE)** (Wilson & Nicoll, 2002), and constitute a form of short-term plasticity that represents the basis of CB_1R physiological function in the CNS and the neuroprotective effects against excitotoxicity (Araque *et al*, 2017). In addition, CB_1R can suppress neurotransmitter release in a long-lasting manner. This pathway has been extensively studied in the hippocampus, were endocannabinoids (mainly, 2-AG) acting on interneurons cause **long-term depression (I-LTD)**, a disinhibition that favors induction of **long-term potentiation (LTP)** at the Schaffer collateral-CA1 circuit (Chevaleyre & Castillo, 2003). This phenomenon is known as **metaplasticity** and is important for associative learning (Xu *et al*, 2014). Cannabinoids also generate LTD in excitatory neurons (E-LTD) (Gerdeman *et al*, 2002; Robbe *et al*, 2002). Recent reports also unveil a neuron-autonomous role for CB_1R in the induction of LTP in the dentate gyrus (Wang *et al*, 2016).

The control that CB_1R exerts on neurotransmitter release is believed to rely on different signaling pathways for short-term and long-term forms of plasticity. DSE and DSI are achieved through the inhibition of presynaptic calcium influx *via* changes in the conductance of voltage-gated calcium channels, likely mediated by the G-protein βγ dimer, whereas the mechanisms that underlie long-lasting plasticity events are poorly understood. LTD has been ascribed to PKA inactivation, presynaptic proteins like Rab3A/RIM1α, modulation of calcium channels and, lately, downstream effectors that could involve changes in protein synthesis and turnover, and synaptic ultrastructure (Castillo *et al*, 2012; Roland *et al*, 2014; Njoo *et al*, 2015; Monday *et al*, 2020). To date, there is not data on the molecular mechanisms behind the neuron-autonomous, cannabinoid-induced, LTP.

Lastly, it is worth mentioning that the ECS is present in astrocytes, where it also participates in synaptic plasticity. In particular, astrocytic CB_1R can trigger the release of glutamate through a calcium-dependent mechanism and modify distant neurons, a process termed lateral potentiation, which adds another layer of complexity to the role of endocannabinoids in neurotransmission (Navarrete & Araque, 2008).

1.5.3 CB_1R function in the brain

The human brain is unarguably the most complex biological system in nature. Classically, molecular components of this system, such as channels, receptors and neurotransmitters have been studied from a 'static' point of view. For instance, in the case of CB_1R, we tend to believe that behavioral outcomes, induced by ligand binding, can be ascribed to the activation of intracellular pathways, such as those described in the previous paragraphs, in specific cells. This paradigm has slowly changed and in the past years the general notion has become that receptors, like CB_1R, have few intrinsic properties but their effects largely emerge from specific contextual constraints (cell type, cellular state, interacting proteins

and so on) (Busquets-Garcia *et al*, 2018). A large body of evidence supports this hypothesis. For example, brain regions with relatively low expression of CB_1R, such as the hypothalamus, display remarkably high receptor activity when compared with other regions enriched in CB_1R (Breivogel *et al*, 1997); telencephalic glutamatergic neurons, which account for ~10% of total CB_1R expression in the hippocampus, are much more efficacious in activating G-proteins than forebrain GABAergic cells, which account for the remainder ~90% of total CB_1R (Steindel *et al*, 2013); coincidental activation of CB_1R and other GPCRs can alter or even block CB_1R function (Glass & Felder, 1997; Bagher *et al*, 2016; Moreno *et al*, 2018); specific interacting proteins can enhance receptor function (Guggenhuber *et al*, 2016); dosage and type of ligand influence functional outcomes (Priestley *et al*, 2017); and, finally, the cellular and subcellular distribution of CB_1R also impact receptor function (Navarrete & Araque, 2008; Bénard *et al*, 2012; Hebert-Chatelain *et al*, 2016; Maroso *et al*, 2016; Robin *et al*, 2018; Jimenez-Blasco *et al*, 2020).

Rising from this complexity, CB_1R emerges as a critical regulator of a plethora of behavioral functions. Classically, acute activation of CB_1R in animal models causes the so-called 'cannabinoid tetrad', which includes antinociceptive, cataleptic, hypokinetic and hypothermic outcomes, but also expands to many other behavioral aspects, such as anxiety-like responses, memory performance or feeding conduct, among several others (Martin, 1986; Busquets-Garcia *et al*, 2015). Selective genetic deletion of CB_1R from neuronal cell subpopulations has been the key tool to link regional contributions from specific brain areas to such a variety of behavioral effects. The first-ever report using a conditional knock-out mouse showed that CB_1R-containing dorsal telencephalic glutamatergic neurons protect against kainic acid-induced seizures (Marsicano *et al*, 2003). By injecting THC in conditional knock-out mouse models devoid of CB_1R in either dorsal telencephalic glutamatergic neurons, forebrain GABAergic interneurons, principal brain neurons or neurons expressing the dopamine 1 receptor (D_1R), it has been shown that 'cannabinoid tetrad' effects mostly require CB_1R molecules selectively expressed in principal neurons of the brain that reside in the cortex and striatum (Monory *et al*, 2007). This notion has been recently corroborated by using conditionally-rescued mice from a CB_1R-null background and complex virally-induced recombination approaches. Furthermore, authors delineated hypothermic and locomotor effects to dorsal telencephalic glutamatergic neurons, while cataleptic and analgesic effects are fulfilled by CB_1R located on medium spiny neurons of the striatum that project to the *substantia nigra* (De Giacomo *et al*, 2020; Soria-Gomez *et al*, 2021). Interestingly, one of these studies also unveiled an unknown role of GABAergic CB_1R for the induction of locomotion that seems occluded in wild-type mice (De Giacomo *et al*, 2020).

The role of CB_1R on memory has also been studied using mouse models. CB_1R-induced short-term amnesia is frequent after cannabinoids intake, appearing not only in the cannabis user but also in animal models (Lundqvist, 2005; Marsicano & Lafenêtre, 2009). By combining pharmacological and genetic inactivation approaches, long-term CB_1R-induced memory loss has been ascribed to CB_1R-containing hippocampal GABAergic interneurons and the ability of the receptor to activate the mTORC1 pathway (Puighermanal *et al*, 2009). Other pieces of evidence indicate that CB_1R present in hippocampal astrocytes or D_1R-expressing neurons is also necessary for CB_1R-induced memory impairment (Han *et al*, 2012; Oliveira da Cruz *et al*, 2020), which highlights the difference between necessity and sufficiency that underlie these types of approaches. In contrast, extinction of aversive memories after traumatic events might constitute a therapeutic option to exploit CB_1R short-term amnesia. This is supported by several evidence. For instance, i) CB_1R is expressed in the hippocampal-amygdala circuitry (Marsicano & Lutz, 1999) ii) mouse models lacking CB_1R do not extinguish aversive memories (Marsicano et al, 2002), and iii)

mice with a point mutation in FAAH that increases AEA levels, which in turn, enhances CB_1R tone, show accelerated fear-extinction (Dincheva et al, 2015).

One interesting concept has emerged from studies analyzing the contribution of CB_1R to feeding behavior and anxiety induction. One of the clearest effects elicited by cannabis intake is the stimulation of appetite, which led to the approval of nabilone, a CB_1R agonist, for the treatment of cancer and AIDS-associated wasting syndrome, and of rimonabant, a CB_1R antagonist, for the treatment of obesity (later withdrawn due to adverse psychiatric side-effects). Nonetheless, treatment with a moderate to high dose of a CB_1R agonist causes hypophagia (Bellocchio *et al*, 2010). Shockingly, mice lacking CB_1R in forebrain GABAergic interneurons showed a hyperphagic phenotype, thus suggesting that CB_1R plays an anorectic role in these neurons. On the contrary, deletion of CB_1R from telencephalic glutamatergic neurons caused appetite loss, consistent with the classical orexigenic function of CB_1R. A similar biphasic profile was found for the role of CB_1R in anxiety. Low doses of a CB_1R agonist showed anxiolytic-like properties that were absent in mice devoid of CB_1R in telencephalic glutamatergic neurons, whereas a high agonist dose induced anxious-like behaviors only in mice that had CB_1R molecules in forebrain GABAergic interneurons, likely mediated by mTORC1 activation (Rey *et al*, 2012; Puighermanal *et al*, 2013).

Taken together, these data provide a fundamental basis for understanding where and how CB_1R modulates behavior. Nonetheless, important questions remain unsolved. How are cell-type differences in signaling achieved? Are these cell-type differences preserved or altered in pathology or across ageing? To which extent do cell-type intrinsic molecular factors (proteins) contribute to this emerging complexity? The pivotal idea of this thesis has been that intracellular proteins, with varying degrees of expression among cell types, contribute a great deal to selectively shape CB_1R function. Thus, identifying proteins that engage CB_1R and the functional consequences of this association could help to further expand our understanding of CB_1R biology, and pave the way for safer therapies aimed at targeting CB_1R.

1.6 CB_1R-associated proteins

Protein-protein interactions are crucial for signaling, trafficking and localization of GPCRs, and CB_1R is not an exception (Magalhaes *et al*, 2012; Oyagawa & Grimsey, 2021). Regarding GPCRs, interactions with cognate signaling G-proteins and β-arrestins are particularly well-characterized and thus subconsciously 'excluded' from the concept of GPCR-associated proteins, although they clearly represent binding partners. As mentioned in previous sections, CB_1R is one of the most promiscuous GPCR and can engage all members of the $G\alpha_{i/o}$ subfamily, but also $G\alpha_s$, $G\alpha_{q/11}$ and $G\alpha_{12/13}$ as well as β-arrestins-1 and -2 (Glass & Felder, 1997; Lauckner *et al*, 2005; Diez-Alarcia *et al*, 2016; Delgado-Peraza *et al*, 2016; Inoue *et al*, 2019). Besides G-proteins and arrestins, oligomerization with other GPCRs (hetero-oligomerization) and even between CB_1R molecules has received considerable attention. Homo-oligomers and hetero-oligomers with cannabinoid 2, dopamine 2 (D_2R), opioid, orexins, adenosine 2A ($A_{2A}R$), β2-adrenergic, serotonin 2a, angiotensin 1, somatostatin 5 and GPR55 receptors, among others, have been reported so far (Xu *et al*, 2005; Callén *et al*, 2012; Kearn *et al*, 2005; Rios *et al*, 2006; Jäntti *et al*, 2014; Moreno *et al*, 2018; Hudson *et al*, 2010; Rozenfeld *et al*, 2011; Viñals *et al*, 2015; Zou *et al*, 2017; Kargl *et al*, 2012). Nonetheless, only CB_1R-D_2R and CB_1R-$A_{2A}R$ heteromers have been properly characterized *in vivo*.

Only a few soluble proteins, apart from G-proteins and β-arrestins have been identified to date as CB_1R-associated proteins. Perhaps the most iconic members of this group are the **cannabinoid receptor interacting proteins 1a and 1b, (CRIP1a/b).** These two proteins are splicing isoforms of the same gene, and were identified as CB_1R-binding proteins using a yeast two-hybrid (Y2H) system with the carboxy-terminal domain of CB_1R as bait (Niehaus *et al*, 2007). CRIP1a is a 164 amino acid-long protein present in all vertebrates, while CRIP1b lacks the last 53 residues in favor of an 18-amino acid insertion and is only expressed in primates. Several reports indicate that CRIP1a influences CB_1R constitutive activity and internalization *in vitro*, likely *via* steric competition with β-arrestins and G-proteins (Niehaus *et al*, 2007; Blume *et al*, 2015, 2017). Nonetheless, studies in mouse brain are inconsistent, since CRIP1a overexpression facilitated CB_1R function in the hippocampus (Guggenhuber *et al*, 2016). CRIP1b is less studied, but it could function as a dominant negative modulator of CRIP1a activity, since initial reports did not find any effect on CB_1R action (Niehaus *et al*, 2007). **Src homology 3-domain growth factor receptor-bound 2-like (endophilin) interacting protein 1 (SGIP1)** is another proposed CB_1R binding partner. Similarly to CRIP1s, it was identified in a Y2H experiment, and experiments with heterologous cells suggest that it reduces internalization and ERK activation, although β-arrestin 2 binding was still preserved (Hájková *et al*, 2016). A follow-up study found enhanced anti-nociceptive and hypothermic effects of THC in SGIP1 knock-out mice, as well as a delayed tolerance development to catalepsy (Dvorakova *et al*, 2021). Intriguingly, a mouse model with two point-mutations in CB_1R that impair β-arrestin-2 recruitment show a similar phenotype (Morgan *et al*, 2014), so one could speculate that SGIP1 facilitates β-arrestin 2 engagement and CB_1R desensitization without internalization, but this was not addressed in the study. **GPCR-associated sorting protein 1 (GASP1)** is another binding partner of CB_1R that was identified almost 15 years ago in a study that focused on the internalization dynamics of the receptor (Martini *et al*, 2007). GASP1 interacts with a series of GPCRs, likely including CB_2R (Bornert *et al*, 2013), to favor post-endocytic sorting to lysosomes in coordination with Beclin 2 (Whistler *et al*, 2002; He *et al*, 2013). Despite GASP1 knock-out mice display altered tolerance development to a CB_1R agonist (Martini *et al*, 2010), this protein resembles a general mechanism for GPCRs, rather than a selective CB_1R interactor. In line with this finding, another protein in charge of cargo delivery throughout the endocytic pathway, **Adaptor protein 3 (AP-3)**, has also been found associated with CB_1R. Like GASP1, AP-3 serves as a pro-degradative factor for CB_1R, in a mechanism that could be common to other GPCRs (Rozenfeld & Devi, 2008).

The first-ever murine CB_1R-associated proteome was published recently (Njoo *et al*, 2015). Among potentially interacting proteins, the authors focused on members of **the Wiskott-Aldrich syndrome protein family verprolin homologous protein 1 (WAVE1) complex**. This complex consists of WAVE1, Abelson-interacting protein 1/2 (ABI1/2), NCK-associated protein 1 (NCKAP1, also known as NAP1), cytoplasmic FMR1-interacting protein 2 (CYFIP2, also known as PIR121 or SRA1) and HSPC300, four of which (WAVE1, ABI2, NCKAP1 and CYFIP2) were consistently immunoprecipitated with CB_1R. By using several approaches, this study elegantly demonstrated for the first time a molecular pathway that links CB_1R and an associated protein with actin nucleation in neurons, both *in vitro* and *in vivo*. This same group has also published cell-type-specific CB_1R-associated proteomes by using virally-induced overexpression with selective promoters, but unfortunately not even a single candidate interactor had been validated so far by the time this thesis started (Mattheus *et al*, 2016).

Finally, there are some anecdotical reports suggesting additional CB_1R interactors. These include **Factor associated with Neutral sphingomyelinase (FAN),** a protein associated

with CB_1R in astrocytes, presumably through its *C*-terminal domain, that could facilitate sphingomyelin hydrolysis (Sánchez *et al*, 2001); **Vang-like protein 2 (VANGL2),** a transmembrane protein essential for trophoblast migration and proper placentation that associates with CB_1R *via* direct transmembrane segments interaction (Kim *et al*, 2021b); and the calcium-regulated proteins **Calneuron-1 and neuronal calcium sensor-1 (NCS-1),** two proteins that interact with both the CTD and the ICL3 of CB_1R and might bias receptor signaling from $G\alpha_{i/o}$ to $G\alpha_s$ depending on intracellular calcium concentrations. Intriguingly, we have also found another calcium-regulated protein that may associate with CB_1R, the **growth-cone associated protein of 43 KDa, GAP43** (Maroto *et al,* manuscript in preparation).

To summarize, proteins associated with CB_1R, namely **the receptor interactome**, only encompass a few binding partners, not studied in detail, especially their physiological role in animal models albeit counted exceptions (Oyagawa & Grimsey, 2021). Data is scarce also from the structural point of view as in many cases interacting regions have not been carefully mapped down (Fig. I9). Given that molecular mechanisms that underlie receptor function have been understudied, particularly context-dependent factors, we sought to identify and characterize CB_1R-associated proteins that contribute to fine-tune receptor action in a spatiotemporally restricted manner, in order to further expand our knowledge on how CB_1R transduces extracellular signals into biological responses.

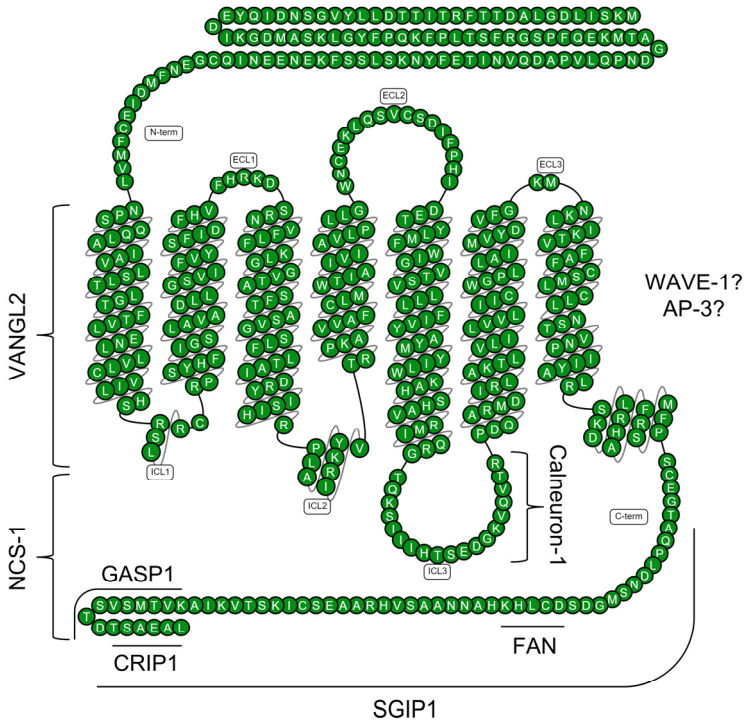

Figure I9. CB_1R and its associated proteins. Data on regions of CB_1R that interact with intracellular proteins are scarce. VANGL2 binds CB_1R through direct transmembrane contacts. NCS1 could engage both the ICL3 and the CTD of the receptor, whereas Calneuron-1 seems to associate exclusively with ICL3. FAN and CRIP1a could bind two 5-amino acid motifs in the mid and final portions of the CTD, respectively, while GASP1 may recognize the last 14 amino acids of the receptor. Structural determinants for WAVE-1 and AP-3 coupling are currently unknown. GPCR scheme was created using https://gpcrdb.org.

INTRODUCTION

AIMS

MATERIALS AND METHODS

RESULTS

DISCUSSION

CONCLUSIONS

REFERENCES

Aims

CB_1R participates in the control of many functions within the CNS. Activation of CB_1R triggers a myriad of signaling pathways, and this process is highly dependent on environmental factors such as the characteristics of the cell type that expresses the receptor, the physiopathological state of the tissue or organism, and the cannabinoid ligand used. Here, we propose that CB_1R-interacting proteins are molecular factors that contribute to shape CB_1R function in a cell-type/population selective manner. So far, very few CB_1R-interacting proteins have been identified, and most reports have not exceeded a mere biochemical characterization of the interaction. Thus, a physiopathological role for these putative CB_1R-interacting proteins has not been addressed yet.

Based on this background, the core aim of this Doctoral Thesis is the identification and characterization of new proteins that bind CB_1R and contribute to specifically fine-tuning receptor action. To achieve it, we initially conducted two high-throughput experiments that rendered two candidate proteins, namely the molecular chaperone BiP/GRP78, and the E3-ubiquitin ligase substrate recognition component Cereblon/CRBN. Upon this starting point, we defined two specific aims:

- Aim 1: Validation and characterization, *in vitro* and *in vivo*, of the interaction between BiP and CB_1R, and assessment of its physiological significance.
- Aim 2: Validation and characterization, *in vitro* and *in vivo*, of the interaction between CRBN and CB_1R, and assessment of its physiological significance.

INTRODUCTION

AIMS

MATERIALS AND METHODS

RESULTS

DISCUSSION

CONCLUSIONS

REFERENCES

Materials and Methods

Reagents

Suppliers of most reagents are indicated in the corresponding Materials and Methods subsection. Buffers, chemicals, oligonucleotides, and common laboratory reagents were obtained from Fisher Scientific if not otherwise indicated.

Plasmids

Several genetic constructs summarized in the tables MM1, MM2 and MM3 were employed in this thesis. Promoters, origins of replication and other genetic elements were adequate to the diverse experimental aims and organisms employed.

Unless otherwise indicated, plasmids were built by using standard molecular biology techniques, generally consisting of PCR amplification with specific oligonucleotides bearing overhangs containing selected restriction sites. PCR products were then inserted in designated vectors by restriction cloning. Point mutants were generated by using a *Quickchange* mutagenesis protocol (Braman *et al*, 1996) optimized in-home. Epitope-tagged vectors were obtained following an *in vivo* assembly approach (García-Nafría *et al*, 2016). Short amino-acid stretches were straight-up cloned in appropriately excised vectors using long annealing oligonucleotides with protruding overhangs.

Small-scale plasmid preparations for cloning procedures were performed by using the NucleoSpin Plasmid Purification kit (Macherey-Nagel, Bethlehem, PA, United States, #740588.50) according to the instructions indicated by the supplier. Likewise, transfection-grade plasmid isolations were achieved by using the Nucleobond Xtra Midi Plasmid Purification Kit (Macherey-Nagel, #740410.50) following the manufacturer's protocol. All plasmid constructs were verified by Sanger sequencing before use.

PLASMID NAME	VECTOR SOURCE	APPLICATION
pKLSLt	Donated by Dr. Jose María Mancheño	Recombinant expression in Escherichia coli
pKLSLt-hCB$_1$R-CTD (amino acids 408 to 472)	This thesis	Recombinant expression in Escherichia coli
pBH4-hCB$_1$R-CTD (amino acids 400 to 472)	This thesis	Recombinant expression in Escherichia coli
pBH4-hCRBN	This thesis	Recombinant expression in Escherichia coli
pBH4-rBiP	This thesis	Recombinant expression in Escherichia coli
pBH4-hBiP-IR (amino acids 497 to 654)	This thesis	Recombinant expression in Escherichia coli

Table MM1. Plasmids used for recombinant protein expression. h: *Homo sapiens* gene, r: *Rattus norvegicus* gene.

PLASMID NAME	VECTOR SOURCE	APPLICATION
pGBT9-hCB1R-CTD (amino acids 408 to 472)	This thesis	Yeast two-hybrid
pGBT9-hCB1R-CTD (amino acids 408 to 449)	This thesis	Yeast two-hybrid
pGBT9-hCB1R-CTD (amino acids 449 to 472)	This thesis	Yeast two-hybrid
pGBT9-hCB1R-CTD-S410D (amino acids 408 to 472)	This thesis	Yeast two-hybrid
pGBT9-hCB1R-CTD-S414D (amino acids 408 to 472)	This thesis	Yeast two-hybrid
pGBT9-hCB1R-CTD-T418D (amino acids 408 to 472)	This thesis	Yeast two-hybrid
pGBT9-hCB1R-CTD-S425D (amino acids 408 to 472)	This thesis	Yeast two-hybrid
pGBT9-hCB1R-CTD-S429D (amino acids 408 to 472)	This thesis	Yeast two-hybrid
pGBT9-hCB1R-CTD-S441D (amino acids 408 to 472)	This thesis	Yeast two-hybrid
pGBT9-hCB1R-CTD-S448D (amino acids 408 to 472)	This thesis	Yeast two-hybrid
pGBT9-hCB1R-CTD-S452D (amino acids 408 to 472)	This thesis	Yeast two-hybrid
pGBT9-hCB1R-CTD-T453D (amino acids 408 to 472)	This thesis	Yeast two-hybrid
pGBT9-hCB1R-CTD-T460D (amino acids 408 to 472)	This thesis	Yeast two-hybrid
pGBT9-hCB1R-CTD-S462D (amino acids 408 to 472)	This thesis	Yeast two-hybrid
pGBT9-hCB1R-CTD-S464D (amino acids 408 to 472)	This thesis	Yeast two-hybrid
pGBT9-hCB1R-CTD-T465D (amino acids 408 to 472)	This thesis	Yeast two-hybrid
pGBT9-hCB1R-CTD-T467D (amino acids 408 to 472)	This thesis	Yeast two-hybrid
pGBT9-hCB1R-CTD-S468D (amino acids 408 to 472)	This thesis	Yeast two-hybrid
pGBT9-hCB2R-CTD (amino acids 307 to 360)	This thesis	Yeast two-hybrid
pACT2-hBiP-IR (amino acids 497 to 654)	This thesis	Yeast two-hybrid

Table MM2. Plasmids used for yeast two-hybrid experiments. h: *Homo sapiens* gene.

PLASMID NAME	VECTOR SOURCE	APPLICATION
pEGFP-N1-3 & pEGFP-C1-3	ClonTech (discontinued)	Mammalian cell expression
pEGFP-C2-hCB1R-CTD (amino acids 400-472)	This thesis	Mammalian cell expression
pEGFP-C2-hCB1R-CTD (amino acids 400-449)	This thesis	Mammalian cell expression
pEGFP-C2-hCB1R-CTD (amino acids 449-472)	This thesis	Mammalian cell expression
pEGFP-C2-hCB1R-CTD (amino acids 449-460)	This thesis	Mammalian cell expression
pEGFP-C2-hCB1R-CTD (amino acids 461-472)	This thesis	Mammalian cell expression
pEGFP-C2-hCB1R-CTD-S452D (amino acids 400-472)	This thesis	Mammalian cell expression
pEGFP-N1-mCB1R	Provided by Dr. Luigi Bellocchio	Mammalian cell expression
pEGFP-C2-hCRIP1a	This thesis	Mammalian cell expression
pcDNA3.1-hCRIP1a	This thesis	Mammalian cell expression
pAM-HA-rCB1R	Provided by Dr. Luigi Bellocchio	Mammalian cell expression
pcDNA3.1(+)	Thermo Scientific (#V79020)	Mammalian cell expression
pcDNA3.1-hCB1R-myc	Provided by Dr. Luigi Bellocchio	Mammalian cell expression
pcDNA3.1-3xFLAG-rBiP	This thesis	Mammalian cell expression
pcDNA3.1-3xFLAG-hBiP-IR (amino acids 497 to 654)	This thesis	Mammalian cell expression
pcDNA3.1-3xFLAG-rBiP-ΔIR (amino acids 1 to 308)	This thesis	Mammalian cell expression
pcDNA3.1-hA1R	Provided by Dr. Estefanía Moreno	Mammalian cell expression
pRluc-N1-hCB1R	Provided by Dr. Estefanía Moreno	Mammalian cell expression
pRluc-N1-hCB1R-S452D	This thesis	Mammalian cell expression
pEGFP-C2-hBiP-IR (amino acids 497 to 654)	This thesis	Mammalian cell expression
pCEFL-GFP	Donated by Dr. J. Silvio Gutkind	Mammalian cell expression
pCEFL-GFP-RGS	Donated by Dr. J. Silvio Gutkind	Mammalian cell expression
pCEFL-GFP-GRK2	Donated by Dr. J. Silvio Gutkind	Mammalian cell expression
pcDNA3.1-3xHA-CB_1R[LgBiT]	Provided by Dr. Peter J. McCormick	Mammalian cell expression
pcDNA3.1-[SmBiT]-ARRB2	Provided by Dr. Peter J. McCormick	Mammalian cell expression
pcDNA3.1-3xHA-hCRBN	This thesis	Mammalian cell expression
pcDNA3.1-3xHA-hCRBN-ΔRGS (lacking amino acids 117 to 258)	This thesis	Mammalian cell expression
pcDNA3.1-3xHA-hCRBN-N (Q120STOP)	This thesis	Mammalian cell expression
pcDNA3.1-3xHA-hCRBN-258 (K258STOP)	This thesis	Mammalian cell expression
pcDNA3.1-3xHA-hCRBN-317 (K317STOP)	This thesis	Mammalian cell expression
pcDNA3.1-3xHA-hCRBN-377 (E377STOP)	This thesis	Mammalian cell expression
pcDNA3.1-3xHA-hCRBN-C (amino acids 80 to 442)	This thesis	Mammalian cell expression
pcDNA3.1-3xFLAG-hCB1R	This thesis	Mammalian cell expression
pcDNA3.1-3xFLAG-hCRBN	This thesis	Mammalian cell expression
pcDNA3.1-3xFLAG-hCRBN-ΔRGS (lacking amino acids 117 to 258)	This thesis	Mammalian cell expression
pEGFP-C2-hCRBN	This thesis	Mammalian cell expression
pRP-V5-hCUL4A	Acquired to VectorBuilder	Mammalian cell expression
pRP-myc-hDDB1	Acquired to VectorBuilder	Mammalian cell expression

Table MM3. Plasmids used for experiments in mammalian cells. h: *Homo sapiens* gene, r: R*attus norvegicus gene*, m: *Mus musculus* gene.

Yeast two-hybrid (Y2H)

The yeast two-hybrid assay is based on the selective transcription of a reporter gene upon the binding of its specific transcription factor (Fields & Song, 1989). This assay can be conducted in several strains of the yeast *Saccharomyces cerevisiae.* Generally, by means of molecular biology methods, the GAL4 transcription factor is split in its activation domain (AD) and DNA-binding domain (BD), and these motifs are in turn fused to different genes or parts of genes. The principle of the technique is the reconstitution of a given protein, being the transcription factor GAL4 the most popular one, if the polypeptides encoded by the fused genes interact. Finally, this reconstitution allows the transcription of selection and reporter proteins (Fig. MM1).

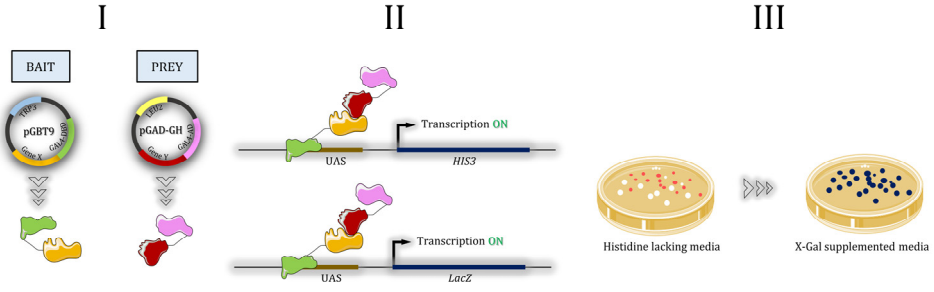

Figure MM1. The yeast two-hybrid system. Yeast are transformed with pGBT9 and pGAD-GH plasmids, that encode GAL4-BD/AD fusion proteins **(I)**. If proteins of interest interact, *HIS3* and *LacZ* genes are transcribed **(II)**. Finally, LacZ expression and activity can be detected by addition of the chromogenic compound X-Gal **(III)**.

Low-throughput experiments were carried out in the *Saccharomyces cerevisiae* strain Y190 [American Type Culture Collection (ATCC), Manassas, VA, US, #96400] (Flick & Johnston, 1990) which has several genetic manipulations (Table MM4). These mutations render an organism with lysine, tryptophan, leucine, histidine, adenine, and uracil auxotrophies. The

histidine auxotrophy can be reverted by the reconstitution of the GAL4 transcription factor, that leads to the expression of imidazoleglycerol-phosphate dehydratase, which is absent in the histidine-auxotrophic host strain Y190.

MUTATION	DESCRIPTION
MATa	Mating type a locus.
Leu2-3, 112	Frameshift mutation in the LEU2 gene, which encodes for beta-isopropylmalate dehydrogenase; that catalyzes the third step in the leucine biosynthesis pathway.
Ura3-52	Insertion of the ty transposable element within the coding region of the URA3 gene, which encodes for Orotidine-5'-phosphate decarboxylase; that catalyzes the sixth enzymatic step in the *de novo* biosynthesis of pyrimidines.
Trp1-901	Deletion within the coding region of the TRP1 gene, which encodes for phosphoribosylanthranilate isomerase; that catalyzes the third step in tryptophan biosynthesis.
His3Δ200	Deletion within the coding region of the HIS3 gene, which encodes for imidazoleglycerol-phosphate dehydratase; that catalyzes the sixth step in histidine biosynthesis.
Ade2101	G to T transversion at nucleotide 190, changing codon 64 from a Glu to a Stop, within the coding region of the ADE2 gene, which encodes for phosphoribosylaminoimidazole carboxylase; that catalyzes a step in the *de novo* purine nucleotide biosynthetic pathway.
Gal4Δ	Complete deletion of the GAL4 gene, which encodes for the DNA-binding transcription factor GAL4, required for activating GAL dependent genes.
Gal80Δ	Complete deletion of the GAL80 gene, which encodes the transcriptional regulator GAL80 involved in the repression of GAL dependent genes in the absence of galactose, via inhibition of GAL4.
Ura3Δ	Complete deletion of the URA3 gene, which encodes for Orotidine-5'-phosphate decarboxylase; that catalyzes the sixth enzymatic step in the *de novo* biosynthesis of pyrimidines.
GAL-LacZ	Insertion of the LacZ gene under the control of the GAL upstream activator sequences (UAS), which encodes for the β-galactosidase enzyme, that catalyzes the conversion of 5-bromo-4-chloro-3-indolyl-β-D-galactopyranoside (hereafter, X-Gal) to 5-bromo-4-chloro-3-hydroxyindole, which spontaneously dimerizes and oxidizes into 5,5'-dibromo-4,4'-dichloro-indigo, an intensely blue product.
LYS	Deletion of the LYS2 gene, which encodes for alpha aminoadipate reductase; that catalyzes the reduction of alpha-aminoadipate to alpha-aminoadipate 6-semialdehyde, which is the fifth step in the biosynthesis of lysine.
GAL-HIS3	Insertion of the HIS3 gene under the control of the GAL UAS.
cyhR	Resistant to cycloheximide

Table MM4. Genomic mutations of the *S. cerevisiae* strain Y190.

Assays were carried out by transforming yeast following a lithium acetate-based protocol previously set up in our laboratory (Merino-Gracia *et al*, 2016a), with different genetic constructs cloned in the plasmids pGAD-GH and pGBT9 (ClonTech, Mountain View, CA, US, products discontinued). The protocol is described in detail in the next paragraph. These plasmids can be used to produce chimeric proteins fused to the activation domain and the DNA-binding domain of the GAL4 transcription factor, respectively. Besides, they carry a copy of the *LEU2* (pGAD-GH vector) and the *TRP1* (pGBT9 vector) genes that rescue yeast growth when plated in media lacking leucine, and tryptophan, respectively.

To achieve transformation, one single colony of *S. cerevisiae* strain Y190 grown in a YPDA-agar plate [1% yeast extract (w/v), 2% peptone (w/v), 2% glucose (w/v), 0.03 mM adenine sulphate and 1.5% bacteriological agar (w/v)], was inoculated in 10-ml of YPDA [1% yeast extract (w/v), 2% peptone (w/v), 2% glucose (w/v), and 0.03 mM adenine sulphate] and grown for 16-18 hours at 30 °C with constant aeration rate (230 rpm). Once the optical density at 580nm (OD_{580}) of the culture reached values between 1.5 – 1.7 (arbitrary units), yeasts were diluted in 40 ml of YPDA and again cultivated at 30 °C with constant aeration rate (230 rpm). Cell growth was controlled again by measuring the OD_{580}, and when a value of 0.4 – 0.6 units (exponential growth phase) was achieved (typically, 2-2.5 hours), cells were collected by centrifugation (1,000x*g*, 10 minutes, room temperature) and the supernatant was discarded. Next, cells were washed with sterile, double-distilled H_2O to ensure all growth media was eliminated and the centrifugation was repeated. The cell pellet was then resuspended with 400 µl of resuspension solution [100 mM lithium acetate (Sigma-Aldrich, Saint Louis, MO, US #213195), 4 mg/ml salmon sperm ssDNA (Sigma-Aldrich, #31149) in water]. One hundred µl of the resultant suspension were added to sterile Eppendorf tubes containing 1 µg of each pGAD/pGBT9 pair (1:1 ratio). Then, 600 µl of transformation solution [33.4% (w/v) PEG-4000 (Merck, Kenilworth, NJ, US, #807490), 100 mM lithium acetate in water] were added to each tube, gently mixed, and incubated for 30 minutes at 30 °C. After the incubation, 70 µl of dimethyl sulfoxide (DMSO) were added to each transformation reaction, and a heat shock was conducted (incubation for 15 minutes at 42 °C followed by a 2-minutes submersion in an ice-water bath). Finally, yeasts were collected by centrifugation (1,000x*g*, 10 minutes at room temperature), supernatants were discarded, and pellets resuspended in 200 µl of sterile, double-distilled H_2O. Samples were

equally split and seeded in SDUAK [0.67% (w/v) yeast nitrogen base, 2% (w/v) glucose, 2.4% (w/v) bacteriological agar, 13.7 mM lysine, 0.18 mM uracyl and 0.18 mM adenine sulphate] plates supplemented either with 7.75 mM histidine (here after, HIS plates) or 10 mM 3-amino-1,2,4-triazole (hereafter, 3-AT plates). The compound 3-amino-1,2,4-triazole is a competitive inhibitor of the imidazoleglycerol-phosphate dehydratase (HIS3 gene product). Thus, cells that are able to grow in 3-AT plates display high enough levels of the enzyme (in this case, directly related to enzymatic activity) to counteract this inhibition, which is indicative of a specific and high-affinity protein-protein interaction that supports an elevated HIS3 transcription rate. Variations in 3-amino-1,2,4-triazole concentration allow the experimenter to raise or lower the experimental threshold for a given protein-protein interaction.

HIS and 3-AT plates were incubated at 30 °C until individual colonies appeared (typically 3-4 days). HIS plates were used as a transformation control, since they only lack amino acids whose biosynthesis is reestablished by the genes incorporated in the plasmids. In turn, 3-AT plates render colonies with positive interactions. Colonies from 3-AT plates were then transferred to histidine plates to favor growth rate and after an additional 3–4-day incubation, a circle of Whatman filter paper (Sigma-Aldrich #WHA1001090) was placed on top of the plate until colonies were adhered. This piece of paper was then used in the β-galactosidase activity assay. The white paper containing the yeast was submerged in liquid nitrogen to lyse cells, then placed on top of a new piece of filter paper previously wetted with 3 ml of buffer Z (100 mM NaH_2PO_4, 10 mM KCl, 10 mM $MgSO_4$ pH 7.0 in water) supplemented with 30 µl of X-Gal [100 mg/ml in dimethylformamide (Sigma-Aldrich #16555 and #807490)], 8 µl of 2-mercaptoethanol and protected from light. The generation of 5,5'-dibromo-4,4'-dichloro-indigo, which appears as a blue precipitate, was followed by visual observation every 15 minutes for at least 2 hours. Representative images were taken 24 hours after the start of the reaction.

A high throughput assay with a human ORF cDNA library (ClonTech, product discontinued) was also performed. The human ORF cDNA library was constructed in the pACT2 plasmid (equivalent to pGAD-GH but with an in-frame HA tag in the *C*-terminus of GAL4-AD) and pre-transformed in the *S. cerevisiae* strain Y187 (ATCC, #96399) (Wade Harper *et al*, 1993) which, similarly to Y190, displays multiple genetic alterations (Table MM5).

MUTATION	DESCRIPTION
MATalpha	Mating type alpha locus.
Leu2-3, 112	Frameshift mutation in the LEU2 gene, which encodes for beta-isopropylmalate dehydrogenase; that catalyzes the third step in the leucine biosynthesis pathway.
Ura3-52	Insertion of the ty transposable element within the coding region of the URA3 gene, which encodes for Orotidine-5'-phosphate decarboxylase; that catalyzes the sixth enzymatic step in the *de novo* biosynthesis of pyrimidines.
Trp1-901	Deletion within the coding region of the TRP1 gene, which encodes for phosphoribosylanthranilate isomerase; that catalyzes the third step in tryptophan biosynthesis.
His3Δ200	Deletion within the coding region of the HIS3 gene, which encodes for imidazoleglycerol-phosphate dehydratase; that catalyzes the sixth step in histidine biosynthesis.
Ade2101	G to T transversion at nucleotide 190, changing codon 64 from a Glu to a Stop, within the coding region of the ADE2 gene, which encodes for phosphoribosylaminoimidazole carboxylase; that catalyzes a step in the *de novo* purine nucleotide biosynthetic pathway.
Gal4Δ	Complete deletion of the GAL4 gene, which encodes for the DNA-binding transcription factor GAL4, required for activating GAL genes.
Gal80Δ	Complete deletion of the GAL80 gene, which encodes the transcriptional regulator GAL80 involved in the repression of GAL genes in the absence of galactose via inhibition of GAL4.
Ura3Δ	Complete deletion of the URA3 gene, which encodes for Orotidine-5'-phosphate decarboxylase; that catalyzes the sixth enzymatic step in the *de novo* biosynthesis of pyrimidines.
GAL-LacZ	Insertion of the LacZ gene under the control of the GAL upstream activating sequences, which encodes for the β-galactosidase enzyme, that catalyzes the conversion of X-gal to 5-bromo-4-chloro-3-hydroxyindole, which spontaneously dimerizes and oxidizes into 5,5'-dibromo-4,4'-dichloro-indigo, an intensely blue product.

Table MM5. Genomic mutations of the S. cerevisiae strain Y187.

In this case, we conducted a single transformation following the above depicted protocol with the plasmid pGBT9-hCB_1R-CTD (amino acids 408 to 472) in *S. cerevisiae* str. Y190. Transformants were selected in SDUAK plates additionally supplemented with 13.7 mM leucine. Once obtained, a single colony was grown in 50 ml of 2xYPDA along with one vial of the library for 24 hours at 30 °C with a constant aeration rate (230 rpm).

The use of two different haploid strains with opposing mating types, MATa (Y190) and MATalpha (Y187), allows the generation of diploid cells when co-cultured *via* sexual reproduction. These diploid cells are stable and harbor the genetic material of both progenitors. Hence, this is a fast method to perform large-scale transformations.

Yeasts were collected by centrifugation (1,000x*g*, 10 minutes, room temperature), resuspended in 10 ml of sterile, double-distilled water and selection of positive transformants was again conducted with HIS and 3-AT plates followed by the β-galactosidase activity assay as explained above. Plasmids from individual colonies able to rescue growth in 3-AT plates were isolated following standard procedures in yeast. Briefly, the colony of interest was resuspended in 50 µl of double-distilled H_2O containing 50 IU of lyticase (Sigma-Aldrich, #04963). The reaction was incubated for 1 hour at 37 °C. Next, SDS was added to a final concentration of 3% (w/v) and the sample was subjected to a freeze-thaw cycle. Then, double-distilled H_2O was added to a final volume of 200 µl, and a mixture of phenol-chloroform-isopropanol (25:24:1) was added in a 1:1 volume ratio. A centrifugation step (10,000x*g*, 10 minutes, room temperature) allowed us to eliminate protein and membrane components. The aqueous, DNA-containing, fraction was isolated and 8 µl of 10M ammonium acetate and 500 µl of pure ethanol were added to precipitate the nucleic acid. The resultant pellet after a new centrifugation step (10,000x*g*, 10 minutes, room temperature) contained the purified DNA, which was resuspended in 20 µl of double-distilled H_2O. DNA purity was checked with conventional spectroscopy. Finally, this DNA was used as template for a standard PCR reaction with specific pACT2 oligonucleotides (see Table MM6) and the subsequent PCR product was purified using the GeneJET PCR Purification Kit (Thermo Scientific, Waltham, MA, US #K0701) following manufacturer's instructions and analyzed with Sanger sequencing. Genes were identified using BLAST (NCBI, Bethesda, MD, US), the search being restricted to the human genome.

OLIGONUCLEOTIDE NAME	SEQUENCE (5'-3')
pACT2.seq.F	TAACGCGTTTGGAATCACTACAGGG
pACT2.seq.R	TGCACGATGCACAGTTGAAG

Table MM6. Sequencing primers for library screening.

Recombinant protein production and purification

Recombinant expression of proteins of interest was performed in *Escherichia coli* str. BL21 DE3 which expresses the T7 phage RNA polymerase. Bacteria were transformed with expression plasmids following a conventional heat shock protocol, which consisted in the addition of 1 µg of the desired DNA to a 50 µl aliquot of competent cells (~10^{13} cfu/ml, produced in-house), followed by a 30-minutes incubation in ice, a fast heating shock in a water bath (37 °C for 45 seconds), and a second incubation in 1 ml of Lysogeny-Broth (LB) media [1% tryptone (w/v), 0.5% yeast extract (w/v) and 1% NaCl (w/v), pH 7.0] for one hour at 37 °C with constant aeration rate (230 rpm), before plating a tenth of the transformation in an LB-agar plate [1% tryptone (w/v), 0.5% yeast extract (w/v), 1% NaCl (w/v) and 1.5% (w/v) bacteriological agar] with the appropriate antibody (Kanamycin: 50 µg/ml; Ampicillin: 100 µg/ml).

Recombinant protein production started with the inoculation of a single colony in a tube containing 10 ml of 2xYT media [1.6% (w/v) tryptone, 1% (w/v) yeast extract and 0.5% (w/v) NaCl, pH 7.0) and incubated in standard conditions (37 °C with constant aeration rate of 230 rpm). Six hours later, this tube was split in larger flasks containing 250 ml of 2xYT and grown in the same way. We produced 2 litters of culture on a day-to-day basis. Culture growth was monitored by the OD_{580nm} and when it reached a late exponential growth phase (0.8 – 1.0 units of optical density), 0.5 mM IPTG was added, and temperature was lowered

to 30 °C to prevent protein aggregation. One day after the induction with IPTG, bacteria were harvested through centrifugation (10,000x*g*, 10 minutes, room temperature) in a Sorvall RC-5B centrifuge with a F10S rotor (Thermo Scientific). Next, the pellet was resuspended with ice-cold lysis buffer (100 mM Tris-HCl, 100 mM NaCl, pH 7.0 supplemented with 1 µg/ml aprotinin, 1 µg/ml leupeptin, 200 µM PMSF, 5 µM 2-mercaptoethanol and 10 mM imidazole in the case of His_6-tagged proteins) and subjected to four cycles of 2-min sonication (40% amplitude) with a 1-minute break in-between on ice with continuous stirring. Undesired contaminants were eliminated through high-speed centrifugation (30,000x*g*, 30 minutes, 4 °C) in a Sorvall RC-5B centrifuge with a F21S rotor. Finally, the bacterial lysate was filtrated using a homemade paper funnel. Lysates were then loaded in chromatography columns with appropriate resins for affinity purification, as described (Merino-Gracia *et al*, 2016a, 2016b). In the case of Lectin-CB_1R-CTD (amino acids 408-472), the lysate was loaded in a Sepharose 4B resin, previously equilibrated with equilibration buffer (100 mM Tris-HCl pH 7.0, 25 mM NaCl). Next, the column was extensively washed (at least 20x times the volume of the column) with washing buffer (100 mM Tris-HCl pH 7.0, 200 mM NaCl). Retained proteins were eluted with 200 mM lactose dissolved in 100 mM Tris-HCl pH 7.0, which competes with Sepharose beads for the binding of the lectin, and 1-ml fractions were collected. Conversely, His_6-tagged constructs (pBH4 plasmids) were sequentially purified with a nickel-nitriloacetic acid affinity column. After extensive washing with washing buffer (50 mM Tris-HCl, pH 7.0, 100 mM NaCl, 25 mM imidazole), proteins were eluted with elution buffer (50 mM Tris-HCl, pH 7.0, 100 mM NaCl, 250 mM imidazole, supplemented with protease inhibitors). In both cases, the column flux was set at a constant value of 1 ml/min. Finally, protein quantity in each sample was estimated by measuring its absorbance at 280 nm, and protein purity was confirmed with SDS-PAGE and Coomassie Brilliant Blue or silver staining (see below). When needed, pure protein solutions were concentrated by centrifugation in Centricon® tubes (Millipore, Burlington, MA, US, product discontinued).

Affinity chromatography and liquid chromatography-mass spectrometry

A fresh sheep (*Ovis aries*) brain was purchased in a local market and homogenized in radioimmunoprecipitation assay (RIPA) buffer [0.1 (w/v) SDS, 0.5% (w/v) sodium deoxycholate, 1% (v/v) NP-40, 150 mM NaCl, 50 mM Tris-HCl pH 8.0 in phosphate-buffered saline] using a glass-Teflon grinder (IKA labortechnik, Satufen, Germany). The insoluble fraction was discarded by centrifugation and the homogenate was loaded in a Sepharose 4B column. The flow-through, containing soluble proteins that do not bind the resin unspecifically, was collected, and was again subjected to an affinity chromatography, in this case using a Sepharose 4B resin previously saturated with either Lectin or Lectin-CB_1R CTD (amino acids 408-472). After extensive wash out with RIPA buffer, retained proteins were eluted with 200 mM lactose and 1-ml fractions were collected. Protein content in each fraction was estimated using the absorbance coefficient at 280 nm. Samples with the highest protein concentration were subjected to SDS-PAGE (see below), but once the samples entered the separating part of the gel, electrophoresis was stopped, the gel was dismounted, stained with Coomassie Colloidal Blue (Sigma-Aldrich #LC6025) overnight, faded with double-distilled water and each lane was cut just above the band corresponding to the recombinant protein using a blade. Every lane was then cut into smaller pieces and subjected to in-gel trypsin digestion as described elsewhere (Cristobo *et al*, 2011). Peptides were retained in an Acclaim Pepmap 100 precolumn (Thermo Scientific, #164567) and eluted in an Acclaim PepMap 100 C18 (25-cm long, with an internal diameter of 75 µm and 3 µm particle size) (Thermo Scientific #164261). Peptides were separated for 110 minutes using a gradient consisting of 90 minutes in 0-35% Buffer B (0.1% formic acid in

acetonitrile), followed by 10 minutes in 45%-95% Buffer B, 9 minutes in 95% Buffer B and 1 minute in 10% Buffer B, with a flow rate of 250 nl/min on an Easy nLC 1000 (Thermo Fisher # LC120) coupled to an ion source with nanoelectrospray (Thermo Scientific).

Mass spectra were acquired in an LTQ-Orbitrap Velos working in positive mode. Whole scan spectra (m/z 400-2000) were obtained at a resolution of 60,000 – 500,000 (m/z = 200) and the 15 most intense ions in each scan were fragmented using collision-induced dissociation in the ionic trap (collision energy was normalized at 35%). Unique charged ions or with unassigned charges were discarded. A dynamic exclusion of 45 seconds was also applied.

Spectral data were challenged with Uniprot databases *Ovis aries* (23,112 sequences) and Mammalian (1,184,488 sequences), using the Sequest search engine built-in Proteome Discoverer v1.1.14 (Thermo Scientific). Carbamydomethylation, cysteine nitrosylation and methionine oxidation were included as dynamic modifications in the search engine. Precursor and product ions selection tolerance was set at a cut-off of 10 ppm and 0.5 Da, respectively. Peptide identification was validated using the Percolator algorithm with a false discovery rate of 1% ($q \leq 0.01$) (Käll *et al*, 2007).

Fluorescence polarization (FP)

Fluorescence polarization is a reliable approach to study molecular interactions in solution. Measuring binding and dissociation of a given pair of proteins is possible when one of them is labeled with a fluorophore and relatively small compared to the other partner (*e.g.,* a peptide). Upon excitation by polarized light, a fluorophore in solution emits light in all space directions due to a rapid molecular rotation, giving rise to a low fluorescence polarization. When a given molecular interaction occurs, this heavier molecular complex slows down rotation and the emitted light no longer remains depolarized. Therefore, it is possible to study molecular associations by monitoring changes in fluorescence polarization while applying increasing concentrations of the non-labeled component (Fig. MM2).

Recombinantly produced and purified His_6-tagged CB_1R-CTD (amino acids 400-472) was labeled with 5-(iodoacetamido)fluorescein (5-IAF, Sigma-Aldrich #I9271). The dye was dissolved in DMSO, and the labeling reaction was performed in sodium bicarbonate buffer, pH 9.0 with a three-fold molar excess of dye for 1 hour at 25 °C protected from light. Subsequently a 3.5 kDa cut-off dialysis membrane (Spectrum chemical MFG, New Brunswick, NJ, US, #888-11362-EA) was used to eliminate non-reacted 5-IAF compound. After extensive dialysis in the assay buffer (20 mM Hepes, 150 mM NaCl, pH 7.0), the concentration of the labeled peptide was calculated using the value 68,000 $cm^{-1}M^{-1}$ as the molar extinction coefficient of the dye at pH 8.0 at 494 nm. Saturation binding experiments were performed as described (Merino-Gracia *et al*, 2016a) with a constant concentration of 5-IAF-CB_1R-CTD of 100 nM. Briefly, a series of samples with increasing concentrations of purified interacting proteins [BiP, BiP-IR (amino acids 497-654) or CRBN, respectively] were prepared with assay buffer in a final volume of 0.5 ml. Fluorescence polarization was obtained in a PerkinElmer Life Sciences MPF 44-E spectrofluorometer. Polarization of the labeled peptides was measured at excitation/emission values of 488/530 nm (bandwidth, 10 nm). The fluorescence polarization values obtained were fitted to the equation:

$$FP = \frac{FPmax \cdot [IP]}{Kd + [IP]}$$

where *FP* is the measured fluorescence polarization, *FPmax* is the maximal fluorescence polarization value, *[IP]* is the added concentration of interacting protein and K_d is the dissociation constant as determined with GraphPad Prism v8.0.1 (GraphPad Software, San

Diego, CA, US). In all cases, the fluorescence in the absence of added protein was established as blank. K_d can be directly derived from this saturation curve as far as the concentration of labeled peptide is well below the true K_d value during the assay (Bach *et al*, 2015).

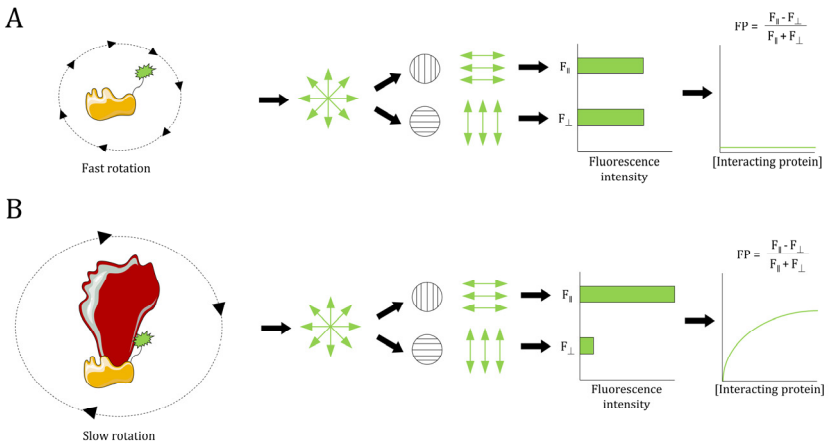

Figure MM2. Fluorescence polarization-based protein-protein interaction assays. ***A,*** Excitation of a freely, fast rotating fluorophore in solution, results in light emitted in all directions of space. ***B,*** Protein-protein interactions slow rotational speed, due to increased molecular weight, which increases polarized light emission after excitation.

Cell culture and transfection

The HEK-293T cell line was from the ATCC (#CRL-3216). HEK-293T cells stably expressing FLAG-CB_1R or FLAG-CB_2R (Kargl *et al*, 2012; Balenga *et al*, 2011) were kindly provided by Dr. Maria Waldhoer (InterAx Biotech, Villigen, Switzerland). Cells were maintained in growth media, which consisted of DMEM (Sigma-Aldrich #D5796) supplemented with 10% FBS (Gibco, #11573397), 1% penicillin/streptomycin (Lonza, Basel, Switzerland #BE17-603E), 1 mM Na-pyruvate (Lonza #BE13-115E) and 1 mM L-glutamine (Gibco #11500626). They were periodically tested for potential mycoplasma contamination by taking an aliquot for PCR with specific oligonucleotides. To ensure stable expression of FLAG-CB_1R/FLAG-CB_2R, 0.22 mg/ml Zeocin (Thermo Fisher Scientific #R25001) was included as a selection marker.

In transfection experiments, cells were plated in transfection media (DMEM supplemented with 10% FBS, 1 mM Na-pyruvate, 1 mM L-glutamine without antibiotics), grown for one day, and then transfection was conducted with polyethyleneimine linear MW25,000 (Polysciences inc. Warrington, PA, US #23966) in a 4:1 mass ratio to DNA according to the manufacturer's instructions. Double transfections were performed with equal amounts of both plasmids unless otherwise indicated. Generally, 5 µg in total were used per 10-cm plate, and this amount was scaled up or down accordingly to surface area when using different growth plates. In all cases, cells were harvested 48 hours post-transfection for further procedures. Co-transfection of CRBN or control siRNAs (Ito *et al*, 2010) and plasmids was conducted by using the Lipofectamine 2000® reagent (Invitrogen #1668019), 10 µg of DNA and 40 nM final siRNA concentration, in a 10-cm plate.

Proximity ligation assay (PLA)

Duolink® Proximity Ligation Assay is an effective tool to detect protein-protein interactions *in situ* (Söderberg *et al*, 2006; Fredriksson *et al*, 2002). A target protein pair can be readily localized in proximity in unaltered cells or tissues using this approach (Fig. MM3). Typically, two primary antibodies are used to detect target proteins, followed by incubation with

oligonucleotide-labeled species-specific secondary antibodies. Only if both proteins are close enough (<40 nm), tails of linked oligonucleotides will hybridize, creating a template for rolling circle amplification. After amplification and polymerization steps, the addition of selective fluorescent probes allows detection of complexes by using standard fluorescence confocal microscopy.

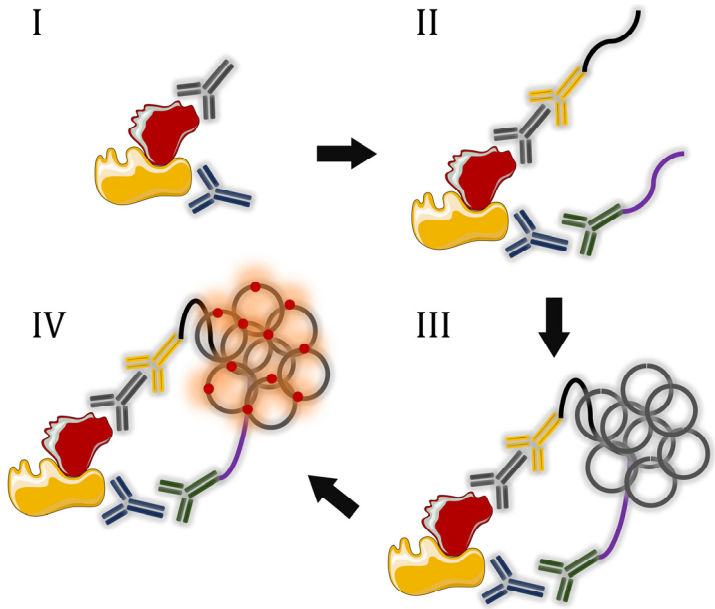

Figure MM3. Proximity ligation assays. Proteins of interest are recognized by primary antibodies **(I)**. Primary antibodies, in turn, are detected with DNA-labeled secondary antibodies **(II)**. If both proteins are close in space, DNA tails hybridize and are replicated by a rolling circle mechanism **(III)**. Finally, these replication events can be detected using fluorescent dyes **(IV)**.

BiP-CB_1R, and CRBN-CB_1R complexes, as well as appropriate negative controls, not described herein for the sake of simplicity, were detected using the Duolink® In Situ PLA detection kit (Sigma-Aldrich #DUO92101) and the In Situ Detection Reagent Red (Sigma-Aldrich #DUO92008). In experiments using the HEK-293T cell line, cells were seeded on poly-L-lysine coated coverslips (200 cells/mm^2), fixed for 15 minutes with 4% PFA and washed three times with PBS. Next, cells were permeabilized by incubation with PBS supplemented with 20 mM Glycine and 0.05% (w/v) Triton X-100 for 5 minutes at room temperature in a rocking platform. After a quick wash with PBS, crystals were blocked with 4 drops of Duolink® blocking solution for 1 hour at 37 °C. Then, coverslips were incubated with primary antibodies [anti-GFP antibody (1:200; Thermo Fisher Scientific, #MA5-15256) and a rabbit anti-CB_1R antibody (1:200 Frontier-Institute, Ishikari, Hokkaido, Japan #CB1-Rb-Af530)] overnight in a wet chamber (a 15-cm plate lined with aluminum foil and containing a wet piece of paper surrounding its border). The day after, samples were washed three times with Duolink® PLA-A buffer (10 minutes each) and incubated with secondary antibodies diluted 1:5 in antibody diluent (both reagents were provided by the supplier) again for 1 hour at 37 °C in a wet chamber. After a new washing step (3 times with Duolink® PLA-A buffer for 10 minutes), ligation was conducted by adding 1x Duolink® ligation buffer (5-fold dilution in double-distilled H_2O) along with 1x Duolink® ligase (40-fold dilution in double-distilled H_2O) and incubating for 1 hour at 37 °C in a wet chamber. Cells were washed twice with Duolink® PLA-A buffer (5 minutes each) and polymerization was performed by adding 1x Duolink® polymerization buffer (5-fold dilution in double-distilled H_2O) along with 1x Duolink® ligase (40-fold dilution in double-distilled H_2O) and incubating for 100 minutes at 37 °C in a wet chamber. Finally, before mounting with Mowiol® mounting media, coverslips were washed with Duolink® PLA-B buffer two times (10 minutes each), being DAPI added on the second wash, and once with Duolink® PLA-B buffer diluted 100-fold.

Synaptosomal preparations were incubated with the same rabbit-anti-CB_1R antibody and a mouse anti-BiP antibody (1:100; Santa Cruz Biotechnology; Dallas, TX, US, #sc-376768, product discontinued). Negative controls were performed with just one primary antibody. Handling of the samples was essentially the same as those stated in the previous paragraph.

For in vivo PLA imaging, mice were deeply anesthetized with a mixture of ketamine/xylazine (87.5 mg/kg and 12.5 mg/kg, of each drug, respectively) and immediately perfused intracardially with PBS followed by 4% paraformaldehyde. After perfusion, brains were removed and post-fixed overnight in the same solution, cryoprotected by immersion in 10, 20, 30% gradient sucrose (24 hours for each sucrose gradient) at 4 °C, and then frozen in dry ice-cooled methylbutane. Serial coronal or sagittal cryostat sections (30 µm) through the whole brain were collected in cryoprotective solution and stored at -20 °C until PLA were performed. Immediately before the assay, mouse brain sections were mounted on glass slides, washed in PBS, permeabilized with PBS containing 0.01% Triton X-100 for 10 minutes, and successively washed with PBS. Interactions were detected as well with Duolink in situ PLA detection and In Situ Detection Reagent Red Kits following the previous guidelines. A mixture of the primary antibodies [mouse anti-GRP78 antibody (1:100; Santa Cruz Biotechnology, #sc-376768, product discontinued) and rabbit anti-CB_1R antibody (1:100; Thermo Scientific, #PA1-745)] was used.

In all cases, samples were analyzed in a Leica SP2 confocal microscope (Leica Microsystems) equipped with an apochromatic 63X oil-immersion objective (1.4 numerical aperture), and a 405 nm and a 561 nm laser lines. In brain slices, for each field of view a stack of two channels (one per staining) and 9 to 13 Z-stacks with a step size of 1 µm were acquired. Images were opened and processed with ImageJ software (National Institutes of Health, Bethesda, MD, US). Quantification of cells containing one or more red dots versus total cells (blue nuclei) was determined by using the Fiji package (https://imagej.net/software/fiji/). The total number of red dots versus total cells (blue nuclei) was determined. Nuclei and red dots were counted on the maximum projections of each image stack. After getting the projection, each channel was processed individually. The blue nuclei and red dots were segmented by filtering with a median filter, subtracting the background, enhancing the contrast with the Contrast Limited Adaptive Histogram Equalization (CLAHE) plug-in, and finally applying a threshold to obtain the binary image and the regions of interest (ROIs). Representative images were prepared with ImageJ software by applying bright and contrast adjustments uniformly.

Protein electrophoresis (SDS-PAGE) and Western blotting (WB)

Bacterial cell lysates and purified recombinant proteins were prepared in 5x Laemmli Sample Buffer [5% (w/v) SDS, 50% (v/v) glycerol, 0.1% Bromophenol Blue (w/v), 250 mM Tris-HCl, pH 6.8, and 5% (v/v) β-mercaptoethanol added before use] and boiled for 5 minutes at 95 °C. Polyacrylamide gels of different concentrations (ranging from 7.5% to 12%) were prepared using Bio-Rad FastCast® solutions (Bio-Rad, Hercules, CA, US #1610181, #1610183, #1610185). Gels were then mounted in the Mini-PROTEAN Tetra Cell System (Bio-Rad, #1658000FC), Tris-Glycine-SDS buffer was added (25 mM Tris-HCl, 192 mM Glycine, 0.1% SDS, pH 8.6) and samples were loaded in each well. Unstained molecular weight markers (Fisher Scientific #11802124) were included. Electrophoresis was conducted at a constant voltage of 90 volts and run stopped when the tracking dye (bromophenol blue), reached the edge of the gel. Next, gels were dismounted, and submerged in a Coomassie Brilliant Blue staining solution (0.25 g of Coomassie Brilliant Blue R-250 in 90 ml of 50% methanol in H_2O and 10 ml of glacial acetic acid) for 15 minutes

in a rocking platform. Then, the staining solution was recovered, gels were briefly washed with tap water and incubated with fading solution [50% (v/v) H_2O, 40% (v/v) methanol, 10% (v/v) acetic acid]. For silver staining, gels were transferred to a petri dish and fixed with fixing solution [50% (v/v) methanol, 12% (v/v) acetic acid, 0.005% (v/v) formaldehyde] for 1 hour at room temperature. Afterwards, gels were washed three times with 50% (v/v) methanol (20 minutes each), incubated with a 0.8 mM sodium thiosulfate solution for 1 minute and washed again three times with double-distilled H_2O (20 minutes each). Then, a silver containing solution was added [11.7 mM $AgNO_3$, 0.03% (v/v) formaldehyde in double-distilled H_2O] for 20 minutes, and three new washes with double-distilled H_2O were conducted. Finally, protein bands were exposed with developing solution [570 mM Na_2CO_3, 0.016 mM $Na_2S_2O_3$, 0.0185% (v/v) formaldehyde in double-distilled H_2O] and made visible after several washes with double-distilled H_2O. At this step, the reaction was stopped by addition of fixing solution without formaldehyde.

Samples for Western blotting were prepared on ice-cold lysis buffer [50 mM, Tris pH 7.5, 1 mM EDTA, 1 mM EGTA, 0.1% (v/v) Triton X-100, 50 mM NaF, 10 mM Na-glycerophosphate, 5 mM Na-pyrophosphate, 1 mM Na-orthovanadate]. Cell lysates were clarified by centrifugation at 12,000x*g* for 15 minutes (4 °C) and total protein content was quantified using the Bradford assay in a 96-well plate with a Rayto RT-6100 microplate reader, using delipidized bovine serum album prepared in lysis buffer as standard. Then, 5-20 µg aliquots of total protein, boiled for 5 minutes at 95 °C (or not boiled, in the case of vGAT and vGLUT1 detection) and prepared in 5x Laemmli Sample Buffer, were resolved by using SDS-PAGE and transferred to PVDF membranes (Bio-Rad #1620177) using Bio-Rad Trans-Blot Turbo transfer system (Bio-Rad #1704150). Membranes were blocked with 5% non-fat milk (w/v) or 5% BSA (w/v) in TBS-Tween-20 [(0.1% (v/v)] for 1 hour and incubated overnight with appropriate antibodies. All antibodies were prepared in TBS-Tween-20 [(0.1% (v/v)] with 5% BSA (w/v). A full list of the antibodies used and their dilutions is provided in Table MM7. In the case of brain structures, the tissue was lysed using RIPA buffer (for synaptic markers detection) or DDM buffer [140 mM NaCl, 2 mM EDTA, 0.5% (w/v) n-dodecyl-β-D-maltoside, 25 mM Tris pH 7.4) (for CB_1R detection) following essentially the same steps.

Membranes were then washed three times with TBS-Tween-20 [(0.1% (v/v)], and HRP-labeled secondary antibodies, selected according to the species of origin of the primary antibodies (Sigma-Aldrich #NA-931-1 & #NA-934V; Invitrogen #A18769), were added for 1 hour at a 1:5,000 dilution in TBS-Tween-20 (0.1%) at room temperature in a rocking platform. Finally, protein bands were detected by incubation with an enhanced chemiluminescence reagent (Bio-Rad, #170561) and exposure to X-ray films in a dark room. Densitometric analysis of the relative expression of the protein of interest versus the corresponding loading control was performed with ImageJ software. Western Blotting images were cropped for clarity. Electrophoretic migration of molecular weight markers is depicted on the left-hand side of each blot.

ANTIBODY	SUPPLIER	DILUTION FACTOR
α-α-Tubulin	Sigma-Aldrich #T9026	1:1,0000
α-β-Actin	Sigma-Aldrich #A5441	1:1,0000
α-BiP	Sigma-Aldrich #G8918	1:1,000
α-BiP	BD Pharmingen #610978	1:1,000
α-c-myc	Roche #11 667 149 001	1:1,000
α-Calnexin	Santa Cruz Biotechnology #sc-6465	1:1,000
α-CB_1R	Frontier Institute, #CB1-GP-Af530	1:2,000
α-CREB	Cell Signaling Technology #9197	1:1,000
α-CRBN	Cell Signaling Technology #71810	1:1,000
α-FLAG M2	Sigma-Aldrich #F3165	1:1,000
α-GAPDH	Cell Signaling Technology #2118S	1:3,000
α-GFP	Thermo Scientific #MA5-15256	1:1,000
α-HA tag	Cell Signaling Technology #3724S	1:1,000
α-HSP90	Santa Cruz Biotechnology #sc-69703	1:3,000
α-p44/42 (ERK1/2)	Cell Signaling Technology #4696	1:1,000
α-p70S6K	Cell Signaling Technology #9202	1:1,000
α-PSD-95	Abcam #ab2723	1:1,000
α-p-CREB (S133)	Cell Signaling Technology #9198	1:1,000
α-p-p44/42 (p-ERK1/2) (T202/Y204)	Cell Signaling Technology #9101	1:1,000
α-p-p70S6K (T389)	Cell Signaling Technology #9206	1:1,000
α-synaptophysin 1	Synaptic systems #101 002	1:1,000
α-Ubiquitin (P4D1)	Santa Cruz Biotechnology #sc-8017	1:1,000
α-V5	Invitrogen #R960-25	1:5,000
α-vGAT	Synaptic systems #131 003	1:1,000
α-vGLUT1	Synaptic systems #135 303	1:1,000

Table MM7. Antibodies source and dilutions.

Co-immunoprecipitation (Co-IP)

For co-immunoprecipitation experiments, 48 hours after transfection, live cells were lysed on ice-cold GST buffer [10% (v/v) glycerol, 100 mM NaCl, 2 mM $MgCl_2$, 1% (v/v) NP-40, 50 mM Tris-HCl, pH 7.4) supplemented with protease inhibitors. Cell lysates were clarified by centrifugation at 12,000x*g* for 15 minutes at 4 °C, and total protein content was quantified using the Bradford assay in a 96-well plate with a Rayto RT-6100 microplate reader, using delipidized bovine serum album prepared in GST buffer as standard. Twenty-µg aliquots were collected to check for transfection levels (herein referred to as whole-cell lysates, WCL), and 1 mg of total protein was incubated with 20 µl of HA-agarose beads (Fisher Scientific #26182) or FLAG M2 agarose beads (Sigma-Aldrich #A2220) for 2-4 hours at 4 °C with a final protein concentration of 1 mg/mL. Next, beads were sedimented by centrifugation (2,000x*g*, 1 minute, 4 °C), resuspended with 1 ml of lysis buffer and sedimented again for three times. Finally, immunoprecipitated proteins were eluted with 30 µl of 2x Laemmli Sample Buffer without β-mercaptoethanol and heated 10 minutes at 55 °C, which is more suitable to detect CB_1R (Esteban *et al*, 2020). Finally, beads were separated and discarded by centrifugation at full speed, and ten µl of the elution were further analyzed by Western blotting as previously described. GFP immunoprecipitation was performed analogously, with a pre-clarification step on 30 µl of Protein A/G mixture (GE Healthcare, Chicago, IL, US #17061801), followed by overnight incubation of the remaining supernatant with 1 µg of a polyclonal anti-GFP antibody (produced in-home), and 2-4 hours of incubation with 30 µl of Protein A/G mixture. The rest of the steps were the same as those mentioned above, with the exception that samples were heated at 95 °C.

For ubiquitination experiments, immunoprecipitations were conducted in a similar set-up, but cell lysis was performed with RIPA buffer supplemented with protease inhibitors, 2-chloroacetamide (inhibitor of ubiquitination and deubiquitination) and DNAse I (Roche Life Science #4716728001, 2 IU/ml) for 30 minutes. The rest of the steps were essentially identical, with the sole exception that washing steps were done as well with RIPA buffer.

CB_1R-induced activation of ERK

Twenty-four hours after transfection with desired plasmids (CB_1R-GFP together with BiP-IR, CRBN or CRBN-ΔRGS), HEK-293T cells were trypsinized, resuspended in growth media and seeded in a six-well plate at a density of 80,000 cells/cm^2. Later that day, medium was changed for serum-free growth media (DMEM supplemented with 1% penicillin-streptomycin, 1 mM Na-pyruvate, 1 mM L-glutamine) and cells were starved for 16 hours. Finally WIN55,212-2 (0.01-1 μM final concentration) (Sigma-Aldrich #W102) or vehicle [DMSO, 0.1% (v/v) final concentration] was added for indicated time points (0-15 minutes). $G\alpha_{q/11}$ inhibition was evaluated by adding YM-254890 (Focus Biomolecules, LLC, Plymouth Meeting, PA, US #10-1590-0100) (1 μM final concentration) or vehicle [(DMSO, 0.1% (v/v)] 30 minutes before Vehicle/WIN55,212-2 treatment. Alternatively, a control plasmid (pCEFL-GFP) or a dominant-negative construct (pCEFL-GFP-GRK2) were co-transfected in a 1:1 mass ratio with CB_1R-GFP. In all cases, after incubation, cells were washed with ice-cold PBS, snap-frozen in liquid nitrogen and stored at -80 °C for further analysis. Samples were then subjected to Western Blotting as described, and levels of p-ERK (T202/Y204), p-CREB (S133) and p-p70S6K (T389) were compared to total ERK, CREB and p70S6K levels, respectively.

Bioluminiscence resonance energy transfer (BRET)

Bioluminiscence resonance energy transfer (BRET) is a reliable tool to study protein-protein interactions in living cells (Xu *et al*, 1999). BRET takes advantage of the *Förster* resonance energy transfer phenomenon (FRET), which is a mechanism of energy transfer between fluorochromophores that are very close in space (<10 nm) and is named after the use of bioluminescence. Despite being an ever-evolving technology, the general scheme remains essentially constant. Typically, putative interacting proteins are engineered to behave as donor and acceptor by fusing them to Renilla luciferase (Rluc) and GFP, respectively. Upon addition of coelenterazine, Rluc oxidizes it into coelenteramide, a reaction that releases light at 395nm, which serves to excite GFP. Excitation of GFP in turn emits a green light at 510nm (Fig. MM4). In the present work, we have undertaken BRET2, which displays better spectral resolution (around 115 nm) and higher signal-to-noise ratio than previous BRET approaches (*i.e.*, BRET1) at the cost of lower light emission and shorter fluorescence lifetime, and uses Biotium Coelenterazine 400a as substrate (DeepBlueC).

HEK-293T cells growing in six-well plates were transiently co-transfected with a constant amount of cDNA encoding the receptor fused to Rluc protein and with increasingly amounts of GFP-tagged interacting protein. To quantify protein-GFP expression, cells (20 μg protein) were distributed in 96-well microplates (black plates with a transparent bottom) (Thermo Scientific #165305) and the fluorescence was read in a FLUOstar Optima fluorimeter (BMG Labtech, Offenburg, Germany) equipped with a high-energy xenon flash lamp using a 10-nm bandwidth excitation filter at 410 nm for protein-GFP reading. Protein-fluorescence expression was determined as fluorescence of the sample minus the fluorescence of cells expressing only the BRET donor. For BRET measurements, cells (20 μg of protein) were distributed in 96-well white microplates (Sigma-Aldrich #CLS3600) and BRET signal was collected 1 minute after addition of 5 μM of DeepBlueC (Molecular Probes, Eugene, OR, US, #NC0621021) using a Mithras LB 940 reader (Berthold Technologies, Bad Wildbad, Germany), that allows the integration of the signals detected in the short-wavelength (λshort) filter at 400 nm and the long-wavelength (λlong) filter at 510 nm. To quantify receptor-Rluc expression luminescence readings were also performed after 10 minutes of adding 5 μM of DeepBlueC. The net BRET is defined as:

$$BRET = \left(\frac{\lambda long}{\lambda short}\right) - Cf$$

where Cf corresponds to $\frac{\lambda long}{\lambda short}$ for the Rluc construct expressed alone in the same experiment. BRET is expressed as milli BRET units (mBU; net BRET x 1,000). In BRET curves BRET was expressed as a function of the ratio between fluorescence and luminescence (GFP/Rluc). To calculate maximum BRET (BRETmax) and BRET50 from saturation curves, data was fitted using a non-linear regression equation and assuming a single phase with GraphPad Prism software v8.0.1.

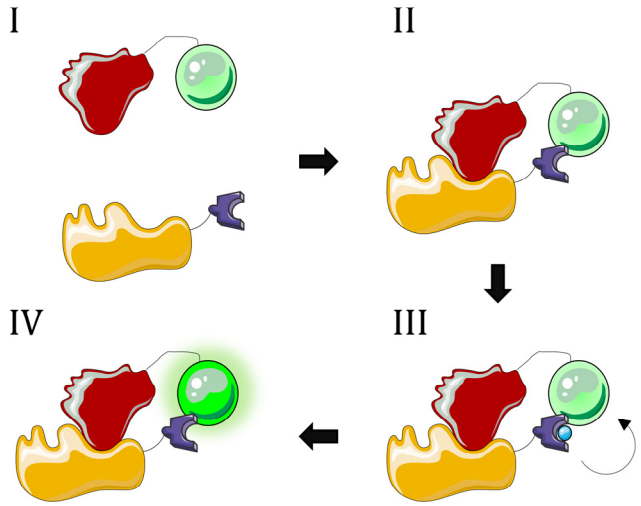

Figure MM4. The Bioluminiscence resonance energy transfer approach (BRET). Proteins of interest are tagged with GFP (green circle) and luciferase (violet c-like form) **(I)**. Interaction occurs, bringing GFP and luciferase in close proximity **(II)**. Addition of the luciferase substrate, and luciferase-mediated oxidation releases light at 395 nm, that excites GFP. **(III)**. Finally, green fluorescence is detected **(IV)**.

Dynamic mass redistribution (DMR)

The dynamic mass redistribution (DMR) technique takes its name from cellular processes that emanate when molecules change its localization within the cell (*e.g.,* cytoskeletal rearrangement, receptors internalization, protein trafficking and adhesion changes, to quote but a few) (Schröder *et al*, 2011). Label-free technology capitalizes on these changes by applying polarized broadband light in the bottom portion of cells seeded in microtiter plates with embedded grating surfaces. This grating interacts with the cells and forms an optical system that can reflect a specific outgoing wavelength (measured in picometers) originating from light penetrating the close part of the cell (~150 nm into the cell, defined as sensing volume). This light resonance is dependent on the mass density within this sensing volume part of the cell. Thus, alterations in this inner cell density, that can be achieved, for example, by pharmacological manipulations of given GPCRs, can shift the outgoing wavelength, allowing a system to quantify receptor signaling non-invasively (Fig. MM5) (Grundmann *et al*, 2018; Moreno *et al*, 2018).

The cell signaling signature was determined using an EnSpire® Multimode Plate Reader (PerkinElmer, Waltham, MA, US). Twenty-four hours before the assay, transfected cells were seeded at a density of 10,000 cells per well in 384-well sensor microplate with 30 µl growth medium and cultured for 24 hours to obtain 70-80% confluent monolayers. Before the assay, cells were washed twice with assay buffer (HBSS with 20 mM Hepes, pH 7.15) and incubated for 2 hours in 30 µl per well of assay-buffer with 0.1% DMSO in the reader at 24°C. Hereafter, the sensor plate was scanned, and a baseline optical signature was recorded before adding 10 µl of test compound dissolved in assay buffer containing 0.1% DMSO. When used, specific protein kinase or G-proteins inhibitors were added 30 minutes before CB_1R activation. These included U0216 (MEK1 inhibitor, Tocris, Bristol, UK, #1144, 5 µM

final concentration), LY294002 (PI3K inhibitor, Tocris, #1130, 5 µM final concentration), and YM-254890 ($G\alpha_{q/11}$ inhibitor, 1 µM final concentration). Then, DMR responses were monitored for at least 5,000 s. Kinetic results were analyzed using EnSpire Workstation software v4.10 (PerkinElmer). Each depicted representative curve is the mean of three technical replicates.

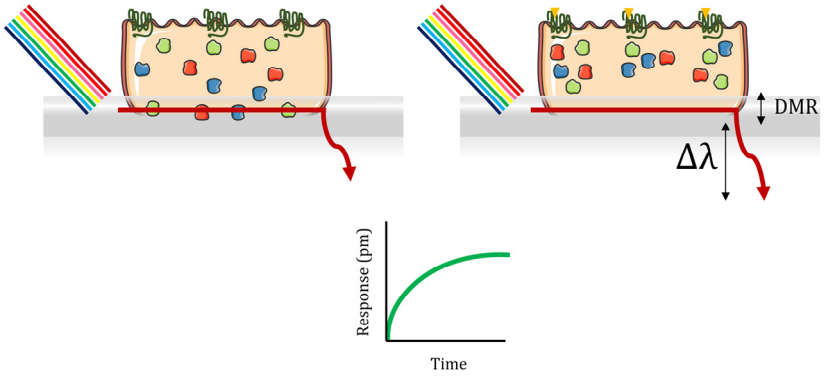

Figure MM5. Dynamic mass redistribution assays (DMR). Cells are plated in specific grating surfaces. The activation of a given GPCR, can cause intracellular changes that modify the reflection of light (measured in picometers), providing a quantifiable signal to the experimenter.

Determination of cAMP concentration

Homogeneous time-resolved fluorescence energy transfer (HTRF) assays were performed using the Lance Ultra cAMP kit (PerkinElmer #TRF0262). This approach combines a classical sandwich ELISA, with two antibodies recognizing an analyte of interest, with FRET technology, by coupling antibodies to donor and acceptor fluorophores. If both antibodies recognize the molecule, the donor will emit fluorescence upon excitation and the energy will be transferred to the nearby acceptor, giving specific acceptor fluorescence. The more analyte there is, the more fluorescence there will be.

HEK-293T-FLAG-CB_1R cells (1,000 per well), growing in medium containing 50 µM zardeverine, were incubated for 15 minutes in white ProxiPlate 384-well microplates (PerkinElmer) at 25°C with vehicle, WIN55,212-2 or CP-55,940 (concentrations ranging from 0.025 to 1 µM) before adding vehicle or forskolin (0.5 µM final concentration) and incubating for 15 additional minutes. Fluorescence at 665 nm was analyzed on a PHERAstar Flagship microplate reader equipped with an HTRF optical module (BMG Lab technologies, Offenburg, Germany).

Phospho-protein array

Phosphorylation status of major cellular kinases after activation of CB_1R was analyzed using the Proteome Profiler Human Phospho-Kinase Array Kit (R&D, Bio-techne, Minneapolis, MN, US, #ARY003C). Cells transfected with CB_1R-GFP, and BiP-IR (or control) plasmids were treated with WIN55,212-2 (100 nM) or vehicle (DMSO, 0.1% v/v) as described above for 5 and 15 minutes. Samples from two independent experiments were processed separately by using 350 µg of total protein per experimental condition and following the instructions from the supplier. Multiple exposition times were obtained in X-Ray films. Densitometric analysis of the relative phosphorylation levels versus the corresponding housekeeping controls and between WIN55,212-2/vehicle treatments was performed with ImageJ software and the Protein Array Analyzer toolset. Phospho-protein status of effectors in selected pathways were validated in the same samples using conventional western blotting as indicated above.

Cellular and hippocampal membrane preparations

Membrane preparations were performed as described elsewhere (Diez-Alarcia *et al*, 2016). Cell pellets (approximately 500 mg from transfected HEK-293T cell lines), or mouse hippocampal samples (approximately 200 mg) from 6 mice each time were gently thawed on ice and lysed using a glass-teflon grinder in cold homogenization buffer (50 mM Tris-HCl, 1 mM EGTA, 3 mM $MgCl_2$, 1 mM DTT, 250 mM sucrose, pH 7.4). Samples were then centrifuged (1,100x*g*, 10 minutes, 4 °C) and nuclei-containing pellets discarded. Membrane enrichment was performed by re-centrifugation (40,000x*g*, 10 minutes, 4 °C) of the supernatants, and the resultant pellet was solubilized in cold centrifugation buffer (50 mM Tris-HCl, 1 mM EGTA, 3 mM $MgCl_2$, 1 mM DTT, pH 7.4) with the aid of a glass stick. Finally, a second centrifugation step was performed (40,000x*g*, 10 minutes, 4 °C), pellets were resuspended in 5 volumes of cold centrifugation buffer and protein content was determined using the Bradford assay. Aliquots of 0.5, 1 and 2 mg were collected (21,000x*g*, 15 minutes, 4 °C), supernatants were discarded, and samples were stored at -80 °C until assayed.

Antibody-capture [^{35}S]GTPγS scintillation proximity assay

CB_1R-mediated activation of different subtypes of protein subunits ($G\alpha_{i1}$, $G\alpha_{i2}$, $G\alpha_{i3}$, $G\alpha_o$, $G\alpha_{q/11}$, $G\alpha_s$, $G\alpha_z$, and $G\alpha_{12/13}$) was addressed using a homogeneous protocol of [^{35}S]GTPγS scintillation proximity assay (Diez-Alarcia *et al*, 2016) coupled to the use of the following antibodies: mouse monoclonal anti-$G\alpha_{i1}$ (1:20 dilution, Santa Cruz Biotechnology, #sc-56536), rabbit polyclonal anti-$G\alpha_{i2}$ (1:20 dilution, Santa Cruz Biotechnology, #sc-7276), rabbit polyclonal anti-$G\alpha_{i3}$ (1:30 dilution, Antibodies on-line, Aachen, Germany, #ABIN6258933), mouse monoclonal anti-$G\alpha_o$ (1:40 dilution, Santa Cruz Biotechnology, #sc-393874), mouse monoclonal anti-$G\alpha_{q/11}$ (1:20 dilution, Santa Cruz Biotechnology, #sc-515689), rabbit polyclonal anti-$G\alpha_s$ (1:20 dilution, Santa Cruz Biotechnology, #sc-383), rabbit polyclonal anti-$G\alpha_z$ (1:20 dilution, Santa Cruz Biotechnology, #sc-388), and rabbit polyclonal anti-$G\alpha_{12/13}$ (1:20 dilution, Santa Cruz Biotechnology, #sc-28588).

Ten μg of protein per well were pipetted in 96-well isoplates (PerkinElmer #6005040) in a final volume of 200 μl of assay buffer (1 mM EGTA, 3 mM $MgCl_2$, 100 mM NaCl, 0.2 mM DTT, 50 mM Tris–HCl pH 7.4, 0.4 nM [^{35}S]GTPγS, GDP 50-100 μM) and incubated for 2 hours at 30 °C. Next, 20 μl of Igepal and SDS was added to each well [1% (v/v) and 0.1% (v/v) in water, respectively), and plates were incubated at room-temperature for 30 minutes with gentle agitation before adding specific antibodies directed against Gα subunits. Ninety minutes after adding the antibodies, polyvinyltoluene SPA beads coated with protein A (PerkinElmer) were added (0.75 mg of beads per well), and plates were incubated for 3 hours at room temperature with gentle agitation. After a final centrifugation (1,000x*g*, 5 minutes at RT), retained radioactivity was detected in a MicroBeta TriLux scintillation counter (PerkinElmer). Different experimental conditions were treated with a single submaximal dose of WIN55,212-2 (10 μM), either alone or in the presence of the CB_1R antagonist O-2050 (10 μM) (Tocris, #1655) as control. Nonspecific binding was defined as the remaining radioactivity count in the presence of 10 μM unlabeled GTPγS. Values were transformed to percentages of the corresponding control (vehicle-treated). Each experimental data point was subjected to a one sample *t*-test against a theoretical mean of 100% of activation and a significant difference was considered when the *p*-value was ≤ 0.05. Comparisons across different experimental conditions were performed using an unpaired Student's *t*-test. Again, a significant difference was considered when the *p*-value was ≤ 0.05.

Receptor internalization measurements

Receptor internalization was quantified by performing a live-cell immunofluorescence towards an *N*-terminal antigen of CB_1R, which only tags receptors in the plasma membrane, followed by a conventional immunofluorescence against a *C*-terminal antigen, which labels all receptors within the cell, and subsequently performing a ratio between both signals (Zhuang & Matsunami, 2008). Briefly, HEK-293T-FLAG-CB_1R cells were seeded on cover glasses and transfected with GFP, or GFP-BiP-IR. Two days after transfection, cells were treated with WIN-55,212-2 (100 nM final concentration) or vehicle [DMSO, 0.1% (v/v) final concentration] for 10 or 40 minutes as described in previous sections, after which agonist was washed out with ice-cold PBS. Cover glasses were then transferred to a new 150 mm dish cell-side up, placed on ice, and incubated with mouse anti-FLAG M2 antibody (Sigma-Aldrich #F3165) diluted 1:1,000 in a staining solution (Minimum Essential Media with 10 mM HEPES and 15 mM NaN_3) for 30-60 minutes. At the end of the incubation, cover glasses were washed 3 times using Hank's Balanced Salt Solution (HBSS) with 10 mM HEPES and 15 mM NaN_3. Then, an Alexa-647-labeled antibody raised in mouse (Invitrogen #A21244) was added (1:1,000 in staining solution). Thirty minutes later, cover glasses were washed again three times. Finally, the washing solution was replaced with 4% PFA for 15 minutes to fix the cells. A subsequent immunostaining step was performed. Cells were permeabilized with PBS containing 0.25% (v/v) Triton X-100 and 5-10% (v/v) goat serum for 1 hour and a standard immunofluorescence (see the paragraph below) with a rabbit anti-CB_1R primary antibody (1:500 dilution, Frontier-Institute) and an Alexa-546-labeled secondary antibody (1:1,000 dilution, Invitrogen #A11010) was performed. Samples were then analyzed with a Leica SP2 confocal microscope (Leica Microsystems), and receptor internalization ratio was calculated as the ratio between FLAG immunoreactivity (surface CB_1R) and CB_1R immunoreactivity (total CB_1R).

The subcellular localization of the receptor was evaluated by conventional double immunofluorescence, using the anti-FLAG M2 antibody in combination with anti-EEA1 antibody (1:100, Cell Signaling Technology, Danvers, MA, US #2411) for early endosomes or anti-LAMP1 antibody (1:1,000, Abcam, Cambridge, UK #ab24170) for lysosomes. Crystals with cells were fixed for 15 minutes with 4% PFA, then washed with PBS and permeabilized with PBS containing 0.25% (v/v) Triton X-100 and 5% goat serum for 1 hour. Next, primary antibodies were added and incubated overnight at 4 °C in a wet chamber. After 3 washes with PBS 0.25% Triton X-100, crystals were incubated one hour with appropriate, fluorophore-labeled (Alexa-488, 546, 594 or 647 nm as required, Invitrogen), secondary antibodies and DAPI at room temperature and protected from light. Finally, samples were washed again three times and mounted in slides with 1 drop of Mowiol®. Samples were again analyzed with a Leica SP2 confocal microscope. For colocalization assays, the resulting binary mask was used along the built-in measure function to acquire the total immunoreactive area among all the pixels inside the binary mask overlaid on top of the original image. The obtained value was then referred to the number of DAPI-positive cell nuclei or to the number of GFP-positive cells in the optical field.

β-arrestin-2 recruitment assays

To assess β-arrestin-2 recruitment to activated CB_1R, we employed a split-reporter reconstitution approach based on the Promega® Nano-BiT system, that employs an engineered luciferase derived from a deep-sea luminous shrimp (Dixon *et al*, 2016). The experimental approach consists of fusing two fragments of the luciferase to a given pair of proteins and then measuring reconstituted luciferase activity.

Briefly, we seeded 50,000 HEK-293T cells per well in a 96-well plate pre-coated with poly-D-lysine, and transfected them with the plasmids pcDNA3.1-3xHA-CB_1R[LgBiT] (10 ng/well), pcDNA3.1-[SmBiT]-ARRB2 (10 ng/well) and pEGFP-BiP-IR or pEGFP (10 ng/well) using Lipofectamine 2000®. Twenty-four hours post-transfection, cells were serum-starved for 4 hours, and then the medium was changed to HBSS supplemented with 24 mM HEPES, 4 mM $NaHCO_3$, 1.3 $CaCl_2$, 1 mM $MgSO_4$ and 0.1% (w/v) bovine serum albumin (100 µl per well). Next, 25 µl of Nano-Glo® 5X reagent was added and luminescence signal was immediately recorded in a CLARIOstar Multimode Plate Reader (BMG Labtech) as the baseline. Once the signal was stable, WIN55,212-2 (10 µM) or vehicle was added, and the luminescence signal was registered for one additional hour. Finally, the area under the curve (AUC), which estimates the amount of recruited β-arrestin-2, was calculated by using GraphPad Prism v8.0.1 and comparisons were made by one-way ANOVA with Bonferroni's post-hoc analysis.

Subcellular fractionation

Subcellular fractionation of brain tissue was achieved following standardized procedures (Bozidis *et al*, 2007). Specific nuclei were dissected from 12-week-old mice and harvested at -80 °C. Tissue samples were lysed by sonication in 2 ml of ice-cold MTE buffer (270 mM D-mannitol, 10 mM Tris-HCl, 0.1 mM EDTA, pH 7.4). Nuclei were discarded by centrifugation (1,400x*g*, 10 minutes, 4 °C) and the supernatant (total cell lysate) was subjected to a second centrifugation (15,000x*g*, 10 minutes, 4 °C) to separate the pelleted mitochondrial crude fraction. Supernatants were then loaded in a sucrose gradient composed of 2 ml of sucrose-buffer A (2 M sucrose, 0.13 mM EDTA, 10 mM Tris-HCl, pH 7.6), 3 ml of sucrose buffer B (1.5 M sucrose, 0.13 mM EDTA, 10 mM Tris-HCl, pH 7.6) and 3 ml of sucrose buffer C (1.3 M sucrose, 0.13 mM EDTA, 10 mM Tris-HCl, pH 7.6) and ER was isolated from the cytosol by ultracentrifugation (152,000x*g*, 70 minutes, 4 °C). The ER fraction appears as a band at the 1.5 M/1.3 M sucrose interphase, while the cytosolic fraction remains at the top of the tube. Both fractions were collected, in the case of the ER with the aid of a 20G needle and a syringe, and the ER fraction was further purified by a subsequent ultracentrifugation step (126,000x*g*, 45 minutes, 4 °C). The ER-containing pellet was resuspended in 100 µl of PBS and immediately frozen. Likewise, aliquots of total cell lysate and cytosolic fractions were collected throughout the process and immediately frozen. Samples were kept at -80 °C for Western blotting analysis.

Synaptosomes preparation

Synaptosomes were prepared as previously described (Martín *et al*, 2010). Striata, hippocampi or cortices from six 3-4-month-old mice were freshly dissected and homogenized in 0.32 M sucrose (pH 7.4). This homogenate was centrifuged twice (2,000x*g*, 2 minutes followed by 12 minutes at 9,500x*g*, both at 4 °C) and the white loosely compacted layer, containing the majority of the synaptosomes was gently resuspended in 8 ml of 0.32 M sucrose (pH 7.4). This synaptosomal suspension was placed onto a 3-ml Percoll discontinuous gradient containing: 0.32 M sucrose, 1 mM EDTA, 0.25 mM dithiothreitol (pH 7.4), and 3, 10, or 23% Percoll (Cytiva, Amersham, UK, #17-0891-01). Synaptosomes were retrieved from the interphase between the 10 and 23% gradients (P2 fraction), diluted in 30 ml of HEPES buffer medium (HBM: 140 mM NaCl, 5 mM KCl, 5 mM $NaHCO_3$, 1.2 mM NaH_2PO_4, 1 mM $MgCl_2$, 10 mM glucose, 10 mM HEPES, pH 7.4) and further purified by centrifugation (22,000x*g*, 10 minutes, 4 °C). Finally, pelleted synaptosomes were resuspended in 6 ml of HBM and plated in poly-D-lysine-coated coverslips for 1 hour and then fixed in PBS containing 4% paraformaldehyde for 15 minutes or harvested for Western

Blotting analysis at -80 °C along with aliquots from total extract, P2 supernatant and P2 fractions.

Animals

All the experimental procedures used were performed in accordance with the guidelines and with the approval of the Animal Welfare Committee of Universidad Complutense de Madrid and Comunidad de Madrid (PROEX 209/18), and in accordance with the directives of the European Commission. Besides C57BL6/N wild-type mice (bred in-home), we made use of several genetically engineered mice. $BiP^{+/-}$ (herein referred to as BiP-HET) (Luo *et al*, 2006) and $CRBN^{floxed/floxed}$ (herein referred to as CRBN-floxed) mice (Rajadhyaksha *et al*, 2012) were purchased from The Jackson Laboratory (Bar Harbor, ME, US #019549 and #017564, respectively). We also used $CB_1R^{floxed/floxed}$ (herein referred to as CB_1R-floxed) mice, $CB_1R^{floxed/floxed;CMV\text{-}Cre}$ (herein referred to as CB_1R-KO) mice (Marsicano *et al*, 2002), conditional $CB_1R^{floxed/floxed;Nex1\text{-}Cre}$ (herein referred to as Glu-CB_1R-KO) mice, and conditional $CB_1R^{floxed/floxed;Dlx5/6\text{-}Cre}$ (herein referred to as GABA-CB_1R-KO) mice (Monory *et al*, 2006); as well as Stop-CB_1R, Stop-$CB_1R^{EIIa\text{-}Cre}$ (herein referred to as CB_1R-RS) mice, conditional Stop-$CB_1R^{Nex1\text{-}Cre}$ (herein referred to as Glu-CB_1R-RS) mice, and conditional Stop-$CB_1R^{Dlx5/6\text{-}Cre}$ (herein referred to as GABA-CB_1R-RS) mice, to allow CB_1R gene-expression rescue from a CB_1R-null background (De Salas-Quiroga *et al*, 2015; De Giacomo *et al*, 2021). $CRBN^{floxed/floxed;Nex1\text{-}Cre}$ (herein referred to as Glu-CRBN-KO) and $CRBN^{floxed/floxed;Dlx5/6\text{-}Cre}$ (herein referred to as GABA-CRBN-KO) were generated by backcrossing $CRBN^{floxed/floxed}$ mice with Nex1-Cre and Dlx5/6-Cre expressing mice, respectively (Schwab *et al*, 2000; Monory *et al*, 2006). A constitutive CRBN knockout (herein referred to as CRBN-KO) was obtained after crossing $CRBN^{floxed/floxed}$ mice with CMV-Cre expressing mice (The Jackson Laboratory #006054). Animal housing and handling was performed in agreement to minimize pain and discomfort of the animals, with a 12h/12h light-dark cycle and *ad libitum* access to food. Assignment to the different experimental groups was conducted randomly. Adult mice (*ca.* 8-weeks old) of both sexes were used. For every single behavioral experiment, animals were habituated to the room for at least 1 hour before the experiment.

Hybridization probes and in situ hybridization histochemistry (ISHH)

For *I*n *S*itu *H*ybridization *H*istochemistry (ISHH) 14-µm thick coronal tissue sections of whole paraformaldehyde-perfused frozen brains were cut on a microtome-cryostat (Microm HM500 OM, Walldorf, Germany), thaw-mounted on 3-aminopropyltriethoxysilane (APTS)-coated slides (Sigma-Aldrich #S4651) and stored at -20 °C until further processing. The oligonucleotides complementary to the mRNAs coding for BiP and CB_1R are listed in Table MM8. Oligonucleotides for each mRNA were labeled at their 3'-end using [α-^{33}P] dATP (3,000 Ci/mmol, New England Nuclear, Boston, MA, US, product discontinued). Labeled probes were purified using ProbeQuant G-50 Micro Columns (Cytiva #28903408).

Frozen tissue sections equilibrated to room temperature were fixed for 20 minutes at 4 °C in 4% paraformaldehyde, then washed three times with 3x times concentrated PBS, followed by two washes with 1x concentrated PBS and incubated for 2 minutes at 20 °C in a solution of predigested pronase (Calbiochem #53702) (24 IU/ml in 5 mM EDTA 50 mM Tris-HCl, pH 7.5). Pronase activity was stopped by adding a solution of 2 mg/ml glycine in 1x PBS, then tissue was rinsed with PBS and dehydrated using a series of 50-70-96% ethanol immersions.

OLIGONUCLEOTIDE NAME	mRNA TARGET	SEQUENCE (5'-3')
mCB1/1	Cannabinoid receptor 1	GATGGTACGGAAGGTGGTATCTGCAAGGCCGTCTAAGATCGACTT
mCB1/2	Cannabinoid receptor 1	ATAGCACCAGCAGGTTCTCCAGAACCGTGAAGGTGCCCAGGGTGA
mCB1/3	Cannabinoid receptor 1	CAGAGCCTCGGCAGACGTGTCTGTGGACACAGACATGGTCACCTT
mGRP78/1	BiP	TCTTGTCCTCCTCCTCGGCCCGCACCGCGCCCAGCAGCAGCAACG
mGRP78/2	BiP	ACACCAGCCTGGACAGCGGCACCATAGGCTACAGCCTCATCGGGG
mGRP78/3	BiP	ATGTATCCTCTTCACCAGTTGGGGGAGGGCCTCCACTTCCATAGA
rmGAD65/1	Glutamic acid decarboxylase 65	CTTGTTTCCGATGCCGCCCGTGAACTTTTGGGCCACCTGGCACCA
rmGAD65/2	Glutamic acid decarboxylase 65	GCGTCAAAATTTCCTCCAGATTTTGCGGTTGGTCTGCCAATTCCC
rGAD/5	Glutamic acid decarboxylase 67	ATAGAGGTATTCAGCCAGCTCCAGGCATTTGTTGATCTGATTTTCAAATCCCAC
rVGluT1/1	vesicular GluT1 Transporter	CAGGGCGCGCCCCGCCAGCTTCCGAAACTCCTCCTGCCGGAACTC

Table MM8. Oligonucleotides for ISHH.

Hybridization was conducted using radioactively labeled and non-radioactively labeled (Digoxigenin-labeled) probes diluted in a solution composed of 50% formamide, 4x Standard Saline Citrate (1 SSC: 150 mM NaCl, 15 mM sodium citrate), 1x Denhardt's solution (0.02% Ficoll, 0.02% polyvinylpyrrolidone, and 0.02% bovine serum albumin), 10% dextran sulfate, 1% sarkosyl, 20 mM phosphate buffer, pH 7.0, 250 µg/mL yeast tRNA, and 500 µg/mL salmon sperm DNA. In every case, the final concentration of each probe was approximately 1.5 nM. After an overnight incubation at 42 °C in a humid box with this solution, tissue sections were washed for 45 minutes with 0.6M NaCl, 10 mM Tris-HCl, pH 7.5 at 60 °C for a total of four times and once for 10 minutes. Next, the slides were submerged for 30 minutes in a buffer containing 0.1 M Tris-HCl pH 7.5, 1 M NaCl, 2 mM $MgCl_2$ and 0.5% (w/v) bovine serum albumin and incubated overnight at 4 °C in the same solution with alkaline phosphate conjugated antidigoxigenin-Fab fragments (1:5,000, Boehringer Mannheim). After three washes in the same buffer without antibody, and two washes in alkaline buffer (0.1 M Tris-HCl, pH 9.5, 0.1 M NaCl, and 5 mM $MgCl_2$), alkaline phosphatase activity was revealed by incubating the sections with 3.3 mg of nitroblue tetrazolium and 1.65 mg of bromochloroindolyl phosphate (Thermo Scientific #N6495 & Sigma-Aldrich #B6149) diluted in 10 ml of alkaline buffer. To block the reaction, alkaline buffer containing 1 mM EDTA was added, sections were briefly immersed in 70% and 96% ethanol, air-dried, and dipped into Ilford K5 nuclear emulsion (Ilford, Mobberly, Cheshire, UK, #10581) diluted 1:1 with distilled water. They were exposed in the dark at 4 °C for 4 to 6 weeks and finally developed in Kodak D19 (Kodak, Rochester, NY) for 5 minutes and fixed in Ilford Hypam fixer (Ilford). For film autoradiography, hybridized sections were exposed to Biomax-MR (Kodak, Rochester, NY, US) films for 1-10 days at -70 °C with intensifying screens.

Images from film autoradiograms were obtained using a Wild 420 macroscope (Leica Microsystems, Wetzlar, Germany) equipped with a digital camera (DXM1200 F, Nikon, Tokyo, Japan) and ACT-1 Nikon software. Microphotography was performed with an Olympus BX51 Stereologic Microscope (Olympus, Tokyo, Japan) equipped with a digital camera (DP71, Olympus). Figures were assembled using Adobe Photoshop (Adobe Systems, San Jose, CA, US); only contrast and brightness were adjusted to optimize images.

RNA isolation, cDNA preparation and qPCR

RNA isolation for multiple tissues was achieved by using the NucleoZOL one phase RNA purification kit (Macherey-Nagel #740404.200) following manufacturer's instructions. Briefly, a small piece of fresh tissue, placed in a microcentrifuge tube, was homogenized using a Kimble motor cordless device (DWK Life sciences #749540-0000) in 500 µl of NucleoZOL reagent and resuspended by up and down pipetting. Next, 200 µl of double-distilled H_2O were added, the tube was vigorously mixed and incubated for 15 minutes at room temperature. Then, the sample was subjected to centrifugation (12,000x*g*, 15 minutes, room temperature) and the supernatant was collected. After that, 100% isopropanol was

added to the tube in a 1:1 volume ratio, and the mix was incubated at room temperature for 10 minutes. Next, RNA was again spun (12,000x*g*, 10 minutes, room temperature), and carefully washed twice with 500 µl of 75% ethanol, with a centrifugation step in-between washes (8,000x*g*, 3 minutes, room temperature). Finally, ethanol was removed, samples were air-dried on ice and double-distilled H_2O was added until concentration of RNA (measured by conventional spectroscopy with a Nanodrop™ apparatus) was approximately 1 µg/µL.

Two µg of RNA were retro-transcribed using the Transcriptor First Strand cDNA Synthesis Kit (Roche Life Science, Penzberg, Upper Bavaria, Germany, #04379012001) with random hexamer primers. Briefly, 2 µg of RNA together with 1 µl of random hexamers in a final volume of 7 µl were denatured for 10 minutes at 65 °C. Next, samples were cooled to 4 °C, dNTPs (2 µl), reverse-transcriptase buffer (1 µl) and the reverse transcriptase enzyme (0.17 µl) were added, and cDNA was generated by incubation at 55 °C for 1 hour, preceded by 10 minutes at 25 °C. Finally, reaction was stopped by heating at 85 °C for 5 minutes.

Real-time quantitative RT-PCR (Q-PCR) was performed in a QuantStudio 7/12k Flex System (Applied Biosystems) using specific Q-PCR primers designed with Primer3 and following standard recommendations (Thornton & Basu, 2011) (Table MM9) Q-PCR was conducted in 384-well plates (Thermo Scientific #4309849) using the LightCycler® Multiplex DNA Master (Roche Life Science #07339577001) and SYBR green (Roche Life Science #4913914001). Relative expression ratio was calculated by using the ΔΔCt method with *HPRT* or *TBP* as housekeeping genes for normalization.

OLIGONUCLEOTIDE NAME	SEQUENCE (5'-3')
CRBN-F	TGAAATGGAAGTTGAAGACCAAGATAG
CRBN-R	AACTCCTCCATATCAGCTCCCAGG
TBP-F	GGGGAGCTGTGATGTGAAGT
TBP-R	CCAGGAAATAATTCTGGCTCA
HPRT-F	CAGTACAGCCCCAAAATGGT
HPRT-R	CAAGGGCATATCCAACAACA

Table MM9. Oligonucleotides for Q-PCR.

Cannabinoid tetrad evaluation

The "tetrad" test comprises four behavioral paradigms in which rodents treated with CB_1R agonists, such as Δ^9-tetrahydrocannabinol, show measurable alterations (Little *et al*, 1988). Thus, the different tasks employed (spontaneous activity, analgesia, hypothermia, and catalepsy) can be used to screen drugs or genes that modulate CB_1R function.

BiP-WT and BiP-HET adult mice were injected intraperitoneally with vehicle [2% (v/v) DMSO, 2% (v/v) Tween-80 saline solution)] or 10 mg/kg THC (THC Pharm). The "cannabinoid tetrad" was assessed 30 minutes after injection following standard guidelines (Metna-Laurent *et al*, 2017). Analgesia was evaluated using the hot-plate paradigm being the temperature set at 52 °C. Animals were placed in the plate inside a transparent cylinder and latency to first pain symptom (paw licking) was annotated. Mice were removed after 30 seconds if no symptoms were visible. In the catalepsy test, animals were placed with both forelimbs on a bar situated at 3.5 cm from the floor. Immobility was considered maximal when animal exceeded 60 seconds of immobility, while it was considered null when the immobility time was lower than 5 seconds. In all cases 3 attempts were performed and the maximal immobility time value was chosen as representative. Animal body temperature was measured before and after drug delivery using a rectal thermometer inserting the probe approximately 2 cm into the animal's rectum. The open field test was conducted in an arena of 70x70 cm. Mice were allowed to explore the arena for 10 minutes and video-recorded for subsequent automated analysis using Smart3.0 software (Panlab, Barcelona,

Spain) to assess locomotor activity. Genotypes and treatments remained blind until analysis was completed. To study anxiety-like behaviors, the number of entries of the animal into the central part of the arena (25x25 cm) relative to total ambulation were assessed, one entry being considered when the animal had placed at least both forelimbs in the square. All tests were performed with a light intensity of 45 ± 10 lux.

In the case of CRBN conditional knockouts, and the CRBN full knockout model, these same behavioral tasks, except the catalepsy test, were conducted independently, without any drug administration.

Novel object recognition (NOR) test

Although originally developed for rats (Ennaceur & Delacour, 1988), the *N*ovel *O*bject *R*ecognition test is widespread used in mice (Ennaceur, 2010). The principle of the test is that a mouse, when presented two objects, if one of them is already familiar, spends more time exploring the unfamiliar one. This purpose is also based in the behavioral fact that mice prefer novelty over familiarity. Generally, after a habituation session to get acquainted with the maze, mice are presented with two identical objects (training phase), and 24 hours later, one of the objects is exchanged for a new one, different in shape, color and texture, and exploration time of each object is analyzed (testing phase) (Fig. MM6). Time between training and testing sessions can be adjusted to assess short or long-term memory function.

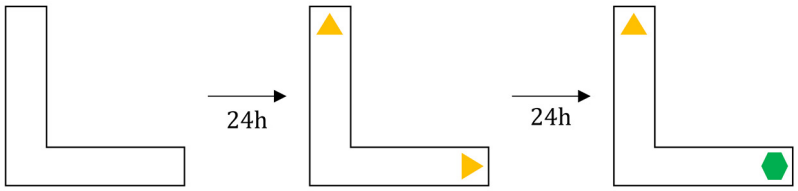

Figure MM6. Novel object recognition test. During the habituation session, mice are placed in an L-maze for 9 minutes. Twenty four hours later, mice are re-exposed to this enviroment containing two identical objects at the end of each arm (training session). Finally, one day after training, mice are presented a different object (testing session).

Alterations in cannabinoid-induced amnesia were studied using the novel object recognition memory task in an L-maze as previously described (Puighermanal *et al*, 2009). The maze was made of grey Plexiglas with two corridors (35-cm and 30-cm long, respectively, for outer and inner walls, 4.5-cm wide and 15-cm high walls) forming a right angle and under weak light intensity (50 lux). The test consisted of a 9-minute trial repeated for three days. On the first day, mice were placed in the maze in the absence of object. The next day, mice were placed in the maze and two equal objects had been placed at the end of each corridor. When administered, SR141716 (0.3 mg/kg), or vehicle [2% (v/v) DMSO, 2% (v/v) Tween-80 saline solution)] was injected intraperitoneally immediately after the training session. Finally, on the third day, one of the objects was exchanged for another different in shape, color and texture and mice were introduced in the maze. Position of novel objects in the arms was randomized, and objects were previously analyzed not be intrinsically favored. In all cases, mouse behavior was video-recorded, and exploration time was manually counted, being exploration considered as mice pointing the nose to the object (distance < 1 cm). Mice with exploration times lower than 15 seconds between both objects were considered outliers. Memory performance was assessed using the discrimination index (DI). Discrimination indexes were calculated as difference in time exploring the new object (TN) versus the familiar one (TF), divided into the total exploration time (sum of TN + TF).

$$DI = \frac{TN - TF}{TN + TF}$$

Elevated plus maze (EPM) test

The *E*levated *P*lus-*M*aze (EPM) test is one of the most used paradigms to study anxiety-like behavior in rodents. Again, this protocol was originally set-up with rats (Handley & Mithani, 1984), and rapidly adapted for mice (Lister, 1987). The principle of the test arises from the conflict between fear and curiosity that originates when an individual encounters a novel environment. Generally, mice are placed in a cross-shaped plastic device with two opposite open arms, and two opposite enclosed arms, connected by a central structure, and elevated from the floor. The time spent in the open arms versus the enclosed ones, as well as the proportion of open to closed arm entries, are usually employed as a measure of anxiety. Anxious animals avoid the open arms, whereas anxiolytic interventions increase the time that mice spent in this zone of the maze (Fig. MM7).

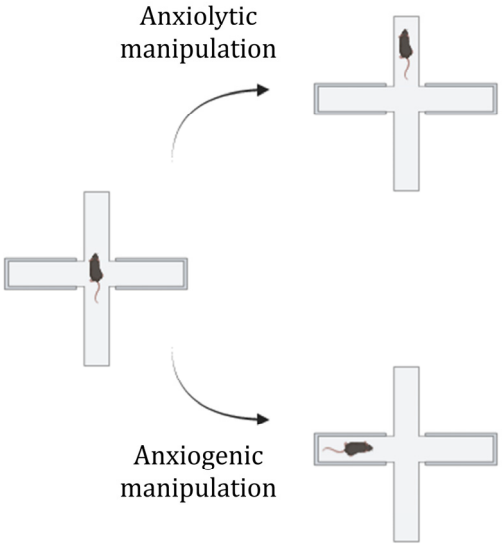

Figure MM7. Elevated plus maze test. Mice are situated in the center of a cross-shaped device, elevated from the floor, with two open arms, and two enclosed arms, and allowed for free exploration. Anxious-like behavior results in the mice spending an increased time in the enclosed part of the maze, whereas anxiolytic manipulations enhance the time spent in the open arms.

We evaluated the anxiety-like behavior 4 hours after acute intraperitoneal injection of vehicle or THC (10 mg/kg). Each mouse was placed in the center of the maze, facing one of the open arms, under dim illumination (20 ± 5 lux) and the exploratory behavior of the animal was video recorded for 5 minutes. The number and duration of entries was measured separately for the open arms and the closed arms, being one arm entry registered when the animal had placed both forepaws in the arm. Our maze followed standard guidelines (arms: 30-cm long, 5-cm wide, two of them with 16-cm high walls, connected with a central structure of 5x5 cm and elevated 50 cm from the floor).

Again, in the case of CRBN conditional knockouts, and the CRBN full knockout model, this same behavioral task was conducted independently, without any drug administration.

Social interaction test

The social interaction test is based in the inherent preference of mice to spend time with another individual (sociability) rather than an object. This type of behavior is usually analyzed in a three-chambered box with openings. One of the lateral compartments contains one caged mouse, while the other lateral one presents only the cage. When placed in the central chamber, mice tend to favor the chamber containing its counterpart. This test is a powerful tool to assess strong deficits in social behavior in transgenic animals that display autism-like traits (Moy *et al*, 2004) (Fig. MM8).

To evaluate social behaviors, we introduced a single mouse in an arena (70-cm long, 40-cm wide, 40-cm high walls) divided in three compartments (approximately, 23.3-cm long each) separated by 2 walls (approximately 17-cm long) with a connector corridor (5-cm wide) and containing two cylindrical cages in the lateral compartments; for 10 minutes and allowed free exploration under light illumination (45 ± 10 lux). One hour later, the mouse was re-exposed to this environment, but this time one of the cages contained one unfamiliar mouse, paired in sex and age, and being a control genotype with the mouse undergoing testing, in one of the cages. Mouse behavior was video recorded for 10 minutes. Finally, time spent sniffing each cage was annotated manually by a blind experimenter. Position of cages containing mice was randomized. Again, mice with exploration times lower than 15 seconds were considered outliers.

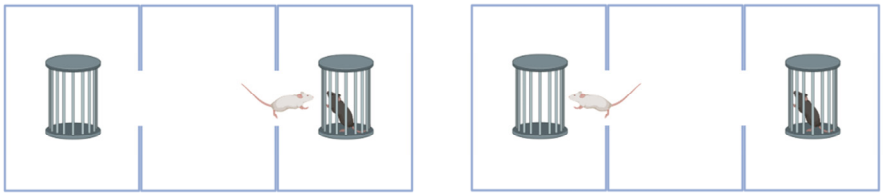

Figure MM8. Social interaction test. Mice placed in a 3-chambered maze tend to spend more time in the compartment containing another mouse. Altered sociability results in decreased time spent in the mouse-containing chamber.

Rota-Rod test

The Rota-Rod test is a widely used paradigm to study motor learning and sensorimotor coordination in mouse (Brooks *et al*, 2012). Classically, a given mouse is placed on a rotating rod, at a constant or increasing speed, and latency to fall is measured. Impaired motor learning or sensorimotor coordination results in diminished falling times.

We employed a 3-day/3-test protocol, that was designed to assess both motor coordination and learning. Each mouse was tested three times each for three consecutive days with an inter-trial interval of 40 minutes under light illumination (45 ± 10 lux). Briefly, the mouse was placed in the rod (Panlab #LE8205) at a constant speed (4 rpm), which was then accelerated (4 to 40 rpm in 300 seconds) once the mouse was put in place. Time to fall was annotated in either test, and the mean of trials 4-9 (days 2 and 3) was calculated to ensure reduced inter-trial variability.

Footprint test

Mouse gait can be simply analyzed by using the footprint pattern test. To obtain footprints, mouse's fore- and hindpaws are painted with non-toxic inks of different colors, and the animal is placed in a corridor placed on top of a white paper. Finally, once the paint dries, distance between each stride (stride length), within both forepaws (front-base width) or hind paws (hind-base width), and the overlap between forepaw and hindpaw placement can be easily measured with a ruler. For the sake of simplicity, we have only considered the stride length.

Forced-swimming test (FST)

The *F*orced-*S*wimming *T*est (FST) (Porsolt *et al*, 1977) is a widespread method to screen not only the action of potentially antidepressant drugs but also genetic or environmental alterations that induce depression-like behaviors in rodents (Armario, 2021). Typically, a

mouse is placed in a cylindrical tank (approximately 25-cm high with a diameter of 10 cm) filled with water at room temperature (21-23 °C) for any given time, and immobility time is calculated. A mouse is considered immobile when it ceases to swim with only sole movements aim to stay floating "motionless".

We conducted a forced swimming test in a square tank (15-cm high, 10-cm wide) filled with 10-cm of water at 22 °C for 5 minutes. Animal behavior was video recorded, and time spent immobile was annotated manually by a blind experimenter.

Y-maze test

The Y-maze test is widely used to assess spatial working memory in mice (Lalonde, 2002). This behavioral task takes its name from the form of the maze, which consists of a Y-shaped device with three opaque arms orientated at 120° angles from one another.

We conducted an adapted protocol to test spatial reference memory as previously described (Kraeuter *et al*, 2019) (Fig. MM9). Briefly, a mouse was placed in one arm of the maze, being one arm of the maze closed off (novel arm), and allowed for free exploration for 15 minutes (training session). One hour later, the mouse was reintroduced into the maze with all three arms accessible, and allowed for free exploration for 5 minutes (testing session). Animal behavior was video-recorded, and the number of entries in each arm was annotated. Mice with proper spatial memory functioning show an enhanced number of entries in the novel arm during the testing session. Mice with less than 20 total entries between all arms were considered outliers.

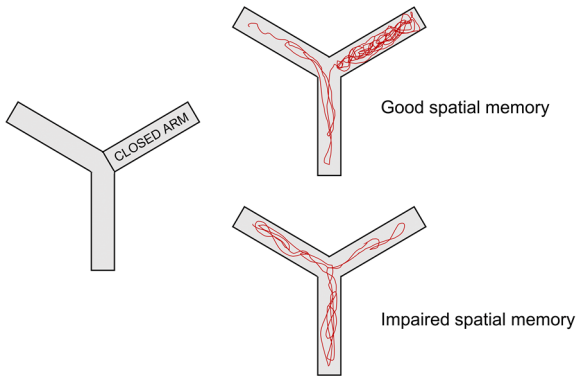

Figure MM9. Y-maze test. Mice are placed in a Y-shaped maze with one arm blocked for 15 minutes. One hour later, mice are reintroduced in the maze with the three arms open for 5 minutes. Control mice tend to spend more time in the previously inaccessible arm.

Statistics

Unless otherwise specified, data are presented as mean ± SEM. Statistical comparisons were conducted by one-way or two-way ANOVA with Tukey's post-hoc test, or by Student's *t*-test, as indicated in each case. All datasets were tested for normality (Kolmogorov-Smirnov's test) and homoscedasticity (Levene's test) prior to analysis. For clarity, only *p* values lower than 0.05 were considered statistically significant. The sample size for each experiment was estimated based on previous studies conducted by our laboratories using similar protein-interaction, cell-culture, brain-sample, and behavioral approaches. The number of biological replicates (*e.g.*, number of mice, number of cell cultures) is provided in the corresponding figure legends. The number of technical replicates (*e.g.*, number of Y2H assays, number of incubations within each cell culture, number of sections microscopically analyzed per mouse brain, number of behavioral trials per mouse) is provided in the corresponding figure legends or in the corresponding Materials and Methods subsections. All the experiments conducted with animals are presented as dot plots. Graphs and statistics were generated by GraphPad Prism v8.0.1.

INTRODUCTION

AIMS

MATERIALS AND METHODS

RESULTS

DISCUSSION

CONCLUSIONS

REFERENCES

Results – Aim 1

Identification of BiP as a CB_1R interacting protein

To identify candidate proteins that interact with CB_1R, we designed a yeast-two hybrid based high-throughput approach.

Yeast two-hybrid experiments were conducted by using the largest region of CB_1R exposed to the cytoplasm, namely the *C*-terminal portion of the protein, since the use of native membrane proteins in this experimental setting is much challenging (Brückner *et al*, 2009). For this purpose, we cloned amino acids 408 to 472 of the receptor (almost the entire carboxy-terminal domain, that starts at amino acid 400) into the pGBT9 vector, fusing this stretch to the DNA-binding domain of the GAL4A transcription factor. Next, we used this region as a bait in a large screening against a human library that contained more than 10^6 individual ORF clones in-frame with the activation domain of the GAL4A transcription factor. Despite several colonies being able to rescue growth in selection plates (*i.e.,* plates lacking essential amino acids, see Materials & Methods section for a detailed description), which is indicative of an interaction, only a single colony was able to display β-galactosidase activity when supplemented with X-Gal, a substrate whose oxidation renders a blue insoluble compound that is easily observable (Fig. R1.1A, upper part). Hence, we concluded that this colony had a plasmid encoding for a CB_1R associated protein. After plasmid isolation and Sanger sequencing, we found that this colony contained a vector encoding for amino acids 497 to 654 of the human protein BiP, also known as Heat shock protein family A member 5 (Hspa5), or Glucose-regulated protein of 78 kDa (GRP78) (Casas, 2017).

Box 1 – What is BiP?

The protein BiP was discovered almost fifty years ago, when three researchers noted a remarkable induction of a 78 kDa protein in chicken fibroblasts that had been cultured in the absence of glucose, and thus, named this polypeptide **glucose-regulated protein of 78 KDa (GRP78)** (Shiu *et al*, 1977)**.** Separately, a study with B lymphocytes identified a protein associated with the immunoglobulin heavy chain, and so termed it **immunoglobulin heavy-chain binding protein (BiP)** (Haas & Wabl, 1983)**.** Soon enough, it was shown that both proteins represented the same molecular entity (Munro & Pelham, 1986). Hence, BiP is an alternative name of GRP78.

The fundamental work by Munro and Pelham, that conjugated BiP and GRP78 into one unique entity, was initially aimed at the identification of heat shock proteins, a family of which BiP became a member after the study (Munro & Pelham, 1986). Heat shock proteins are a large group of proteins, conserved throughout evolution, whose expression is increased when cells suffer from stresses of multiple types, such as heat, hypo- or hyperosmosis and oxidation (Munro & Pelham, 1985). **BiP is the fifth member of the heat shock protein family A** (**Hspa5,** another alternative name) and one of the most abundant and studied proteins within the **heat shock protein family of 70 KDa (Hsp70s)**. Paradoxically, the *Hspa5* gene does not respond to heat. Instead, a variety of signals such as alterations in intracellular calcium concentration, or glycosylation inhibition, which explains its regulation by glucose, can up-regulate BiP. All these stressors converge in causing intracellular accumulation of unfolded or denatured proteins. BiP is a **molecular chaperone**. Thus, its main function within the cell consists of assisting the folding and assembly of unfolded hydrophobic polypeptides through direct protein-protein interactions (Gething, 1999).

BiP belongs to the highly conserved Hsp70 family of molecular chaperones. These proteins consist of two different domains: an *N*-terminal nucleotide-binding domain (NBD) with ATPase activity, and a *C*-terminal substrate-binding domain (SBD). The SBD, in turn, is composed of a β-sandwich domain (SBDβ) and an α-helical lid (SBDα), which are interlinked by a hydrophobic stretch (Wieteska *et al*, 2017). It is generally believed that ATP-assisted, BiP-mediated protein refolding proceeds when hydrophobic peptides bind to a conserved groove in the SBDβ domain of BiP (see Box 2). Conversely, here, we found that CB_1R-CTD interacts essentially with the lid domain in the absence of the groove. Specifically, according to the reported structures (Yang *et al*, 2015, 2017), BiP-IR would span the entire SBDα and two strands of the SBDβ (Fig. R1.1A, bottom diagram).

We next aimed to validate the molecular specificity of the interaction between CB_1R-CTD and BiP-IR. First, by using directed Y2H assays, we delimitated the BiP-IR-binding site to a restricted 23 amino-acid stretch (residues 449-472) at the edge of CB_1R-CTD (Fig. R1.1B). Second, we found that the CTD of CB_2R, the GPCR with the highest sequence homology to CB_1R, did not bind BiP-IR (Fig. R1.1B). Third, as the phosphorylation state of specific S and T residues in the CTD of a GPCR can determine its interaction with intracellular proteins, we challenged BiP-IR to every possible single phosphomimetic mutant (S/T → D) within CB_1R-CTD, and found that only the S452D point mutation, which is precisely located in the last 23 amino-acid portion of CB_1R, impaired the association (Table R1.1). Fourth, we expressed and purified recombinant CB_1R-CTD, BiP-IR and BiP, and found that BiP and BiP-IR bind CB_1R-CTD with a similar high affinity, as measured by fluorescence polarization-based protein-protein binding assays (Fig. R1.1C).

We subsequently conducted experiments in HEK-293T cells. First, co-immunoprecipitation studies showed that (i) CB_1R-CTD, and specifically its 449-460 amino-acid stretch, was sufficient to bind BiP-IR (Fig. R1.1D); (ii) full-length CB_1R also interacted with both BiP and BiP-IR (Fig. R1.1E); and (iii) BiP-IR exhibited little association with the S452D point-mutant of CB_1R-CTD (Fig. R1.1F). Second, BRET experiments conducted with an Rluc-tagged version of CB_1R also supported the protein-protein interaction (Fig. R1.1G, upper panel), and adding non-GFP-tagged versions of BiP as competitors decreased the BRET peak only when the BiP-IR was present (Fig. R1.1G, lower panel). Moreover, there was no overt binding between GFP-BiP-IR and CB_1R-Rluc when the S452D single mutation was introduced in the receptor (Fig. R1.1G, upper panel).

Taken together, these data show that BiP interacts specifically with CB_1R in vitro, both in purified-protein assays and in HEK-293T cells.

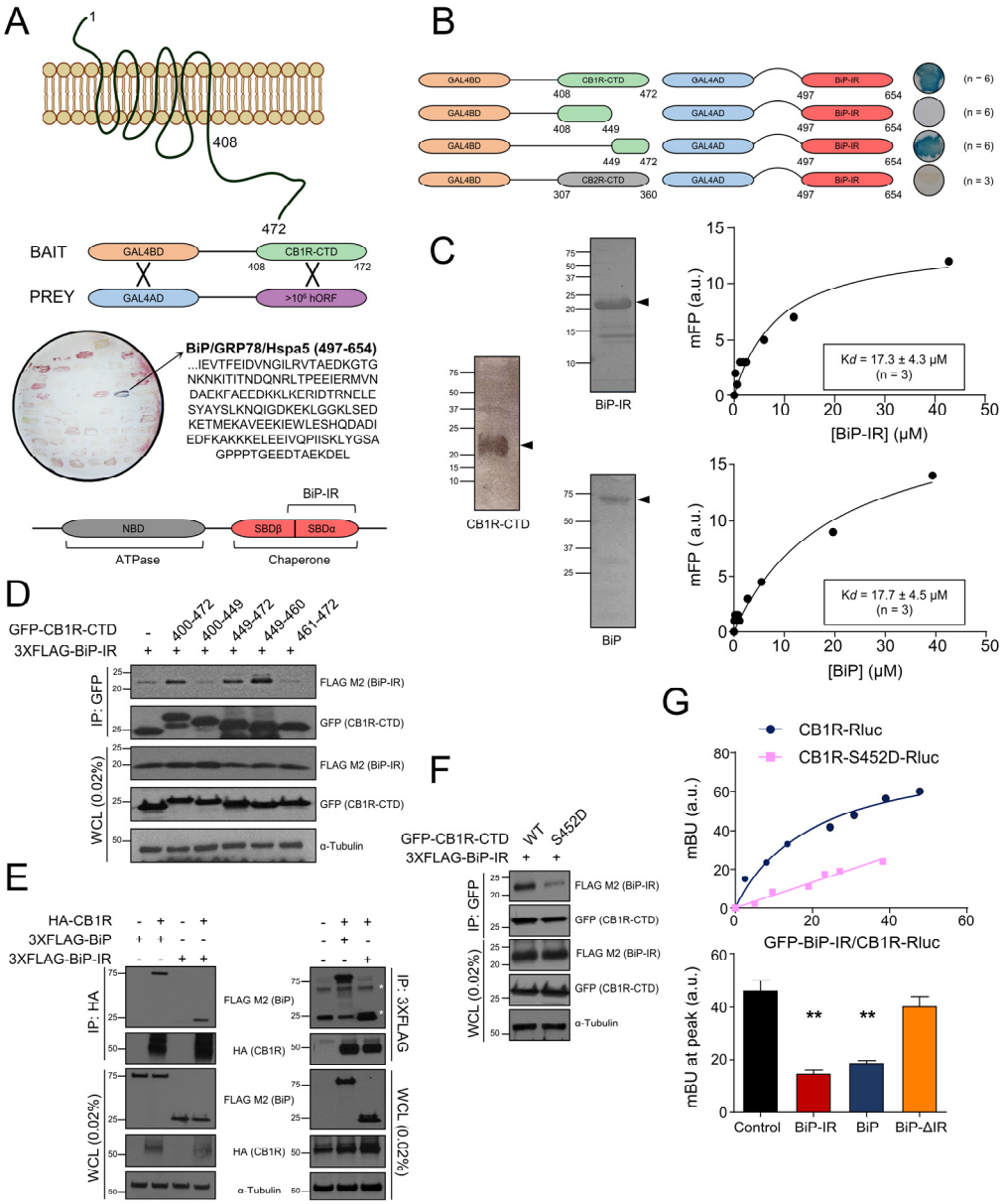

Figure R1.1. BiP interacts with CB$_1$R *in vitro*. *A,* Scheme of the Y2H experiment using CB$_1$R-CTD (amino acids 408-472) as bait and a human cDNA library (> 10^6 clones) as prey. One cDNA clone (stained in blue) contained BiP/GRP78/Hspa5 amino acids 497-654 (BiP-IR). A diagram represents the main structural domains of BiP/GRP78/Hspa5. ***B,*** Scheme of the Y2H experiment using fragments of CB$_1$R-CTD or CB$_2$R-CTD as bait and BiP-IR as prey. ***C,*** Fluorescence polarization-based protein–protein binding experiments using 5-IAF-labeled CB$_1$R-CTD and increasing amounts of unlabeled BiP-IR (top) or BiP (bottom). A representative experiment, including the gels of the purified proteins, is shown (n = 3). ***D,*** Co-immunoprecipitation experiments in HEK293T cells expressing fragments of GFP-CB$_1$R-CTD and 3xFLAG-BiP-IR. Immunoprecipitation (IP) was conducted with anti-GFP antibody. WCL, Whole-cell lysate. A representative experiment is shown (n = 3). ***E,*** Co-immunoprecipitation experiments in HEK-293T cells expressing HA-CB$_1$R and 3xFLAG-BiP or 3xFLAG-BiP-IR. IP was conducted with anti-HA antibody (left) or anti-FLAG antibody (right). Asterisk indicates immunoglobulin heavy and light chains. A representative experiment is shown (n = 3). ***F,*** Co-immunoprecipitation experiments in HEK-293T cells expressing GFP-CB$_1$R-CTD WT or an S452D point mutant form, along with 3xFLAG-BiP-IR. IP was conducted with anti-GFP antibody. A representative experiment is shown (n = 3). ***G,*** BRET experiments in HEK-293T cells expressing CB$_1$R-Rluc or CB$_1$R-S452D-Rluc and increasing amounts of GFP-BiP-IR (top; a representative experiment is shown; n = 3), together or not with nontagged versions of BiP, BiP-IR, or BiP-ΔIR as competitors (bottom). ** $p < 0.01$ from control vector by one-way ANOVA with Tukey's multiple comparisons test (n = 3).

Bait plasmid	Prey plasmid	Interaction
pGBT9 CB1R-CTD (amino acids 408 to 472)	pACT2 BiP-IR	+ (n = 3)
pGBT9 CB1R-CTD-S410D (amino acids 408 to 472)	pACT2 BiP-IR	+ (n = 3)
pGBT9 CB1R-CTD-S414D (amino acids 408 to 472)	pACT2 BiP-IR	+ (n = 3)
pGBT9 CB1R-CTD-T418D (amino acids 408 to 472)	pACT2 BiP-IR	+ (n = 3)
pGBT9 CB1R-CTD-S425D (amino acids 408 to 472)	pACT2 BiP-IR	+ (n = 3)
pGBT9 CB1R-CTD-S429D (amino acids 408 to 472)	pACT2 BiP-IR	+ (n = 3)
pGBT9 CB1R-CTD-S441D (amino acids 408 to 472)	pACT2 BiP-IR	+ (n = 3)
pGBT9 CB1R-CTD-S448D (amino acids 408 to 472)	pACT2 BiP-IR	+ (n = 3)
pGBT9 CB1R-CTD-S452D (amino acids 408 to 472)	pACT2 BiP-IR	- (n = 3)
pGBT9 CB1R-CTD-T453D (amino acids 408 to 472)	pACT2 BiP-IR	+ (n = 3)
pGBT9 CB1R-CTD-T460D (amino acids 408 to 472)	pACT2 BiP-IR	+ (n = 3)
pGBT9 CB1R-CTD-S462D (amino acids 408 to 472)	pACT2 BiP-IR	+ (n = 3)
pGBT9 CB1R-CTD-S464D (amino acids 408 to 472)	pACT2 BiP-IR	+ (n = 3)
pGBT9 CB1R-CTD-T465D (amino acids 408 to 472)	pACT2 BiP-IR	+ (n = 3)
pGBT9 CB1R-CTD-T467D (amino acids 408 to 472)	pACT2 BiP-IR	+ (n = 3)
pGBT9 CB1R-CTD-S468D (amino acids 408 to 472)	pACT2 BiP-IR	+ (n = 3)

Table R1.1. Effect of CB_1R-CTD phosphomimetic mutants on CB_1R-BiP interaction. Scheme of the Y2H experiment using every possible single phosphomimetic mutant (S/T⟶D) within CB_1R-CTD as bait, and BiP-IR as prey. Absence of interaction was only found when using the clone CB_1R-CTD-S452D.

Box 2 – Structure-activity relationship of BiP

Like every Hps70s chaperone, BiP displays a highly conserved protein sequence and structure reminiscent of other Hsp70 family members, such as HS71A (HSPA1A), HS71B (HSPA1B), GRP75 (HSPA9), HSP7C (HSPA8), HSP72 (HSPA2), HSP76 (HSPA6), and HSP71L (HSPA1L) (Wang *et al*, 2017).

Crystal structures show that BiP contains two differentiated domains (Yang *et al*, 2015, 2017). The *N*-terminal part of the protein establishes a nucleotide-binding domain (NBD) composed of a bilobular structure that has ATP hydrolytic activity, whereas the *C*-terminus conforms a substrate-binding domain (SBD) with eight β-strands (SBDβ) and a triple α-helical bundle (SBDα) as lid; bound with a linker sequence. Polypeptide binding proceeds at two loops between the β-strands of SBDβ and is finely controlled by the nucleotide-bound state of the protein. Several evidence have led to a consensus model, namely the Hsp70 ATPase cycle (Pobre *et al*, 2019) (Fig. Box-2). As a fantastic example of protein gymnastics, when BiP binds ATP, the SBD with its lid open docks into the NBD, which results in a high $K_{on/off}$ rate for interaction with protein clients, that is, favoring binding and release of associated peptides but at the cost of a low overall affinity. In turn, ATP hydrolysis extends the SBD away from the NBD and closes the lid (SBDα) over SBDβ, which poises the protein to receive substrates with low $K_{on/off}$ rates but high affinity. This cycle allows the efficient binding and folding of substrates with the energy provided by ATP hydrolysis.

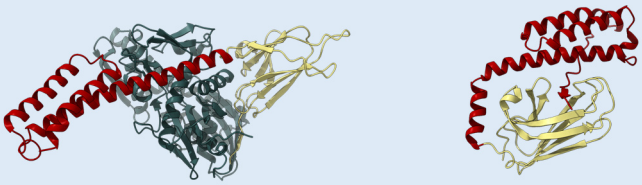

Figure Box-2. ATP and ADP-bound states of BiP. The NBD domain is shown in grey, the SBDβ in yellow and the SBDα (lid) in red. Note the relaxed conformation of the lid in the ATP-bound structure (left), and how it bends over the SBDα domain when ADP is bound (right). Images were created using ChimeraX (UCSF®) and Protein Data Bank accession numbers *5e84* for full-length, ATP-bound BiP, and *5e85* for isolated, ADP-bound, SBD.

BiP modulates CB_1R-evoked signaling

Dynamic mass redistribution (DMR) is a powerful tool to assess the overall signal triggered by the agonist-evoked activation of a particular receptor in living cells (Fang *et al*, 2007). In fact, our group and others have previously used DMR to investigate CB_1R-evoked signaling (Viñals *et al*, 2015; Moreno *et al*, 2018; Navarro *et al*, 2020). Here, by using HEK-293T cells expressing CB_1R, we found a well-defined and saturating curve after adding the cannabinoid receptor-selective agonist WIN55,212-2 (Fig. R1.2A). Of note, co-expression of full-length BiP led to a strong inhibition of CB_1R signaling (Fig. R1.2A) but did not alter the agonist-evoked response of two other $G\alpha_{i/o}$-coupled receptors (CB_2R and adenosine A_1 receptor) that were used as controls (Fig. R1.3A). The effect of BiP on CB_1R relied selectively on BiP-IR, as expressing this region rendered a comparable inhibition, and no change was found with BiP-ΔIR (Fig. R1.2A). This effect was again subverted when the S452D point mutation was inserted in CB_1R (Fig. R1.3B) and was also evident –though with a slower kinetics- when the endocannabinoids anandamide and 2-arachidonoylglycerol were used as receptor agonists (Fig. R1.2B). Given the similar behavior of full-length BiP and BiP-IR, we used only BiP-IR for further signaling experiments.

Box 3 – Functions of BiP

BiP is a ubiquitously expressed protein that can be found mainly in the lumen of the endoplasmic reticulum (ER), but also at other subcellular locations (Casas, 2017). As a chaperone, the main role of BiP is to assist the folding of cellular proteins but it also fulfills other functions. For instance, BiP is required to import polypeptides into the ER lumen and also to retro-translocate misfolded/unfolded proteins to the cytoplasm for degradation in the proteasome, a process known as ER-associated protein degradation (ERAD) (Vogel *et al*, 1990; Feige & Hendershot, 2013). Perhaps the most studied function of BiP is its role in the unfolded protein response (UPR). The UPR is a conserved signaling pathway that takes place when an overload of misfolded proteins occurs in the ER. Three transducers, namely, inositol-requiring enzyme 1 (IRE1), protein kinase-like ER kinase (PERK), and activating transcription factor 6 (ATF6), trigger signaling cascades that detain protein synthesis, increase the expression of target genes to augment folding capacity, and ultimately, induce cell cycle arrest and apoptosis if homeostasis is not reestablished (Ron & Walter, 2007). BiP evidently represents an UPR target gene, but its main function in UPR resides in inhibiting IRE1, PERK, and ATF6 in the absence of stress by direct protein-protein interactions (Bertolotti *et al*, 2000; Shen *et al*, 2002). Additionally, BiP is essential for ER-stress induced autophagy (Li *et al*, 2008) and Ca^{2+} storage in the ER, where it binds approximately 25 % of total Ca^{2+} load within that organelle (Lièvremont *et al*, 1997). Recently, BiP has been found on the cell surface under a set of pathological conditions, where it acts as a receptor and enables pro-survival signaling pathways (Misra *et al*, 2002; Gopal & Pizzo, 2021).

CB_1R activation modulates multiple signaling pathways, being cAMP/PKA, ERK and PI3K/Akt/mTORC1 the best characterized (Pertwee *et al*, 2010; Nogueras-Ortiz & Yudowski, 2016). We thus aimed to dissect in detail the inhibitory effect of BiP-IR on CB_1R overall signaling observed in DMR assays. First, we found that BiP-IR did not markedly alter the archetypical $G\alpha_{i/o}$-coupling profile of CB_1R (Fig. R1.2C), nor affected the WIN55,212-2-evoked reduction of forskolin-augmented cAMP concentration (Fig. R1.2D). Next, we analyzed the phosphorylation (activation) state of major cellular protein kinases by using a

phosphoprotein array. HEK-293T cells were transfected with the same constructs used in the aforementioned DMR assays, and subsequently treated with vehicle or WIN55,212-2. Among the different pathways activated by the cannabinoid, BiP-IR preferentially hampered the Akt/mTORC1 pathway (as inferred from Akt1/2/3-T308, PRAS40-T246 and p70S6K-T389 phosphorylation) and the ERK pathway (as inferred from ERK1/2-T202/Y204 phosphorylation) (Fig. R1.2E). The WIN55,212-2-mediated activation of CREB, an archetypical convergent substrate of the Akt/mTORC1 and ERK pathways, was also inhibited by BiP-IR (as inferred from CREB-S133 phosphorylation). We confirmed this BiP-mediated inhibition of CB_1R-evoked signaling by analyzing pERK1/2-T202/Y204, pp70S6K-T389, and pCREB-S133 with conventional western blotting (Fig. R1.2F). Accordingly, the PI3K inhibitor LY294002 and the MEK1 inhibitor U0126 blunted the WIN55,212-2-evoked DMR signal (Fig. R1.3C).

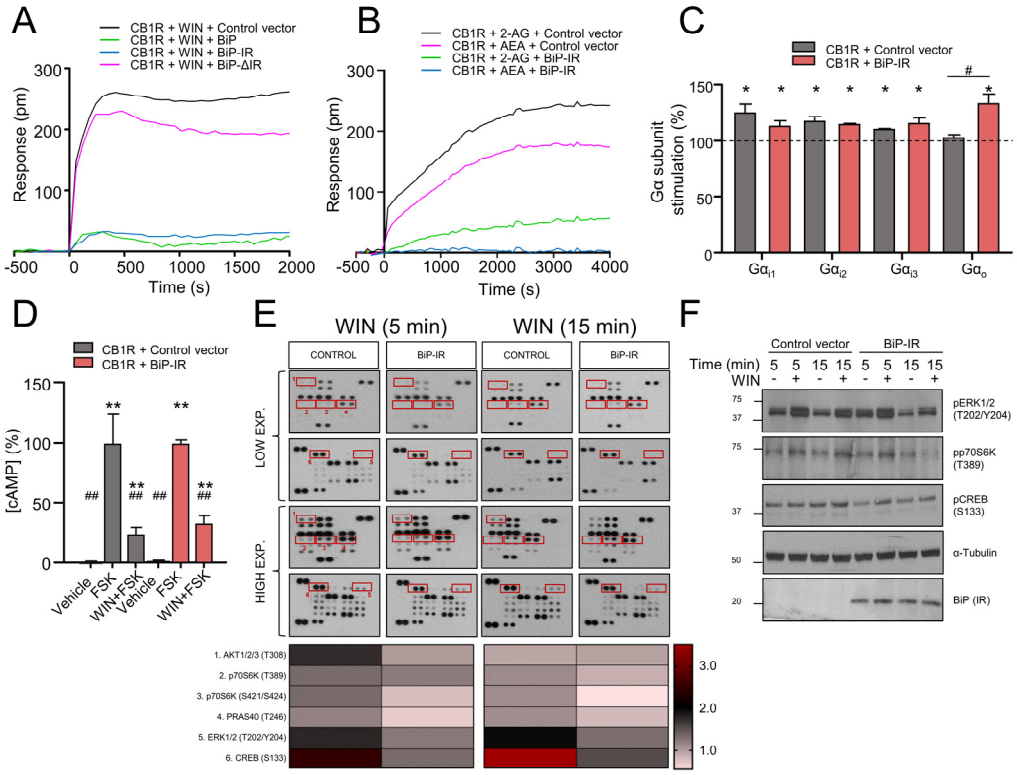

Figure R1.2. BiP modulates CB_1R-evoked signaling (I). ***A,*** DMR experiments in HEK-293T cells expressing CB_1R, together or not with BiP, BiP-IR, or BiP-ΔIR, and incubated with WIN55,212-2 (100 nM). A representative experiment is shown (n = 3). ***B,*** DMR experiments in HEK-293T cells expressing CB_1R, together or not with BiP-IR, and incubated with endocannabinoid (10 μM; 2-AG, 2-arachidonoylglycerol; AEA, anandamide). A representative experiment is shown (n = 3). ***C,*** Coupling of CB_1R to $G\alpha_{i/o}$ proteins in membrane extracts from HEK-293T cells expressing CB_1R, together or not with BiP-IR. * $p < 0.05$ from basal (dashed line), or $^{\#}$ $p < 0.05$ from control vector; one-sample Student's *t*-test or unpaired Student's *t*-test, respectively (n = 3). ***D,*** cAMP concentration in HEK-293T cells expressing CB_1R, together or not with BiP-IR. Cells were incubated first for 15 min with vehicle or WIN55,212-2 (100 nM), and then for 15 min with vehicle or forskolin (FSK; 500 nM). ** $p <$ 0.01 from vehicle, or $^{\#\#}$ $p < 0.01$ from FSK alone; two-way ANOVA with Tukey's multiple comparisons test (n = 3). ***E,*** HEK-293T cells expressing CB_1R, together or not with BiP-IR, were incubated for 5 or 15 min with vehicle or WIN55,212-2 (100 nM), and cell extracts were blotted on a phosphoprotein array. Two different times of membrane exposure are shown to allow an appropriate visualization of the main proteins affected (framed spots). A representative experiment is shown (n = 2; membranes from vehicle-treated cells are omitted for clarity). Heat map represents values of mean fold-activation by WIN55,212-2 over vehicle. ***F,*** Validation of some of the phosphoarray hits by conventional western blotting in the same cell extracts used in D. A representative experiment is shown (n = 2).

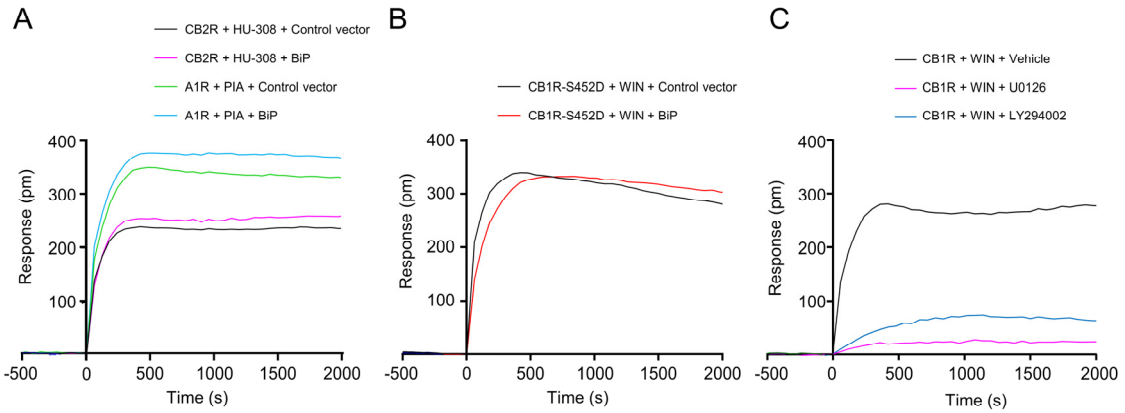

Figure R1.3. Controls of specificity of the CB_1R-BiP DMR experiments. ***A,*** DMR experiments in HEK-293T cells expressing CB_2R, together or not with BiP, and incubated with the CB_2R-selective agonist HU-308 (100 nM); or in HEK-293T cells expressing A_1R, together or not with BiP, and incubated with the A_1R-selective agonist PIA (50 nM). A representative experiment is shown (n = 3). ***B,*** DMR experiments in HEK-293T cells expressing CB_1R-S452D, together or not with BiP, and incubated with WIN55,212-2 (100 nM). A representative experiment is shown (n = 3). ***C,*** DMR experiments in HEK-293T cells expressing CB_1R and incubated with WIN55,212-2 (100 nM) plus vehicle or U0126 (5 μM) or LY294002 (5 μM). A representative experiment is shown (n = 3).

To study how BiP selectively alters CB_1R-mediated signaling independently of $G\alpha_{i/o}$ proteins, we evaluated the coupling of the receptor to non-$G\alpha_{i/o}$ G proteins. Of note, we found that CB_1R also coupled to $G\alpha_{q/11}$, and this association was impaired by BiP-IR (Fig. R1.4A). Moreover, WIN55,212-2-mediated ERK activation was mitigated by either pharmacological blockade of $G\alpha_{q/11}$ (with the drug YM-254890) or genetic interference of $G\alpha_{q/11}$ signaling (with a dominant-negative GFP-GRK2 construct) (Andradas *et al*, 2016) (Fig. R1.4B). Likewise, YM-254890 and dominant-negative $G\alpha_{q/11}$ reduced the WIN55,212-2-evoked DMR response (Fig. R1.4C). We next analyzed the coupling of CB_1R to $G\alpha_{q/11}$ in hippocampal extracts from adult $BiP^{+/-}$ (hereafter BiP-HET) and $BiP^{+/+}$ (hereafter BiP-WT) mice [Note that very early embryonic lethality occurs in $BiP^{-/-}$ mice (Luo *et al*, 2006).] In line with the aforementioned data from HEK-293T cells, CB_1R showed a preference for $G\alpha_{q/11}$ coupling in BiP-HET mice compared to their BiP-WT littermates (Fig. R1.4D).

G protein-dependent GPCR signaling often proceeds with β-arrestin binding and receptor internalization. Although BiP-IR did not compete markedly with β-arrestin-2 binding to CB_1R (Fig. R1.5A), by using cells expressing an *N*-terminally FLAG-tagged CB_1R (Kargl *et al*, 2012), we observed that prolonged incubation with WIN decreased cell-surface CB_1R (Fig. R1.5B), and this was prevented by BiP-IR overexpression. Under this experimental setting, CB_1R turned to be localized in early endosomes (as identified by the early endosome antigen 1, EEA1) with negligible trafficking to lysosomes (as identified by lysosomal-associated membrane protein 1, LAMP1) (Fig. R1.5C-D). Of note, CB_1R internalization to early endosomes was precluded by BiP-IR (Fig. R1.4B).

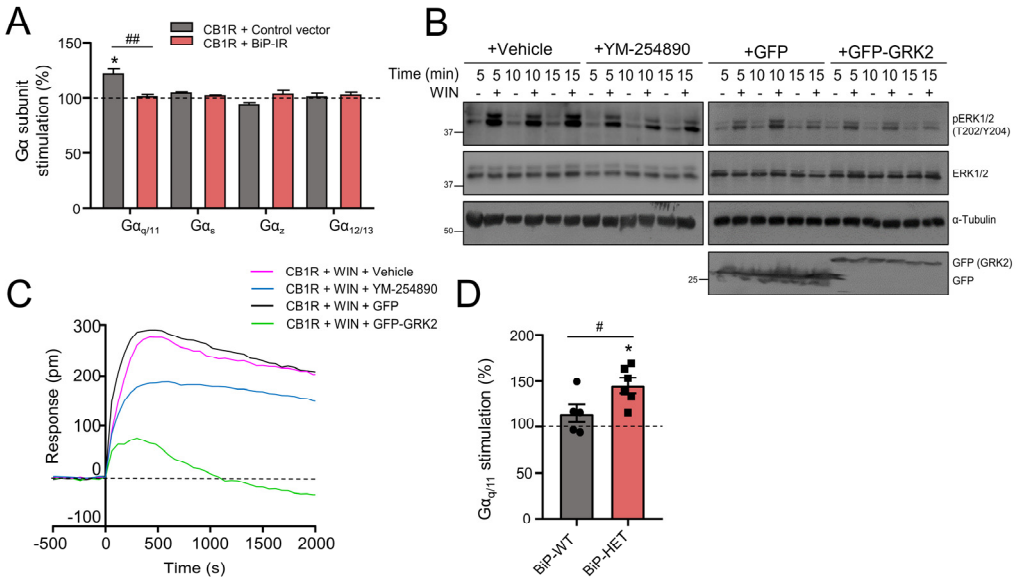

Figure R1.4. BiP modulates CB_1R-evoked signaling (II). ***A,*** Coupling of CB_1R to non-$G\alpha_{i/o}$ Gα proteins in membrane extracts from HEK-293T cells expressing CB_1R, together or not with BiP-IR. * $p < 0.05$ from basal (dashed line), or ## $p < 0.01$ from control vector; one-sample Student's *t*-test or unpaired Student's *t*-test, respectively (n = 3). ***B,*** Western blotting of phospho-ERK in HEK-293T cells expressing CB_1R, and incubated for 5, 10, or 15 min with vehicle or WIN55,212-2 (100 nM). Top, cells were preincubated for 30 min with vehicle or YM-254890 (1 μM). Bottom, cells coexpressed control vector (GFP) or $G\alpha_{q/11}$ dominant-negative vector (GFP-GRK2). A representative experiment is shown (n = 3). ***C,*** DMR experiments in HEK-293T cells expressing CB_1R under the same experimental conditions as in G. A representative experiment is shown (n = 3). ***D,*** Coupling of CB_1R to $G\alpha_{q/11}$ protein in hippocampal extracts from 3- to 4-month-old $BiP^{+/+}$ (BiP-WT) and $BiP^{+/-}$ (BiP-HET) mice. * $p < 0.05$ from basal (dashed line), or # $p < 0.05$ from BiP-WT group; one-sample Student's *t*-test or unpaired Student's *t*-test, respectively (n = 5 or 6 mice per group).

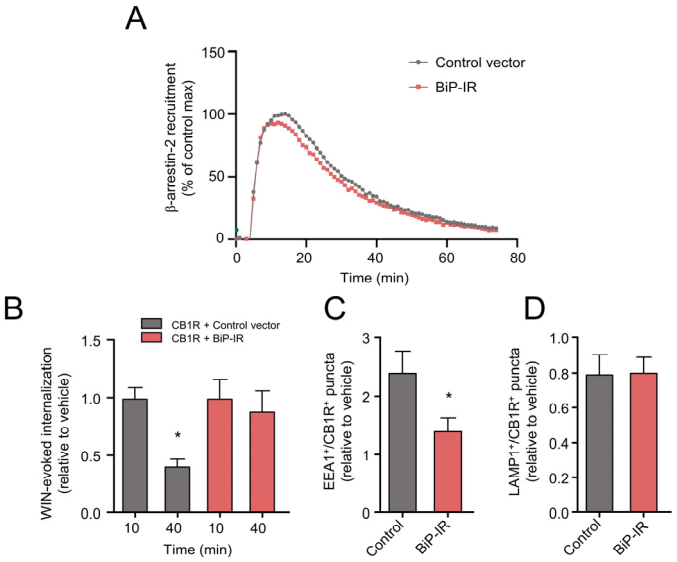

Figure R1.5. BiP prevents agonist-induced CB_1R internalization leaving β-arrestin-2 recruitment unaffected. ***A,*** β-arrestin-2 recruitment assay in HEK-293T cells expressing or not BiP-IR. ***B,*** HEK-293T-FLAG-CB_1R cells expressing or not BiP-IR were treated with WIN55,212-2 (100 nM) for 10 or 40 minutes. CB_1R internalization was calculated as ratio between superficial versus total CB_1R immunoreactivity (left panel). Internalized receptors colocalized with the early endosome marker EEA1 (***C***), but not with the lysosomal marker, LAMP1 (***D***).

Taken together, these data show that BiP-IR affects CB_1R-evoked signaling through the selective attenuation of an "alternative" $G\alpha_{q/11}$ protein-driven module, while leaving the "classical" $G\alpha_{i/o}$ protein-driven module essentially unaffected.

CB_1R-BiP complexes reside on GABAergic terminals of the mouse brain

It is well established that CB_1R resides largely on terminals of GABAergic neurons (Marsicano & Lutz, 1999; Katona & Freund, 2008). However, the precise neurochemical phenotype of BiP-expressing cells remains unclear (*cf*. Jin et al., 2018). Hence, we analyzed the expression of BiP mRNA in GABAergic *vs*. glutamatergic neurons by in situ hybridization histochemistry. BiP mRNA was localized throughout the mouse brain (Fig. R1.6A), showing a more ubiquitous expression pattern than CB_1R mRNA (Fig. R1.6B). Of note, nearly all the hippocampal high CB_1R mRNA-expressing cells were also positive for BiP mRNA (Figs. R1.6C and R1.6D). In the CA1/3 hippocampal areas, as reported for CB_1R mRNA (Marsicano and Lutz, 1999), BiP mRNA showed a high co-localization with GAD65/67 mRNA (Figs. R1.7A and R1.7B), while co-localization with vGluT1 mRNA was hardly detectable in the scattered BiP-expressing cells adjacent to the BiP/vGluT1 mRNA-enriched pyramidal cell layer (Figs. R1.7C and R1.7D). In the DG, the distribution of BiP mRNA between disseminated GAD65/67 mRNA-expressing neurons (Figs. R1.7A and R1.7B) and vGluT1 mRNA-expressing neurons (Figs. R1.7C and R1.7D) was more balanced, although again with a preference towards inhibitory cells.

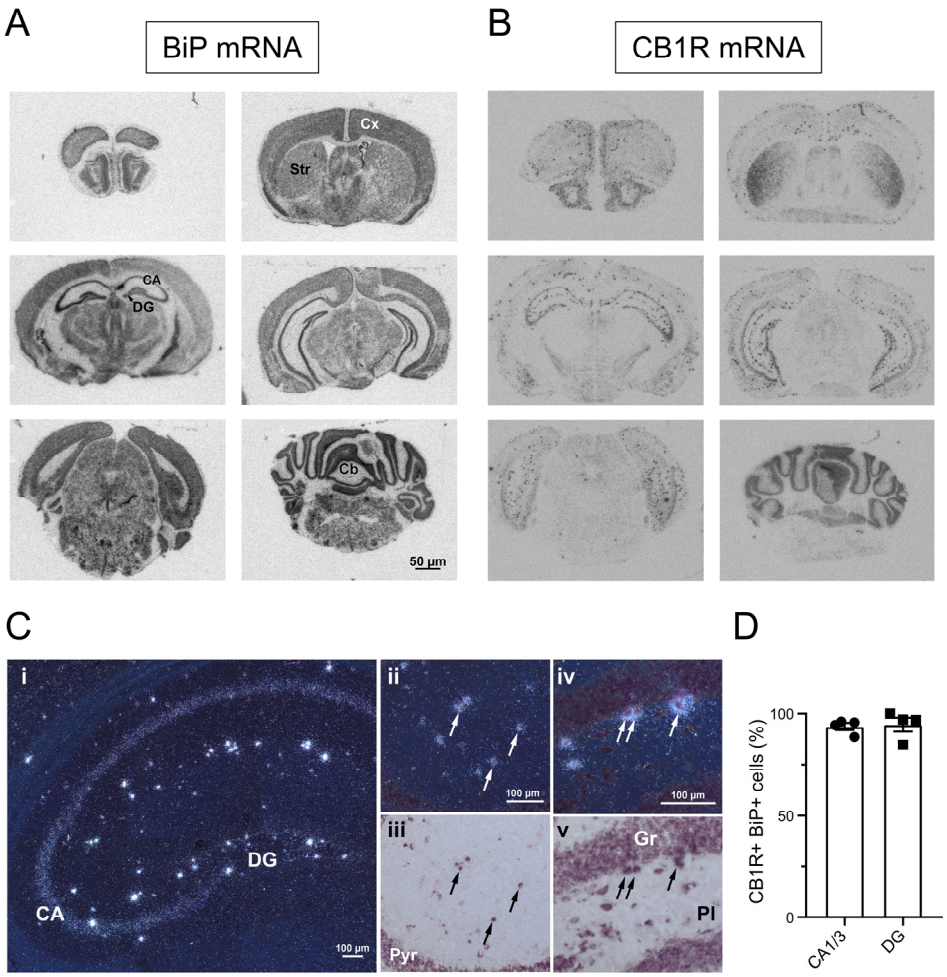

Figure R1.6. Expression of BiP and CB_1R mRNA in the mouse brain. ***A, B,*** Representative autoradiographic images of coronal sections from adult mouse brain showing the mRNA hybridization pattern of BiP (***A***) and CB_1R (***B***). CA, Cornu ammonis; DG, dentate gyrus; Str, striatum; Cx, cortex; Cb, cerebellum. ***C,*** Distribution of CB_1R mRNA in the mouse hippocampus. ***Ci,*** Representative dark field image from a section hybridized with ^{33}P-labeled oligonucleotide probes for CB_1R mRNA. A positive signal is evident as clusters/accumulation of bright silver grains. Note the moderate signal on the pyramidal cell layer of CA and the very intense signal on scattered cells in the various hippocampal layers. ***Cii, Ciii,*** Colocalization of CB_1R mRNA and BiP mRNA in cells of the stratum radiatum and stratum lacunosum moleculare of CA. Pyr, Pyramidal cell layer of CA. ***Civ, Cv***, Colocalization of

CB_1R mRNA and BiP mRNA in cells of the polymorphic layer (Pl). Gr, Granular cell layer. Sections were hybridized with ^{33}P-labeled probes for CB_1R mRNA (signal visualized as clusters of bright silver grains in dark field images) and with digoxigenin-labeled probes for BiP mRNA (signal visualized as dark precipitate in bright field images). Arrows point to some double-labeled cells. ***D,*** Quantification of CB_1R mRNA-positive cells that coexpress BiP mRNA (n = 4 mice per group).

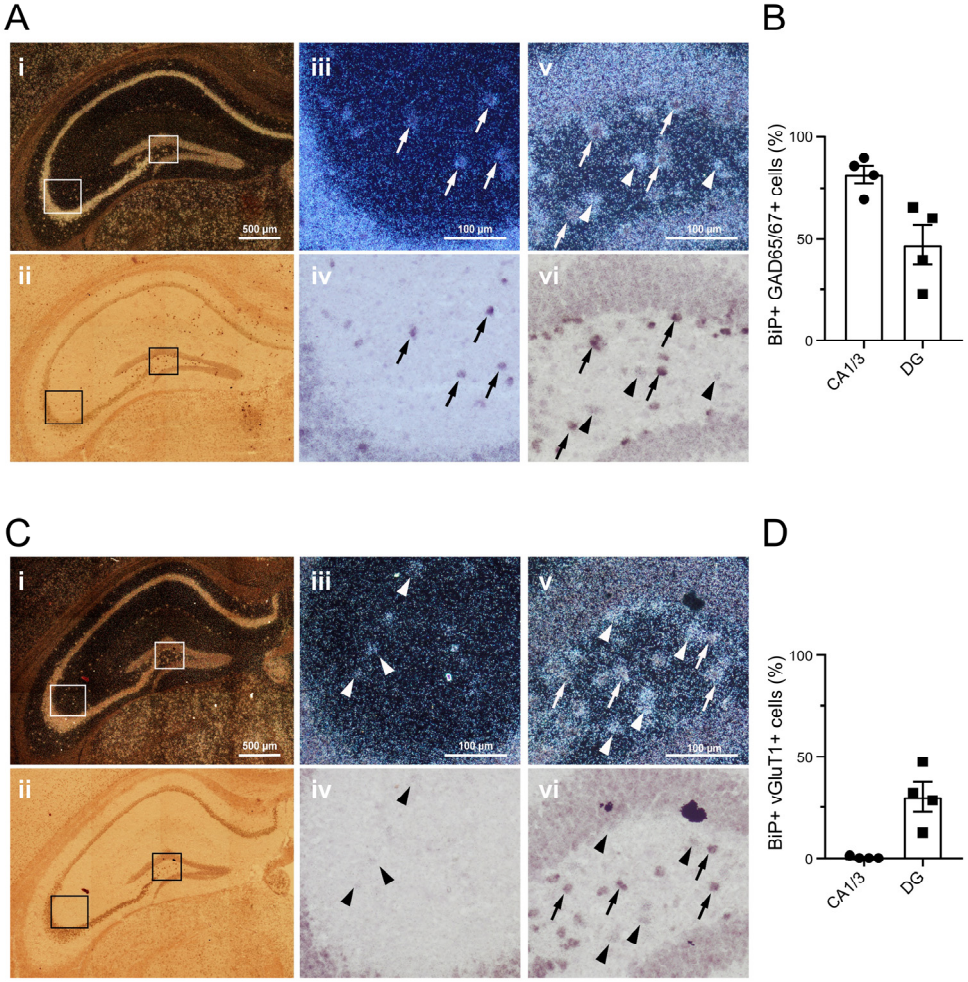

Figure R1.7. Colocalization of BiP mRNA with GAD65/67 or vGlut1 mRNA in the mouse hippocampus. ***A,*** Representative mosaic superimages of sections from the adult mouse hippocampus that were hybridized with ^{33}P-labeled probes for BiP mRNA (signal visualized as clusters/accumulation of bright silver grains in the dark field image ***Ai***) and with a mixture of digoxigenin-labeled probes for GAD65 and GAD67 mRNAs (labeled cells showing dark precipitate in the bright field image ***Aii***). Higher-magnification images of cornu ammonis (CA; ***Aiii, Aiv***) and dentate gyrus (DG; ***Av, Avi***) are shown. Arrows point to some double-labeled cells. Arrowheads point to some cells that express BiP mRNA but not GAD65/67 mRNA. ***B,*** Quantification of BiP mRNA-positive cells that coexpress GAD65/67 mRNA (n = 4 mice per group). ***C,*** Representative mosaic superimages of sections from the adult mouse hippocampus that were hybridized with ^{33}P-labeled probes for BiP mRNA (signal visualized as clusters/accumulation of bright silver grains in the dark field image ***Ci***) and with digoxigenin-labeled probes for vGluT1 mRNA (labeled cells showing dark precipitate in the bright field image ***Cii***). Higher-magnification images of CA (***Ciii, Civ***) and DG (***Cv, Cvi***) are shown. Arrows point to some double-labeled cells. Arrowheads point to some cells that express BiP mRNA but not vGluT1 mRNA. ***D,*** Quantification of BiP mRNA-positive cells that coexpress vGluT1 mRNA (n = 4 mice per group).

The most widely reported subcellular localization of BiP is the endoplasmic reticulum (ER) lumen, while CB_1R is largely located at the plasma membrane, and its CTD faces the cytoplasm since its biosynthesis starts on the ER. To assess this apparent inconsistency, we performed subcellular fractionation experiments in mouse brain samples. Analysis of hippocampal, striatal, and cortical tissue extracts showed that BiP is present not only in the ER but also in the cytosolic fraction (Figs. R1.8A and R1.8B). This observation supports the

notion that cytoplasmic BiP binds to CB_1R-CTD, and aligns with previous reports showing that not all BiP functions can be attributed to its interaction with ER-resident proteins (Belfi *et al*, 1999; Cha-Molstad *et al*, 2015; Shim *et al*, 2018; Anwar *et al*, 2021), and that a population of BiP molecules is found adjacent to the plasma membrane (Tsai *et al*, 2015). As the majority of CB_1R resides at the presynapse, where it controls neurotransmitter release (Piomelli, 2003), we also evaluated whether CB_1R-BiP complexes are present in this subcellular location. PLA analyses revealed a pronounced positive signal in synaptosomes from the hippocampus, striatum, and cortex of CB_1R-WT mice, but not of CB_1R-KO littermates (Fig. R1.8C).

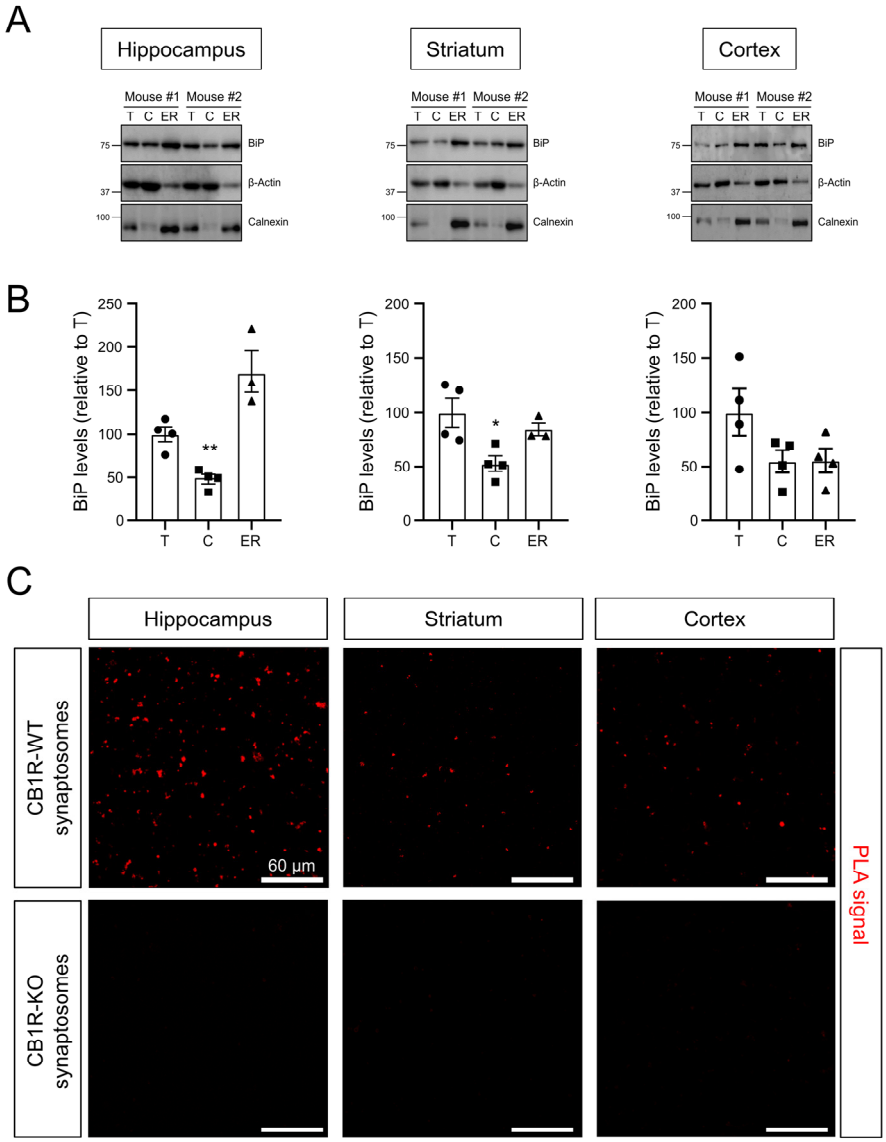

Figure R1.8. Subcellular localization of BiP in the mouse brain. ***A,*** Western blotting of BiP in total-extract (T), cytosolic (C), and ER fractions from the hippocampus, striatum, and cortex of 3- to 4-month-old WT mice. Calnexin was included as an ER-specific marker. Representative blots from 2 mice are shown. ***B,*** Quantification of BiP levels in the C and ER fractions relative to BiP levels in the T fraction. * $p < 0.05$, ** $p < 0.01$ from the corresponding ER fraction by one-way ANOVA with Tukey's multiple comparisons test (n = 3 or 4 mice per group). ***C,*** PLA experiments conducted on synaptosomal fractions isolated from the hippocampus, striatum, and cortex of 3- to 4-month-old CB_1R-WT and CB_1R-KO mice. Representative images of hippocampal (left column), striatal (middle column), and cortical (right column) synaptosomes, with CB_1R-BiP complexes depicted in red, are shown (n = 5 mice per group).

Next, to obtain a detailed neuroanatomical map of CB_1R-BiP protein complexes, we conducted in situ PLA assays on brain slices from various genetic mouse models of conditional loss or gain of CB_1R expression (Fig. R1.9A). We first used hippocampi from conditional CB_1R-KO models (Marsicano *et al*, 2002) (Figs. R1.9B, R1.9D, R1.9E and R1.9G). PLA experiments conducted on hippocampal sections from control adult $CB_1R^{floxed/floxed}$ (hereafter CB_1R-floxed) mice showed that 63.2 ± 4.7% and 62.9 ± 11.2% of the cells contained positive puncta in the DG and CA1, respectively. This signal was strongly reduced in sections from $CB_1R^{floxed/floxed;CMV\text{-}Cre}$ (hereafter CB_1R-KO) mice (DG: 14.8 ± 5.0%; CA1: 18.8 ± 4.5%). In conditional knockout mice in which the gene encoding CB_1R had been selectively deleted from forebrain GABAergic neurons ($CB_1R^{floxed/floxed;Dlx5/6\text{-}Cre}$ hereafter GABA-CB_1R-KO), we found a notable decrease in the percentage of cells expressing positive dots (DG: 31.9 ± 6.2%; CA1: 33.9 ± 7.8%). In contrast, sections from mice in which the gene encoding CB_1R had been selectively deleted from dorsal telencephalic glutamatergic neurons ($CB_1R^{floxed/floxed;Nex1\text{-}Cre}$ hereafter Glu-CB_1R-KO) displayed a similar pattern of PLA staining than their CB_1R-floxed counterparts (DG: 58.6 ± 5.9%; CA1: 60.8 ± 1.1%). Comparable overall data were obtained in sections from mouse striatum (Figs. R1.10B and R1.10D) and cortex (Figs. R1.10E and R1.10G).

We subsequently made use of a Cre-mediated, lineage-specific, CB_1R gene expression-rescue strategy from a CB_1R-null background (hereafter Stop-CB_1R mice) (De Salas-Quiroga *et al*, 2015; De Giacomo *et al*, 2020) (Figs. R1.9C, R1.9D, R1.9F and R1.9G). PLA assays in hippocampal sections from these mice showed, as expected, a marginal CB_1R-KO-like background signal (DG: 20.1 ± 3.2%, CA1: 21.2 ± 3.2%). In line with the data from conditional knockout mice, rescuing CB_1R gene expression in Stop-CB_1R mice with a constitutive Cre recombinase (Stop-$CB_1R^{EIIa\text{-}Cre}$, hereafter, CB_1R-RS) restored CB_1R-BiP complexes to the levels of control CB_1R-floxed mice (DG: 59.6 ± 5.5%, CA1: 58.5 ± 5.8%). This effect was paralleled in brain sections from conditionally-rescued Stop-$CB_1R^{Dlx5/6\text{-}Cre}$ (hereafter, GABA-CB_1R-RS) mice (DG: 58.1 ± 9.6%; CA1: 56.9 ± 5.5%), but not from conditionally-rescued Stop-$CB_1R^{Nex1\text{-}Cre}$ (hereafter, Glu-CB1R-RS) mice (DG: 21.1 ± 3.2%; CA1: 20.0 ± 2.5%). As in the aforementioned conditional knockout mouse experiments, these CB_1R gene expression-rescue data in the mouse hippocampus displayed a similar global pattern in the mouse striatum (Figs. R1.10C and R1.10D) and cortex (Figs. R1.10F and R1.10G).

Taken together, these data support the interaction between CB_1R and BiP in three key regions of the mouse brain, and, more specifically, a restricted occurrence of CB_1R-BiP complexes in GABAergic neurons.

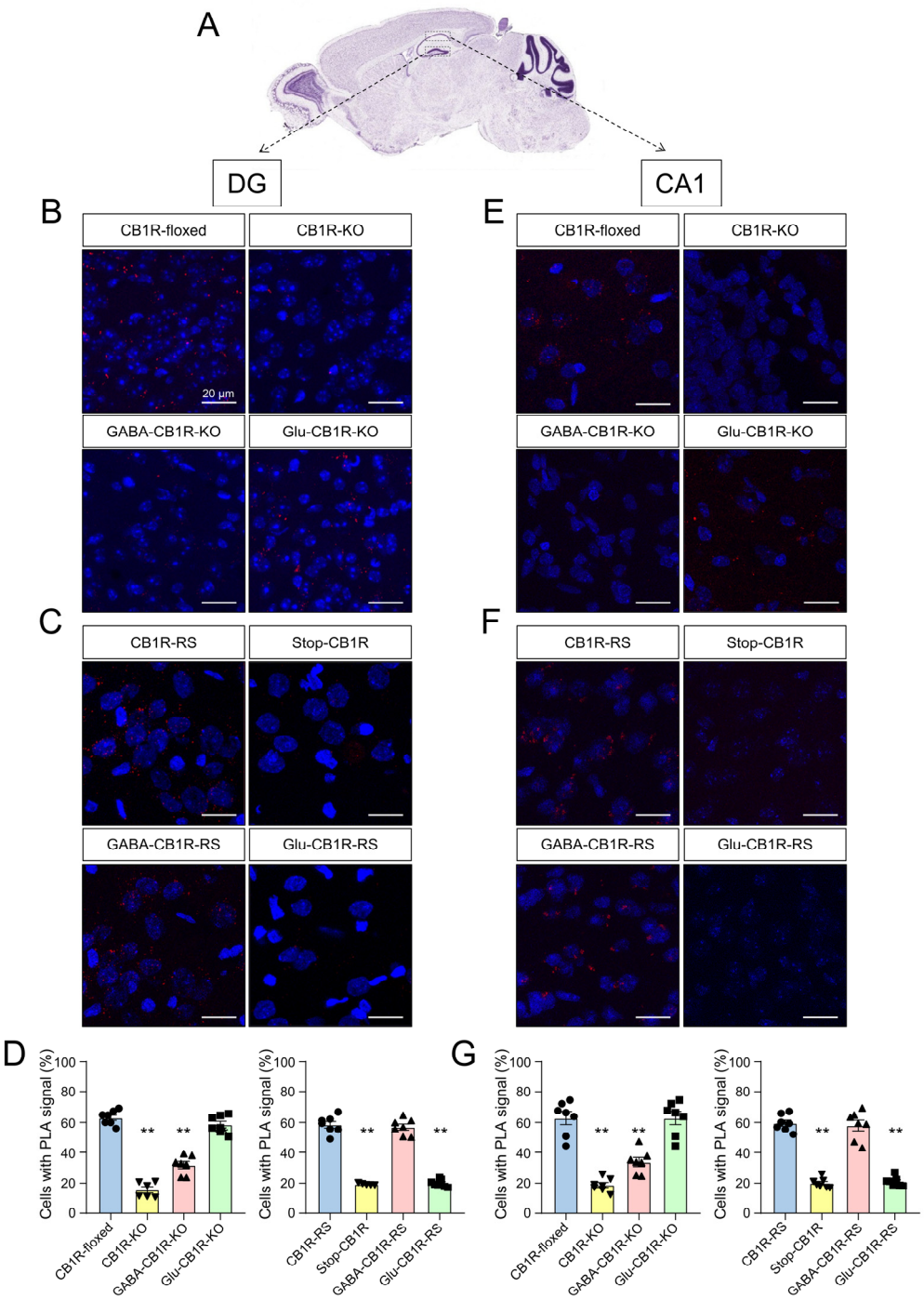

Figure R1.9. CB_1R-BiP complexes reside on GABAergic terminals of the mouse hippocampus. ***A,*** PLA experiments were conducted on hippocampal sections from 3- to 4-month-old mice of different genotypes. Representative low-magnification image and selected regions for analysis are shown. Image credit: Allen Institute. In the rest of the panels, CB_1R-BiP complexes are shown as red dots, and nuclei are colored in blue by DAPI staining. ***B,*** Representative images of dentate gyrus (DG) sections from CB_1R-floxed, CB_1R-KO, GABA-CB_1R-KO, and Glu-CB_1R-KO mice. ***C,*** Representative images of DG sections from Stop-CB_1R, CB_1R-RS, GABA-CB_1R-RS, and Glu-CB_1R-RS mice. ***D,*** Quantification of the number of cells containing one or more dots expressed as the percentage of the total number of cells (DAPI-stained nuclei) in DG sections. ** $p < 0.01$ from the corresponding CB_1R-floxed group or the corresponding CB_1R-RS group by one-way ANOVA with Tukey's multiple comparisons test (n = 6 or 7 fields from 3 different animals per group). ***E,*** Representative images of CA1 sections from CB_1R-floxed, CB_1R-KO, GABA-CB_1R-KO, and Glu-CB_1R-KO mice. ***F,*** Representative images of CA1 sections from Stop-CB_1R, CB_1R-RS, GABA-CB_1R-RS, and Glu-CB_1R-RS mice. ***G,*** Quantification of the number of cells containing one or more dots expressed as the percentage of the total number of cells (DAPI-stained nuclei) in CA1 sections. ** $p < 0.01$ from the corresponding CB_1R-floxed group or the corresponding CB_1R-RS group by one-way ANOVA with Tukey's multiple comparisons test (n = 6 or 7 fields from 3 different animals per group).

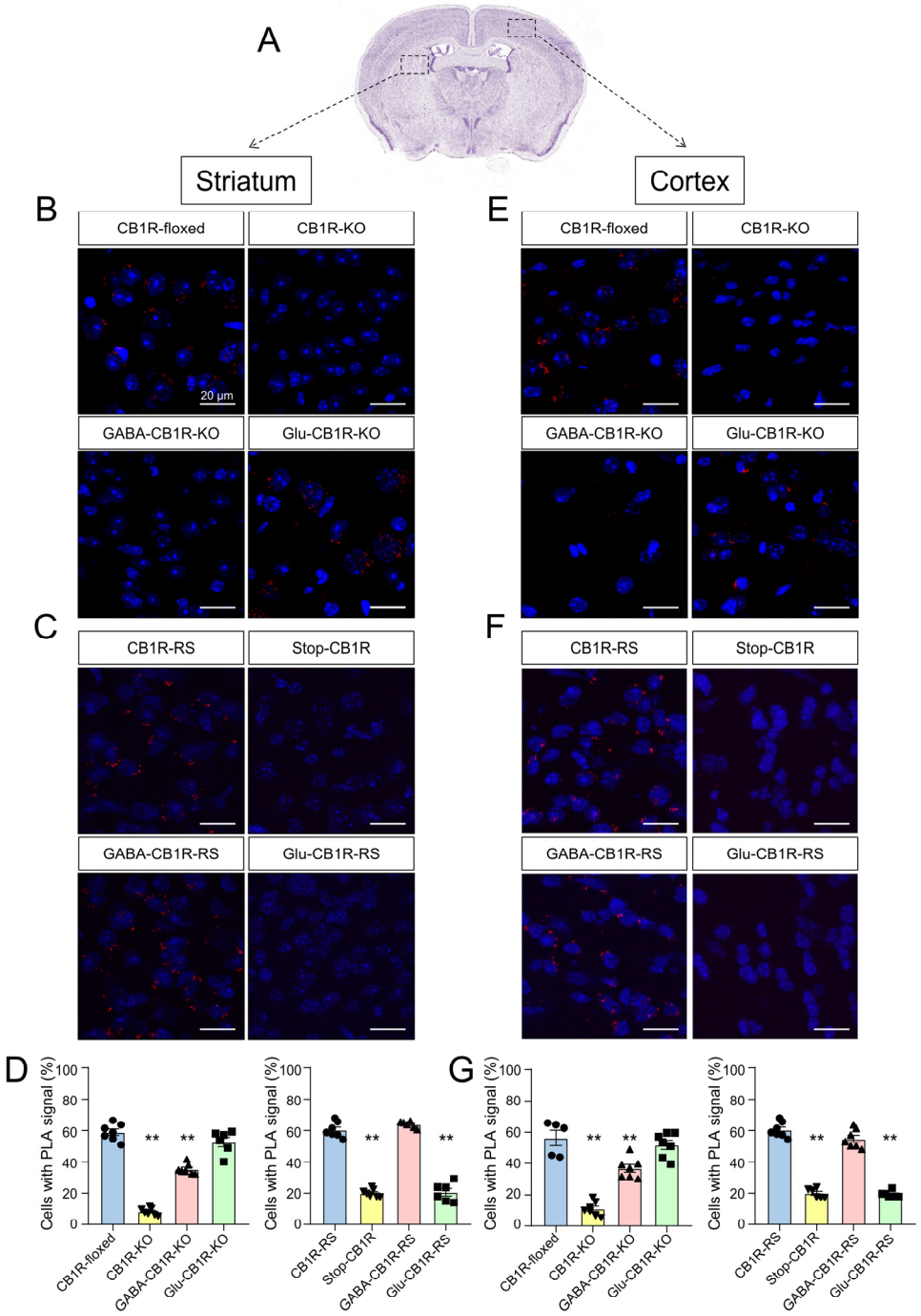

Figure R1.10. CB$_1$R-BiP complexes reside on GABAergic terminals of the mouse striatum and cortex. ***A,*** PLA experiments were conducted on striatal and cortical sections from 3- to 4-month-old mice of different genotypes. Representative low-magnification image and selected regions for analysis are shown. Image credit: Allen Institute. In the rest of the panels, CB$_1$R-BiP complexes are shown as red dots, and nuclei are colored in blue by DAPI staining. ***B,*** Representative images of striatal sections from CB$_1$R-floxed, CB$_1$R-KO, GABA-CB$_1$R-KO, and Glu-CB$_1$R-KO mice. ***C,*** Representative images of striatal sections from Stop-CB$_1$R, CB$_1$R-RS, GABA-CB$_1$R-RS, and Glu-CB$_1$R-RS mice. ***D,*** Quantification of the number of cells containing one or more dots expressed as the percentage of the total number of cells (DAPI-stained nuclei) in striatal sections. ** $p < 0.01$ from the corresponding CB$_1$R-floxed group or the corresponding CB$_1$R-RS group by one-way ANOVA with Tukey's multiple comparisons test (n = 6 or 7 fields from 3 different animals per group). ***E,*** Representative images of cortical sections from CB$_1$R-floxed, CB$_1$R-KO, GABA-CB$_1$R-KO, and Glu-CB$_1$R-KO mice. ***F,*** Representative images of cortical sections from Stop-CB$_1$R, CB$_1$R-RS, GABA-CB$_1$R-RS, and Glu-CB$_1$R-RS mice. ***G,*** Quantification of the number of cells containing one or more dots expressed as the percentage of the total number of cells (DAPI-stained nuclei) in cortical sections. ** $p < 0.01$ from the corresponding CB$_1$R-floxed group or the corresponding CB$_1$R-RS group by one-way ANOVA with Tukey's multiple comparisons test (n = 6 or 7 fields from 3 different animals per group).

BiP affects CB_1R function in vivo

THC induces numerous behavioral changes in laboratory animals and humans. The combination of hypolocomotion, analgesia, catalepsy, and hypothermia, usually designated as the "cannabinoid tetrad", has evolved as a powerful tool to identify pharmacological or genetic interventions that target CB_1R (Martin, 1986; Metna-Laurent *et al*, 2017). Previous studies have shown that these four behavioral traits rely selectively on the activation of CB_1R molecules located on various populations of glutamatergic or dopamine D_1 receptor-expressing projection neurons, but not on GABAergic interneurons, thus allowing a neurobiological correlate between CB_1R cellular expression and function (Monory *et al*, 2007; De Giacomo *et al*, 2020). We studied the "cannabinoid tetrad" in BiP-HET and BiP-WT littermates (Fig. R1.11A) and found that acute THC injection (10 mg/kg, i.p.) elicited the four archetypical effects of the "cannabinoid tetrad" to the same extent in BiP-HET and BiP-WT animals (Fig. R1.11B-E, left panels). In addition, following a 5-day sustained treatment, BiP-HET and BiP-WT mice developed a comparable tolerance to THC (Fig. R1.11B-E, right panels).

As the CB_1R-BiP complexes reside selectively on GABAergic neurons (see above), it is not surprising that the deletion of a BiP allele does not modify any of the classical "cannabinoid tetrad" behavioral traits. Of note, anxiety-like behaviors induced by cannabinoid intoxication have been shown to rely selectively on the activation of CB_1R molecules located on GABAergic interneurons (Rey *et al*, 2012; De Giacomo *et al*, 2020, 2021). Because the open-field test of the "cannabinoid tetrad" can also be used to define anxious phenotypes by evaluating the relative ambulation of the animals across the center of the arena (Seibenhener & Wooten, 2015), we conducted these analyses in our experimental setting. A single THC injection reduced the ambulation of the mice across the center of the arena equally in BiP-HET and BiP-WT mice (Fig. R1.12A, left panel). However, after a 5-day continuing THC treatment, the ambulation across the center of the arena remained lowered by acute THC in BiP-HET mice but not in their BiP-WT littermates (Fig. R1.12A, right panel).

To provide further support to the control of CB_1R-mediated anxiety by BiP, we used the elevated plus maze test, a widely recognized measure of anxiety that served originally to define the anxiogenic activity of the CB_1R pool located on GABAergic neurons (Rey *et al*, 2012). We injected BiP-WT and BiP-HET mice with vehicle or THC (10 mg/kg, i.p.), and found that the drug induced only an anxiogenic trend in BiP-WT mice but a significant anxiogenic effect in BiP-HET littermates, as evidenced by the decrease in both the number of entries (Fig. R1.12B, left panel) and the time of permanence (Fig. 1.12B, right panel) in the open arms of the device.

Taken together, these data support that BiP, by interacting with CB_1R on GABAergic neurons, modulates anxiety-like behaviors upon cannabinoid administration.

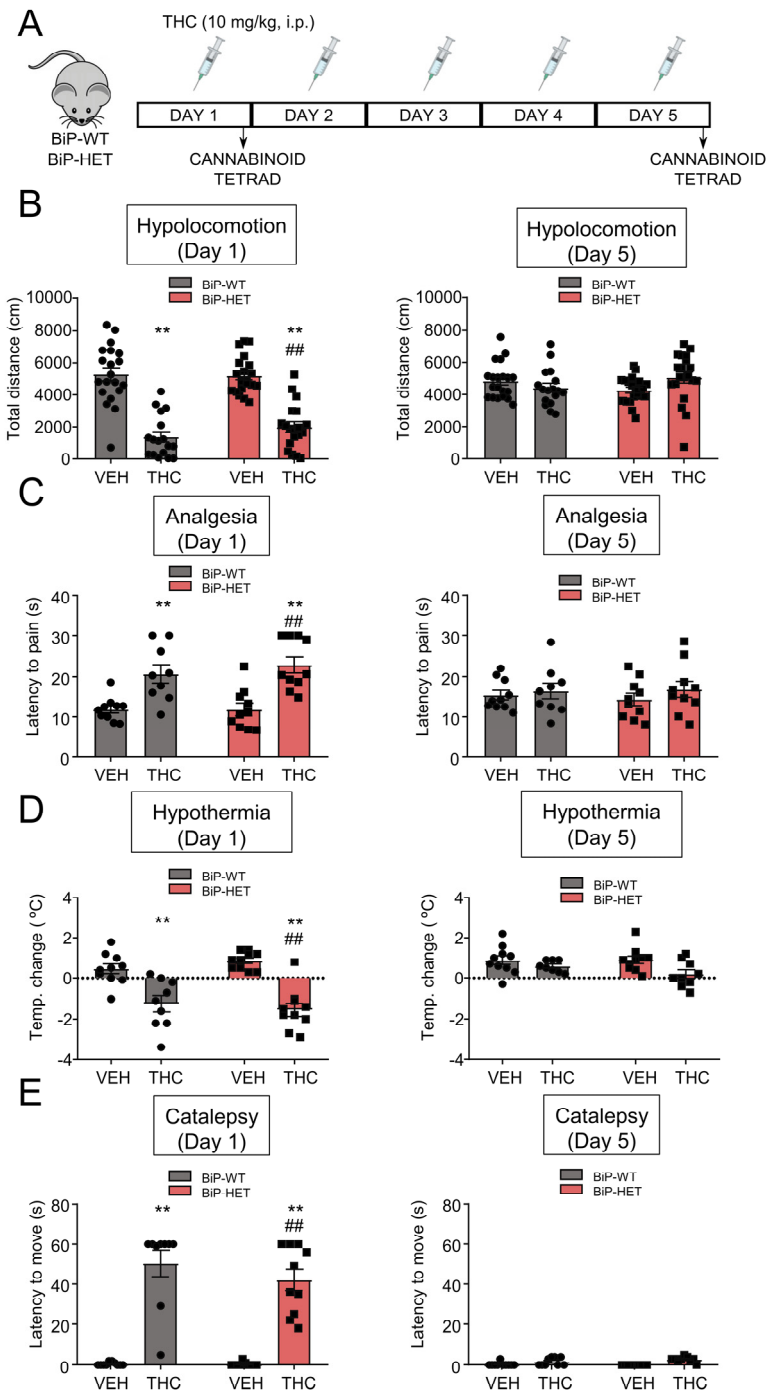

Figure R1.11. BiP does not affect CB_1R-evoked hypolocomotion, analgesia, hypothermia, and catalepsy *in vivo*. *A,* Scheme of the experiments. Vehicle or THC (10 mg/kg, 1 i.p. injection per day) was administered for 5 d to 3- to 4-month-old $BiP^{+/+}$ (BiP-WT) and $BiP^{+/-}$ (BiP-HET) mice. The "cannabinoid tetrad" was evaluated on days 1 and 5, starting 30 min after the corresponding acute-drug injections. ***B,*** Ambulation (total distance traveled, cm) in the open-field test on day 1 (left) and day 5 (right). ***C,*** Analgesia (latency to pain, s) in the hotplate test on day 1 (left) and day 5 (right). ***D,*** Hypothermia (change in body temperature, °C) as measured with a rectal thermometer on day 1 (left) and day 5 (right). ***E,*** Catalepsy (latency to move, s) as measured on a horizontal bar on day 1 (left) and day 5 (right). ***B-E:*** ** $p < 0.01$ from the corresponding vehicle group; ## $p < 0.01$ from the BiP-WT-vehicle group; two-way ANOVA with Tukey's multiple comparisons test (***B,*** n = 17-20 mice per group; ***C-E,*** n = 9 or 10 mice per group).

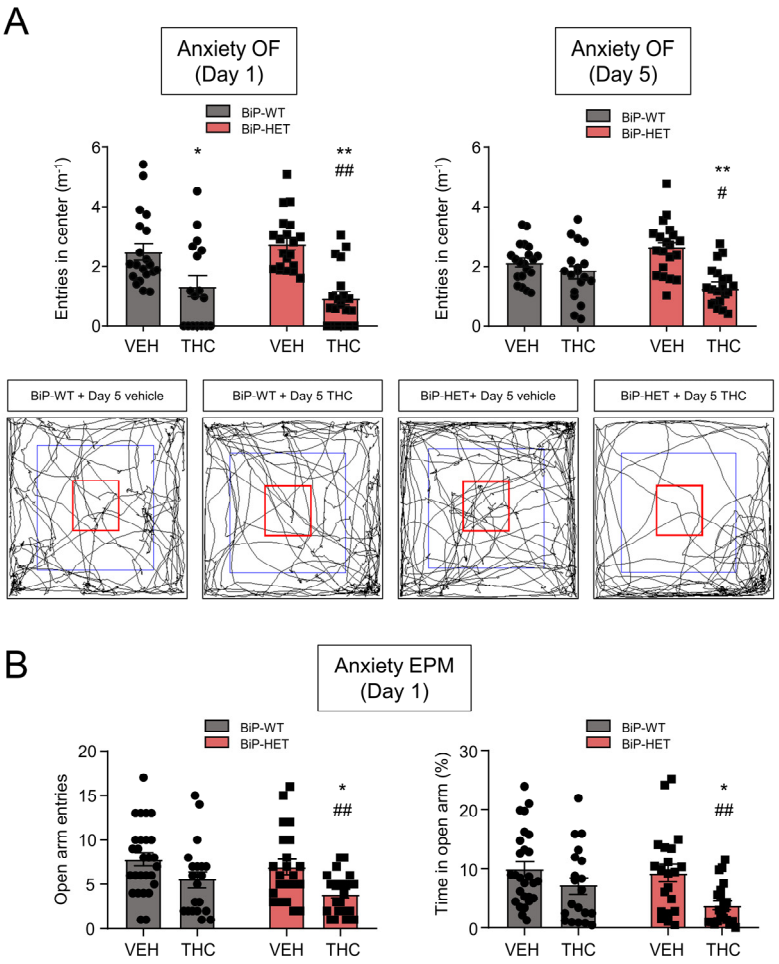

Figure R1.12. BiP modulates CB_1R-evoked anxiety *in vivo*. Anxiety-like behaviors were measured on an experimental scheme similar to that shown in Figure 9A. ***A,*** Anxiety (normalized entries in the center, m^{-1}) in the open-field (OF) test on day 1 (left) and day 5 (right). Arenas (with their centers outlined in red) illustrating the ambulation of a representative animal per group on day 5 are shown (bottom). ***B,*** Anxiety (left: number of entries in the open arms; right: time spent in the open arms, %) in the elevated plus maze (EPM) test on day 1. ***A, B***: * $p < 0.05$, ** $p < 0.01$ from the corresponding vehicle group, or # $p < 0.05$, ## $p < 0.01$ from the BiP-WT-vehicle group; two-way ANOVA with Tukey's multiple comparisons test (***A,*** n = 18-20 mice per group; ***B,*** n = 20-27 mice per group).

Results – Aim 2

Identification of CRBN as a CB_1R-interacting protein

To identify additional candidate proteins that interact with CB_1R, we designed an affinity-purification assay followed by a mass spectrometry proteomics protocol.

Initially, we set up the recombinant expression and subsequent purification of CB_1R-CTD (again, amino acids 408 to 472) in bacteria by using the expression vector pKLSLt (Merino-Gracia *et al*, 2016a), which uses lectin, a sugar-binding protein from the fungus *Laetiporus sulphureus*, as a purification tag, and allows the isolation of proteins based upon Sepharose 4B chromatography columns and a eluting lactose solution (Angulo *et al*, 2011). Once this purification was optimized, we saturated a column either with free lectin or lectin-CB_1R-CTD and loaded a whole-brain sheep homogenate onto it. After extensive washing, we eluted retained lectin or lectin-CB_1R-CTD and bound proteins with free lactose, collected fractions, and subjected those with higher protein content, measured by conventional spectroscopy, to proteomic evaluation (Fig. R2.1A). Following deep *in silico* analysis, which excluded proteins that bound free lectin, but also proteins common to this type of approaches by using the CRAPome database (https://reprint-apms.org/?q=chooseworkflow), we obtained a list of potential binding partners that comprised approximately 30 proteins (Table R2.1). Among the candidates, we decided to focus on cereblon (CRBN) for various reasons: *i)* Despite being a protein with high expression and known functions in the adult CNS, many of its neurobiological functions remain unsolved (Kim *et al*, 2016), *ii)* it is the pharmacological target of a controversial drug, namely thalidomide and its subsequent derivatives (IMiDs) which are currently used to treat several diseases (Ito *et al*, 2010), *iii)* a point mutation in human CRBN (R419X) causes a rare form of autosomal, non-syndromic, mild mental retardation (Higgins *et al*, 2004) and *iv)* although excluded after using the CRAPome database, DNA-damage binding protein 1 (DDB1), a known CRBN interactor (Ito *et al*, 2010; Fischer *et al*, 2014), was also identified in the experiment, which further strengthens the possibility of CRBN being present in the sample.

Accession identifier	Gene symbol	Score	Coverage	#Proteins	#Unique Peptides	#Peptides	#PSMs	#AAs	CRAPome database
Q63441	PLP1	2,7	16,4	26	1	1	1	67	0 / 411
E1BF13	KBTBD11	3,6	2,4	3	1	1	1	624	0 / 411
B5B0D4	PAEP	21,9	6,2	7	1	1	6	178	0 / 411
I3LTW2	GAP43	7,9	8,3	1	1	1	2	205	0 / 411
M3YD82	CNR1	71,2	9,5	28	2	2	16	411	0 / 411
I3LFP8	SLC6A11	4,4	12,9	1	1	1	1	132	0 / 411
F1SQ09	LUM	12,9	8,5	34	3	3	4	341	0 / 411
G5C004	PLA2R1	3,8	1,1	1	1	1	1	1393	0 / 411
F1SDF9	SV2A	4,5	1,8	7	1	1	1	742	0 / 411
F7AJ24	SLC7A13	0,0	5,2	1	1	1	1	481	0 / 411
L8HNF2	CRBN	15,0	9,0	43	3	3	4	444	0 / 411
Q9QX63	CRTAC1	4,0	7,3	47	1	1	1	193	0 / 411
Q60FB3	SMR3B	4,2	37,5	3	1	1	1	56	1 / 411
I3LAG0	FNTA	4,1	22,4	1	1	1	1	58	1 / 411
F5BZ34	MFGE8	3,5	3,4	20	1	1	1	294	1 / 411
F1S4D5	CCBL2	4,1	2,8	1	1	1	1	430	1 / 411
W5PDX4	NRXN2	0,0	2,8	1	1	1	1	1430	2 / 411
W5NV42	SRPX2	0,0	40,6	2	1	1	1	101	3 / 411
U6DIA1	CFB	5,3	7,8	44	1	1	1	206	3 / 411
I3LPF5	FBXO3	15,7	11,5	48	2	2	3	269	4 / 411
W5PNY4	PDXK	0,0	11,6	2	1	1	1	285	6 / 411
I3LIW1	LANCL2	44,2	17,2	42	7	7	12	412	9 / 411
F6Y9D4	ATP2B1	3,4	8,7	252	1	1	1	127	12 / 411
K7EBP8	MAPK1	3,2	6,0	106	1	1	1	150	15 / 411
P82317	DEFA1B	3,0	30,0	11	1	1	1	30	23 / 411
G9KG48	PFKM	3,3	2,3	40	1	1	1	482	30 / 411
P00432	CAT	2,7	1,7	1	1	1	1	527	37 / 411
A9RA89	SERPINB12	4,5	8,7	18	1	1	1	183	37 / 411
S9XN82	DDB1	36,5	5,4	60	4	4	8	1091	103 / 411

Table R2.1. Potential CB_1R binding partners. Several peptides corresponding to > 60 proteins were identified in the screening after identity comparison across mammalian genomes**.** Putative false positives were discarded using the CRAPome database. PSMs: Number of times that peptides have been detected in the MS/MS spectrometer. AAs: Number of amino acids in the protein.

Box 4 – Discovery of CRBN

Cereblon (CRBN) was originally discovered in 2004 as a gene responsible for an **autosomal recessive non-syndromic form of mental retardation (ARNSMR)** (Higgins *et al*, 2004). Patients that suffer from ARNSMR show intelligence quotient values that range from 50 to 70 but do not display congenital anomalies or dysmorphic features. This disorder had been previously found in an American family whose origins traced back to southwest Germany, and mapped to a loci in chromosome 3 (Higgins *et al*, 2000). CRBN is a 442-amino acid long protein encoded at chromosome 3 in humans and highly expressed in the brain. Individuals affected by ARNSMR harbor a mutation that causes the appearance of a **premature stop codon at amino acid 419 (R419X).** Nonetheless, no further efforts were made at that time to identify molecular mechanism(s) underlying this mutation.

CRBN drew back much attention when a pioneer study identified this protein as the pharmacological target of thalidomide, a teratogenic drug prescribed to pregnant women that affected thousands of children with severe malformations in the last century and was withdrawn from the market. The authors found that **CRBN establishes a E3-ubiquitin ligase complex with the proteins Cullin4A/B, DNA-damage binding protein 1 (DDB1) and Ring box protein 1 (Rbx1/Roc1) ($CRL4^{CRBN}$)** where it acts as a substrate recognition component, and proposed that thalidomide inhibits ubiquitin ligase function (Ito *et al*, 2010). Although this notion has been further expanded (see next box), this finding laid the ground for structural and mechanistical studies of CRBN function, and only a few years later, the structure of the DDB1-CRBN complex bound to thalidomide was reported (Fischer *et al*, 2014) (Fig. Box-3)

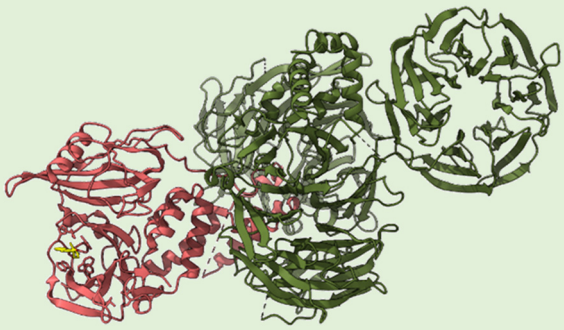

Figure Box-3. Three-dimensional structure of chicken CRBN-DDB1 complex bound to thalidomide. CRBN is shown in red, DDB1 is depicted in green, and the thalidomide molecule is yellow-colored Image was created using ChimeraX (UCSF®) and Protein Data Bank accession number *4ci1*.

To validate the molecular interaction between CB_1R and CRBN, we designed a series of experimental approaches. First, we recombinantly expressed and purified CRBN and found that it bound with high affinity to purified 5-IAF-CB_1R-CTD in solution in a fluorescence polarization-based assay (Fig. R2.1B). Second, co-immunoprecipitation experiments using a set of CB_1R-CTD deletion mutants in HEK-293T allowed us to allocate the CRBN binding site to a 11-amino acid stretch of the CB_1R-CTD cells (Fig. R2.1C). Third, PLA and co-immunoprecipitation experiments showed that both native proteins interact in this same cellular system (Figs. R2.1D and R2.1E). Finally, incubation of the cells with thalidomide, lenalidomide or pomalidomide, three drugs that target CRBN, prevented complex formation by approximately ~35% in all cases (Fig. R2.1F).

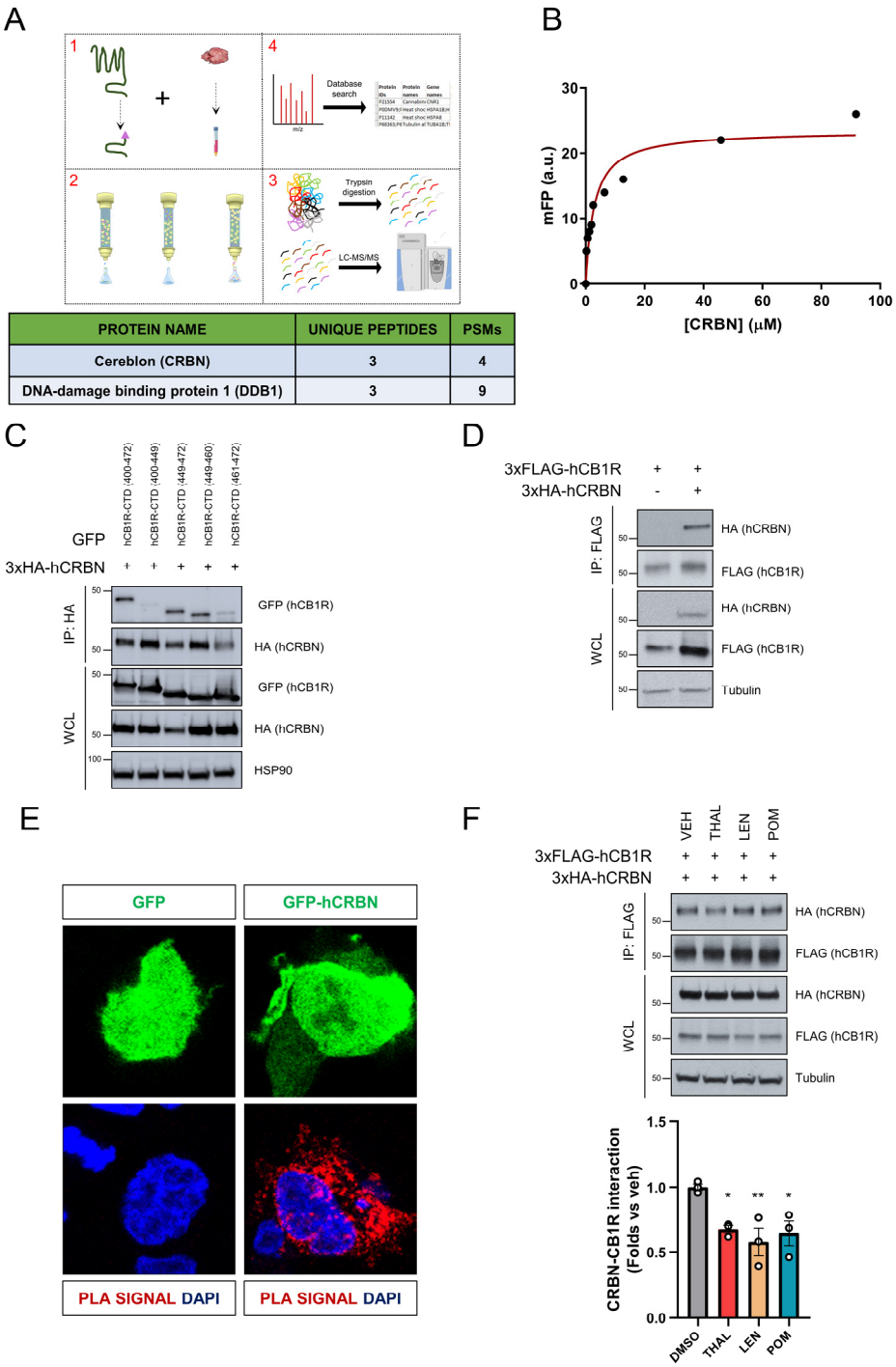

PROTEIN NAME	UNIQUE PEPTIDES	PSMs
Cereblon (CRBN)	3	4
DNA-damage binding protein 1 (DDB1)	3	9

Figure R2.1. CRBN interacts with CB$_1$R *in vitro*. ***A,*** Scheme of the proteomic experiment using CB$_1$R-CTD (amino acids 408-472) and a sheep brain homogenate. CRBN and DDB1 were identified in the MS/MS experiment. ***B,*** Fluorescence polarization-based protein-protein binding experiments using 5-IAF-labeled CB$_1$R-CTD and increasing amounts of unlabeled CRBN. A representative experiment is shown (n = 3). ***C,*** Co-immunoprecipitation experiments in HEK-293T cells expressing fragments of GFP-hCB$_1$R-CTD and 3xHA-hCRBN. Immunoprecipitation (IP) was conducted with anti-HA antibody. WCL: whole-cell lysate. A representative experiment is shown (n = 3). ***D,*** Co-immunoprecipitation experiments in HEK-293T cells expressing 3xFLAG-hCB$_1$R and 3xHA-hCRBN. IP was conducted with anti-FLAG M2 agarose. A representative experiment is shown (n = 3). ***E,*** Proximity ligation assay in HEK-293T cells expressing GFP-hCRBN and hCB$_1$R-myc. A representative experiment is shown (n = 3). ***F,*** Co-immunoprecipitation experiments in HEK-293T cells expressing 3xFLAG-hCB$_1$R and 3xHA-hCRBN incubated with vehicle, 100 μM thalidomide (THAL), 10 μM lenalidomide (LEN) or 2 μM pomalidomide (POM). IP was conducted with anti-FLAG M2 agarose. A representative experiment (upper panel) and the quantification (lower panel) are shown. * $p < 0.05$, ** $p < 0.01$ from control vector by one-way ANOVA with Tukey's multiple comparisons test (n = 3).

Box 5 – Cereblon, ubiquitination and IMiDs

CRBN is the substrate recognition component of the $CRL4^{CRBN}$ complex. This macromolecular assembly facilitates ubiquitination of target proteins. **Ubiquitination** is a post-translational modification that consists of the **covalent bondage of a ubiquitin protein to a lysine residue of a target protein** by the sequential action of **three enzymes: the E1-activating enzyme, the E2-conjugating enzyme and the E3-ligase enzyme** (Hershko & Ciechanover, 1998). Mammalian cells display > 600 ubiquitin E3-ligases, which allow for selective substrate targeting (Berndsen & Wolberger, 2014). Classically, ubiquitin was considered as a tag for protein degradation by the 26S proteasome (Ciechanover, 2015), but this dogma has changed enormously, and now it is widely accepted that ubiquitin tagging exerts a plethora of functions, including protein degradation, signaling or trafficking (Akutsu *et al*, 2016; Mattern *et al*, 2019).

As mentioned above, CRBN is the molecular target of thalidomide. Thalidomide and other CRBN-targeting, derivative drugs (*e.g.,* lenalidomide, pomalidomide) are widely known as **immunomodulatory drugs (IMiDs)** and are currently used for the treatment of various malignancies, including multiple myeloma (Kim *et al*, 2016). Initially, these drugs were considered $CRL4^{CRBN}$ inhibitors, since CRBN autoubiquitination was prevented by thalidomide treatment (Ito *et al*, 2010), but this notion was challenged by the fact that IMiDs induced, rather than prevented, ubiquitination and degradation of the transcription factors Ikaros (IKZF1) and Aiolos (IKZF3) in tumoral lymphoid cells (Lu *et al*, 2014; Krönke *et al*, 2014). Quite shockingly, these proteins do not represent endogenous substrates of CRBN. To complicate things even more, it has been found that the ubiquitination of a given substrate is IMiD-specific. For example, casein kinase 1 α is ubiquitinated in the presence of lenalidomide, but not thalidomide (Krönke *et al*, 2015). Combining these findings with studies that show IMiD-dependent diminished ubiquitination of other CRBN substrates (Tao *et al*, 2018) a complex system comes out where these drugs can bias CRBN function by displacing endogenous substrates and favoring 'neo-substrates', in a drug-specific manner (Kim *et al*, 2021a).

The molecular architecture of CRBN comprises an *N*-terminal domain (residues 1-185, chicken protein numbering) that consists of a seven-stranded β-sheet, a DDB1-binding domain formed by seven α-helices (residues 186-317) and a *C*-terminal domain composed of eight β-sheets (residues 318-445) (Fischer *et al*, 2014) (Box 4). To date, known CRBN substrates bind distinct portions of the protein and show differential sensitivity towards CRBN-mediated ubiquitination and/or to IMiDs treatments (Tao *et al*, 2018), issues that together support the notion that specific interacting regions influence CRBN biological function on given substrates. To identify which region/s of CRBN bind CB_1R, we performed co-immunoprecipitation experiments using several CRBN chimeras, and found that both the *N*-terminus and the *C*-terminus regions of CRBN are involved in CB_1R binding (Figs. R2.2A and R2.2B). In this context, it is worth mentioning that a previous study had proposed that amino acids 119-255 of the rat CRBN protein -partially overlapping with the DDB1-binding site-, harbor a regulators of G-protein-like (RGS) domain (Jo *et al*, 2005). We conducted an i*n silico* modelling with the RGS domains of RGS4 and GRK2, two proteins that have been linked to CB_1R function (Bosier *et al*, 2015; Dalton *et al*, 2020), and one published CRBN structure (Nowak *et al*, 2018), and noticed a very similar fold (Fig. R2.2C). We made use of a mutant that lacks this putative domain (CRBN-ΔRGS) and found that, despite retaining the ability of binding CB_1R (Fig. R2.2A), this modified form was unable to associate with DDB1, thus rendering a ubiquitin-ligase dominant-negative CRBN, which is a very valuable tool to

discriminate between CUL4A-mediated and non-CUL4A-mediated effects on CB_1R (Fig. R2.2D).

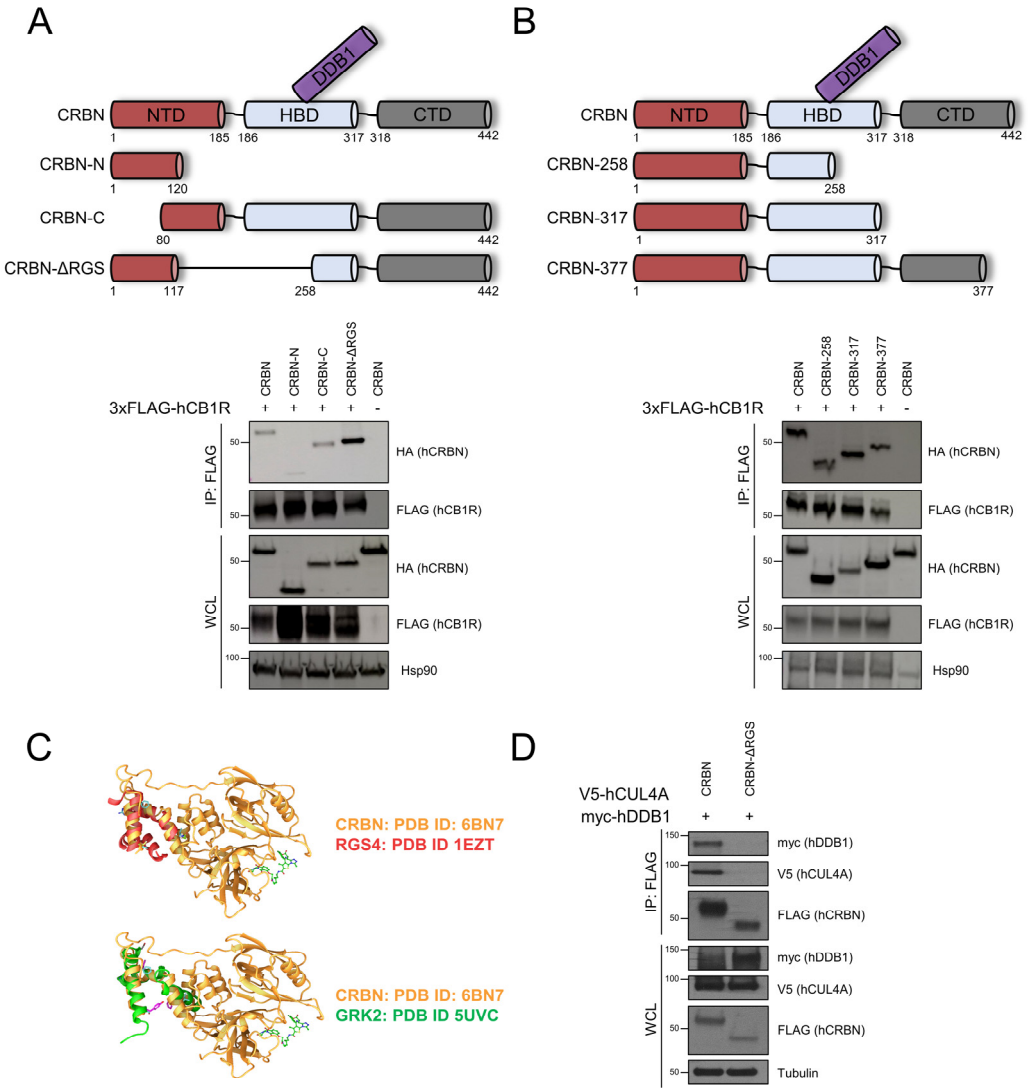

Figure R2.2. Different regions of CRBN bind CB_1R. ***A,*** Co-immunoprecipitation experiments in HEK-293T cells expressing fragments of 3xHA-hCRBN and 3xFLAG-hCB_1R. Immunoprecipitation (IP) was conducted with anti-FLAG M2 agarose. WCL: whole-cell lysate. A representative experiment is shown (n = 3). ***B,*** Co-immunoprecipitation experiments in HEK-293T cells expressing fragments of 3xHA-hCRBN and 3xFLAG-hCB_1R. Immunoprecipitation (IP) was conducted with anti-FLAG M2 agarose. WCL: whole-cell lysate. A representative experiment is shown (n = 3). ***C,*** Structural comparison of the putative RGS domain of hCRBN with the RGS domains of rRGS4 (upper panel) or hGRK2 (lower panel). ***D,*** Co-immunoprecipitation experiments in HEK-293T cells expressing 3xFLAG-hCRBN or 3xFLAG-hCRBN-ΔRGS together with V5-hCUL4A and myc-tagged hDDB1. Immunoprecipitation (IP) was conducted with anti-FLAG M2 agarose. WCL: whole-cell lysate. A representative experiment is shown (n = 3).

CRBN modulates CB_1R-evoked signaling

We first employed DMR assays to assess the action of CRBN on CB_1R global signaling profile in HEK-293T cells, and found that CRBN partially inhibited WIN55,212-2-induced CB_1R activation. Of note, CRIP1a, a *bona fide* CB_1R-interacting protein exerted an inhibition of similar extent (Fig. R2.3A). To dissect in detail which molecular pathways are affected by CRBN overexpression, we first studied the canonical inhibition of cAMP production triggered by $G\alpha_{i/o}$ protein coupling to CB_1R. CRBN overexpression diminished the WIN55,212-2-evoked reduction of forskolin-augmented cAMP concentration in a dose-

dependent manner (Fig. R2.3B). This effect was also evident when using a different CB_1R agonist, specifically CP-55,940 (Fig. R2.3C). This inhibition did not extend to other pathways, activated by CB_1R, as CRBN overexpression did not attenuate CB_1R-induced ERK activation (Fig. R2.3D). CRBN forms part of a large ubiquitin E3 ligase complex. Thus, CRBN-mediated CB_1R ubiquitination comes as a straight-forward hypothesis to explain the observed reduction in receptor signaling. Nonetheless, neither CRBN overexpression, nor CRBN knockdown with 2 independent siRNAs influenced CB_1R basal ubiquitination in heterologous cells, although a trend towards increased CB_1R protein levels upon CRBN silencing was observed (Figs. R2.3E and R2.3F).

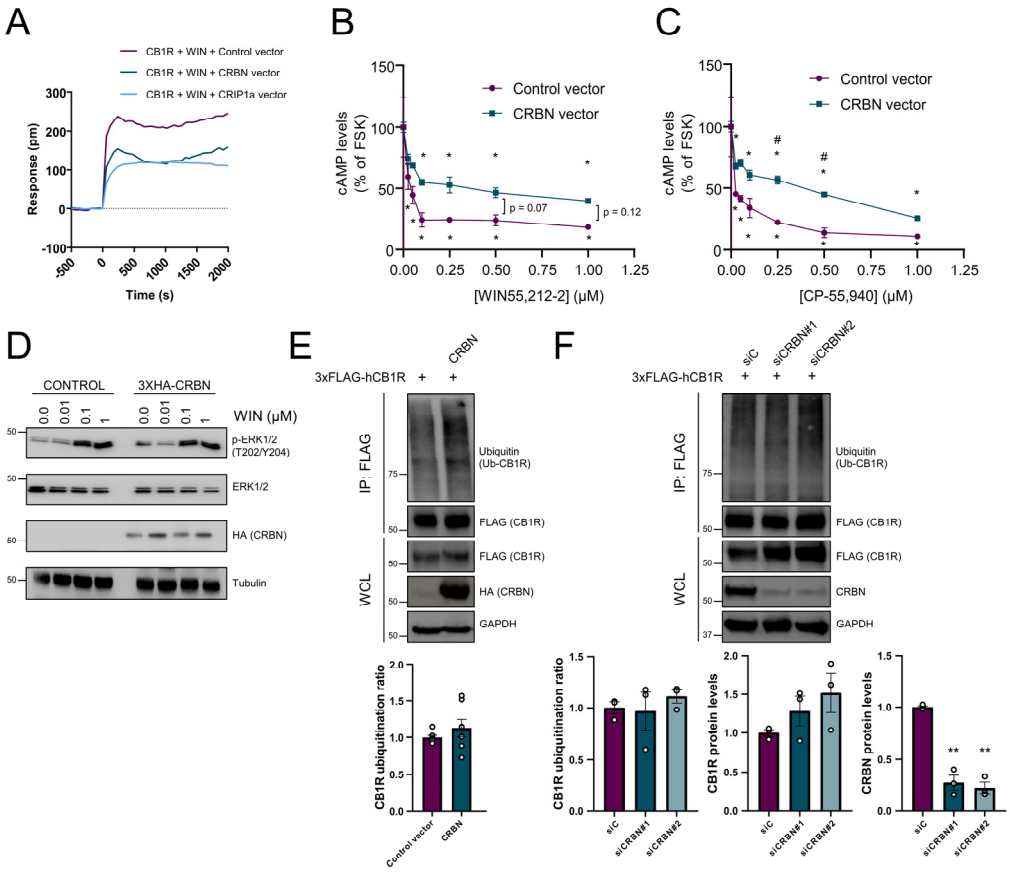

Figure R2.3. BiP modulates CB_1R-evoked signaling. A, DMR experiments in HEK-293T cells expressing hCB_1R, together or not with hCRBN or hCRIP1a, and incubated with WIN55,212-2 (100 nM). A representative experiment is shown (n = 3). **B,** cAMP concentration in HEK-293T cells expressing hCB_1R, together or not with hCRBN. Cells were incubated first for 15 min with vehicle or WIN55,212-2 (doses ranging from 25 to 1000 nM), and then for 15 min with forskolin (FSK; 500 nM). * $p < 0.05$ from vehicle, or # $p < 0.05$ from paired control, by two-way ANOVA with *Tukey's* multiple comparisons test (n = 3). ***C,*** cAMP concentration in HEK-293T cells expressing CB_1R, together or not with CRBN. Cells were incubated first for 15 min with vehicle or CP-55,940 (doses ranging from 25 to 1000 nM), and then for 15 min with forskolin (FSK; 500 nM). * $p < 0.05$ from vehicle, or # $p < 0.05$ from paired control, by two-way ANOVA with Tukey's multiple comparisons test. ***D,*** HEK-293T cells expressing 3xFLAG-hCB_1R, together or not with 3xHA-hCRBN, were incubated for 10 min with vehicle or WIN55,212-2 (doses ranging from 10 to 1000 nM), and cell extracts were blotted for ERK phosphorylation. A representative experiment is shown (n = 3). ***E,*** Basal hCB_1R ubiquitination is not affected by hCRBN overexpression. Immunoprecipitation (IP) was conducted with anti-FLAG M2 agarose. WCL: whole-cell lysate. A representative experiment is shown (n = 7). ***F,*** Basal hCB_1R ubiquitination is not affected by hCRBN knockdown. Immunoprecipitation (IP) was conducted with anti-FLAG M2 agarose. WCL: whole-cell lysate. A representative experiment is shown (n = 3). ** $p < 0.01$ from siControl condition, by one-way ANOVA with Tukey's multiple comparisons test.

Generation of CRBN loss-of-function mouse models

Our *in vitro* findings demonstrate that CRBN selectively inhibits CB_1R action on the cAMP pathway. Hence, we aimed to develop CRBN loss-of-function mouse models to study how CRBN deficiency impacts CB_1R action *in vivo*. For this purpose we made use of the *Cre-LoxP* technology, and back-crossed mice carrying *LoxP* sites flanking alleles 3 and 4 of the *CRBN* gene (Rajadhyaksha *et al*, 2012) (hereafter, CRBN-floxed) with mice expressing the Cre recombinase under the control of different promoters. This allowed us to generate a full knockout model (hereafter CRBN-KO), by using the CMV-Cre mouse (Schwenk *et al*, 1995), which expresses the recombinase in the germline, and two conditional mouse models, where CRBN is absent in dorsal telencephalic glutamatergic neurons, by using the Nex1-Cre mouse (hereafter, Glu-CRBN-KO) (Schwab *et al*, 2000), or forebrain GABAergic neurons, by using the Dlx5/6-Cre mouse (hereafter, GABA-CRBN-KO) (Monory *et al*, 2006) (Fig. R2.4A). All three mouse strains were viable and fertile, showed normal body parameters, such as weight and temperature and did not display any gross physical alteration (Figs. R2.4B and R2.4C).

To analyze recombination, first we used Q-PCR, and found that *CRBN* mRNA was totally absent in CRBN-KO mice in every tissue analyzed, which included peripheral organs with high CRBN expression (Xin *et al*, 2008) (Figs. R2.5A and R2.6A), while only region-specific differences were found in the brain of conditional knockout models (Fig. R2.7A and R2.8A). We validated these results by using western blotting. Again, CRBN-KO mice showed undetectable levels of CRBN in every tissue analyzed (Figs. R2.5B and R2.6B). Glu-CRBN-KO mice, consistently with the Q-PCR results, displayed drastic decreases of protein level in the cortex and hippocampus, and a trend to lower CRBN expression in striatum, while other regions that do not express Cre-recombinase under the Nex1 promoter, as the cerebellum, were unaffected (Fig. R2.7B). In contrast, GABA-CRBN-KO mice showed a 50% reduction in striatal CRBN levels, and just a trend towards a lower expression in cortex, while hippocampal and cerebellar CRBN levels remained unchanged (Fig. R2.8B). Again, this was in line with the Q-PCR data. Taken together, these data indicates that CRBN expression occurs predominantly in glutamatergic neurons of the hippocampus and cortex, whereas in striatum, the expression seems more balanced between excitatory and inhibitory neuron subtypes.

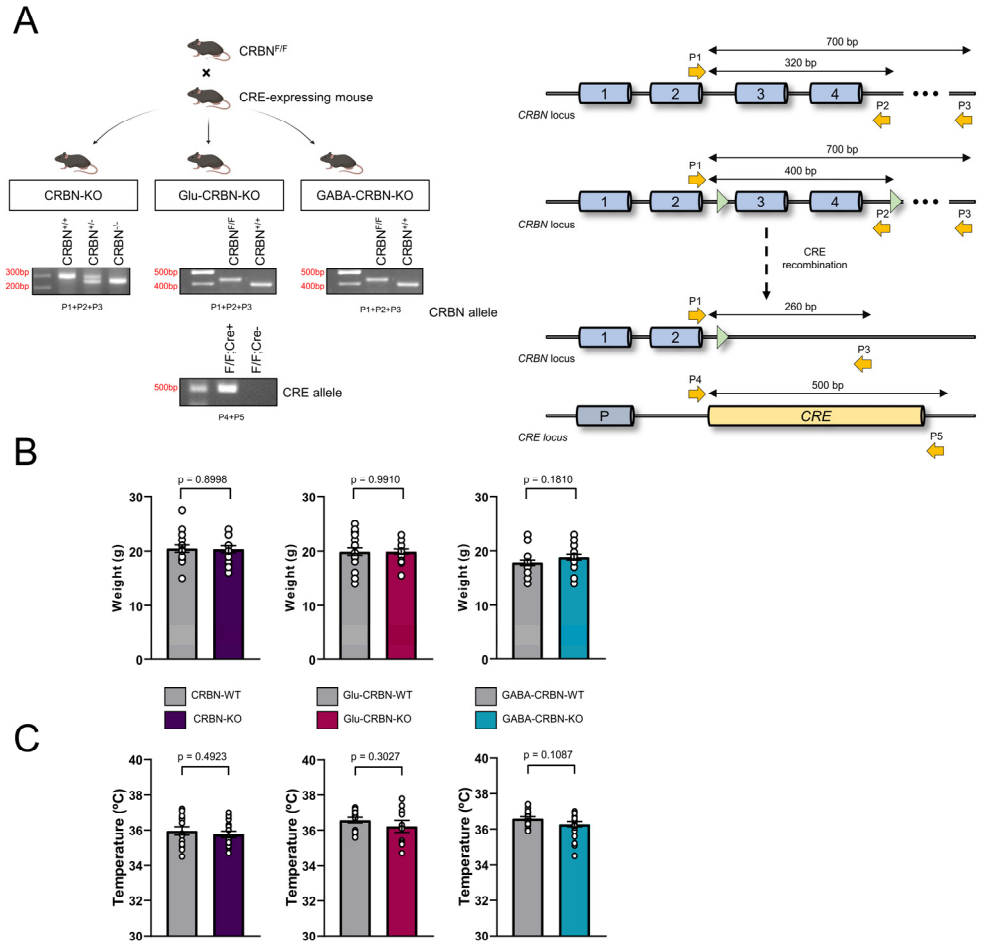

Figure R2.4. Generation of conditional and full CRBN knockout models. ***A,*** Scheme of the breeding strategy (left panel), and the resulting genetic architecture after recombination (right panel). Location of primers employed and representative genotyping images are shown. ***B,*** Body weight, in grams, of adult (*ca.* 8 weeks) CRBN-WT or CRBN-KO mice (left panel), Glu-CRBN-WT or Glu-CRBN-KO mice (mid panel), or GABA-CRBN-WT or GABA-CRBN-KO mice (right panel) (n > 10 animals per experimental group). *p*-values were calculated by unpaired Student's *t*-test ***C,*** Body temperature, in degrees Celsius, of adult (*ca.* 8 weeks) CRBN-WT or CRBN-KO mice (left panel), Glu-CRBN-WT or Glu-CRBN-KO mice (mid panel), GABA-CRBN-WT or GABA-CRBN-KO mice (right panel) (n > 10 animals per experimental group). *p*-values were calculated by unpaired Student's *t*-test.

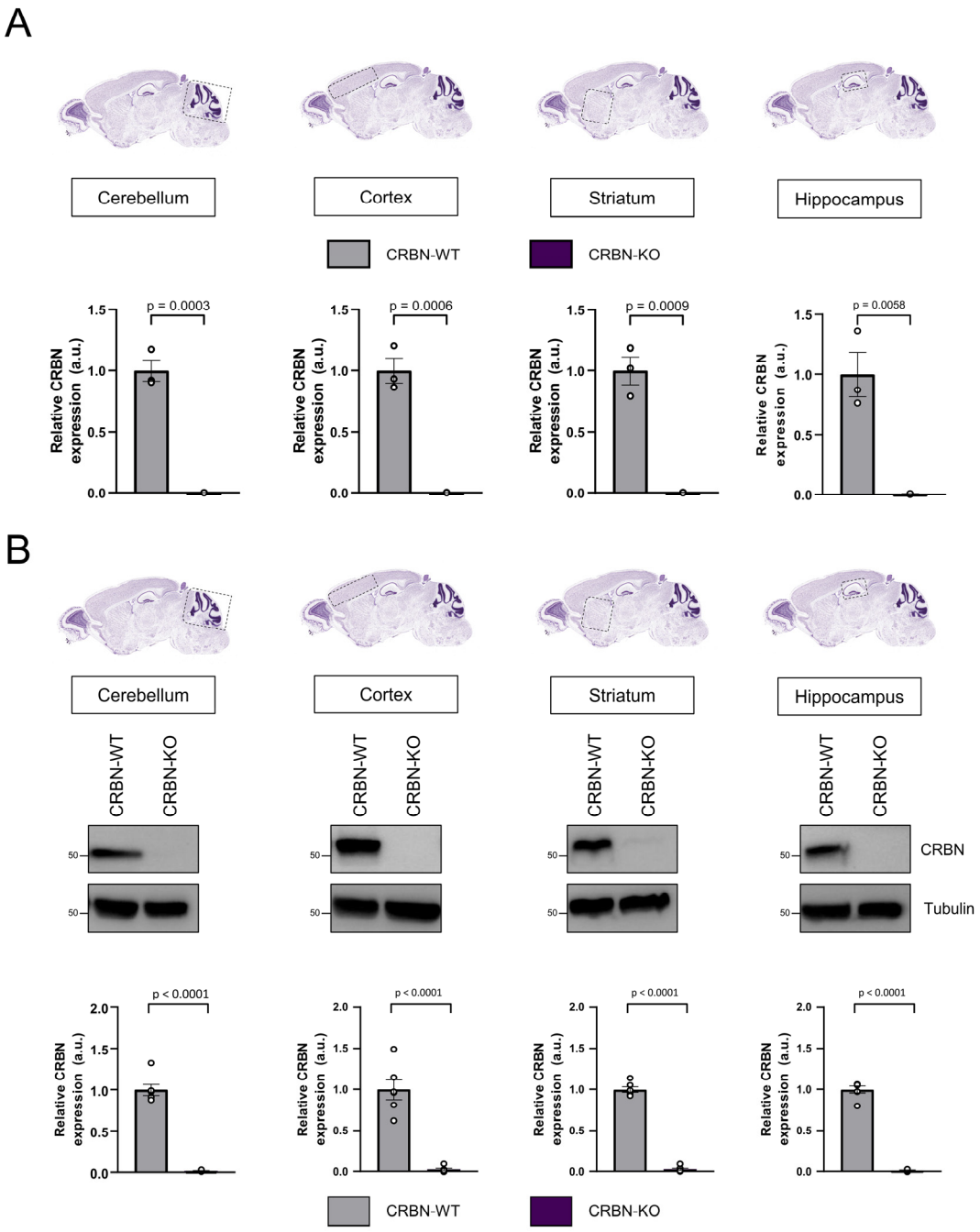

Figure R2.5. Characterization of the recombination in CRBN full knockout mice (I). ***A,*** Relative mRNA levels of CRBN in cerebellum, cortex, striatum or hippocampus as assessed by Q-PCR (n = 3). A caption of selected brain regions is shown for clarity. Image credit: Allen institute. *p*-values were calculated by unpaired Student's *t*-test. ***B,*** CRBN protein levels in cerebellum, cortex, striatum or hippocampus as assessed by western blotting. A representative image is shown (n = 6). A caption of selected brain regions is shown for clarity. Image credit: Allen institute. *p*-values were calculated by unpaired Student's *t*-test.

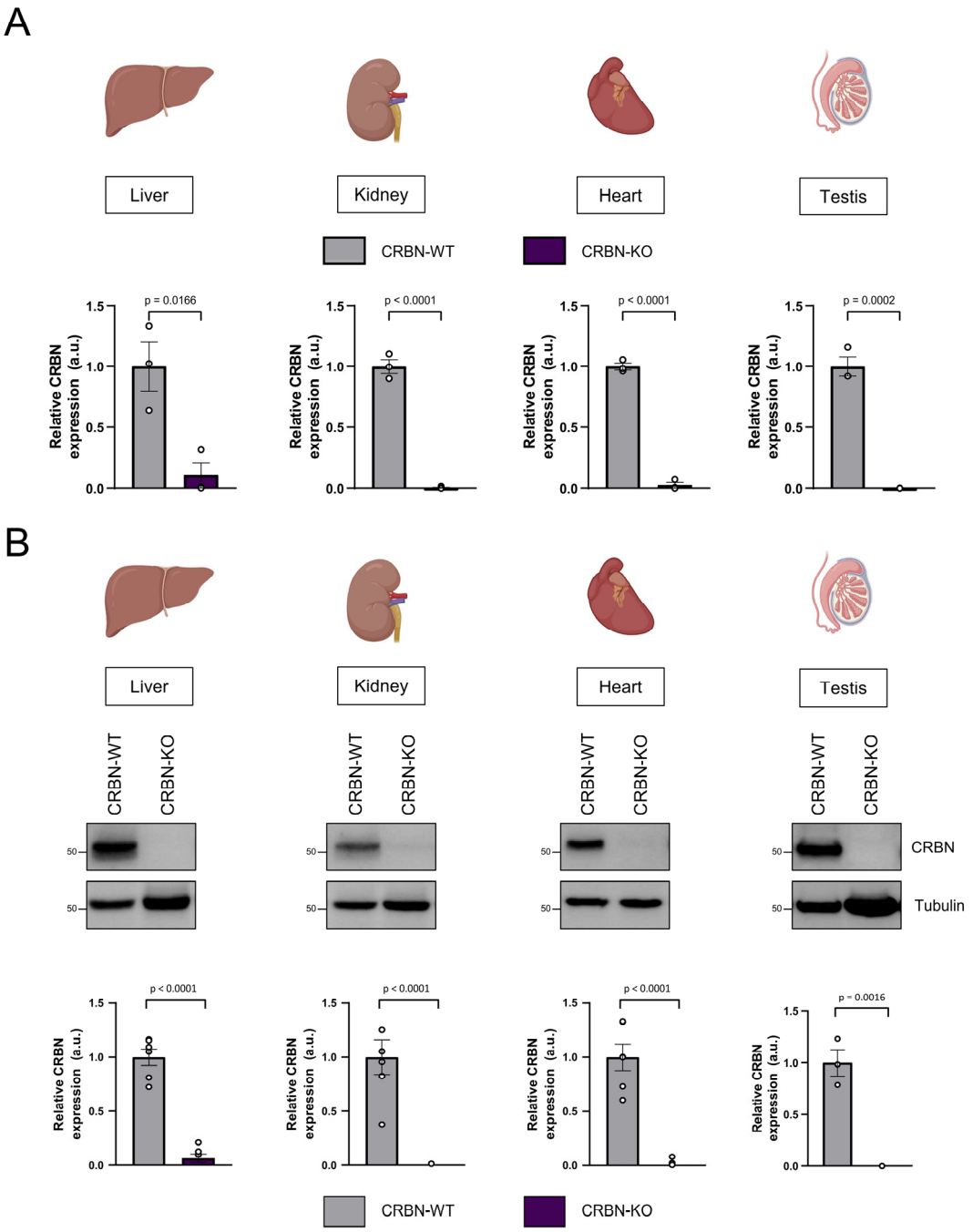

Figure R2.6. Characterization of the recombination in CRBN full knockout mice (II). ***A,*** Relative mRNA levels of CRBN in liver, kidney, heart or testis as assessed by Q-PCR (n = 3). A caption of the selected organs is shown for clarity. Image credit: BioRender. *p*-values were calculated by unpaired Student's *t*-test. ***B,*** CRBN protein levels in liver, kidney, heart or testis as assessed by western blotting. A representative image is shown (n = 6 for liver, kidney and heart; n = 3 for testis). A caption of the selected organs is shown for clarity. Image credit: BioRender. *p*-values were calculated by unpaired Student's *t*-test.

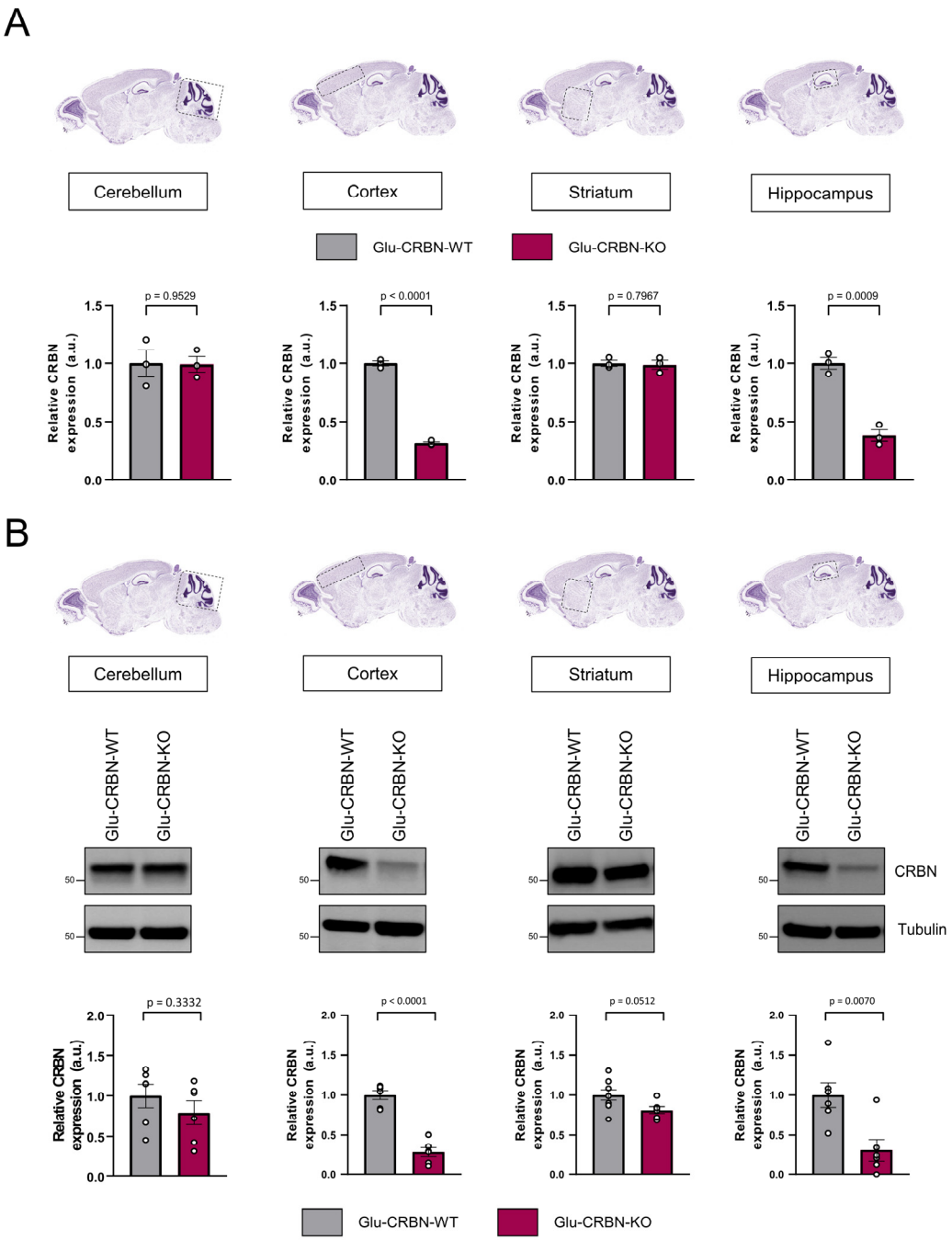

Figure R2.7. Characterization of the recombination in Glu-CRBN-knockout mice. ***A,*** Relative mRNA levels of CRBN in cerebellum, cortex, striatum or hippocampus as assessed by Q-PCR (n = 3). A caption of selected brain regions is shown for clarity. Image credit: Allen institute. *p*-values were calculated by unpaired Student's *t*-test. ***B,*** CRBN protein levels in cerebellum, cortex, striatum or hippocampus as assessed by western blotting. A representative image is shown (n = 6). A caption of selected brain regions is shown for clarity. Image credit: Allen institute. *p*-values were calculated by unpaired Student's *t*-test.

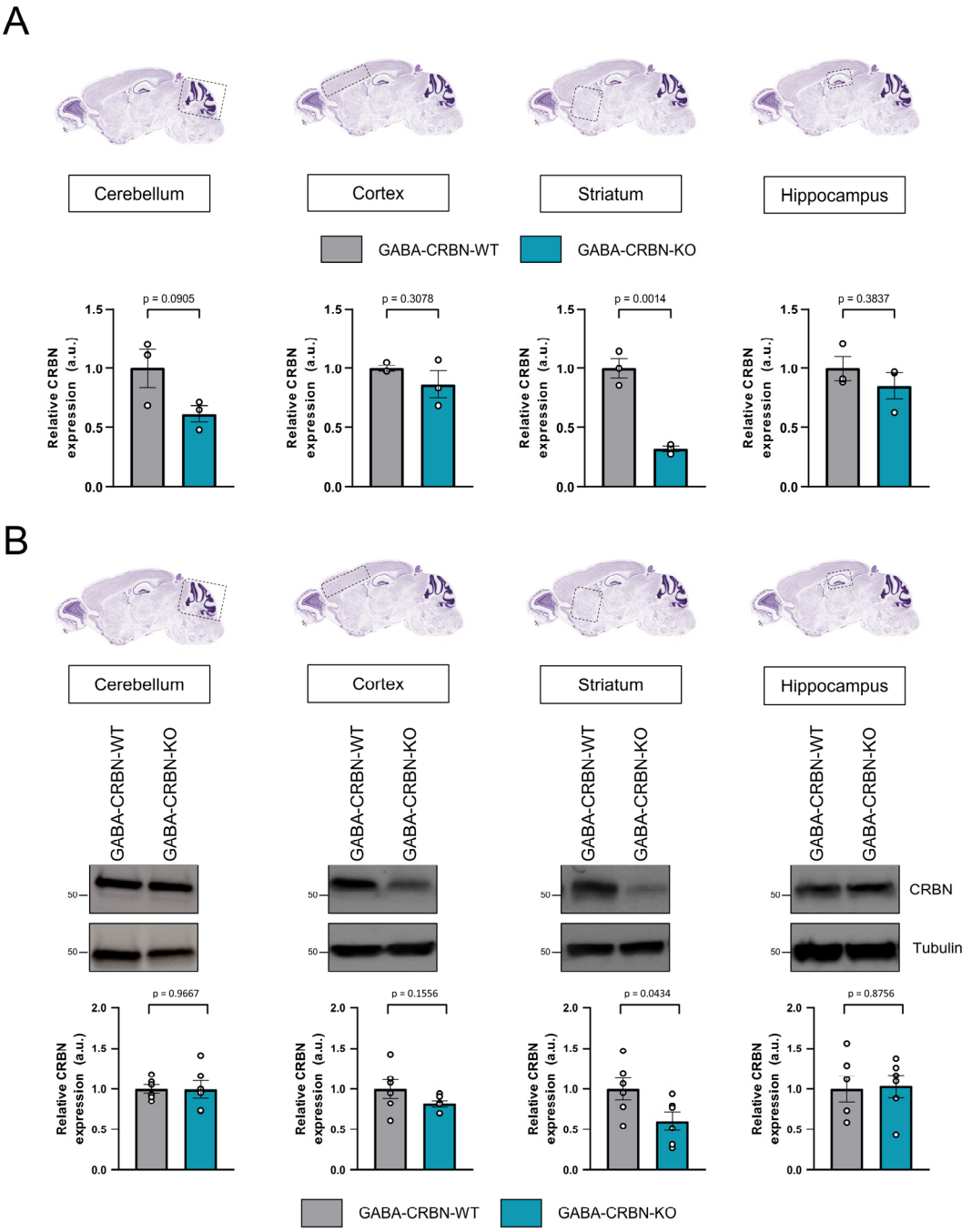

Figure R2.8. Characterization of the recombination in GABA-CRBN-knockout mice. ***A,*** Relative mRNA levels of CRBN in cerebellum, cortex, striatum or hippocampus as assessed by Q-PCR (n = 3). A caption of selected brain regions is shown for clarity. Image credit: Allen institute. *p*-values were calculated by unpaired Student's *t*-test. ***B,*** CRBN protein levels in cerebellum, cortex, striatum or hippocampus as assessed by western blotting. A representative image is shown (n = 6). A caption of selected brain regions is shown for clarity. Image credit: Allen institute. *p*-values were calculated by unpaired Student's *t*-test.

Box 6 – Endogenous substrates of CRBN

IMiDs have attracted much attention to CRBN biology. Nonetheless, many CRBN functions in a 'drug-naïve' context are currently unaddressed. Endogenous substrates of CRBN encompass a variety of proteins, that include the potassium channel BK_{Ca}, the chloride channels CLC-1 and CLC-2, the calcium channel Orai1, the γ subunit of the AMP activated protein kinase (AMPK), glutamine synthetase, amyloid precursor protein, the Toll-like receptor 4 adapter proteins TAK1 and TRAF6, c-Jun, tau, Hsp70 or DNAJA1 (Jo *et al*, 2005; Hohberger & Enz, 2009; Chen *et al*, 2015; Moon *et al*, 2020; Lee *et al*, 2011; Nguyen *et al*, 2016; Prete *et al*, 2016; Min *et al*, 2016; Akber *et al*, 2021) are the most representative substrates described so far. However, data on the biological significance of these interactions is scarce. Specifically, given this list, How ARNSMR arises from CRBN R419X mutation? Does CRBN R419X intervene in neurodegenerative diseases such as Alzheimer's? Does CRBN R419X alter the conductance of BKCa, CLC1, CLC-2 or Ora1? What is the role of CRBN R419X in glutamine metabolism? are straight-away questions that one could ask. In addition, recent evidence locates CRBN not only in the cytoplasm, but also in the mitochondria, the nucleus and adjacent to the plasma membrane, localizations that could increase its substrate repertoire and its biological functions (Kataoka *et al*, 2016; Wada *et al*, 2016). Thus, studies that expand our knowledge on how CRBN exert its functions in our body are warranted.

The recent development of CRBN knockout mouse models by two independent groups has contributed substantially to our understanding of CRBN biology. Interestingly, in the first mouse model generated, genetic inactivation of CRBN impaired associative learning, both when CRBN was deleted from the germline or in principal neurons of the brain that express the *Camk2a* gene (Rajadhyaksha *et al*, 2012). Characterization of a second knockout mouse model suggested that hyperactivity of BK_{Ca} potassium channels underlies these cognitive shortfalls, thus providing a first-in-class molecular mechanism behind ARNSMR (Choi *et al*, 2018). Previous reports had already indicated that CRBN controls BK_{Ca} channel function by preventing its anterograde trafficking to the plasma membrane, and identified inactivation of $CRL4^{CRBN}$, by knocking-out DDB1 or treating with thalidomide, as a sensitizing factor for drug-induced seizures (Jo *et al*, 2005; Liu *et al*, 2014). However, these CRBN knockout mice are not more prone to drug induced seizures (Jeon *et al*, 2020). In line with this data, a follow up study by Rajadhyaksha et al, found that memory alterations in the CRBN knockout could be reversed by inhibition of AMPK, thus, providing another plausible molecular mechanism lying beneath ARNSMR (Bavley *et al*, 2018). However, serious inconsistencies regarding electrophysiological recordings and neural plasticity have been found between both models, which undermines the validity of these findings.

Despite causing cognitive impairments, knocking-out CRBN could be beneficial for several diseases. For instance, CRBN knockout mice are resistant to diet induced obesity, heart or brain ischemia, diabetes-induced osteoporosis, lung fibrosis or tauopathies (Lee *et al*, 2013; Kim *et al*, 2014; Sawamura *et al*, 2018; Yao *et al*, 2018; Kang *et al*, 2021; Akber *et al*, 2021). Nonetheless, CRBN knockout mice also show impaired lymphocyte T maturation and inflammatory responses or altered skin barrier function (Min *et al*, 2016; Kang *et al*, 2016; Kim *et al*, 2019; Jeon *et al*, 2021). Thus, defining when and where CRBN becomes 'druggable' is an ongoing topic of research.

Knocking-out the *Crbn* gene from the germline mimics cognitive deficits found in patients with the R419X mutations (Gil *et al*, 2018; Choi *et al*, 2018), likely because lacking the *C*-terminus of the protein causes its instability (Xu *et al*, 2013). We carried out an extensive

behavioral phenotyping in CRBN-KO, Glu-CRBN-KO and GABA-CRBN-KO mice and found no overt alterations in pain sensitivity (hot plate test), locomotion (open field test, gait analysis), motor coordination (Rota-Rod test), depression-like behaviors (forced-swimming test) or sociability (3-chamber test) (Fig. R2.9A-F). Subtle differences were found regarding anxiety-like behaviors, with CRBN-KO mice showing no phenotype, but Glu-CRBN-KO and GABA-CRBN-KO mice displaying a trend toward hyper-anxious and hypo-anxious performances, respectively, in the elevated plus maze test (Fig. 2.10A). Nonetheless only the trend observed in Glu-CRBN-KO was reproduced when analyzing entries in the center of the arena in the open field test, an alternative way to measure anxiety-like behaviors (Fig. 2.10B). When using a different experimental set-up, others had found that complete CRBN deficiency causes hyper-anxious behavior (Choi *et al*, 2018), thus, a role for CRBN in anxiogenesis cannot be ruled out. In contrast, when we assessed long-term recognition memory performance using the novel object recognition paradigm (NOR), we found that CRBN-KO mice were unable to discriminate between a familiar and an unfamiliar object, and this phenotype was also found in Glu-CRBN-KO mice, but not in the GABA-CRBN-KO mouse line (Fig. 2.10C). In addition, Glu-CRBN-KO mice showed impaired spatial memory in a Y-maze-based spatial memory task (Fig. 2.10D). Previous studies had shown alterations in hippocampal-dependent behaviors, such as context recall, when CRBN is deleted from forebrain projection neurons (Rajadhyaksha *et al*, 2012) but this thesis is the first work in which the neurochemical identity of CRBN-expressing neurons involved in memory processing is unveiled.

Next, we aimed to dissect the molecular mechanism underlying this phenotype. First, we analyzed the levels of a certain synaptic proteins involved in neurotransmitter release and synaptic architecture and found no significant differences in either genotype (Fig. 2.11A-C). Since CRBN behaved as a CB_1R inhibitor *in vitro*, we hypothesized that CB_1R function could be increased in CRBN-KO and Glu-CRBN-KO mice. CB_1R protein levels did not vary across the different genotypes (Fig. 2.12A). Given that CB_1R is mainly a presynaptic protein, we asked if CRBN compartmentalizes to this subcellular localization. Western blotting in a preparation of hippocampal synaptosomes substantiated this notion (Fig. 2.12B). Finally, a preliminary experiment, that is currently being completed with additional mice, showed a trend towards cognitive rescue in Glu-CRBN-KO mice upon injection of the CB_1R-selective antagonist SR141716 (0.3 mg/kg, i.p.) right after the training session (Fig. 2.12C). Taken together, these data support an overactivated CB_1R as a plausible underlying factor of the cognitive deficits arising from CRBN deficiency.

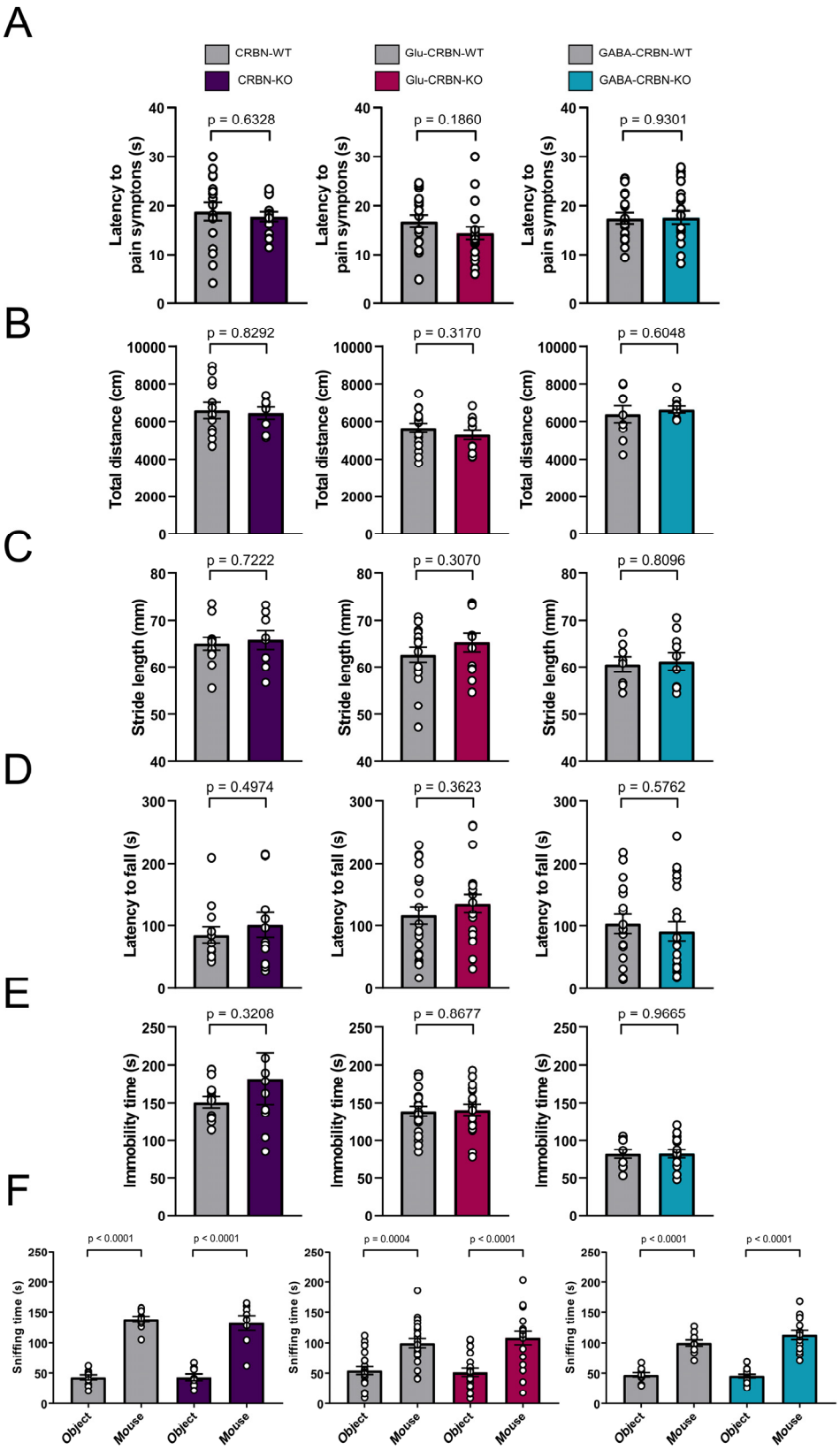

Figure R2.9. Behavioral phenotyping of CRBN knockout mouse lines (I). ***A,*** Pain sensitivity (hot plate test, latency to show pain symptoms). ***B,*** Spontaneous locomotion (open field test, total distance traveled). ***C,*** Gait analysis (footprint test, distance between forepaws along strides). ***D,*** Motor coordination (RotaRod test, time to fall). ***E,*** Depression-like behavior (forced-swimming test, time spent immobile). ***F,*** Sociability (3-chamber test, time spent in sniffing each cage). n > 10 animals per experimental group. *p*-values were calculated by unpaired Student's *t*-test in all cases.

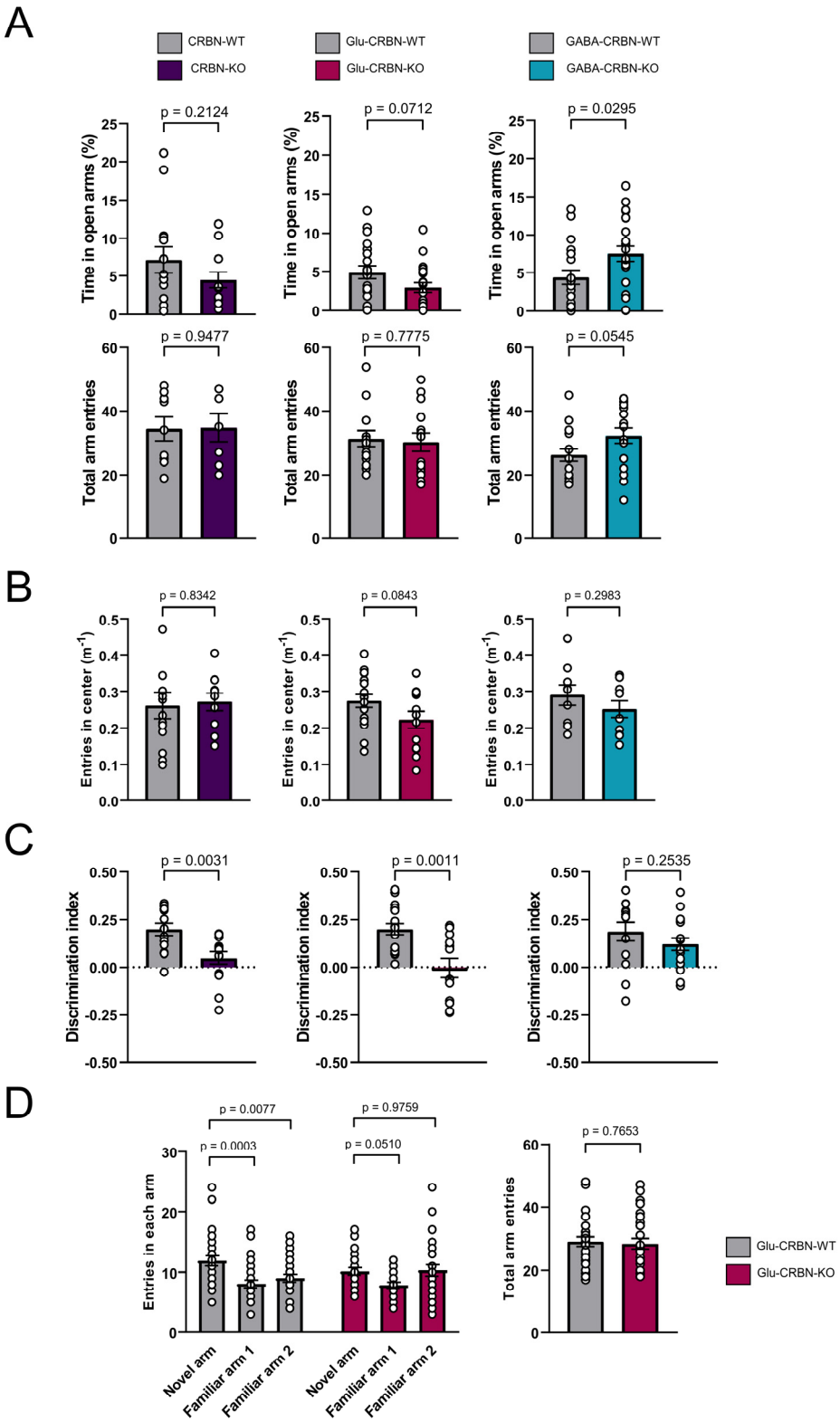

Figure R2.10. Behavioral phenotyping of CRBN knockout mouse lines (II). ***A,*** Anxiety-like behavior (elevated plus maze test, time spent in open arms, as well as total entries) (n > 10 animals per experimental group). ***B,*** Anxiety-like behavior (open field test, entries in the center relative to total ambulation) (n > 10 animals per experimental group). ***C,*** Long-term recognition memory (novel object recognition test, discrimination index between novel and familiar objects) (n > 10 animals per experimental group). ***D,*** Spatial memory (Y-maze-based spatial memory test, number of entries in each arm, as well as total entries) (n > 10 animals per experimental group). *p*-values were calculated by unpaired Student's *t*-test in all cases.

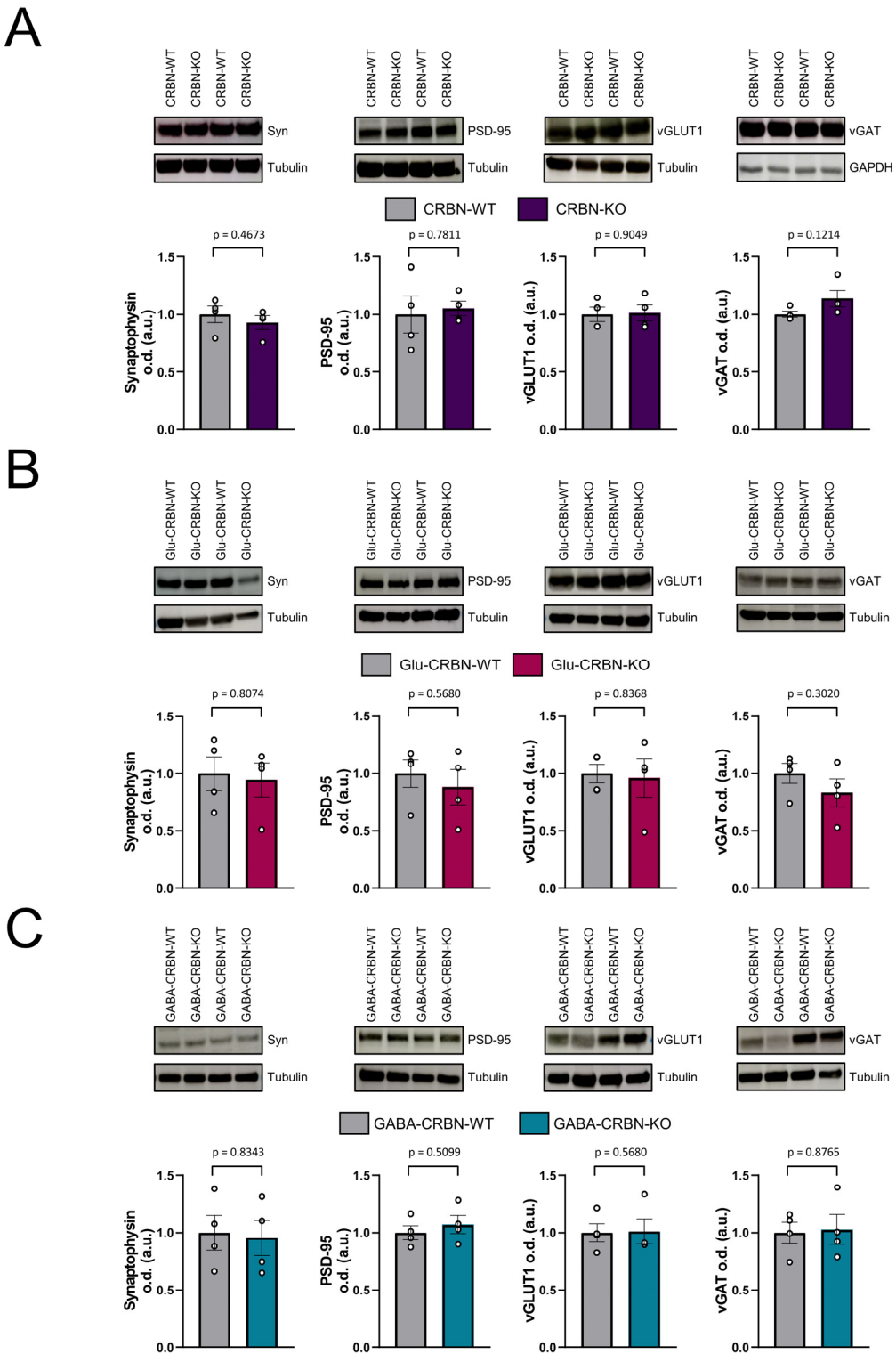

Figure R2.11. CRBN genetic inactivation does not affect certain synaptic protein levels. ***A,*** Protein levels of synaptophysin, PSD-95, vGLUT1 or vGAT in the hippocampus of CRBN-WT and CRBN-KO mice as assessed by western blotting (n = 4). A representative image of 2 samples from independent mice of each genotype is shown. ***B,*** Protein levels of synaptophysin, PSD-95, vGLUT1 or vGAT in the hippocampus of Glu-CRBN-WT and Glu-CRBN-KO mice as assessed by western blotting (n = 4). A representative image of 2 samples from independent mice of each genotype is shown. ***C,*** Protein levels of synaptophysin, PSD-95, vGLUT1 or vGAT in the hippocampus of GABA-CRBN-WT and GABA-CRBN-KO mice as assessed by western blotting (n = 4). A representative image of 2 samples from independent mice of each genotype is shown. *p*-values were calculated by unpaired Student's *t*-test in all cases.

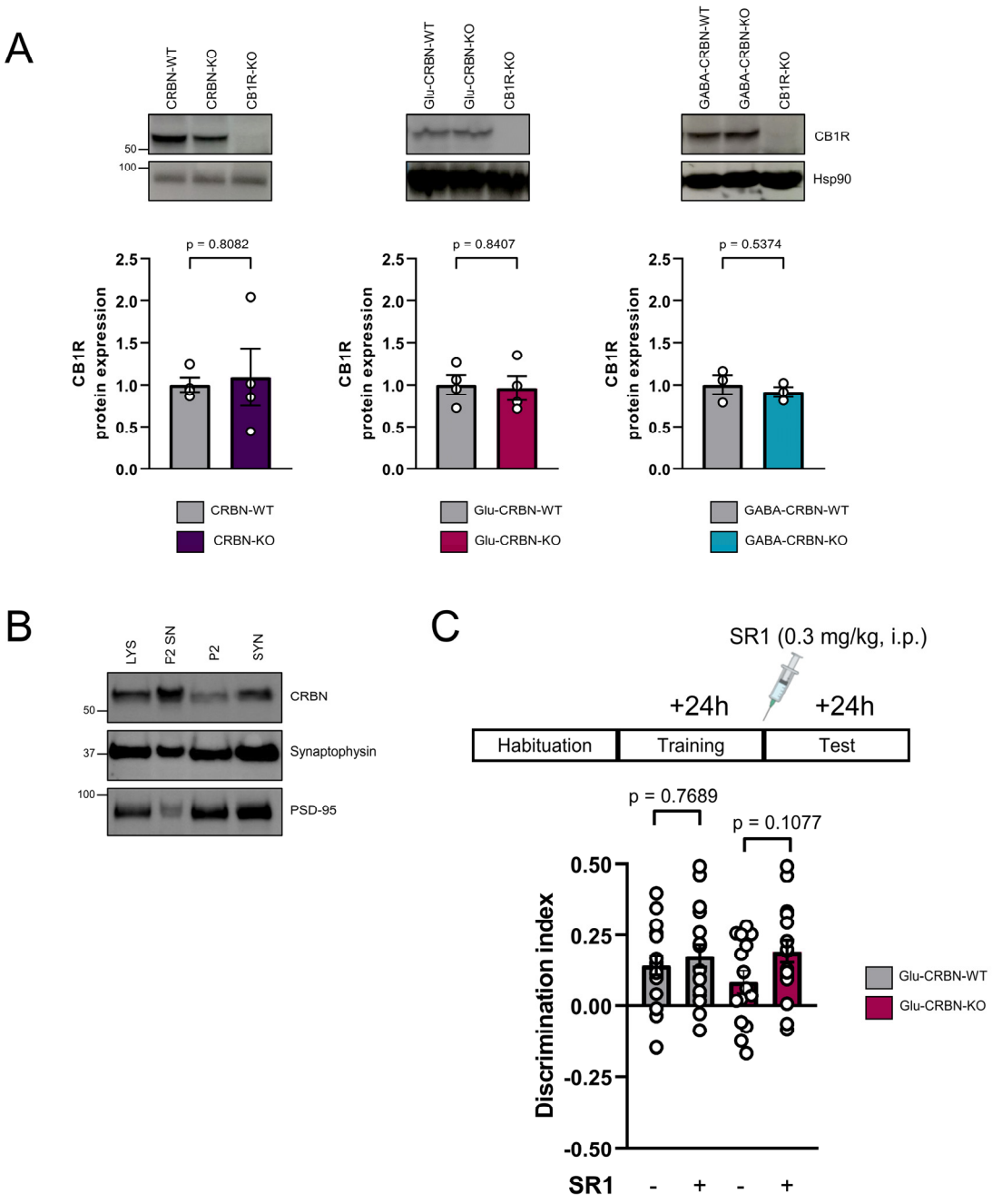

Figure R2.12. CB$_1$R may be involved in CRBN genetic inactivation-induced memory shortfalls. ***A,*** CB$_1$R protein levels in the hippocampus of CRBN-WT and CRBN-KO (left panel), Glu-CRBN-WT and Glu-CRBN-KO (mid panel) and GABA-CRBN-WT and GABA-CRBN-KO (right panel) mice as assessed by western blotting (n = 4). A representative image is shown. *p*-values were calculated by unpaired Student's *t*-test. ***B,*** CRBN protein levels in a total brain lysate (LYS), the supernatant of the P2 fraction (P2 SN), the P2 fraction and the synaptosomal preparation (SYN) of the hippocampus of six mice, as assessed by western blotting. ***C,*** Long-term recognition memory assessment (novel object recognition test, discrimination index between novel and familiar objects) of Glu-CRBN-WT and Glu-CRBN-KO after SR141716 injection (0.3 mg/kg, i.p.) right after the training session (*i.e.*, 24 h before the test session) (n > 10 animals per experimental group). *p*-values were calculated by two-way ANOVA with *Tukey's* multiple comparisons tes

Discussion

CB_1R is arguably one of the most complex GPCRs in the human body. It is involved in a myriad of physiopathological events and cell signaling cascades across many tissues, but especially in the brain. Even though it has been the focus of intense scientific and clinical research in the last years, many molecular aspects underlying cell type-specific CB_1R-mediated functions are still unknown. In this thesis, we have addressed the possibility that intracellular proteins selectively fine-tune CB_1R action by establishing physical interactions with the receptor in a neuron population-selective manner. Aim 1 of this thesis has unveiled BiP, a molecular chaperone, as a novel CB_1R-interacting protein. BiP, upon binding the receptor, inhibits it by blocking $G\alpha_{q/11}$-dependent signaling events, thus biasing receptor function. In contrast with other reports that had identified CB_1R-interacting proteins, we have gone one step beyond and have located CB_1R-BiP complexes through different mouse brain regions on forebrain GABAergic neurons. Moreover, we have unveiled that CB_1R-BiP complexes participate in a behavioral outcome controlled by CB_1R molecules present in GABAergic cells, namely the induction of anxiety. Aim 2 of this thesis has provided another potential binding partner of CB_1R, the protein CRBN. Contrary to the action of BiP, CRBN selectively attenuates the canonical cAMP pathway down-regulation triggered by CB_1R. Loss of CRBN was known to cause memory impairment in mice, and we have found that this is mediated by CRBN molecules selectively located on dorsal telencephalic glutamatergic neurons. Finally, we have obtained preliminary data supporting that CB_1R pharmacological antagonism reverts the alterations caused by the genetic inactivation of CRBN, which further strengthens the notion that CB_1R-CRBN complexes are important for the control of key brain functions. Taken together, we believe that this thesis contributes substantially to our understanding of how CB_1R exerts actions in the brain in a neuron population-restricted manner.

Validation of BiP as a CB_1R-interacting protein

The Y2H system has been used before to identify CB_1R interacting proteins with relative success (Niehaus *et al*, 2007; Hájková *et al*, 2016). This approach is easy to perform and provides fast results at inexpensive costs (Fields, 2005). However, the classical Y2H is not well-suited for membrane proteins and, as such, we had to delimitate the search to proteins interacting with isolated cytoplasmic regions of CB_1R. Thus, this is an important setback in our study, since it limits the identification of potential interacting proteins engaging membrane helixes or more than one cytoplasmic surface. We selected the CTD since it represents the largest surface exposed to the intracellular milieu. In contrast with previous studies, our experimental setup employed almost the entire CTD of CB_1R to identify interacting partners. We conducted a prospective experiment using a human cDNA library and serendipitously found that the last ~150 amino acids of the molecular chaperone BiP, herein referred to as BiP-IR, interacts with CB_1R-CTD. BiP is known to assist some GPCRs during their folding (Siffroi-Fernandez *et al*, 2002; Mizrachi & Segaloff, 2004; Langer *et al*, 2008), and the CTD of CB_1R is mostly unfolded in solution (Ahn *et al*, 2009). Thus, we initially hypothesized that this interaction was rather non-specific, chaperone-like. Perhaps for this same reason, the BiP-CB1R interaction identified in proteomic assays (Mattheus *et al*, 2016) was probably discarded as non-specific (see below). Surprisingly, a deeper analysis challenged our thoughts. First, the region of BiP that interacted with CB_1R did not encompass the substrate-binding domain β, which holds the loops necessary to bind and fold denatured peptides (Yang *et al*, 2015); second, a follow-up Y2H experiment conducted with several deletion mutants of CB_1R-CTD revealed that the interaction only occurred when the last 23 amino acids of CB_1R were present; and third, the CTD of CB_2R, the GPCR

with highest amino acid identity with CB_1R, did not associate with BiP. To the best of our knowledge, the region comprising BiP-IR had never been implicated in the binding of BiP to membrane receptors. Next, by using purified recombinant proteins, BRET assays and co-immunoprecipitations, we verified that either BiP or BiP-IR and CB_1R physically interact in solution and in HEK-293T cells, and further narrowed down the interaction region within CB_1R-CTD to an 11-amino acid stretch extending from cysteine-449 to threonine-460. From this set of experiments, we concluded that BiP selectively associated to the mid-*C*-terminus of CB_1R. The extensive structural mapping of interacting regions within both proteins helped us to hypothesize the biological significance of this interaction. BiP-IR and CB_1R-CTD are remarkably conserved throughout evolution (Fig. D1); thus, the CB_1R-BiP interaction is most likely preserved in many organisms apart from humans and mice. Interestingly, the amino acid sequence of BiP-IR is highly divergent across Hsp70s family members, which could confer BiP selectivity in terms of CB_1R binding. On the other hand, a sequence similar to the region of CB_1R engaged by BiP can be found in caspase-7, which has also been reported associated with BiP, although other regions of the proteins were identified in the study (Rao *et al*, 2002; Kong *et al*, 2013). In the absence of three-dimensional structures of both caspase-7-BiP and CB_1R-BiP complexes, one could speculate that two or more surfaces of the protein partners interact. Would not this be the case, another interesting idea emerges. BiP is an astonishing promiscuous protein in terms of protein-protein interactions, with more than a thousand unique interactors already reported in the Biogrid protein-protein interaction repository (https://thebiogrid.org/109541/summary/homo-sapiens/hspa5.html). Hence, the simultaneous binding of CB_1R and other proteins is an exciting possibility that could expand the CB_1R interactome beyond imagination. In addition, the BiP interaction region of CB_1R falls within the putative helix 9 of the receptor (Ahn *et al*, 2009; Fletcher-Jones *et al*, 2019), and this could have fundamental implications for CB_1R biology (see below). Finally, given that ligand binding to CB_1R, and ATP hydrolysis by BiP, cause remarkable conformational changes, and even post-translational modifications (see next paragraph), future experiments should assess whether these events affect the CB_1R-BiP interaction.

Using a mutational scan approach, we assessed if the phosphorylation status of any of the serine or threonine residues in CB_1R-CTD affects BiP binding by means of directed Y2H assays. Intriguingly, the sole mutation of the amino acid serine-452 to aspartic acid prevented BiP association. Similar to other GPCRs, the occurrence of phosphorylation events in intracellular portions of CB_1R is well-accepted in the field, but the specific amino acid(s) that are modified, and the pairs of kinases/phosphatases involved in the process, remain elusive. To date, only three residues in CB_1R-CTD, namely serine-317, serine-425 and serine-429, are *bona fide* phosphorylated residues (Garcia *et al*, 1998; Bakshi *et al*, 2007; Morgan *et al*, 2014). Serine-317 is phosphorylated by protein kinase C, whereas serine-425 and serine-429 suffer GRK-mediated phosphorylation, although the exact GRK isoform responsible for this modification has not been elucidated (Delgado-Peraza *et al*, 2016). This is striking because when one consults high-throughput databases, such as PhosphoSite (https://www.phosphosite.org/homeAction.action), one finds tens of residues that have been found phosphorylated in massive approaches. To the best of our knowledge, serine-452 has been found modified in a single study (Wiśniewski *et al*, 2010) and not validated experimentally. We are currently addressing this issue by using mass-spectrometry. Unfortunately, structural constraints make this experiment technically challenging, since the closest amino acid (threonine-453) is also phosphorylatable, and both amino acids are located within a cluster of lysine residues, which complicates the classical approach that includes trypsin digestion (trypsin cuts after basic amino acids). So far, we

have found phosphorylated peptides corresponding to this region, but we have been unable to discern whether it represents phosphorylated-serine-452 or phosphorylated-threonine-453. Noteworthy, an *in silico* analysis tool for kinase prediction (NetPhos 3.0 - https://services.healthtech.dtu.dk/service.php?NetPhos-3.1; Blom *et al*, 2004) indicates that serine-452 could be phosphorylated by p90 ribosomal S6 kinase (p90^{RSK}). Another tool that includes an expanded set of protein kinases (GPS 5.0 - http://gps.biocuckoo.cn/; Wang *et al*, 2020) also predicts GRK-mediated phosphorylation. To summarize, deciphering if, how, where and when serine-452 is phosphorylated is an important matter for a deeper understanding of CB_1R-BiP complexes and maybe the association of CB_1R to other partners.

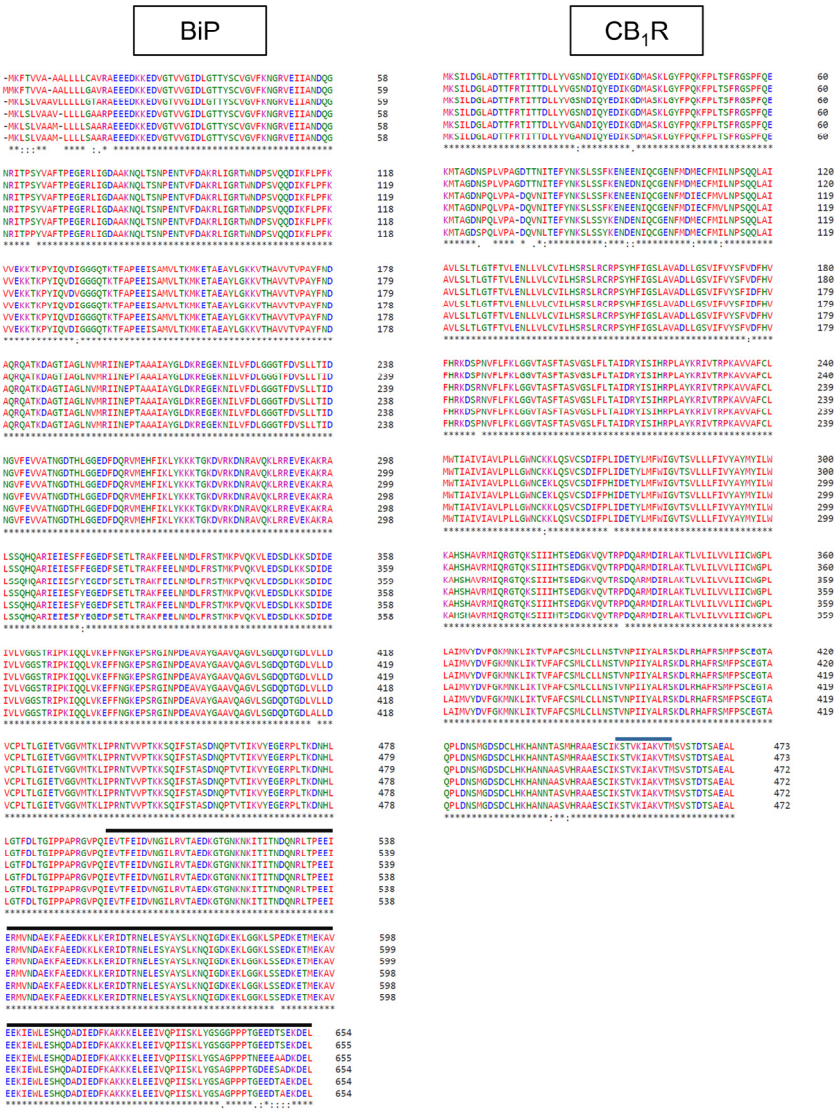

Figure D1. BiP and CB_1R sequence alignments. Amino acid sequences of human (*Homo sapiens*), orangutan (*Pongo abelii*), pig (*Sus scrofa*), sheep (*Ovis aries*), rat (*Rattus norvegicus*) and mouse (*Mus musculus*) BiP and CB_1R proteins. The black bar highlights BiP-IR, whereas the blue bar indicates the interacting region of CB_1R. Hydrophobic and aromatic (except tyrosine) residues are shown in red, acidic in blue, basic in magenta and polar in green. An asterisk (*) indicates a fully conserved residue, a semicolon (:) indicates a conservative mutation, and a dot (.) indicates a substitution by an amino acid with weakly similar properties.

BiP modulates CB_1R function in vitro

BiP binding inhibits global CB_1R signaling as assessed by DMR assays in transiently-transfected HEK-293T cells. This finding contrasts with the subtle effect of CRIP1a on CB_1R/G-protein coupling (Blume *et al*, 2015), and with the BiP-mediated facilitation of

melanocortin MC4 receptor activation (Yoon *et al*, 2018). Given that we obtained equivalent effects using either full-length BiP or BiP-IR, we performed subsequent experiments with BiP-IR. Although data with BiP loss-of-function mice was consistent with all our findings (see below), it is important to mention that BiP-IR might not behave exactly as BiP, particularly if a macromolecular assembly, as suggested above, took place. In addition, the three-dimensional conformation of BiP-IR also fails to be regulated by ATP binding and release. Thus, this is an important caveat in our study. DMR technology is by definition a holistic approach, and the cellular response encompasses a plethora of cellular events (Schröder *et al*, 2010). To dissect in detail how BiP impairs CB_1R action, we first studied the canonical signaling action of CB_1R, *i.e.*, inhibition of the adenylyl cyclase/cAMP/PKA pathway, and found that this blockade was unaffected upon BiP-IR overexpression. Likewise, the $G\alpha_{i/o}$-protein coupling pattern profile of CB_1R showed only minor differences when BiP-IR was overexpressed. Next, we widened the analysis to CB_1R-induced activation of other cell signaling pathways by using an array of phosphorylated kinases. We employed two different time points to analyze both G-protein and β-arrestin-dependent signaling events (Nogueras-Ortiz & Yudowski, 2016), and found that BiP-IR mainly precluded WIN55,212-2-induced activation of ERK, Akt, p70S6K, CREB and related proteins. To identify the molecular mechanism(s) underlying this inhibition, we turned our view to alternative G proteins. CB_1R is known to activate $G\alpha_s$, $G\alpha_{q/11}$ and $G\alpha_{12/13}$ proteins under different experimental settings (Priestley *et al*, 2017). Intriguingly, in our G-protein-coupling immunoprecipitation assays, we found a pool of CB_1R molecules that engaged $G\alpha_{q/11}$ protein subunits, and this was prevented by BiP-IR overexpression. $G\alpha_{q/11}$ proteins can readily activate ERK (Sugden & Clerk, 1997). Genetic or pharmacological inhibition of $G\alpha_{q/11}$ diminished CB_1R-mediated phosphorylation of ERK, and abolished the DMR response. Even more, deletion of one BiP allele in mice increased CB_1R-$G\alpha_{q/11}$ coupling in hippocampal membrane extracts. To summarize, the remarkable blockade exerted by BiP overexpression in DMR assays presumably arises from $G\alpha_{q/11}$ displacement from CB_1R upon BiP binding. This is in line with previous findings indicating that G-proteins activation is the main post-receptor trigger leading to the captured responses with the DMR approach (Schröder *et al*, 2010). $G\alpha_{q/11}$ displacement by BiP starkly contrasts with the subtle effects on $G\alpha_{i/o}$ protein subunits. This observation may have its rationale in the structural determinants of CB_1R that participate in G-protein binding. A series of studies have identified that amino acids 401-417 in CB_1R-CTD can efficiently bind and activate $G\alpha_{i3}$ and $G\alpha_o$ proteins, whereas peptides containing the mid- and *C*-terminal portions of ICL3 of CB_1R associate with $G\alpha_{i1}$ and $G\alpha_{i2}$ (Mukhopadhyay *et al*, 2000; Mukhopadhyay & Howlett, 2001). Unfortunately, the regions involved in $G\alpha_{q/11}$ binding have not been unveiled yet. Interestingly, the helix 9 of the receptor, which overlaps with the BiP-binding site, is analogous to the $G\alpha_{q/11}$ binding site present in squid rhodopsin, which is implicated in its activation (Murakami & Kouyama, 2008). Following this reasoning, steric competition between BiP and $G\alpha_{q/11}$ might explain the absence of $G\alpha_{q/11}$ bound to CB_1R in cells overexpressing BiP-IR. Noteworthy, studies on adrenergic, dopaminergic and vasopressin receptors have reported that the cooperation of two different types of G-proteins can act synergistically to increase the extent of receptor activation (Gupte *et al*, 2017), thus suggesting that a change in $G\alpha_{q/11}$ coupling, as triggered by BiP binding, might impact on the non-$G\alpha_{q/11}$-mediated effects of CB_1R. Additionally, the putative helix 9 has been proposed as an axon-targeting signal. Of note, these authors proposed that the mechanism lying beneath this action might be an interacting protein (Fletcher-Jones *et al*, 2019). In line with this hypothesis, we have found that BiP-IR alters CB_1R trafficking by impairing agonist-induced CB_1R internalization. Thus, whether BiP participates in axonal targeting of CB_1R is a stimulating idea that would require further experiments using primary neuron cultures or

even an *in vivo* setup. Noteworthy, our data with synaptosomal preparations, in line with previous reports (Willis *et al*, 2005; Pendyala *et al*, 2015), shows that BiP is present in axon terminals, and can associate to CB_1R molecules; so it is feasible that BiP ensures proper CB_1R axonal targeting. Similar to the aforementioned data on $G\alpha_{i/o}$ proteins, BiP did not compete with β-arrestin-2 for CB_1R binding. This is consistent with a previous report that locates the β-arrestin-2 binding site of the receptor between amino acids 419 and 439, a region that does not fall within the BiP-binding site (Bakshi *et al*, 2007). Nonetheless, the mechanism that underlies the BiP-mediated blockade of CB_1R-internalization needs to be clarified in further studies. Intriguingly, a recent report showed that cytoplasmic BiP sequesters phosphorylated sphingosine-1-phospate receptor in the ER and prevents recycling to the plasma membrane (Anwar *et al*, 2021). Furthermore, although we have provided an extensive characterization of the effects that BiP exerts upon binding CB_1R, we have only employed heterologous cell systems and overexpression approaches. Given that CB_1R function is highly heterogeneous, and cell-type dependent, experiments using more physiologically relevant methodologies, such as primary neuron cultures or *in vivo* setups, are warranted.

CB_1R-BiP complexes are present in GABAergic neurons

BiP is a very ubiquitous protein. In agreement with this notion, we found elevated expression of BiP mRNA throughout the brain by using ISH. Classically, the subcellular localization of BiP has been ascribed to the lumen of the endoplasmic reticulum, but lately, this issue has been challenged. For instance, various reports have identified BiP in the mitochondria, at the outer leaflet of the plasma membrane, adjacent to the plasma membrane, and even one cytoplasmic-exclusive isoform has been found (Misra *et al*, 2002; Hayashi & Su, 2007; Ni *et al*, 2009; Tsai *et al*, 2015). By using subcellular fractionation assays, we have found a significant amount of BiP present in the cytoplasm. To the best of our knowledge, the subcellular distribution of BiP in neurons had never been studied. Thus, although containing other cell types apart from neurons, this fractionation is the first approach that locates BiP in the cytoplasm of brain cells. High-resolution microscopy analysis could be of great help to unveil the subcellular distribution of BiP across cell-types in the brain parenchyma. Our detailed mapping of CB_1R-BiP complexes in the mouse brain shows that GABAergic neurons constitute the foremost cell population expressing these complexes. In fact, data with gene rescue-mice from a CB_1R-null background shows that CB_1R-BiP complexes are exclusively located in inhibitory cells. This is in line with a previous high-throughput proteomic study showing that BiP co-immunoprecipitates in a significant amount with CB_1R in mouse GABAergic but not in glutamatergic neurons (Mattheus *et al*, 2016). How this selectively-located BiP-CB_1R complex formation takes place is one of the most exciting questions that arises from our study. Probably, the degree of BiP and CB_1R expression in GABAergic is one of the key reasons to answer this question. GABAergic terminals contain large amounts of CB_1R (Marsicano & Lutz, 1999; Katona & Freund, 2008), and we have found that the expression of BiP in GABAergic *vs.* glutamatergic cells of the hippocampus is markedly different, with the former cell population displaying the highest expression level. Nonetheless, glutamatergic cells across the brain express CB_1R, and are also BiP-enriched (*e.g.*, the granular cell layer of the hippocampus in Figs. R1.5 & R1.6), thus theoretically allowing complex formation. Merely speculating, the mechanism that ensures proper distribution of CB_1R-BiP complexes could arise from a combination of factors, apart (or derived) from the number of interacting molecules that a particular cell expresses, that would ultimately impact fundamental aspects of protein-protein interactions (such as affinity constants or 'entropic' components). For instance, cell-intrinsic properties such as cytoplasmic (and/or axonal/somatodendritic) compartmentalization of BiP; the activity of

cellular kinases responsible for serine-452 phosphorylation (if actually occurring *in vivo*); differential stoichiometry ratios of steric competitors such as $G\alpha_{q/11}$ and/or the activity of other $G\alpha_{q/11}$-coupled GPCRs (that could act as $G\alpha_{q/11}$ "buffers") may differ between GABAergic and glutamatergic cells. Going one step ahead from basic mechanisms to biological functions, it is worth mentioning that GABAergic CB_1R presents a high-tonic activity (Roberto *et al*, 2010). Thus, given its inhibitory nature, BiP binding may represent a counterpoint to ensure a balanced CB_1R activity in the physiological control of glutamatergic/GABAergic neurotransmission. This is consistent with the low G-protein binding efficacy displayed by CB_1R in GABAergic cells, in contrast with glutamatergic terminals (Steindel *et al*, 2013). Additionally, given that agonist-induced receptor internalization presents regional-specific differences (it is most pronounced in the neocortex and hippocampus, and essentially absent in basal ganglia) (Thibault *et al*, 2013), cell-population selective dissociation of CB_1R-BiP complexes after chronic receptor activation might represent another physiological mechanism to ensure proper CB_1R function. Of note, in neuroblastoma cells, anandamide increases BiP expression through CB_1R activation (Pasquariello *et al*, 2009); thus, one could speculate that excessive CB_1R function could lead to increased CB_1R-BiP complex formation in some cell types/contexts.

BiP modulates CB_1R function in vivo

To determine if CB_1R function is affected by BiP *in vivo* we injected BiP-HET mice, that lack ~50% of BiP protein (Li *et al*, 2008), with the CB_1R partial -yet clinically and recreationally most relevant- agonist THC. Classical behavioral effects of cannabinoids (*i.e.*, the "cannabinoid tetrad") have been ascribed to the activation of CB_1R molecules located selectively on glutamatergic neurons or dopamine D_1 receptor-expressing neurons (Monory *et al*, 2007; Soria-Gomez *et al*, 2021). Consistent with our detailed mapping in brain slices, that showed that CB_1R-BiP complexes are highly selective of GABAergic cells, we did not find any differences between BiP-WT and BiP-HET mice after acute or 5-day THC administration (10 mg/kg, i.p.) in terms of cannabinoid-induced hypokinesia, analgesia, catalepsy, or hypothermia. A more thorough analysis of the open field test revealed that at day 5, when animals do not display THC-induced hypolocomotion any longer, BiP-HET mice showed signs of anxiety, since entries in the center of the maze relative to total ambulation were significantly reduced compared to WT littermates. CB_1R has a complex role in anxiety (Ruehle *et al*, 2012). Thus, CB_1R agonists display biphasic effects, with low doses causing anxiolytic-like effects and high doses favoring anxiogenesis, in a process known to require CB_1R molecules located on glutamatergic or GABAergic cells, respectively (Ruehle *et al*, 2012; Rey *et al*, 2012). More specifically, (high dose) THC-elicited anxiety relies on mTORC1 activation upon engagement of CB_1R on hippocampal GABAergic interneurons (Rubino *et al*, 2008; Rey *et al*, 2012; Puighermanal *et al*, 2013; De Giacomo *et al*, 2021, 2020). To assess if BiP participates in CB_1R-induced anxiety, we performed the elevated plus-maze test in BiP-WT and BiP-HET mice acutely injected with THC (10 mg/kg, i.p.). In contrast with BiP-WT mice, where THC elicited a milder effect, BiP-HET mice spent less time -and also showed reduced entries- in the open arms when compared with vehicle-injected littermates. Given that BiP likely blocks CB_1R-induced Akt/mTORC1 activation *in vitro* through $G\alpha_{q/11}$ displacement, as discussed above, we propose a mechanism by which a restricted $G\alpha_{q/11}$-coupled pool of CB_1R molecules located on hippocampal GABAergic interneurons, *via* the mTORC1 signaling axis, triggers anxiety-like behaviors, a process plausibly controlled by BiP binding to CB_1R at the presynapse (Fig. D2). This would provide an unprecedented mechanism for the spatially-selective control of CB_1R signaling in the brain, and supports that favoring CB_1R-BiP association (for instance, by inhibiting CB_1R serine-452 phosphorylation or boosting BiP expression) would reduce anxiety, a frequent negative

effect of CB_1R over-activation. In fact, a role for $G\alpha_{q/11}$ protein-coupled receptors (*e.g.*, serotonin 5-HT_{2C} receptor) in the induction of anxiety has been proposed (Mazzone *et al*, 2018). Intriguingly, THC-induced anxiety can also arise from activation of CB_1R in the prefrontal cortex in rats (Rubino *et al*, 2008), and we also detected CB_1R-BiP complexes in cortical interneurons; thus, it would be of interest to compare the ability of cortical CB_1R to bind $G\alpha_{q/11}$ proteins to that of other brain regions, such as the amygdala, where CB_1R preferentially mediates anxiolytic responses (Rubino *et al*, 2008). Moreover, given this wide brain distribution of CB_1R-BiP complexes, the possibility that BiP binding controls additional CB_1R-related behaviors remains to be determined. Accruing evidence has linked ERK and Akt/mTORC1 activation to various key CB_1R-evoked effects in the brain (Rubino *et al*, 2007; Guegan *et al*, 2013; Puighermanal *et al*, 2013; Blázquez *et al*, 2020), so BiP could be involved in the modulation of these processes. Specifically, motor impairment caused by cannabinoid intoxication, as measured by the Rota-Rod test, requires CB_1R-induced mTORC1 activation in striatal medium spiny neurons expressing the dopamine D_1 receptor (D_1R-MSNs) (Blázquez *et al*, 2020). A recent study has performed Rota-Rod trials in BiP-HET mice, and, although no significant differences were observed, there was a tendency for the BiP-HET mice to perform worse in the task (Gómez-Almería *et al*, 2021). Merely speculating, it is feasible that CB_1R-BiP complexes present in (GABAergic-)D_1R-MSNs are reduced in BiP-HET mice, leading to exacerbated CB_1R-evoked mTORC1 activation. Similarly, memory impairment by cannabinoids involves hippocampal GABAergic-neuron CB_1R (Puighermanal *et al*, 2009), and we have noted that BiP-HET mice also perform worse in the novel object recognition task when compared to WT littermates (Espina-Cortés et al, manuscript in preparation). Hence, this phenotype could as well be caused by an exacerbated CB_1R function. Another provocative hypothesis, partially introduced in the previous section, is that BiP represents a sensitizing factor for CB_1R stimulation (*i.e.*, THC treatment in this context), lowering (if absent) or increasing (if present) the threshold for maximal CB_1R activation. Given that all our data come from experiments using a unique and rather high THC injection, administering various THC doses to BiP-HET mice, as well as different cannabinoid agonists, would be greatly informative. Finally, it is worth mentioning that our *in vivo* approach has the obvious pitfall of being highly correlational -as usually in this type of studies. For instance, we have not shown increased mTORC1 activation after THC administration. We also lacked cellular specificity in our loss-of-function approach, because we could not access to BiP-floxed mice (Luo *et al*, 2006), although this could be solved in the future by using this strain, since it has been recently deposited at JAX (#035444), or by conducting virally-driven rescues in BiP-HET mice using neuron-population-specific promoters. Finally, electrophysiology recordings to study the effect of BiP on classical CB_1R functions, such as DSE/DSI, would also be desirable. These issues notwithstanding, we frankly believe that by combining our extensive data *in vitro*, the detailed *in vivo* mapping, and the behavioral outcomes after THC injection to BiP-HET mice, we provide herein compelling evidence supporting that CB_1R-BiP complexes are important in the CB_1R-evoked signaling events signal that lead to anxiogenesis.

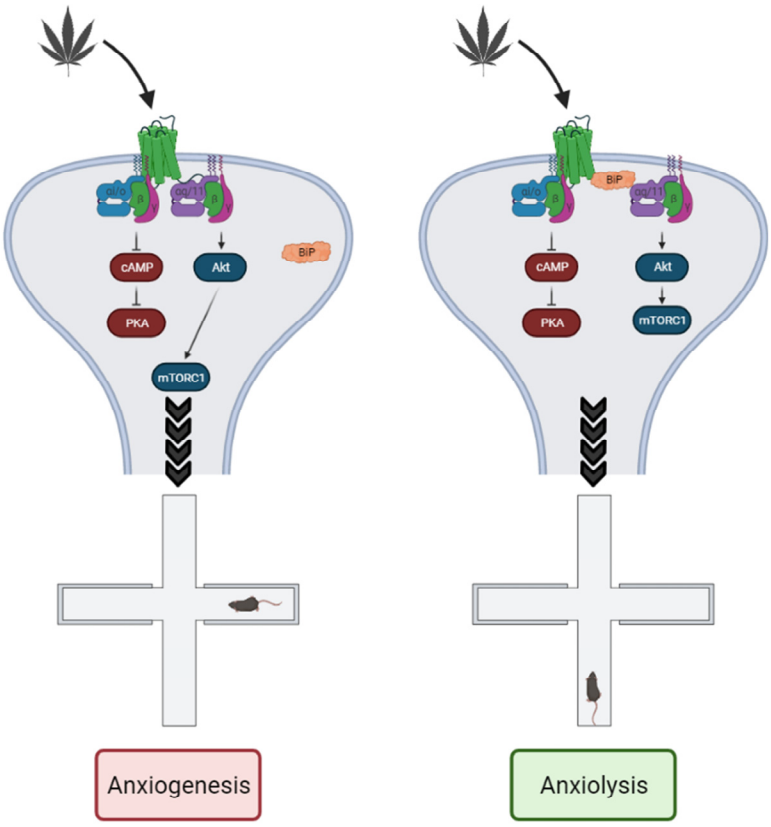

Figure D2. Proposed model for the control of anxiety by CB_1R-BiP complexes. Activation of CB_1R triggers anxiety, measured as an increased permanence in the closed arms of an elevated plus-maze, by engaging $G\alpha_{q/11}$ proteins, which ultimately activates the Akt/mTORC1 pathway. BiP binding to CB_1R acts as a brake, by displacing $G\alpha_{q/11}$ proteins and elevating the threshold for anxiety induction, measured as an increased permanence in the open arms of an elevated plus-maze, after THC administration.

Validation of CRBN as a CB_1R-interacting protein

Affinity purification/mass spectrometry-based proteomics (AP-MS) is an excellent approach to assess protein interactome profiling. As such, it has already been applied to map both the global cell interactome (Huttlin *et al*, 2015, 2017, 2021) and, specifically, the CB_1R interactome (Njoo *et al*, 2015; Mattheus *et al*, 2016; Molina-Holgado *et al*, 2021). One important caveat of AP-MS is that it generally involves overexpression of tagged baits, and immunoprecipitation with specific antibodies, which can occlude protein-protein interaction (PPI) sites promote the non-specific pull down of large proteins, protein complexes or membrane inserted polypeptides. We tried to avoid this issue by using a chromatography-based affinity-purification protocol previously set up in our laboratory (Merino-Gracia *et al*, 2016a). Despite this theoretical advantage, there are two main drawbacks to our approach. First, contrary to previous analysis that studied CB_1R PPIs, we did not use the full-length receptor, but instead solely the CTD, which limits the potential repertoire of interacting proteins; and second, we did not limit beforehand the cellular specificity of the interactions, as we used a whole-brain homogenate, in contrast with the previous cell-type selective immunoprecipitations (Mattheus *et al*, 2016). This initial experiment provided a list of ~30 potential interactors. Strikingly, we were not able to detect known CB_1R binding partners, such as CRIP1a, GASP1, or WAVE1. This outcome might be explained by various reasons, including the heterogeneity of the starting materials (different species, whole-brain *vs*. specific nuclei, cell-type selectivity, and so on), experimental conditions (such as stringency of washing steps), technical sensitivity of the mass spectrometer, the bait employed across (full-length receptor *vs*. the CTD) studies; and, of course, the dynamic nature of PPIs. In fact, the CB_1R interactome varies greatly between days in cultured neurons (Molina-Holgado *et al*, 2021). Therefore, this list represents a picture of an ever-evolving scenario, and as such, we considered it a '*terminos a quo*' that would ultimately lead to a more reductionist-based approach. As indicated in the Results section, we selected CRBN based on its unknown neurobiological function, the existence of a drug targeting this protein, and its involvement in human pathology, in addition to the presence of a known CRBN-interacting protein, DDB1, in the PPI sample.

We have validated the interaction between CRBN and CB_1R by several approaches, including, fluorescence polarization, co-immunoprecipitation and PLA. This has allowed us to define the CRBN-binding site to the same 11-amino acid stretch that binds BiP (see above). Thus, this region might constitute an important interaction hub of the receptor. Immediately answering the reader's mind, to date we have not tested if both CRBN and BiP compete for receptor binding, or how S452 phosphorylation affects the association with CRBN. Merely speculating, this scenario could well explain why the CB_1R-BiP association is restricted to GABAergic cells in some brain regions, as CRBN is expressed predominantly in glutamatergic neurons (see below). On the other hand, the region of CRBN involved in CB_1R binding has not been fully elucidated yet. Two independent possibilities can be extracted from our experiments with CRBN deletion mutants, either i) the CB_1R-interacting region falls between amino acids 80 and 117, or ii) there are at least two independent binding sites, located in the *N*-terminus (residues 1-120) and *C*-terminus (residues 258-onward). Further experiments using CRBN chimeras lacking additional regions (*e.g.*, amino acids 1–80 or 80–120) are necessary to solve this puzzle. Noteworthy, we have found that the CRBN-CB_1R interaction is preserved with the mouse orthologs (data not shown), thus suggesting a conserved mode of interaction throughout evolution. In this context, it is worth mentioning that the CRBN protein sequence is highly conserved between humans and mice (94% sequence identity), with a maximum sequence variation in the very *N*-terminal portion of the protein (residues 30-40). Thus, in this case, sequence alignment cannot provide any

further information on how both proteins interact. Even though the CB_1R-interacting region has not been fully elucidated, our structural data is consistent with previous studies that have defined the *N*-terminus and the *C*-terminus of CRBN as protein-interacting surfaces (Tao *et al*, 2018). Since thalidomide and derivatives attenuated the CRBN-CB_1R interaction, and thalidomide binds to a conserved groove in the *C*-terminal part of CRBN, this might represent indirect evidence of a CB_1R-interacting site in the most distal end of CRBN. The potential implication of CRBN displacement from CB_1R by thalidomide will be discussed in detail below.

We are well aware that one weakness of our study is the lack of validation of the interaction with endogenous proteins in a more physiologically relevant cellular setting. The lack of cell lines expressing large amounts of CB_1R, and, particularly, until recently, of proper anti-CRBN antibodies, has represented an important setback to undertake these experiments, which would be undoubtedly conducted in our laboratory in the forthcoming months. Finally, it is of utmost importance to clarify if CRBN binding involves the concomitant engagement of the CUL4A complex to CB_1R (discussed in detail below). Shortcomings aside, to the best of our knowledge CB_1R is the first-ever GPCR shown to interact with CRBN under a physiological setting. Interestingly, a recent report has used a synthetic drug, consisting of prazosin (an α_{1A}-adrenergic receptor inhibitor) linked to pomalidomide, to trigger CRBN-dependent degradation of the α_{1A}-adrenergic receptor, thus suggesting that CRBN can readily distribute to GPCRs present in cellular membranes.

CRBN modulates CB_1R function in vitro

CRBN binding partially inhibits global CB_1R signaling, as assessed by DMR assays in transiently-transfected HEK-293T cells, to an extent similar to that of CRIP1a. To dissect in detail how CRBN impairs CB_1R action, we first studied the canonical pathway of CB_1R, *i.e.*, inhibition of the adenylyl cyclase/cAMP/PKA pathway, and found that this blockade was attenuated when CRBN was overexpressed with two different CB_1R agonists, namely WIN55,212-2 and CP-55,940. This effect seems pathway-selective, as ERK activation (although, analyzed at a single time point) was not influenced by CRBN overexpression. Since CRBN is the substrate recognition component of a CUL4A E3-ubiquitin ligase complex, we analyzed whether basal CB_1R ubiquitination was affected by CRBN overexpression and/or knockdown, and found no overt differences. Ubiquitination of GPCRs plays important roles in receptor trafficking and signal transduction upon activation, although this modification is still understudied for many receptors, including CB_1R (Shenoy *et al*, 2001; Marchese & Trejo, 2013; Skieterska *et al*, 2017; Burton & Grimsey, 2019; Lee *et al*, 2019). The finding that CB_1R is basally ubiquitinated in HEK-293T cells has prompted us to study the role of ubiquitin in the signal transduction of CB_1R. Preliminary experiments show that ubiquitination of CB_1R peaks at 15 minutes after activation (Fig. D3), and the role of CRBN in this process will be tested soon. Somehow related, CB_1R activation is well-known to induce directed protein ubiquitination, in some cases leading to degradation, under some cellular settings (Jordan *et al*, 2005; Díaz-Alonso *et al*, 2017; Monday *et al*, 2020), but molecular mechanisms underlying these events are unknown. Recently, a hallmark study has shown that a set of GPCRs can effectively induce directed-ubiquitination of Atg14L through activation of GSK3β-CUL3 to block autophagy (Zhang *et al*, 2015) [of note, an effect also triggered by CB_1R activation (Blázquez *et al*, 2020)]. In addition, CRBN-mediated degradation of CK1α can be induced by the Wnt-stimulated GPCR Frizzled (Shen *et al*, 2021). Thus, CRBN-binding to favor CB_1R-mediated activation of $CUL4A^{CRBN}$ complex is an interesting possibility to be explored in the future.

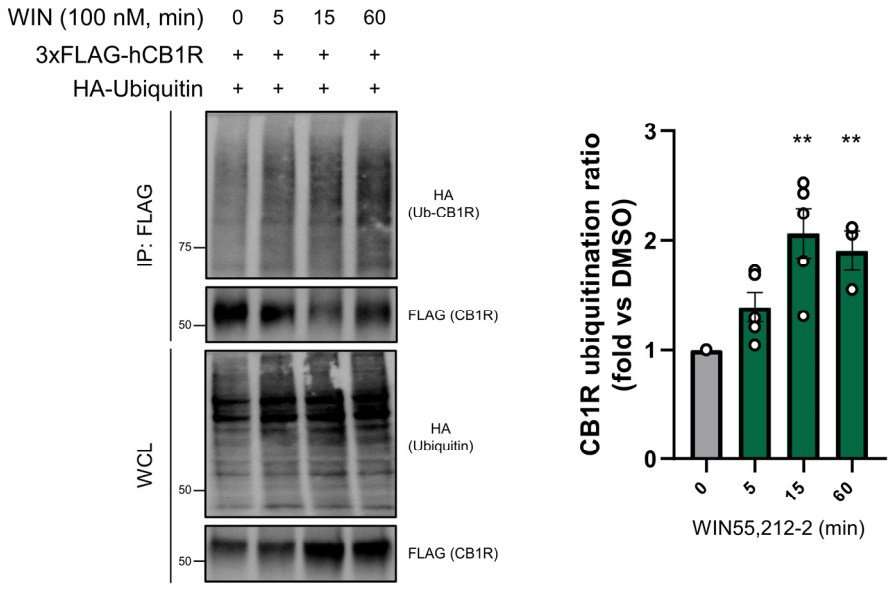

Figure D3. CB_1R activation leads to receptor ubiquitination. Activation of CB_1R produces a time dependent ubiquitination of the receptor, that peaks at 15 minutes, as assessed by co-immunoprecipitation. Immunoprecipitation (IP) was conducted with anti-FLAG M2 agarose. WCL: whole-cell lysate. A representative experiment is shown (n = 4).

An alternative explanation for the CRBN-mediated modulation of CB_1R-signaling might involve a putative RGS-like domain present in CRBN (Jo *et al*, 2005). A key determinant of G-protein action is the duration of their active state. G proteins are activated by the binding of GTP to the Gα subunit, which releases it from the βγ dimer, and their deactivation proceeds with GTP hydrolysis to GDP due to the GTPase enzymatic activity of Gα. The temporal resolution of this process is tightly regulated by guanine nucleotide exchange factors (GEFs), that promote GTP binding and subsequent GDP release, and GTPase-activating proteins (GAPs), which accelerate GTP turnover. GPCRs represent the archetypical GEF functional superfamily, whereas the most well characterized GAPs belong to the regulator of G-protein signaling family (RGS) (Masuho *et al*, 2020). CRBN-RGS-like domain, which spans through amino acids 120–255 of the rat protein, was suggested almost 15 years ago. This putative motif shows low overall sequence identity with well-established RGS members (32%), but the comparison of key residues for G-protein interaction with those of RGS4 and RGS9, two proteins that display tuned selectivity for $G\alpha_{i/o}$, shows elevated conservation (Jo *et al*, 2005; Masuho *et al*, 2020). In fact, RGS4 acts as a GAP for CB_1R-stimulated $G\alpha_{i2}$ protein (Sutor *et al*, 2011). Our structural modeling shows similarities between the CRBN-RGS domain and those of RGS4 and GRK2 (Fig. R2.2), which strengthens the hypothesis that CRBN might function as an RGS within the cell. In line with this idea, CB_1R-mediated cAMP down-regulation is blocked by RGS4 overexpression in HEK-293T cells, similarly to our data obtained with CRBN overexpression (Bosier *et al*, 2015). Thus, experiments using the CRBN-ΔRGS mutant are warranted to confirm this possibility.

Another stimulating idea can be envisaged upon considering known CRBN and CB_1R information. A series of fundamental studies have recently identified a novel, ubiquitin-independent, function of CRBN: the stabilization of membrane proteins (Eichner *et al*, 2016; Heider *et al*, 2021). CRBN acts synergistically with HSP90 and AHA1 proteins to ensure the proper maturation of membrane proteins. AHA1 stimulates the ATPase activity of HSP90, favoring client release. CRBN seems to counteract AHA1 *via* direct PPI with both HSP90 and AHA1. Alterations in CRBN levels result in altered AHA1 function, which in turn, causes membrane protein instability due to accelerated release from HSP90 (Wang *et al*, 2006b;

Heider *et al*, 2021). Interestingly, others have found that chronic THC enhances AHA1 expression in the cerebellum (Filipeanu *et al*, 2011). Shockingly, experiments in heterologous cells show that AHA1 overexpression enhances CB_1R protein levels in the plasma membrane, which ultimately leads to augmented CB_1R-mediated cAMP down-regulation (Filipeanu *et al*, 2011). If one combines both pieces of data with the observation that CRBN attenuates the canonical CB_1R/cAMP pathway, the possibility of CRBN counteracting AHA1 for the trafficking of CB_1R seems highly likely. Thus, assessing if CRBN overexpression modifies membrane levels of CB_1R, as observed for other CRBN binding partners (Liu *et al*, 2014; Chen *et al*, 2015), would be of great interest.

Generation of CRBN loss-of-function mouse models

To assess the role of CRBN function on CB_1R-signaling *in vivo*, we developed genetically-modified mice devoid of the *Crbn* gene not only in the germline (CRBN-KO), but also in dorsal telencephalic glutamatergic neurons (Glu-CRBN-KO), or in forebrain GABAergic neurons (GABA-CRBN-KO). This strategy had been employed before to unveil the neuron-populations responsible for CB_1R actions with enormous success (*e.g.,* Monory *et al*, 2007). By the time this thesis started, two CRBN knockout mice, and one conditional model [lacking CRBN in neurons expressing the alpha subunit of calcium/calmodulin-dependent protein kinase type II (CaMKIIα); hereafter, CaMKII-CRBN-KO] had already been generated (Rajadhyaksha *et al*, 2012; Lee *et al*, 2013). Nonetheless, although knockout mice are a valuable research tool, unexpected compensatory or redundant mechanisms can lead to deceitful conclusions. On the other hand, cells expressing the *CamK2a* gene include virtually all principal neurons of the forebrain, but this gene is also expressed in many neurons of subcortical and diencephalic regions, including the striatum, thalamus, and hypothalamus (Casanova *et al*, 2001; Monory *et al*, 2007). Thus, results obtained with these mice can also be misleading. Therefore, the generation of neuron-population-selective conditional knockouts represents a further layer of complexity needed to study CRBN function.

All the CRBN mouse lines generated in our laboratory were viable and fertile, and did not show any overt general-health alteration. We analyzed the recombination pattern of conditional knockouts by using Q-PCR and western blotting. As expected, CRBN mRNA or protein levels were undetectable in constitutive CRBN-KO mice in every tissue analyzed. In contrast, CRBN expression was reduced selectively in the hippocampus and the cortex of Glu-CRBN-KO mice and a similar trend was observed in the striatum. These data are in line with the previous characterization of the CaMKII-CRBN-KO mouse model, which showed lowered mRNA levels of CRBN in the hippocampus and the cortex (Rajadhyaksha *et al*, 2012). On the other hand, GABA-CRBN-KO showed a decreased mRNA and protein expression in the striatum, and the same trend was noticed in the cortex. Unfortunately, not a single study that has mapped CRBN expression to GABAergic cells is available to compare. One major limitation of this characterization is the use of brain extracts, which fail to provide cell-type specificity. Since we were unable to characterize recombination by conventional protein immunofluorescence methods, due to the lack of appropriate anti-CRBN antibodies, we are currently optimizing *in situ* hybridization assays to detect CRBN mRNA in brain sections, and we will combine this labeling with cell-type-specific probes to address this gap. This issue notwithstanding, the Nex1- and Dlx5/6-Cre expressing mouse lines have been validated to a great extent before (Schwab *et al*, 2000; Monory *et al*, 2006).

Our extensive phenotypical characterization shows that neither CRBN global knockout nor CRBN conditional knockouts display overt behavioral alterations. A mutation in CRBN has been found in individuals affected by autism spectrum disorders (ASDs) (Pinto *et al*, 2010) Since impaired sociability and intellectual disability are core symptoms of ASDs, we

examined sociability-like behaviors in the three-chamber test, and found a normal preference for mouse congeners, aligning with previous reports using a different CRBN-KO mouse model (Bavley *et al*, 2018). Depression-like behaviors, which are also common in individuals suffering from ASDs (Hollocks *et al*, 2019), were also unaffected by CRBN genetic inactivation in either genotype analyzed. Therefore, the lack of CRBN does not seem to cause an ASD-like phenotype in mice. Interestingly, increased anxiety has been observed in one of the two CRBN-KO models when using the EPM test (Rajadhyaksha *et al*, 2012; Choi *et al*, 2018). Likewise, here we have found a trend towards increased anxiety in CRBN-KO mice, and specifically in Glu-CRBN-KO mice, whereas deletion of CRBN in GABAergic neurons led to the opposite outcome, with mice showing anxiolytic-like behavior. Nonetheless, by using an alternative way to measure anxiety, such as the number of entries in the center of an open-field arena, we only reproduced the results of the Glu-CRBN-KO mouse line. These differences with published data might reside on the protocol and type of device employed. We followed the guidelines described in the original study that adapted the EPM approach for mice, and our maze had standard dimensions (Lister, 1987; Walf & Frye, 2007). In contrast, data showing increased anxiety in CRBN-KO mice use a significantly larger maze, as well as an extended testing time (Choi *et al*, 2018), which might explain this discrepancy. In addition, the lack of consistency between the EPM and OFT results might arise from the fact that the avoidance of open arms in the EPM test has a component of acrophobia (fear of height), whereas the OFT mostly evaluates agoraphobia-induced anxiety (fear of open spaces) (Singh Bora & Sharma, 2012). Thus, additional behavioral paradigms (*e.g.*, novelty suppressed feeding, light-dark box test), would be necessary to clarify the role of CRBN in anxiety.

CRBN-KO mice display memory shortfalls, as assessed by NOR, Morris water maze or context-dependent fear conditioning tests (Rajadhyaksha *et al*, 2012; Bavley *et al*, 2018; Choi *et al*, 2018). Altogether, the phenotype of CRBN-KO mice reminds of that of patients suffering from the R419X mutation causing ARNSMR (Higgins *et al*, 2004). Experiments with cell lines suggest that this mutation enhances CRBN protein degradation through increased *C*-terminal ubiquitination (Xu *et al*, 2013), which reconciles with CRBN-KO mice resembling the alterations of individuals with ARNSMR. Our data add to previous information that CRBN molecules exquisitely located on telencephalic glutamatergic neurons are responsible for this long-term recognition memory impairment, as both CRBN-KO and Glu-CRBN-KO, but not GABA-CRBN-KO mice, underperformed the NOR test. In addition, Glu-CRBN-KO mice also showed impaired memory in a Y-maze-based spatial memory paradigm. This is consistent with previous studies showing that CaMKII-CRBN-KO mice freeze less when re-exposed to an aversive environment. Since focal deletion of CRBN in the dorsal hippocampus by using a constitutive Cre recombinase impairs spatial memory (Bavley *et al*, 2018), and, as shown here, CRBN protein levels in hippocampal extracts come mostly from excitatory cells, it seems most likely that this phenotype arises from the loss of CRBN molecules in glutamatergic cells of the dorsal hippocampus (presumably, granular cells). In the forthcoming months, we intend to substantiate this notion by using i) acute genetic-inactivation of CRBN by stereotaxic injection of viral vectors expressing Cre recombinase under the control of cell-type selective promoters in the dorsal hippocampus of CRBN-floxed mice, and ii) Cre-dependent genetic-rescue of CRBN expression in the dorsal hippocampus of Glu-CRBN-KO by using DIO-CRBN vectors that we have already generated. Moreover, the acute knockout of CRBN in adult mice is essential to clarify whether developmental alterations in CRBN mouse lines contribute to the alteration of learning and memory processes. Nonetheless, this seems unlikely as CRBN expression peaks at the adult age (Higgins *et al*, 2010). Of note, a very recent study has found that CRBN controls neural

stem cell proliferation during zebrafish development (Ando *et al*, 2019). Since adult neural stem cells play essential roles in learning, episodic memory and spatial navigation tasks (Gonçalves *et al*, 2016), whether altered adult neurogenesis underlies the memory impairment observed in CRBN-KO mice should be assessed in the future.

To decipher molecular mechanisms underlying CRBN knockout-induced memory shortfalls, we started by analyzing the levels of a series of proteins involved in synaptic organization. We did not detect expression changes in any of the proteins analyzed (PSD-95, synaptophysin 1, vGAT and vGLUT1) neither in the global nor in the conditional knockouts. This finding contrasts with published data of CRBN-KO mice that found alterations in some of these proteins, although recurrent inconsistencies exist between reports (Bavley *et al*, 2018; Choi *et al*, 2018). Again, this question may have its explanation in methodological issues, as one study used very young mice (3-5-week-old), and the other one used hippocampal synaptosomal fractions of mice whose age was not indicated, in contrast with our experimental approach, that used whole hippocampal homogenates of adult (*ca.* 8-week-old) mice. Nonetheless, protein levels of major synaptic components, such as glutamate and GABA receptor subunits, as well as proteins involved in the exocytosis of neurotransmitter vesicles, should be determined in the future, particularly after finding that CRBN (to bear in mind, a 'protein degrader' in nature) was identified at synaptosomal preparations, which suggests a presynaptic localization.

CRBN knockout mouse models might represent a valuable tool to identify novel treatments for ARNSMR. The involvement of CB_1R in the disease seems likely for various reasons. First, our data shows that CRBN is an inhibitor of CB_1R function in heterologous cells. Second, CRBN-KO mice show decreased probability of release in excitatory neurons (Choi *et al*, 2018). Third, molecular targets linked to this phenotype, such as BK_{Ca} or AMPK (Bavley *et al*, 2018; Choi *et al*, 2018), can be effectively activated by CB_1R (Stumpff *et al*, 2005; Kola *et al*, 2005; Romano & Lograno, 2006). Fourth, CB_1R hyperactivity occurs in mouse models of fragile X and Down syndromes, other diseases that cause intellectual disability, and CB_1R antagonism ameliorates the pathology symptoms (Busquets-Garcia *et al*, 2013; Gomis-González *et al*, 2016; Navarro-Romero *et al*, 2019). Thus, we tried to revert memory deficits induced by CRBN loss with the acute administration of a low dose (0.3 mg/kg) of the CB_1R-selective antagonist rimonabant, and found a trend towards improved memory function. Importantly, this dose is significantly lower than that employed to reduce food intake in mice (Wiley *et al*, 2005). Since rimonabant was withdrawn from the market due to serious psychiatric side-effects, lower doses might represent a safer therapeutic approach (Gomis-González *et al*, 2016). In addition, at this dose, rimonabant might be used in a sustained-administration regime (Gomis-González *et al*, 2016). Taken together, we propose a model in which CRBN deficiency-induced CB_1R overactivation in excitatory cells underlies the memory shortfalls observed in CRBN-KO and Glu-CRBN-KO mice, a notion that might extend to individuals suffering from ARNSMR (Fig. D4).

Finally, I would like to speculate on the potential implication of CB_1R in thalidomide-mediated deleterious effects. During the late 1950s until the early 1960s, thalidomide was prescribed as an antiemetic, tranquilizer and sedative for treating morning sickness. Usage by pregnant woman led to one of the biggest tragedies in the history of drug development, as it caused severe malformations in thousands of children (Franks *et al*, 2004; Zhou *et al*, 2013). Considering our data in full caption (and of course, being fully aware that they represent very preliminary results), thalidomide (and derivatives) might disengage CRBN from CB_1R. Since CRBN behaves as a CB_1R inhibitor *in vitro*, this could lead to an enhanced CB_1R function. Were this model correct, thalidomide intake could trigger increased CB_1R

signaling. Several researchers, including our group, have focused on teratogenic effects of cannabis, particularly THC. Although THC consumption during pregnancy can lead to detrimental effects *via* CB_1R, none of them has the extension of those caused by thalidomide (De Salas-Quiroga *et al*, 2015; Díaz-Alonso *et al*, 2017; de Salas-Quiroga *et al*, 2020; Bara *et al*, 2021). Thus, the involvement of CB_1R in the teratogenesis caused by thalidomide seems highly unlikely. Accordingly, several CRBN substrates have been linked to the origin of congenital malformations induced by this drug (*e.g.,* Matyskiela *et al*, 2018; Asatsuma-Okumura *et al*, 2019). In fact, since the discovery of CRBN as the molecular target of thalidomide, most research efforts have been put on finding molecular culprits of teratogenesis, as well as identifying proteins responsible for the antitumoral effects, as its most common therapeutic use is the treatment of haematological cancers (Krönke *et al*, 2014; Lu *et al*, 2014; Sievers *et al*, 2018; Yamamoto *et al*, 2020). Ironically, very few reports have searched for the mechanism of action underlying the sedative and antiemetic effects of thalidomide, actions for which it was initially prescribed. Molecular pathways eliciting thalidomide-induced antiemesis remain largely unexplored. Interestingly, the CB_1R agonists dronabinol and nabilone are approved by the FDA for antiemesis in cancer patients treated with chemotherapy (Todaro, 2012). Thus, to what extent activation of CB_1R following CRBN disengagement might underlie the antiemetic effect of thalidomide is a very exciting hypothesis. On the other hand, to the best of our knowledge, only one study has assessed the molecular determinants of thalidomide-induced sedation, and found that it did not involve CRBN (Hirose *et al*, 2020). Nonetheless, since hypnotic effects or cannabinoids have long been known (Kesner & Lovinger, 2020), we dare proposing that thalidomide-mediated disruption of the CB_1R-CRBN function might be regarded as a potential sedative mechanism of thalidomide to be addressed in the future. Taken together, the potential implication of CB_1R in the mechanism of action of thalidomide looks like an exciting journey ahead of us.

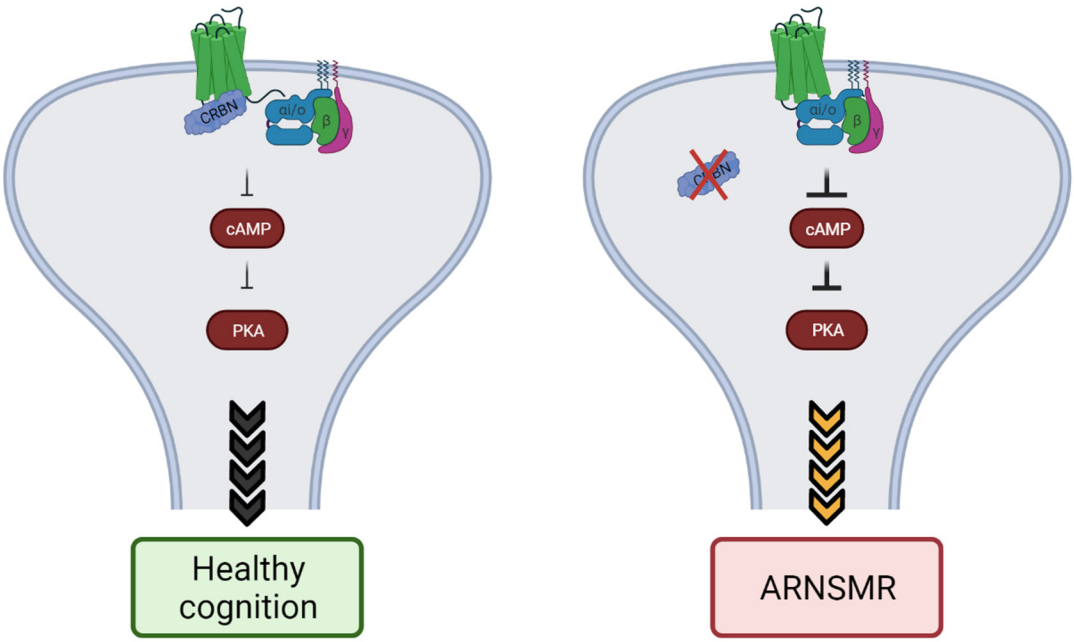

Figure D4. Proposed model for the control of memory by CB_1R-CRBN complexes. In a physiological state, CRBN associates to CB_1R and attenuates the activation of the canonical cAMP/PKA pathway. Mice devoid of THE *Crbn* gene, might present an overactivated CB_1R tone, leading to diminished cAMP/PKA axis activity, that in turn could underlie the neurotransmission and memory deficits present in CRBN-KO and Glu-CRBN-KO mice. This alteration might extend to individuals affected by ARNSMR.

INTRODUCTION

AIMS

MATERIALS AND METHODS

RESULTS

DISCUSSION

CONCLUSIONS

REFERENCES

Conclusions

The data obtained in this Doctoral Thesis allow us to extract the following conclusions.

1. BiP and CRBN are new CB_1R-interacting proteins.
2. The *C*-terminal region of BiP interacts with a 11-amino acid stretch of CB_1R-CTD.
3. BiP binding modulates CB_1R action by inhibiting a $G\alpha_{q/11}$-driven activation of the ERK and Akt pathways.
4. The BiP-CB_1R interaction occurs in GABAergic neurons of the mouse forebrain.
5. BiP, likely by binding CB_1R, modulates CB_1R-evoked anxiety in mice.
6. CRBN, through hitherto unknown region(s), interacts with a 11-amino acid stretch of CB_1R-CTD.
7. CRBN binding modulates CB_1R action by attenuating the $G\alpha_{i/o}$-driven inhibition of the canonical adenylyl cyclase/cAMP pathway.
8. Genetic inactivation of CRBN in telencephalic excitatory neurons causes memory shortfalls in mice.
9. CB_1R overactivation might be involved in CRBN genetic-inactivation-induced memory deficits in mice.

References

Aguado T, Monory K, Palazuelos J, Stella N, Cravatt B, Lutz B, Marsicano G, Kokaia Z, Guzmán M & Galve-Roperh I (2005) The endocannabinoid system drives neural progenitor proliferation. *FASEB J* 19: 1704–1706

Ahn KH, Mahmoud MM, Shim JY & Kendall DA (2013) Distinct roles of β-arrestin 1 and β-arrestin 2 in ORG27569-induced biased signaling and internalization of the cannabinoid receptor 1 (CB1). *J Biol Chem* 288: 9790–9800

Ahn KH, Pellegrini M, Tsomaia N, Yatawara AK, Kendall DA & Mierke DF (2009) Structural analysis of the human cannabinoid receptor one carboxyl-terminus identifies two amphipathic helices. *Biopolymers* 91: 565–573

Akber U, Jo H, Jeon S, Yang SJ, Bong S, Lim S, Kim YK, Park ZY & Park CS (2021) Cereblon regulates the proteotoxicity of tau by tuning the chaperone activity of DNAJA1. *J Neurosci* 41: 5138–5156

Akutsu M, Dikic I & Bremm A (2016) Ubiquitin chain diversity at a glance. *J Cell Sci* 129: 875–880

Albarran E, Sun Y, Liu Y, Raju K, Dong A, Li Y, Wang S, Südhof TC & Ding JB (2021) Postsynaptic synucleins mediate vesicular exocytosis of endocannabinoids. *bioRxiv*: 2021.10.04.462870

Ando H, Sato T, Ito T, Yamamoto J, Sakamoto S, Nitta N, Asatsuma-Okumura T, Shimizu N, Mizushima R, Aoki I, *et al* (2019) Cereblon control of zebrafish brain size by regulation of neural stem cell proliferation. *iScience* 15: 95–108

Andradas C, Blasco-Benito S, Castillo-Lluva S, Dillenburg-Pilla P, Diez-Alarcia R, Juanes-García A, García-Taboada E, Hernando-Llorente R, Soriano J, Hamann S, *et al* (2016) Activation of the orphan receptor GPR55 by lysophosphatidylinositol promotes metastasis in triple-negative breast cancer. *Oncotarget* 7: 47565–47575

Angulo I, Acebrón I, De Las Rivas B, Muñoz R, Rodríguez-Crespo I, Menéndez M, García P, Tateno H, Goldstein IJ, Pérez-Agote B, *et al* (2011) High-resolution structural insights on the sugar-recognition and fusion tag properties of a versatile-trefoil lectin domain from the mushroom Laetiporus sulphureus. *Glycobiology* 21: 1349–1361

Anwar M, Amin MR, Ragunathrao VAB, Matsche J, Karginov A, Minshall RD, Mo GH, Komarova Y & Mehta D (2021) Tyrosine phosphorylation of S1PR1 leads to chaperone bip-mediated import to the endoplasmic reticulum. *J Cell Biol* 220(12)

Araque A, Castillo PE, Manzoni OJ & Tonini R (2017) Synaptic functions of endocannabinoid signaling in health and disease. *Neuropharmacology* 124: 13–24

Armario A (2021) The forced swim test: Historical, conceptual and methodological considerations and its relationship with individual behavioral traits. *Neurosci Biobehav Rev* 128: 74–86

Asatsuma-Okumura T, Ando H, De Simone M, Yamamoto J, Sato T, Shimizu N, Asakawa K, Yamaguchi Y, Ito T, Guerrini L, *et al* (2019) P63 is a cereblon substrate nvolved in thalidomide teratogenicity. *Nat Chem Biol* 15: 1077–1084

Bach A, Pedersen SW, Dorr LA, Vallon G, Ripoche I, Ducki S & Lian LY (2015) Biochemical investigations of the mechanism of action of small molecules ZL006 and IC87201 as potential inhibitors of the nNOS-PDZ/PSD-95-PDZ interactions. *Sci Rep* 5: 12157

Baggelaar MP, Maccarrone M & van der Stelt M (2018) 2-Arachidonoylglycerol: A signaling lipid with manifold actions in the brain. *Prog Lipid Res* 71: 1–17

Bagher AM, Laprairie RB, Kelly MEM & Denovan-Wright EM (2016) Antagonism of dopamine receptor 2 long affects cannabinoid receptor 1 signaling in a cell culture model of striatal medium spiny projection neurons. *Mol Pharmacol* 89: 652–666

Bakshi K, Mercier RW & Pavlopoulos S (2007) Interaction of a fragment of the cannabinoid CB1 receptor C-terminus with arrestin-2. *FEBS Lett* 581: 5009–5016

Balenga NAB, Aflaki E, Kargl J, Platzer W, Schröder R, Blättermann S, Kostenis E, Brown AJ, Heinemann A & Waldhoer M (2011) GPR55 regulates cannabinoid 2 receptor-mediated responses in human neutrophils. *Cell Res* 21: 1452–1469

Bara A, Ferland JMN, Rompala G, Szutorisz H & Hurd YL (2021) Cannabis and synaptic reprogramming of the developing brain. *Nat Rev Neurosci* 22: 423–438

Bari M, Paradisi A, Pasquariello N & Maccarrone M (2005) Cholesterol-dependent modulation of type 1 cannabinoid receptors in nerve cells. *J Neurosci Res* 81: 275–283

Bavley CC, Rice RC, Fischer DK, Fakira AK, Byrne M, Kosovsky M, Rizzo BK, Del Prete D, Alaedini A, Morón JA, *et al* (2018) Rescue of learning and memory deficits in the human nonsyndromic intellectual disability cereblon knock-out mouse model by targeting the AMP-activated protein kinase–mTORC1 translational pathway. *J Neurosci* 38: 2780–2795

Belfi CA, Chatterjee S, Gosky DM, Berger SJ & Berger NA (1999) Increased sensitivity of human colon cancer cells to DNA cross-linking agents after GRP78 up-regulation. *Biochem Biophys Res Commun* 257: 361–368

Bellocchio L, Lafenetre P, Cannich A, Cota D, Puente N, Grandes P, Chaouloff F, Piazza PV & Marsicano G (2010) Bimodal control of stimulated food intake by the endocannabinoid system. *Nat Neurosci* 13: 281–283

Bénard G, Massa F, Puente N, Lourenço J, Bellocchio L, Soria-Gómez E, Matias I, Delamarre A, Metna-Laurent M, Cannich A, *et al* (2012) Mitochondrial CB1 receptors regulate neuronal energy metabolism. *Nat Neurosci* 15: 558–564

Benito C, Romero JP, Tolón RM, Clemente D, Docagne F, Hillard CJ, Guaza C & Romero J (2007) Cannabinoid CB1 and CB2 receptors and fatty acid amide hydrolase are specific markers of plaque cell subtypes in human multiple sclerosis. *J Neurosci* 27: 2396–2402

Berndsen CE & Wolberger C (2014) New insights into ubiquitin E3 ligase mechanism. *Nat Struct Mol Biol* 21: 301–307

Bertolotti A, Zhang Y, Hendershot LM, Harding HP & Ron D (2000) Dynamic interaction of BiP and ER stress transducers in the unfolded-protein response. *Nat Cell Biol* 2: 326–332

Biringer RG (2021) The rise and fall of anandamide: processes that control synthesis, degradation, and storage. *Mol Cell Biochem* 476: 2753–2775

Bisogno T, Howell F, Williams G, Minassi A, Cascio MG, Ligresti A, Matias I, Schiano-Moriello A, Paul P, Williams EJ, *et al* (2003) Cloning of the first sn1-DAG lipases points to the spatial and temporal regulation of endocannabinoid signaling in the brain. *J Cell Biol* 163: 463–468

Blankman JL, Simon GM & Cravatt BF (2007) A comprehensive profile of brain enzymes that hydrolyze the endocannabinoid 2-arachidonoylglycerol. *Chem Biol* 14: 1347–1356

Blázquez C, Ruiz-Calvo A, Bajo-Grañeras R, Baufreton JM, Resel E, Varilh M, Zottola ACP, Mariani Y, Cannich A, Rodríguez-Navarro JA, *et al* (2020) Inhibition of striatonigral autophagy as a link between cannabinoid intoxication and impairment of motor coordination. *Elife* 9: 1–24

Blom N, Sicheritz-Pontén T, Gupta R, Gammeltoft S & Brunak S (2004) Prediction of post-translational glycosylation and phosphorylation of proteins from the amino acid sequence. *Proteomics* 4: 1633–1649

Blume LC, Eldeeb K, Bass CE, Selley DE & Howlett AC (2015) Cannabinoid receptor interacting protein (CRIP1a) attenuates CB1R signaling in neuronal cells. *Cell Signal* 27: 716–726

Blume LC, Patten T, Eldeeb K, Leone-Kabler S, Ilyasov AA, Keegan BM, O'Neal JE, Bass CE, Hantgan RR, Lowther WT, *et al* (2017) Cannabinoid receptor interacting protein 1a competition with β-arrestin for CB1 receptor binding sites. *Mol Pharmacol* 91: 75–86

Bornert O, Møller TC, Boeuf J, Candusso MP, Wagner R, Martinez KL & Simonin F (2013) Identification of a novel protein-protein interaction motif mediating interaction of GPCR-associated sorting proteins with G Protein-coupled receptors. *PLoS One* 8: e56336

Bosier B, Doyen PJ, Brolet A, Muccioli GG, Ahmed E, Desmet N, Hermans E & Deumens R (2015) Inhibition of the regulator of G protein signalling RGS4 in the spinal cord decreases neuropathic hyperalgesia and restores cannabinoid CB1 receptor signalling. *Br J Pharmacol* 172: 5333–5346

Bouaboula M, Hilairet S, Marchand J, Fajas L, Le Fur G & Casellas P (2005) Anandamide induced PPARγ transcriptional activation and 3T3-L1 preadipocyte differentiation. *Eur J Pharmacol* 517: 174–181

Bouaboula M, Rinaldi M, Carayon P, Carillon C, Delpech B, Shire D, Le Fur G & Casellas P (1993) Cannabinoid-receptor expression in human leukocytes. *Eur J Biochem* 214: 173–180

Bozidis P, Williamson CD & Colberg-Poley AM (2007) Isolation of endoplasmic reticulum, mitochondria, and mitochondria-associated membrane fractions from transfected cells and from human cytomegalovirus-infected primary fibroblasts. *Curr Protoc Cell Biol* 37(1)

Braman J, Papworth C & Greener A (1996) Site-directed mutagenesis using double-stranded plasmid DNA templates. *Methods Mol Biol* 57: 31–44

Breivogel CS, Sim LJ & Childers SR (1997) Regional differences in cannabinoid receptor/G-protein coupling in rat brain. *J Pharmacol Exp Ther* 282: 1632–1642

Brooks SP, Trueman RC & Dunnett SB (2012) Assessment of motor coordination and balance in mice using the Rotarod, elevated bridge, and footprint tests. *Current Protocols in Mouse Biology* 2: 37-53

Brown SM, Wager-Miller J & Mackie K (2002) Cloning and molecular characterization of the rat CB2 cannabinoid receptor. *Biochim Biophys Acta - Gene Struct Expr* 1576: 255–264

Brückner A, Polge C, Lentze N, Auerbach D & Schlattner U (2009) Yeast two-hybrid, a powerful tool for systems biology. *Int J Mol Sci* 10: 2763–2788

Burton JC & Grimsey NJ (2019) Ubiquitination as a key regulator of endosomal signaling by GPCRs. *Front Cell Dev Biol* 7: 43

Busquets-Garcia A, Bains J & Marsicano G (2018) CB1 receptor signaling in the brain: extracting pecificity from ubiquity. *Neuropsychopharmacology* 43: 4–20

Busquets-Garcia A, Desprez T, Metna-Laurent M, Bellocchio L, Marsicano G & Soria-Gomez E (2015) Dissecting the cannabinergic control of behavior: The where matters. *BioEssays* 37: 1215–1225

Busquets-Garcia A, Gomis-González M, Guegan T, Agustín-Pavón C, Pastor A, Mato S, Pérez-Samartín A, Matute C, De La Torre R, Dierssen M, *et al* (2013) Targeting the endocannabinoid system in the treatment of fragile X syndrome. *Nat Med* 19: 603–607

Cadas H, Gaillet S, Beltramo M, Venance L & Piomelli D (1996) Biosynthesis of an endogenous cannabinoid precursor in neurons and its control by calcium and cAMP. 16: 3934–3942

Callén L, Moreno E, Barroso-Chinea P, Moreno-Delgado D, Cortés A, Mallol J, Casadó V, Lanciego JL, Franco R, Lluis C, *et al* (2012) Cannabinoid receptors CB1 and CB2 form functional heteromers in brain. *J Biol Chem* 287: 20851–20865

Casanova E, Fehsenfeld S, Mantamadiotis T, Lemberger T, Greiner E, Stewart AF & Schtz G (2001) A CamKIIα iCre BAC allows brain-specific gene inactivation. *Genesis* 31: 37–42

Casas C (2017) GRP78 at the centre of the stage in cancer and neuroprotection. *Front Neurosci* 11: 1–15

Castillo PE, Younts TJ, Chávez AE & Hashimotodani Y (2012) Endocannabinoid signaling and synaptic function. *Neuron* 76: 70–81

Cha-Molstad H, Sung KS, Hwang J, Kim KA, Yu JE, Yoo YD, Jang JM, Han DH, Molstad M, Kim JG, *et al* (2015) Amino-terminal arginylation targets endoplasmic reticulum chaperone BiP for autophagy through p62 binding. *Nat Cell Biol* 17: 917–929

Chen X, Yang W, Fan Y, Luo J, Hong K, Wang Z, Yan J, Chen X, Lu J, Benovic J, *et al* (2010) Structural determinants in the second intracellular loop of the human cannabinoid CB1 receptor mediate selective coupling to Gs and Gi. *Br J Pharmacol* 161: 1817–1834

Chen YA, Peng YJ, Hu MC, Huang JJ, Chien YC, Wu JT, Chen TY & Tang CY (2015) The cullin 4A/B-DDB1-cereblon E3 ubiquitin ligase complex mediates the degradation of CLC-1 chloride channels. *Sci Rep* 5: 1–13

Cheng X, Ji Z, Tsalkova T & Mei F (2008) Epac and PKA: A tale of two intracellular cAMP receptors. *Acta Biochim Biophys Sin (Shanghai)* 40: 651–662

Chevaleyre V & Castillo PE (2003) Heterosynaptic LTD of hippocampal GABAergic synapses: A novel role of endocannabinoids in regulating excitability. *Neuron* 38: 461–472

Choi TY, Lee SH, Kim YJ, Bae JR, Lee KM, Jo Y, Kim SJ, Lee AR, Choi S, Choi LM, *et al* (2018) Cereblon maintains synaptic and cognitive function by regulating BK channel. *J Neurosci* 38: 3571–3583

Ciechanover A (2015) The unravelling of the ubiquitin system. *Nat Rev Mol Cell Biol* 16: 322–324

Cravatt BF, Demarest K, Patricelli MP, Bracey MH, Giang DK, Martin BR & Lichtman AH (2001) Supersensitivity to anandamide and enhanced endogenous cannabinoid signaling in mice lacking fatty acid amide hydrolase. *Proc Natl Acad Sci U S A* 98: 9371–9376

Cravatt BF, Giang DK, Mayfield SP, Boger DL, Lerner RA & Gilula NB (1996) Molecular characterization of an enzyme that degrades neuromodulatory fatty-acid amides. *Nature* 384: 83–87

Cristino L, Bisogno T & Di Marzo V (2020) Cannabinoids and the expanded endocannabinoid system in neurological disorders. *Nat Rev Neurol* 16: 9–29

Cristobo I, Larriba MJ, Ríos V de los, García F, Muñoz A & Casal JI (2011) Proteomic analysis of 1α,25-Dihydroxyvitamin D 3 action on human colon cancer cells reveals a link to splicing regulation. *J Proteomics* 75: 384–397

Crocq MA (2020) History of cannabis and the endocannabinoid system. *Dialogues Clin Neurosci* 22: 223–228

Daigle TL, Kwok ML & Mackie K (2008) Regulation of CB1 cannabinoid receptor internalization by a promiscuous phosphorylation-dependent mechanism. *J Neurochem* 106: 70–82

Dalton GD, Carney ST, Marshburn JD, Norford DC & Howlett AC (2020) CB1 cannabinoid receptors stimulate Gβγ-GRK2-mediated FAK phosphorylation at tyrosine 925 to regulate ERK activation involving neuronal focal adhesions. *Front Cell Neurosci* 14: 176

Dalton GD & Howlett AC (2012) Cannabinoid CB1 receptors transactivate multiple receptor tyrosine kinases and regulate serine/ threonine kinases to activate ERK in neuronal cells. *Br J Pharmacol* 165: 2497–2511

Delgado-Peraza F, Ahn KH, Nogueras-Ortiz C, Mungrue IN, Mackie K, Kendall DA & Yudowski GA (2016) Mechanisms of biased β-arrestin-mediated signaling downstream from the cannabinoid 1 receptor. *Mol Pharmacol* 89: 618–629

Devane WA, Dysarz FA, Johnson MR, Melvin LS & Howlett AC (1988) Determination and characterization of a cannabinoid receptor in rat brain. *Mol Pharmacol* 34: 605-613

Devane WA, Hanuš L, Breuer A, Pertwee RG, Stevenson LA, Griffin G, Gibson D, Mandelbaum A, Etinger A & Mechoulam R (1992) Isolation and structure of a brain constituent that binds to the cannabinoid receptor. *Science* 258: 1946–1949

Devinsky O, Cross JH, Laux L, Marsh E, Miller I, Nabbout R, Scheffer IE, Thiele EA & Wright S (2017) Trial of cannabidiol for drug-resistant seizures in the Dravet syndrome. *N Engl J Med* 376: 2011–2020

Díaz-Alonso J, De Salas-Quiroga A, Paraíso-Luna J, García-Rincón D, Garcez PP, Parsons M, Andradas C, Sánchez C, Guillemot F, Guzmán M, *et al* (2017) Loss of cannabinoid CB1 receptors induces

cortical migration malformations and increases seizure susceptibility. *Cereb Cortex* 27: 5303–5317

Diez-Alarcia R, Ibarra-Lecue I, Lopez-Cardona ÁP, Meana J, Gutierrez-Adán A, Callado LF, Agirregoitia E & Urigüen L (2016) Biased agonism of three different cannabinoid receptor agonists in mouse brain cortex. *Front Pharmacol* 7: 1–13

Dinh TP, Carpenter D, Leslie FM, Freund TF, Katona I, Sensi SL, Kathuria S & Piomelli D (2002) Brain monoglyceride lipase participating in endocannabinoid inactivation. *Proc Natl Acad Sci U S A* 99: 10819–10824

Dixon AS, Schwinn MK, Hall MP, Zimmerman K, Otto P, Lubben TH, Butler BL, Binkowski BF, MacHleidt T, Kirkland TA, *et al* (2016) NanoLuc complementation reporter optimized for accurate measurement of protein interactions in cells. *ACS Chem Biol* 11: 400–408

Dvorakova M, Kubik-Zahorodna A, Straiker A, Sedlacek R, Hajkova A, Mackie K & Blahos J (2021) SGIP1 is involved in regulation of emotionality, mood, and nociception and modulates in vivo signalling of cannabinoid CB1 receptors. *Br J Pharmacol* 178: 1588–1604

Egertova M, Giang DK, Cravatt BF & Elphick MR (1998) A new perspective on cannabinoid signalling: Complementary localization of fatty acid amide hydrolase and the CB1 receptor in rat brain. *Proc R Soc B Biol Sci* 265: 2081–2085

Egertová M, Simon GM, Cravatt BF & Elphick MR (2008) Localization of N-acyl phosphatidylethanolamine phospholipase D (NAPE-PLD) expression in mouse brain: A new perspective on N- acylethanolamines as neural signaling molecules. *J Comp Neurol* 506: 604–615

Van Egmond N, Straub VM & Van Der Stelt M (2021) Targeting endocannabinoid signaling: FAAH and MAG lipase inhibitors. *Annu Rev Pharmacol Toxicol* 61: 441–463

Eichner R, Heider M, Fernández-Sáiz V, Van Bebber F, Garz AK, Lemeer S, Rudelius M, Targosz BS, Jacobs L, Knorn AM, *et al* (2016) Immunomodulatory drugs disrupt the cereblon-CD147-MCT1 axis to exert antitumor activity and teratogenicity. *Nat Med* 22: 735–743

Elphick MR (2012) The evolution and comparative neurobiology of endocannabinoid signalling. *Philos Trans R Soc B Biol Sci* 367: 3201–3215

Elphick MR, Satou Y & Satoh N (2003) The invertebrate ancestry of endocannabinoid signalling: An orthologue of vertebrate cannabinoid receptors in the urochordate Ciona intestinalis. *Gene* 302: 95–101

Ennaceur A (2010) One-trial object recognition in rats and mice: Methodological and theoretical issues. *Behav Brain Res* 215: 244–254

Ennaceur A & Delacour J (1988) A new one-trial test for neurobiological studies of memory in rats: Behavioral data. *Behav Brain Res* 31: 47–59

Esteban PF, Garcia-Ovejero D, Paniagua-Torija B, Moreno-Luna R, Arredondo LF, Zimmer A, Martín ÁA & Molina-Holgado E (2020) Revisiting CB1 cannabinoid receptor detection and the exploration of its interacting partners. *J Neurosci Methods* 337: 108680

Fang Y, Li G & Ferrie AM (2007) Non-invasive optical biosensor for assaying endogenous G protein-coupled receptors in adherent cells. *J Pharmacol Toxicol Methods* 55: 314–322

Feige MJ & Hendershot LM (2013) Quality control of integral membrane proteins by assembly-dependent membrane integration. *Mol Cell* 51: 297–309

Fields S (2005) High-throughput two-hybrid analysis: The promise and the peril. *FEBS Journal* 272: 5391–5399.

Fields S & Song OK (1989) A novel genetic system to detect protein-protein interactions. *Nature* 340: 245–246

Filipeanu CM, Guidry JJ, Leonard ST & Winsauer PJ (2011) Δ9-THC increases endogenous AHA1

expression in rat cerebellum and may modulate CB1 receptor function during chronic use. *J Neurochem* 118: 1101–1112

Fischer ES, Böhm K, Lydeard JR, Yang H, Stadler MB, Cavadini S, Nagel J, Serluca F, Acker V, Lingaraju GM, *et al* (2014) Structure of the DDB1-CRBN E3 ubiquitin ligase in complex with thalidomide. *Nature* 512: 49–53

Fletcher-Jones A, Hildick KL, Evans AJ, Nakamura Y, Wilkinson KA & Henley JM (2019) The C-Terminal helix 9 motif in rat cannabinoid receptor type 1 regulates axonal trafficking and surface expression. *Elife* 8: 1–26

Flick JS & Johnston M (1990) Two systems of glucose repression of the GAL1 promoter in Saccharomyces cerevisiae. *Mol Cell Biol* 10: 4757–4769

Franks ME, Macpherson GR & Figg WD (2004) Thalidomide. *Lancet* 363: 1802–1811

Fredriksson S, Gullberg M, Jarvius J, Olsson C, Pietras K, Gústafsdóttir SM, Östman A & Landegren U (2002) Protein detection using proximity-dependent DNA ligation assays. *Nat Biotechnol* 20: 473–477

Galiègue S, Mary S, Marchand J, Dussossoy D, Carrière D, Carayon P, Bouaboula M, Shire D, LE Fur G & Casellas P (1995) Expression of central and peripheral cannabinoid receptors in human immune tissues and leukocyte subpopulations. *Eur J Biochem* 232: 54–61

Galve-Roperh I, Chiurchiù V, Díaz-Alonso J, Bari M, Guzmán M & Maccarrone M (2013) Cannabinoid receptor signaling in progenitor/stem cell proliferation and differentiation. *Prog Lipid Res* 52: 633–650

Galve-Roperh I, Rueda D, Del Pulgar TG, Velasco G & Guzmán M (2002) Mechanism of extracellular signal-regulated kinase activation by the CB1 cannabinoid receptor. *Mol Pharmacol* 62: 1385–1392

Gao Y, Vasilyev D V., Goncalves MB, Howell F V., Hobbs C, Reisenberg M, Shen R, Zhang MY, Strassle BW, Lu P, *et al* (2010) Loss of retrograde endocannabinoid signaling and reduced adult neurogenesis in diacylglycerol lipase knock-out mice. *J Neurosci* 30: 2017–2024

Gaoni Y & Mechoulam R (1964) Isolation, structure, and partial synthesis of an active constituent of hashish. *J Am Chem Soc* 86: 1646–1647

García-Nafría J, Watson JF & Greger IH (2016) IVA cloning: A single-tube universal cloning system exploiting bacterial In Vivo Assembly. *Sci Rep* 6: 1–12

Garcia DE, Brown S, Hille B & Mackie K (1998) Protein kinase C disrupts cannabinoid actions by phosphorylation of the CB1 cannabinoid receptor. *J Neurosci* 18: 2834–2841

Gerdeman GL, Ronesi J & Lovinger DM (2002) Postsynaptic endocannabinoid release is critical to long-term depression in the striatum. *Nat Neurosci* 5: 446–451

Gething MJ (1999) Role and regulation of the ER chaperone BiP. *Semin Cell Dev Biol* 10: 465–472

De Giacomo V, Ruehle S, Lutz B, Häring M & Remmers F (2020) Differential glutamatergic and GABAergic contributions to the tetrad effects of Δ(9)-tetrahydrocannabinol revealed by cell-type-specific reconstitution of the CB1 receptor. *Neuropharmacology* 179: 108287

De Giacomo V, Ruehle S, Lutz B, Häring M & Remmers F (2021) Cell type-specific genetic reconstitution of CB1 receptor subsets to assess their role in exploratory behaviour, sociability, and memory. *Eur J Neurosci* 00: 1– 13

Giang DK & Cravatt BF (1997) Molecular characterization of human and mouse fatty acid amide hydrolases. *Proc Natl Acad Sci U S A* 94: 2238–2242

Gil M, Kim YK, kim HY, Pak HK, Park CS & Lee KJ (2018) Cereblon deficiency confers resistance against polymicrobial sepsis by the activation of AMP activated protein kinase and heme-oxygenase-1. *Biochem Biophys Res Commun* 495: 976–981

Glass M & Felder CC (1997) Concurrent stimulation of cannabinoid CB1 and dopamine D2 receptors augments cAMP accumulation in striatal neurons: Evidence for a G(s) linkage to the CB1 receptor. *J Neurosci* 17: 5327–5333

Gómez-Almería M, Burgaz S, Costas-Insua C, Rodríguez-Cueto C, Santos-García I, Rodríguez-Crespo I, García C, Guzmán M, de Lago E & Fernández-Ruiz J (2021) Bip heterozigosity aggravates pathological deterioration in experimental amyotrophic lateral sclerosis. *Int J Mol Sci* 22: 12533

Gómez Del Pulgar T, Velasco G & Guzmán M (2000) The CB1 cannabinoid receptor is coupled to the activation of protein kinase B/Akt. *Biochem J* 347: 369–373

Gomis-González M, Matute C, Maldonado R, Mato S & Ozaita A (2016) Possible therapeutic doses of cannabinoid type 1 receptor antagonist reverses key alterations in fragile X syndrome mouse model. *Genes (Basel)* 7

Gonçalves JT, Schafer ST & Gage FH (2016) Adult neurogenesis in the hippocampus: from stem cells to behavior. *Cell* 167: 897–914

Gopal U & Pizzo S V. (2021) Cell surface GRP78 signaling: An emerging role as a transcriptional modulator in cancer. *J Cell Physiol* 236: 2352–2363

Goparaju SK, Ueda N, Taniguchi K & Yamamoto S (1999) Enzymes of porcine brain hydrolyzing 2-arachidonoylglycerol, an endogenous ligand of cannabinoid receptors. *Biochem Pharmacol* 57: 417–423

Grundmann M, Merten N, Malfacini D, Inoue A, Preis P, Simon K, Rüttiger N, Ziegler N, Benkel T, Schmitt NK, *et al* (2018) Lack of beta-arrestin signaling in the absence of active G proteins. *Nat Commun* 9: 1–7

Guegan T, Cutando L, Gangarossa G, Santini E, Fisone G, Martinez A, Valjent E, Maldonado R & Martin M (2013) Operant behavior to obtain palatable food modifies ERK activity in the brain reward circuit. *Eur Neuropsychopharmacol* 23: 240–252

Guggenhuber S, Alpar A, Chen R, Schmitz N, Wickert M, Mattheus T, Harasta AE, Purrio M, Kaiser N, Elphick MR, *et al* (2016) Cannabinoid receptor-interacting protein Crip1a modulates CB1 receptor signaling in mouse hippocampus. *Brain Struct Funct* 221: 2061–2074

Gupte TM, Malik RU, Sommese RF, Ritt M & Sivaramakrishnan S (2017) Priming GPCR signaling through the synergistic effect of two G proteins. *Proc Natl Acad Sci U S A* 114: 3756–3761

Haas IG & Wabl M (1983) Immunoglobulin heavy chain binding protein. *Nature* 306: 387–389

Hájková A, Techlovská Š, Dvořáková M, Chambers JN, Kumpošt J, Hubálková P, Prezeau L & Blahos J (2016) SGIP1 alters internalization and modulates signaling of activated cannabinoid receptor 1 in a biased manner. *Neuropharmacology* 107: 201–214

Han J, Kesner P, Metna-Laurent M, Duan T, Xu L, Georges F, Koehl M, Abrous DN, Mendizabal-Zubiaga J, Grandes P, *et al* (2012) Acute cannabinoids impair working memory through astroglial CB1 receptor modulation of hippocampal LTD. *Cell* 148: 1039–1050

Handley SL & Mithani S (1984) Effects of alpha-adrenoceptor agonists and antagonists in a maze-exploration model of 'fear'-motivated behaviour. *Naunyn Schmiedebergs Arch Pharmacol* 327: 1–5

Hashimotodani Y, Ohno-Shosaku T & Kano M (2007) Presynaptic monoacylglycerol lipase activity determines basal endocannabinoid tone and terminates retrograde endocannabinoid signaling in the hippocampus. *J Neurosci* 27: 1211–1219

Hayashi T & Su TP (2007) Sigma-1 Receptor chaperones at the ER- mitochondrion interface regulate Ca2+ signaling and cell survival. *Cell* 131: 596–610

He C, Wei Y, Sun K, Li B, Dong X, Zou Z, Liu Y, Kinch LN, Khan S, Sinha S, *et al* (2013) Beclin 2 functions in autophagy, degradation of G protein-coupled receptors, and metabolism. *Cell* 154: 1085–1099

Hebert-Chatelain E, Desprez T, Serrat R, Bellocchio L, Soria-Gomez E, Busquets-Garcia A, Pagano Zottola AC, Delamarre A, Cannich A, Vincent P, *et al* (2016) A cannabinoid link between mitochondria and memory. *Nature* 539: 555–559

Heider M, Eichner R, Stroh J, Morath V, Kuisl A, Zecha J, Lawatscheck J, Baek K, Garz AK, Rudelius M, *et al* (2021) The IMiD target CRBN determines HSP90 activity toward transmembrane proteins essential in multiple myeloma. *Mol Cell* 81: 1170-1186.e10

Herkenham M, Lynn AB, Little MD, Johnson MR, Melvin LS, De Costa BR & Rice KC (1990) Cannabinoid receptor localization in brain. *Proc Natl Acad Sci U S A* 87: 1932–1936

Hershko A & Ciechanover A (1998) The ubiquitin system. *Annu Rev Biochem* 67: 425–479

Higgins JJ, Pucilowska J, Lombardi RQ & Rooney JP (2004) A mutation in a novel ATP-dependent Lon protease gene in a kindred with mild mental retardation. *Neurology* 63: 1927–1931

Higgins JJ, Rosen DR, Loveless JM, Clyman JC & Grau MJ (2000) A gene for nonsyndromic mental retardation maps to chromosome 3p25-pter. *Neurology* 55: 335–340

Higgins JJ, Tal AL, Sun X, Hauck SCR, Hao J, Kosofosky BE & Rajadhyaksha AM (2010) Temporal and spatial mouse brain expression of cereblon, an ionic channel regulator involved in human intelligence. *J Neurogenet* 24: 18–26

Hirose Y, Kitazono T, Sezaki M, Abe M, Sakimura K, Funato H, Handa H, Vogt KE & Yanagisawa M (2020) Hypnotic effect of thalidomide is independent of teratogenic ubiquitin/proteasome pathway. *Proc Natl Acad Sci* 117: 23106–23112

Hohberger B & Enz R (2009) Cereblon is expressed in the retina and binds to voltage-gated chloride channels. *FEBS Lett* 583: 633–637

Hollocks MJ, Lerh JW, Magiati I, Meiser-Stedman R & Brugha TS (2019) Anxiety and depression in adults with autism spectrum disorder: A systematic review and meta-analysis. *Psychol Med* 49: 559–572

Howlett AC & Abood ME (2017) CB1 and CB2 Receptor Pharmacology. *Adv in Pharmacol* 80: 169–206.

Hua T, Li X, Wu L, Iliopoulos-Tsoutsouvas C, Wang Y, Wu M, Shen L, Brust CA, Nikas SP, Song F, *et al* (2020) Activation and signaling mechanism revealed by cannabinoid receptor-Gi complex structures. *Cell* 180: 655-665.e18

Hua T, Vemuri K, Nikas SP, Laprairie RB, Wu Y, Qu L, Pu M, Korde A, Jiang S, Ho JH, *et al* (2017) Crystal structures of agonist-bound human cannabinoid receptor CB1. *Nature* 547: 468–471

Hua T, Vemuri K, Pu M, Qu L, Han GW, Wu Y, Zhao S, Shui W, Li S, Korde A, *et al* (2016) Crystal structure of the human cannabinoid receptor CB1. *Cell* 167: 750-762.e14

Hudson BD, Hébert TE & Kelly ME (2010) Physical and functional interaction between CB1 cannabinoid receptors and β2-adrenoceptors. *Br J Pharmacol* 160: 627–642

Hussain Z, Uyama T, Tsuboi K & Ueda N (2017) Mammalian enzymes responsible for the biosynthesis of N-acylethanolamines. *Biochim Biophys Acta - Mol Cell Biol Lipids* 1862: 1546–1561

Huttlin EL, Bruckner RJ, Navarrete-Perea J, Cannon JR, Baltier K, Gebreab F, Gygi MP, Thornock A, Zarraga G, Tam S, *et al* (2021) Dual proteome-scale networks reveal cell-specific remodeling of the human interactome. *Cell* 184: 3022-3040.e28

Huttlin EL, Bruckner RJ, Paulo JA, Cannon JR, Ting L, Baltier K, Colby G, Gebreab F, Gygi MP, Parzen H, *et al* (2017) Architecture of the human interactome defines protein communities and disease networks. *Nature* 545: 505–509

Huttlin EL, Ting L, Bruckner RJ, Gebreab F, Gygi MP, Szpyt J, Tam S, Zarraga G, Colby G, Baltier K, *et al* (2015) The BioPlex network: a systematic exploration of the human interactome. *Cell* 162: 425–440

Inoue A, Raimondi F, Kadji FMN, Singh G, Kishi T, Uwamizu A, Ono Y, Shinjo Y, Ishida S, Arang N, *et al* (2019) Illuminating G-protein-coupling selectivity of GPCRs. *Cell* 177: 1933-1947.e25

Ito T, Ando H, Suzuki T, Ogura T, Hotta K, Imamura Y, Yamaguchi Y & Handa H (2010) Identification of a primary target of thalidomide teratogenicity. *Science* 327: 1345–1350

Jäntti MH, Mandrika I & Kukkonen JP (2014) Human orexin/hypocretin receptors form constitutive homo- and heteromeric complexes with each other and with human CB1 cannabinoid receptors. *Biochem Biophys Res Commun* 445: 486–490

Jeon S, Yoon YS, Kim HK, Han J, Lee KM, Seol JE, Cho SK & Park CS (2021) Ablation of CRBN induces loss of type I collagen and SCH in mouse skin by fibroblast senescence via the p38 MAPK pathway. *Aging (Albany NY)* 13: 6406–6419

Jeon SJ, Ham J, Park CS & Lee B (2020) Susceptibility of pentylenetetrazole-induced seizures in mice with Cereblon gene knockout. *BMB Rep* 53: 484–489

Jimenez-Blasco D, Busquets-Garcia A, Hebert-Chatelain E, Serrat R, Vicente-Gutierrez C, Ioannidou C, Gómez-Sotres P, Lopez-Fabuel I, Resch-Beusher M, Resel E, *et al* (2020) Glucose metabolism links astroglial mitochondria to cannabinoid effects. *Nature* 583: 603–608

Jo S, Lee KH, Song S, Jung YK & Park CS (2005) Identification and functional characterization of cereblon as a binding protein for large-conductance calcium-activated potassium channel in rat brain. *J Neurochem* 94: 1212–1224

Jordan JD, He JC, Eungdamrong NJ, Gomes I, Ali W, Nguyen T, Bivona TG, Philips MR, Devi LA & Iyengar R (2005) Cannabinoid receptor-induced neurite outgrowth is mediated by Rap1 activation through Gαo/i-triggered proteasomal degradation of Rap1GAPII. *J Biol Chem* 280: 11413–11421

Kaczocha M & Haj-Dahmane S (2021) Mechanisms of endocannabinoid transport in the brain. *Br J Pharmacol* 1: 11

Käll L, Canterbury JD, Weston J, Noble WS & MacCoss MJ (2007) Semi-supervised learning for peptide identification from shotgun proteomics datasets. *Nat Methods* 4: 923–925

Kang HJ, Lee KJ, Woo J, Kim J, Kim YK, Lee CH, Yoo CG & Lee KH (2021) Cereblon contributes to the development of pulmonary fibrosis via inactivation of adenosine monophosphate-activated protein kinase α1. *Exp Mol Med* 53: 885–893

Kang JA, Park SH, Jeong SP, Han MH, Lee CR, Lee KM, Kim N, Song MR, Choi M, Ye M, *et al* (2016) Epigenetic regulation of Kcna3-encoding Kv1.3 potassium channel by cereblon contributes to regulation of CD4+ T-cell activation. *Proc Natl Acad Sci U S A* 113: 8771–8776

Kargl J, Balenga N, Parzmair GP, Brown AJ, Heinemann A & Waldhoer M (2012) The cannabinoid receptor CB1 modulates the signaling properties of the lysophosphatidylinositol receptor GPR55. *J Biol Chem* 287: 44234–44248

Kataoka K, Nakamura C, Asahi T & Sawamura N (2016) Mitochondrial cereblon functions as a Lon-type protease. *Sci Rep* 6: 29986

Katona I & Freund TF (2008) Endocannabinoid signaling as a synaptic circuit breaker in neurological disease. *Nat Med* 14: 923–930

Kearn CS, Blake-Palmer K, Daniel E, Mackie K & Glass M (2005) Concurrent stimulation of cannabinoid CB1 and dopamine D2 receptors enhances heterodimer formation: A mechanism for receptor cross-talk? *Mol Pharmacol* 67: 1697–1704

Kesner AJ & Lovinger DM (2020) Cannabinoids, endocannabinoids and sleep. *Front Mol Neurosci* 13: 125

Kim HK, Ko TH, Nyamaa B, Lee SR, Kim N, Ko KS, Rhee BD, Park CS, Nilius B & Han J (2016) Cereblon in health and disease. *Pflugers Arch Eur J Physiol* 468: 1299–1309

Kim HK, Seol JE, Ahn SW, Jeon S, Park CS & Han J (2021a) Cereblon: promise and challenges for

combating human diseases. *Pflugers Arch Eur J Physiol* 473: 1695–1711

Kim J, Lee KM, Park CS & Park WJ (2014) Ablation of cereblon attenuates myocardial ischemia-reperfusion injury. *Biochem Biophys Res Commun* 447: 649–654

Kim MJ, Min Y, Shim JH, Chun E & Lee KY (2019) CRBN is a negative regulator of bactericidal activity and autophagy activation through inhibiting the ubiquitination of ECSIT and BECN1. *Front Immunol* 10: 2203

Kim YS, Li Y, Yuan J, Borg JP, Sun X & Dey SK (2021b) Cannabinoid and planar cell polarity signaling converges to direct placentation. *Proc Natl Acad Sci U S A* 118: 1–12

Kola B, Hubina E, Tucci SA, Kirkham TC, Garcia EA, Mitchell SE, Williams LM, Hawley SA, Hardie DG, Grossman AB, *et al* (2005) Cannabinoids and ghrelin have both central and peripheral metabolic and cardiac effects via AMP-activated protein kinase. *J Biol Chem* 280: 25196–25201

Kong DH, Zhang Q, Meng X, Zong ZH, Li C, Liu BQ, Guan Y & Wang HQ (2013) BAG3 sensitizes cancer cells exposed to DNA damaging agents via direct interaction with GRP78. *Biochim Biophys Acta - Mol Cell Res* 1833: 3245–3253

Kraeuter AK, Guest PC & Sarnyai Z (2019) The Y-Maze for assessment of spatial working and reference memory in mice. *Methods Mol Biol* 1916: 105–111

Krishna Kumar K, Shalev-Benami M, Robertson MJ, Hu H, Banister SD, Hollingsworth SA, Latorraca NR, Kato HE, Hilger D, Maeda S, *et al* (2019) Structure of a signaling cannabinoid receptor 1-G protein complex. *Cell* 176: 448-458.e12

Krönke J, Fink EC, Hollenbach PW, MacBeth KJ, Hurst SN, Udeshi ND, Chamberlain PP, Mani DR, Man HW, Gandhi AK, *et al* (2015) Lenalidomide induces ubiquitination and degradation of CK1α in del(5q) MDS. *Nature* 523: 183–188

Krönke J, Udeshi ND, Narla A, Grauman P, Hurst SN, McConkey M, Svinkina T, Heckl D, Comer E, Li X, *et al* (2014) Lenalidomide causes selective degradation of IKZF1 and IKZF3 in multiple myeloma cells. *Science* 343: 301–305

Kumar P, Mahato DK, Kamle M, Borah R, Sharma B, Pandhi S, Tripathi V, Yadav HS, Devi S, Patil U, *et al* (2021) Pharmacological properties, therapeutic potential, and legal status of Cannabis sativa L.: An overview. *Phyther Res* 35: 6010–6029

Lalonde R (2002) The neurobiological basis of spontaneous alternation. *Neurosci Biobehav Rev* 26: 91–104

Langer I, Leroy K, Gaspard N, Brion JP & Robberecht P (2008) Cell surface targeting of VPAC1 receptors: Evidence for implication of a quality control system and the proteasome. *Biochim Biophys Acta - Mol Cell Res* 1783: 1663–1672

Laprairie RB, Bagher AM, Kelly MEM & Denovan-Wright EM (2015) Cannabidiol is a negative allosteric modulator of the cannabinoid CB1 receptor. *Br J Pharmacol* 172: 4790–4805

Lauckner JE, Hille B & Mackie K (2005) The cannabinoid agonist WIN55,212-2 increases intracellular calcium via CB1 receptor coupling to Gq/11 G proteins. *Proc Natl Acad Sci U S A* 102: 19144–19149

Lee KM, Jo S, Kim H, Lee J & Park CS (2011) Functional modulation of AMP-activated protein kinase by cereblon. *Biochim Biophys Acta - Mol Cell Res* 1813: 448–455

Lee KM, Yang SJ, Kim YD, Choi YD, Nam JH, Choi CS, Choi HS & Park CS (2013) Disruption of the cereblon gene enhances hepatic AMPK activity and prevents high-fat diet-induced obesity and insulin resistance in mice. *Diabetes* 62: 1855–1864

Lee S, Park S, Lee H, Han S, Song JM, Han D & Suh YH (2019) Nedd4 E3 ligase and beta-arrestins regulate ubiquitination, trafficking, and stability of the mGlu7 receptor. *Elife* 8: e44502

Leterrier C, Lainé J, Darmon M, Boudin H, Rossier J & Lenkei Z (2006) Constitutive activation drives

compartment-selective endocytosis and axonal targeting of type 1 cannabinoid receptors. *J Neurosci* 26: 3141–3153

Leung D, Saghatelian A, Simon GM & Cravatt BF (2006) Inactivation of N-Acyl phosphatidylethanolamine phospholipase D reveals multiple mechanisms for the biosynthesis of endocannabinoids. *Biochemistry* 45: 4720–4726

Li J, Ni M, Lee B, Barron E, Hinton DR & Lee AS (2008) The unfolded protein response regulator GRP78/BiP is required for endoplasmic reticulum integrity and stress-induced autophagy in mammalian cells. *Cell Death Differ* 15: 1460–1471

Li X, Hua T, Vemuri K, Ho JH, Wu Y, Wu L, Popov P, Benchama O, Zvonok N, Locke K, *et al* (2019) Crystal structure of the human cannabinoid receptor CB2. *Cell* 176: 459-467.e13

Li X, Shen L, Hua T & Liu ZJ (2020) Structural and functional insights into cannabinoid receptors. *Trends Pharmacol Sci* 41: 665–677

Lièvremont JP, Rizzuto R, Hendershot L & Meldolesi J (1997) BiP, a major chaperone protein of the endoplasmic reticulum lumen, plays a direct and important role in the storage of the rapidly exchanging pool of Ca2+. *J Biol Chem* 272: 30873–30879

Lister RG (1987) The use of a plus-maze to measure anxiety in the mouse. *Psychopharmacology (Berl)* 92: 180–185

Little PJ, Compton DR, Johnson MR, Melvin LS & Martin BR (1988) Pharmacology and stereoselectivity of structurally novel cannabinoids in mice. *J Pharmacol Exp Ther* 247: 1046–1051

Liu J, Ye J, Zou X, Xu Z, Feng Y, Zou X, Chen Z, Li Y & Cang Y (2014) CRL4A CRBN E3 ubiquitin ligase restricts BK channel activity and prevents epileptogenesis. *Nat Commun* 5: 1–9

Liu QR, Pan CH, Hishimoto A, Li CY, Xi ZX, Llorente-Berzal A, Viveros MP, Ishiguro H, Arinami T, Onaivi ES, *et al* (2009) Species differences in cannabinoid receptor 2 (CNR2 gene): Identification of novel human and rodent CB2 isoforms, differential tissue expression and regulation by cannabinoid receptor ligands. *Genes, Brain Behav* 8: 519–530

Lobato-Freitas C, Brito-Da-costa AM, Dinis-Oliveira RJ, Carmo H, Carvalho F, Silva JP & Dias-Da-silva D (2021) Overview of synthetic cannabinoids adb-fubinaca and amb-fubinaca: Clinical, analytical, and forensic implications. *Pharmaceuticals* 14: 1–39

Lu G, Middleton RE, Sun H, Naniong MV, Ott CJ, Mitsiades CS, Wong KK, Bradner JE & Kaelin WG (2014) The myeloma drug lenalidomide promotes the cereblon-dependent destruction of Ikaros proteins. *Science* 343: 305–309

Lundqvist T (2005) Cognitive consequences of cannabis use: Comparison with abuse of stimulants and heroin with regard to attention, memory and executive functions. *Pharmacol Biochem Behav r* 81: 319–330.

Luo S, Mao C, Lee B & Lee AS (2006) GRP78/BiP is required for cell proliferation and protecting the inner cell mass from apoptosis during early mouse embryonic development. *Mol Cell Biol* 26: 5688–5697

Lutz B, Marsicano G, Maldonado R & Hillard CJ (2015) The endocannabinoid system in guarding against fear, anxiety and stress. *Nat Rev Neurosci* 16: 705–718

Mackie K, Lai Y, Westenbroek R & Mitchell R (1995) Cannabinoids activate an inwardly rectifying potassium conductance and inhibit Q-type calcium currents in AtT20 cells transfected with rat brain cannabinoid receptor. *J Neurosci* 15: 6552–6561

Magalhaes AC, Dunn H & Ferguson SSGSSG (2012) Regulation of GPCR activity, trafficking and localization by GPCR-interacting proteins. *Br J Pharmacol* 165: 1717–1736

Magotti P, Bauer I, Igarashi M, Babagoli M, Marotta R, Piomelli D & Garau G (2015) Structure of human N-acylphosphatidylethanolamine-hydrolyzing phospholipase D: Regulation of fatty acid ethanolamide biosynthesis by bile acids. *Structure* 23: 598–604

Malfitano AM, Basu S, Maresz K, Bifulco M & Dittel BN (2014) What we know and do not know about the cannabinoid receptor 2 (CB2). *Semin Immunol* 26: 369–379

Marchese A & Trejo JA (2013) Ubiquitin-dependent regulation of G protein-coupled receptor trafficking and signaling. *Cell Signal* 25: 707–716

Maroso M, Szabo GG, Kim HK, Alexander A, Bui AD, Lee SH, Lutz B & Soltesz I (2016) Cannabinoid control of learning and memory through HCN channels. *Neuron* 89: 1059–1073

Marsicano G, Goodenough S, Monory K, Hermann H, Eder M, Cannich A, Azad SC, Cascio MG, Ortega-Gutiérrez S, Van der Stelt M, *et al* (2003) CB1 cannabinoid receptors and on-demand defense against excitotoxicity. *Science* 302: 84–88

Marsicano G & Lafenêtre P (2009) Roles of the endocannabinoid system in learning and memory. *Curr Top Behav Neurosci* 1: 201–230

Marsicano G & Lutz B (1999) Expression of the cannabinoid receptor CB1 in distinct neuronal subpopulations in the adult mouse forebrain. *Eur J Neurosci* 11: 4213–4225

Marsicano G, Wotjak CT, Azad SC, Bisogno T, Rammes G, Cascioll MG, Hermann H, Tang J, Hofmann C, Zieglgänsberger W, *et al* (2002) The endogenous cannabinoid system controls extinction of aversive memories. *Nature* 418: 530–534

Martin BR (1986) Cellular effects of cannabinoids. *Pharmacol Rev* 38: 45–74

Martín R, Durroux T, Ciruela F, Torres M, Pin J-P, Sánchez-Prieto J & Sá Nchez-Prieto J (2010) The metabotropic glutamate receptor mGlu7 activates phospholipase C, translocates munc-13-1 protein, and potentiates glutamate release at cerebrocortical nerve terminals. *J Biol Chem* 285: 17907–17917

Martini L, Thompson D, Kharazia V & Whistler JL (2010) Differential regulation of behavioral tolerance to WIN55,212-2 by GASP1. *Neuropsychopharmacology* 35: 1363–1373

Martini L, Waldhoer M, Pusch M, Kharazia V, Fong J, Lee JH, Freissmuth C & Whistler JL (2007) Ligand-induced down-regulation of the cannabinoid 1 receptor is mediated by the G-protein-coupled receptor-associated sorting protein GASP1. *FASEB J* 21: 802–811

Masuho I, Balaji S, Muntean BS, Skamangas NK, Chavali S, Tesmer JJG, Babu MM & Martemyanov KA (2020) A global map of G protein signaling regulation by RGS proteins. *Cell* 183: 503-521.e19

Matsuda LA, Lolait SJ, Brownstein MJ, Young AC & Bonner TI (1990) Structure of a cannabinoid receptor and functional expression of the cloned cDNA. *Nature* 346: 561–564

Mattern M, Sutherland J, Kadimisetty K, Barrio R & Rodriguez MS (2019) Using ubiquitin binders to decipher the ubiquitin code. *Trends Biochem Sci* 44: 599–615

Mattheus T, Kukla K, Zimmermann T, Tenzer S & Lutz B (2016) Cell type-specific tandem affinity purification of the mouse hippocampal CB1 receptor-associated proteome. *J Proteome Res* 15: 3585–3601

Matyskiela ME, Couto S, Zheng X, Lu G, Hui J, Stamp K, Drew C, Ren Y, Wang M, Carpenter A, *et al* (2018) SALL4 mediates teratogenicity as a thalidomide-dependent cereblon substrate. *Nat Chem Biol* 14: 981–987

Mazzone CM, Pati D, Michaelides M, DiBerto J, Fox JH, Tipton G, Anderson C, Duffy K, McKlveen JM, Hardaway JA, *et al* (2018) Acute engagement of Gq-mediated signaling in the bed nucleus of the stria terminalis induces anxiety-like behavior. *Mol Psychiatry* 23: 143–153

Mechoulam R, Ben-Shabat S, Hanus L, Ligumsky M, Kaminski NE, Schatz AR, Gopher A, Almog S, Martin BR, Compton DR, *et al* (1995) Identification of an endogenous 2-monoglyceride, present in canine gut, that binds to cannabinoid receptors. *Biochem Pharmacol* 50: 83–90

Mechoulam R, Hanuš LO, Pertwee R & Howlett AC (2014) Early phytocannabinoid chemistry to endocannabinoids and beyond. *Nat Rev Neurosci* 15: 757–764

Mechoulam R, Shani A, Edery H & Grunfeld Y (1970) Chemical basis of hashish activity. *Science* 169: 611–612

Mechoulam R & Shvo Y (1963) Hashish-I. The structure of Cannabidiol. *Tetrahedron* 19: 2073–2078

Merino-Gracia J, Costas-Insua C, Ángeles Canales M & Rodríguez-Crespo I (2016a) Insights into the C-terminal peptide binding specificity of the PDZ domain of neuronal nitric-oxide synthase: Characterization of the interaction with the tight junction protein claudin-3. *J Biol Chem* 291: 11581–11595

Merino-Gracia J, Zamora-Carreras H, Bruix M & Rodríguez-Crespo I (2016b) Molecular basis for the protein recognition specificity of the dynein light chain DYNLT1/Tctex1: Characterization of the interaction with activin receptor IIB. *J Biol Chem* 291: 20962–20975

Metna-Laurent M, Mondésir M, Grel A, Vallée M & Piazza PV (2017) Cannabinoid-induced tetrad in mice. *Curr Protoc Neurosci* 2017: 9.59.1-9.59.10

Min Y, Wi SM, Kang JA, Yang T, Park CS, Park SG, Chung S, Shim JH, Chun E & Lee KY (2016) Cereblon negatively regulates TLR4 signaling through the attenuation of ubiquitination of TRAF6. *Cell Death Dis* 7: e2313–e2313

Misra UK, Gonzalez-Gronow M, Gawdi G, Hart JP, Johnson CE & Pizzo S V. (2002) The role of Grp 78 in α2-macroglobulin-induced signal transduction: Evidence from RNA interference that the low density lipoprotein receptor-related protein is associated with, but not necessary for, GRP 78-mediated signal transduction. *J Biol Chem* 277: 42082–42087

Mizrachi D & Segaloff DL (2004) Intracellularly located misfolded glycoprotein hormone receptors associate with different chaperone proteins than their cognate wild-type receptors. *Mol Endocrinol* 18: 1768–1777

Molina-Holgado E, Paniagua-Torija B, Arevalo-Martin A, Moreno-Luna R, Esteban PF, Le MQU, Del Cerro M del M & Garcia-Ovejero D (2021) Cannabinoid receptor 1 associates to different molecular complexes during GABAergic neuron maturation. *J Neurochem* 158: 640–656

Molina-Holgado E, Vela JM, Arévalo-Martín A, Almazán G, Molina-Holgado F, Borrell J & Guaza C (2002) Cannabinoids promote oligodendrocyte progenitor survival: Involvement of cannabinoid receptors and phosphatidylinositol-3 kinase/Akt signaling. *J Neurosci* 22: 9742–9753

Monday HR, Bourdenx M, Jordan BA & Castillo PE (2020) CB1-receptor-mediated inhibitory LTD triggers presynaptic remodeling via protein synthesis and ubiquitination. *Elife* 9: 1–25

Monory K, Blaudzun H, Massa F, Kaiser N, Lemberger T, Schütz G, Wotjak CT, Lutz B & Marsicano G (2007) Genetic dissection of behavioural and autonomic effects of Δ9-tetrahydrocannabinol in mice. *PLoS Biol* 5: e269

Monory K, Massa F, Egertová M, Eder M, Blaudzun H, Westenbroek R, Kelsch W, Jacob W, Marsch R, Ekker M, *et al* (2006) The endocannabinoid system controls key epileptogenic circuits in the hippocampus. *Neuron* 51: 455–466

Moon H, Min C, Kim G, Kim D, Kim K, Lee SA, Moon B, Yang S, Lee J, Yang SJ, *et al* (2020) Crbn modulates calcium influx by regulating Orai1 during efferocytosis. *Nat Commun* 11: 5489

Moreno E, Chiarlone A, Medrano M, Puigdellívol M, Bibic L, Howell LA, Resel E, Puente N, Casarejos MJ, Perucho J, *et al* (2018) Singular location and signaling profile of adenosine A2A-cannabinoid CB1 Receptor heteromers in the dorsal striatum. *Neuropsychopharmacology* 43: 964–977

Morgan DJ, Davis BJ, Kearn CS, Marcus D, Cook AJ, Wager-Miller J, Straiker A, Myoga MH, Karduck J, Leishman E, *et al* (2014) Mutation of putative GRK phosphorylation sites in the cannabinoid receptor 1 (CB1R) confers resistance to cannabinoid tolerance and hypersensitivity to cannabinoids in mice. *J Neurosci* 34: 5152–5163

Moy SS, Nadler JJ, Perez A, Barbaro RP, Johns JM, Magnuson TR, Piven J & Crawley JN (2004)

Sociability and preference for social novelty in five inbred strains: An approach to assess autistic-like behavior in mice. *Genes, Brain Behav* 3: 287–302

Mukhopadhyay S & Howlett AC (2001) CB1 receptor-G protein association: Subtype selectivity is determined by distinct intracellular domains. *Eur J Biochem* 268: 499–505

Mukhopadhyay S, McIntosh HH, Houston DB & Howlett AC (2000) The CB1 cannabinoid receptor juxtamembrane C-terminal peptide confers activation to specific G proteins in brain. *Mol Pharmacol* 57: 162–170

Munro S & Pelham H (1985) What turns on heat shock genes? *Nature* 317: 477–478

Munro S & Pelham HRB (1986) An hsp70-like protein in the ER: Identity with the 78 kd glucose-regulated protein and immunoglobulin heavy chain binding protein. *Cell* 46: 291–300

Munro S, Thomas KL & Abu-Shaar M (1993) Molecular characterization of a peripheral receptor for cannabinoids. *Nature* 365: 61–65

Murakami M & Kouyama T (2008) Crystal structure of squid rhodopsin. *Nature* 453: 363–367

National Institute for Health and Care Excellence (UK) (2019) Cannabis-based medicinal products. Evidence review for chronic pain. London

Navarrete M & Araque A (2008) Endocannabinoids mediate neuron-astrocyte Communication. *Neuron* 57: 883–893

Navarro-Romero A, Vázquez-Oliver A, Gomis-González M, Garzón-Montesinos C, Falcón-Moya R, Pastor A, Martín-García E, Pizarro N, Busquets-Garcia A, Revest JM, *et al* (2019) Cannabinoid type-1 receptor blockade restores neurological phenotypes in two models for Down syndrome. *Neurobiol Dis* 125: 92–106

Navarro G, Varani K, Lillo A, Vincenzi F, Rivas-Santisteban R, Raïch I, Reyes-Resina I, Ferreiro-Vera C, Borea PA, Sánchez de Medina V, *et al* (2020) Pharmacological data of cannabidiol- and cannabigerol-type phytocannabinoids acting on cannabinoid CB(1), CB(2) and CB(1)/CB(2) heteromer receptors. *Pharmacol Res* 159: 104940

Nguyen T Van, Lee JE, Sweredoski MJ, Yang SJ, Jeon SJ, Harrison JS, Yim JH, Lee SG, Handa H, Kuhlman B, *et al* (2016) Glutamine triggers acetylation-dependent degradation of glutamine synthetase via the thalidomide receptor cereblon. *Mol Cell* 61: 809–820

Ni M, Zhou H, Wey S, Baumeister P & Lee AS (2009) Regulation of PERK signaling and leukemic cell survival by a novel cytosolic isoform of the UPR regulator GRP78/BiP. *PLoS One* 4: e6868

Niehaus JL, Liu Y, Wallis KT, Egertová M, Bhartur SG, Mukhopadhyay S, Shi S, He H, Selley DE, Howlett AC, *et al* (2007) CB1 cannabinoid receptor activity is modulated by the cannabinoid receptor interacting protein CRIP 1a. *Mol Pharmacol* 72: 1557–1566

Njoo C, Agarwal N, Lutz B & Kuner R (2015) The cannabinoid receptor CB1 interacts with the WAVE1 complex and plays a role in actin dynamics and structural plasticity in neurons. *PLoS Biol* 13: 1–36

Nogueras-Ortiz C & Yudowski GA (2016) The multiple waves of cannabinoid 1 receptor signaling. *Mol Pharmacol* 90: 620–626

Novotna A, Mares J, Ratcliffe S, Novakova I, Vachova M, Zapletalova O, Gasperini C, Pozzilli C, Cefaro L, Comi G, *et al* (2011) A randomized, double-blind, placebo-controlled, parallel-group, enriched-design study of nabiximols* (Sativex®), as add-on therapy, in subjects with refractory spasticity caused by multiple sclerosis. *Eur J Neurol* 18: 1122–1131

Nowak RP, Deangelo SL, Buckley D, He Z, Donovan KA, An J, Safaee N, Jedrychowski MP, Ponthier CM, Ishoey M, *et al* (2018) Plasticity in binding confers selectivity in ligand-induced protein degradation article. *Nat Chem Biol* 14: 706–714

Ogura Y, Parsons WH, Kamat SS & Cravatt BF (2016) A calcium-dependent acyltransferase that produces N-Acyl phosphatidylethanolamines. *Nat Chem Biol* 12: 669–671

Ohno-Shosaku T, Shosaku J, Tsubokawa H & Kano M (2002) Cooperative endocannabinoid production by neuronal depolarization and group I metabotropic glutamate receptor activation. *Eur J Neurosci* 15: 953–961

Okamoto Y, Morishita J, Tsuboi K, Tonai T & Ueda N (2004) Molecular characterization of a phospholipase D generating anandamide and its congeners. *J Biol Chem* 279: 5298–5305

Oliveira da Cruz JF, Busquets-Garcia A, Zhao Z, Varilh M, Lavanco G, Bellocchio L, Robin L, Cannich A, Julio-Kalajzić F, Lesté-Lasserre T, *et al* (2020) Specific hippocampal interneurons shape consolidation of recognition memory. *Cell Rep* 32(7): 108046

Oyagawa CRM & Grimsey NL (2021) Cannabinoid receptor CB1 and CB2 interacting proteins: Techniques, progress and perspectives *Methods in Cell Biology* 166: 83–132

Palazuelos J, Aguado T, Egia A, Mechoulam R, Guzmán M, Galve-Roperh I, Palazuelos J, Aguado T, Egia A, Mechoulam R, *et al* (2006) Non-psychoactive CB2 cannabinoid agonists stimulate neural progenitor proliferation. *FASEB J* 20: 2405–2407

Pasquariello N, Catanzaro G, Marzano V, Amadio D, Barcaroli D, Oddi S, Federici G, Urbani A, Agrò AF & Maccarrone M (2009) Characterization of the endocannabinoid system in human neuronal cells and proteomic analysis of anandamide-induced apoptosis. *J Biol Chem* 284: 29413–29426

Pendyala G, Periyasamy P, Callen S, Fox HS, Lisco SJ & Buch SJ (2015) Chronic SIV and morphine treatment increases heat shock protein 5 expression at the synapse. 21: 592–598

Pertwee RG, Howlett AC, Abood ME, Alexander SPH, Di Marzo V, Elphick MR, Greasley PJ, Hansen HS, Kunos G, Mackie K, *et al* (2010) International Union of Basic and Clinical Pharmacology. LXXIX. Cannabinoid receptors and their ligands: beyond CB_1 and CB_2. *Pharmacol Rev* 62: 588–631

Piazza PV, Cota D & Marsicano G (2017) The CB1 Receptor as the Cornerstone of Exostasis. *Neuron* 93: 1252–1274

Pinto D, Pagnamenta AT, Klei L, Anney R, Merico D, Regan R, Conroy J, Magalhaes TR, Correia C, Abrahams BS, *et al* (2010) Functional impact of global rare copy number variation in autism spectrum disorders. *Nature* 466: 368–372

Piomelli D (2003) The molecular logic of endocannabinoid signalling. *Nat Rev Neurosci* 4: 873–884

Piomelli D, Beltramo M, Glasnapp S, Lin SY, Goutopoulos A, Xie XQ & Makriyannis A (1999) Structural determinants for recognition and translocation by the anandamide transporter. *Proc Natl Acad Sci U S A* 96: 5802–5807

Pisanti S & Bifulco M (2019) Medical Cannabis: A plurimillennial history of an evergreen. *J Cell Physiol* 234: 8342–8351

Pobre KFR, Poet GJ & Hendershot LM (2019) The endoplasmic reticulum (ER) chaperone BiP is a master regulator of ER functions: Getting by with a little help from ERdj friends. *J Biol Chem* 294: 2098–2108

Porsolt RD, Bertin A & Jalfre M (1977) Behavioral despair in mice: A primary screening test for antidepressants. *Arch Int Pharmacodyn Ther* 229: 327–336

Prete D Del, Rice RC, Rajadhyaksha AM & D'Adamio L (2016) Amyloid precursor protein (APP) may act as a substrate and a recognition unit for CRL4 CRBN and stub1 E3 ligases facilitating ubiquitination of proteins involved in presynaptic functions and neurodegeneration. *J Biol Chem* 291: 17209–17227

Price MR, Baillie GL, Thomas A, Stevenson LA, Easson M, Goodwin R, McLean A, McIntosh L, Goodwin G, Walker G, *et al* (2005) Allosteric modulation of the cannabinoid CB1 receptor. *Mol Pharmacol* 68: 1484–1495

Priestley R, Glass M & Kendall D (2017) Functional Selectivity at Cannabinoid Receptors *Adv in Pharmacol* 80: 207–221

Puighermanal E, Busquets-Garcia A, Gomis-González M, Marsicano G, Maldonado R & Ozaita A (2013) Dissociation of the pharmacological effects of THC by mTOR blockade. *Neuropsychopharmacology* 38: 1334–1343

Puighermanal E, Marsicano G, Busquets-Garcia A, Lutz B, Maldonado R & Ozaita A (2009) Cannabinoid modulation of hippocampal long-term memory is mediated by mTOR signaling. *Nat Neurosci* 12: 1152–1158

Rajadhyaksha AM, Ra S, Kishinevsky S, Lee AS, Romanienko P, DuBoff M, Yang C, Zupan B, Byrne M, Daruwalla ZR, *et al* (2012) Behavioral characterization of cereblon forebrain-specific conditional null mice: A model for human non-syndromic intellectual disability. *Behav Brain Res* 226: 428–434

Ramesh K & Rosenbaum DM (2021) Molecular basis for ligand modulation of the cannabinoid CB1 receptor. *Br J Pharmacol* 1-9

Rao R V., Peel A, Logvinova A, Del Rio G, Hermel E, Yokota T, Goldsmith PC, Ellerby LM, Ellerby HM & Bredesen DE (2002) Coupling endoplasmic reticulum stress to the cell death program: Role of the ER chaperone GRP78. *FEBS Lett* 514: 122–128

Rey AA, Purrio M, Viveros MP & Lutz B (2012) Biphasic effects of cannabinoids in anxiety responses: CB1 and GABA B receptors in the balance of gabaergic and glutamatergic neurotransmission. *Neuropsychopharmacology* 37: 2624–2634

Rios C, Gomes I & Devi LA (2006) μ opioid and CB1 cannabinoid receptor interactions: Reciprocal inhibition of receptor signaling and neuritogenesis. *Br J Pharmacol* 148: 387–395

Robbe D, Kopf M, Remaury A, Bockaert J & Manzoni OJ (2002) Endogenous cannabinoids mediate long-term synaptic depression in the nucleus accumbens. *Proc Natl Acad Sci U S A* 99: 8384–8388

Roberto M, Cruz M, Bajo M, Siggins GR, Parsons LH & Schweitzer P (2010) The endocannabinoid system tonically regulates inhibitory transmission and depresses the effect of ethanol in central amygdala. *Neuropsychopharmacology* 35: 1962–1972

Robin LM, Oliveira da Cruz JF, Langlais VC, Martin-Fernandez M, Metna-Laurent M, Busquets-Garcia A, Bellocchio L, Soria-Gomez E, Papouin T, Varilh M, *et al* (2018) Astroglial CB1 Receptors determine synaptic D-Serine availability to enable recognition memory. *Neuron* 98: 935-944.e5

Roland AB, Ricobaraza A, Carrel D, Jordan BM, Rico F, Simon A, Humbert-Claude M, Ferrier J, McFadden MH, Scheuring S, *et al* (2014) Cannabinoid-induced actomyosin contractility shapes neuronal morphology and growth. *Elife* 3: e03159

Romano MR & Lograno MD (2006) Cannabinoid agonists induce relaxation in the bovine ophthalmic artery: Evidences for CB1 receptors, nitric oxide and potassium channels. *Br J Pharmacol* 147: 917–925

Ron D & Walter P (2007) Signal integration in the endoplasmic reticulum unfolded protein response. *Nat Rev Mol Cell Biol* 8: 519–529

Rozenfeld R & Devi LA (2008) Regulation of CB1 cannabinoid receptor trafficking by the adaptor protein AP-3 . *FASEB J* 22: 2311–2322

Rozenfeld R, Gupta A, Gagnidze K, Lim MP, Gomes I, Lee-Ramos D, Nieto N & Devi LA (2011) AT1R-CB1R heteromerization reveals a new mechanism for the pathogenic properties of angiotensin II. *EMBO J* 30: 2350–2363

Rubino T, Guidali C, Vigano D, Realini N, Valenti M, Massi P & Parolaro D (2008) CB1 receptor stimulation in specific brain areas differently modulate anxiety-related behaviour. *Neuropharmacology* 54: 151–160

Rubino T, Sala M, Viganò D, Braida D, Castiglioni C, Limonta V, Guidali C, Realini N & Parolaro D (2007) Cellular mechanisms underlying the anxiolytic effect of low doses of peripheral Δ9-

tetrahydrocannabinol in rats. *Neuropsychopharmacology* 32: 2036–2045

Ruehle S, Rey AA, Remmers F & Lutz B (2012) The endocannabinoid system in anxiety, fear memory and habituation. *J Psychopharmacol* 26: 23–39

Ruehle S, Wager-Miller J, Straiker A, Farnsworth J, Murphy MN, Loch S, Monory K, Mackie K & Lutz B (2017) Discovery and characterization of two novel CB1 receptor splice variants with modified N-termini in mouse. *J Neurochem* 142: 521–533

De Salas-Quiroga A, Díaz-Alonso J, García-Rincón D, Remmers F, Vega D, Gómez-Cañas M, Lutz B, Guzmán M & Galve-Roperh I (2015) Prenatal exposure to cannabinoids evokes long-lasting functional alterations by targeting CB1 receptors on developing cortical neurons. *Proc Natl Acad Sci U S A* 112: 13693–13698

de Salas-Quiroga A, García-Rincón D, Gómez-Domínguez D, Valero M, Simón-Sánchez S, Paraíso-Luna J, Aguareles J, Pujadas M, Muguruza C, Callado LF, *et al* (2020) Long-term hippocampal interneuronopathy drives sex-dimorphic spatial memory impairment induced by prenatal THC exposure. *Neuropsychopharmacology* 45: 877–886

Sánchez C, Rueda D, Ségui B, Galve-Roperh I, Levade T & Guzmáan M (2001) The CB1 cannabinoid receptor of astrocytes is coupled to sphingomyelin hydrolysis through the adaptor protein fan. *Mol Pharmacol* 59: 955–959

Sawamura N, Yamada M, Fujiwara M, Yamada H, Hayashi H, Takagi N & Asahi T (2018) The neuroprotective effect of thalidomide against ischemia through the Cereblon-mediated repression of AMPK activity. *Sci Rep* 8: 1–9

Scherma M, Masia P, Satta V, Fratta W, Fadda P & Tanda G (2019) Brain activity of anandamide: a rewarding bliss? *Acta Pharmacol Sin* 40: 309–323

Schröder R, Janssen N, Schmidt J, Kebig A, Merten N, Hennen S, Müller A, Blättermann S, Mohr-Andrä M, Zahn S, *et al* (2010) Deconvolution of complex G protein-coupled receptor signaling in live cells using dynamic mass redistribution measurements. *Nat Biotechnol* 28: 943–949

Schröder R, Schmidt J, Blättermann S, Peters L, Janssen N, Grundmann M, Seemann W, Kaufel D, Merten N, Drewke C, *et al* (2011) Applying label-free dynamic mass redistribution technology to frame signaling of G protein-coupled receptors noninvasively in living cells. *Nat Protoc* 6: 1748–1760

Schwab MH, Bartholomae A, Heimrich B, Feldmeyer D, Druffel-Augustin S, Goebbels S, Naya FJ, Zhao S, Frotscher M, Tsai MJ, *et al* (2000) Neuronal basic helix-loop-helix proteins (NEX and BETA2/Neuro D) regulate terminal granule cell differentiation in the hippocampus. *J Neurosci* 20: 3714–3724

Schwenk F, Baron U & Rajewsky K (1995) A cre-transgenic mouse strain for the ubiquitous deletion of loxP-flanked gene segments including deletion in germ cells. *Nucleic Acids Res* 23: 5080–5081

Seibenhener ML & Wooten MC (2015) Use of the open field maze to measure locomotor and anxiety-like behavior in mice. *J Vis Exp*: 52434

Shao Z, Yan W, Chapman K, Ramesh K, Ferrell AJ, Yin J, Wang X, Xu Q & Rosenbaum DM (2019) Structure of an allosteric modulator bound to the CB1 cannabinoid receptor. *Nat Chem Biol* 15: 1199–1205

Shao Z, Yin J, Chapman K, Grzemska M, Clark L, Wang J & Rosenbaum DM (2016) High-resolution crystal structure of the human CB1 cannabinoid receptor. *Nature* 540: 602–606

Shen C, Nayak A, Neitzel LR, Adams AA, Silver-Isenstadt M, Sawyer LM, Benchabane H, Wang H, Bunnag N, Li B, *et al* (2021) The E3 ubiquitin ligase component, Cereblon, is an evolutionarily conserved regulator of Wnt signaling. *Nat Commun* 12: 1–10

Shen J, Chen X, Hendershot L & Prywes R (2002) ER stress regulation of ATF6 localization by dissociation of BiP/GRP78 binding and unmasking of golgi localization signals. *Dev Cell* 3: 99–

111

Shenoy SK, McDonald PH, Kohout TA & Lefkowitz RJ (2001) Regulation of receptor fate by ubiquitination of activated β2-adrenergic receptor and β-arrestin. *Science* 294: 1307–1313

Shim SM, Choi HR, Sung KW, Lee YJ, Kim ST, Kim D, Mun SR, Hwang J, Cha-Molstad H, Ciechanover A, *et al* (2018) The endoplasmic reticulum-residing chaperone BiP is short-lived and metabolized through N-terminal arginylation. *Sci Signal* 11: 511

Shire D, Calandra B, Rinaldi-Carmona M, Oustric D, Pessègue B, Bonnin-Cabanne O, Le Fur G, Caput D & Ferrara P (1996) Molecular cloning, expression and function of the murine CB2 peripheral cannabinoid receptor. *Biochim Biophys Acta - Gene Struct Expr* 1307: 132–136

Shire D, Carillon C, Kaghad M, Calandra B, Rinaldi-Carmona M, Le Fur G, Caput D & Ferrara P (1995) An amino-terminal variant of the central cannabinoid receptor resulting from alternative splicing. *J Biol Chem* 270: 3726–3731

Shiu RPC, Pouyssegur J & Pastan I (1977) Glucose depletion accounts for the induction of two transformation-sensitive membrane proteins in Rous sarcoma virus-transformed chick embryo fibroblasts. *Proc Natl Acad Sci U S A* 74: 3840–3844

Sievers QL, Petzold G, Bunker RD, Renneville A, Słabicki M, Liddicoat BJ, Abdulrahman W, Mikkelsen T, Ebert BL & Thomä NH (2018) Defining the human C2H2 zinc finger degrome targeted by thalidomide analogs through CRBN. *Science* 362: 6414

Siffroi-Fernandez S, Giraud A, Lanet J & Franc JL (2002) Association of the thyrotropin receptor with calnexin, calreticulin and BiP: Effects on the maturation of the receptor. *Eur J Biochem* 269: 4930–4937

Singh Bora K & Sharma A (2012) Evaluation of anxiolytic effect of Medicago sativa in mice. *Pharm Biol* 50: 878–882

Skieterska K, Rondou P & Van Craenenbroeck K (2017) Regulation of G protein-coupled receptors by ubiquitination. *Int J Mol Sci* 18: 10–13

Söderberg O, Gullberg M, Jarvius M, Ridderstråle K, Leuchowius KJ, Jarvius J, Wester K, Hydbring P, Bahram F, Larsson LG, *et al* (2006) Direct observation of individual endogenous protein complexes in situ by proximity ligation. *Nat Methods* 3: 995–1000

Soria-Gomez E, Pagano Zottola AC, Mariani Y, Desprez T, Barresi M, Bonilla-Del Río I, Muguruza C, Le Bon-Jego M, Julio-Kalajzić F, Flynn R, *et al* (2021) Subcellular specificity of cannabinoid effects in striatonigral circuits. *Neuron* 109: 1513-1526.e11

Steindel F, Lerner R, Häring M, Ruehle S, Marsicano G, Lutz B & Monory K (2013) Neuron-type specific cannabinoid-mediated G protein signalling in mouse hippocampus. *J Neurochem* 124: 795–807

Stella N (2004) Cannabinoid signaling in glial cells. *Glia* 48: 267–277

Stella N, Schweitzer P & Plomelli D (1997) A second endogenous' cannabinoid that modulates long-term potentiation. *Nature* 388: 773–778

Straiker A, Wager-Miller J, Hutchens J & Mackie K (2012) Differential signalling in human cannabinoid CB1 receptors and their splice variants in autaptic hippocampal neurones. *Br J Pharmacol* 165: 2660–2671

Stumpff F, Boxberger M, Krauss A, Rosenthal R, Meissner S, Choritz L, Wiederholt M & Thieme H (2005) Stimulation of cannabinoid (CB1) and prostanoid (EP2) receptors opens BKCa channels and relaxes ocular trabecular meshwork. *Exp Eye Res* 80: 697–708

Sugden PH & Clerk A (1997) Regulation of the ERK subgroup of MAP kinase cascades through G protein-coupled receptors. *Cell Signal* 9: 337–351

Sugiura T, Kondo S, Sukagawa A, Nakane S, Shinoda A, Itoh K, Yamashita A & Waku K (1995) 2-arachidonoylglycerol: A possible endogenous cannabinoid receptor ligand in brain. *Biochem*

Biophys Res Commun 215: 89–97

Sutor S, Heilmann J & Seifert R (2011) Impact of fusion to Gα i2 and co-expression with RGS proteins on pharmacological properties of human cannabinoid receptors CB1R and CB2R. *J Pharm Pharmacol* 63: 1043–1055

Tanimura A, Yamazaki M, Hashimotodani Y, Uchigashima M, Kawata S, Abe M, Kita Y, Hashimoto K, Shimizu T, Watanabe M, *et al* (2010) The endocannabinoid 2-arachidonoylglycerol produced by diacylglycerol lipase α mediates retrograde suppression of synaptic transmission. *Neuron* 65: 320–327

Tao J, Yang J & Xu G (2018) The interacting domains in cereblon differentially modulate the immunomodulatory drug-mediated ubiquitination and degradation of its binding partners. *Biochem Biophys Res Commun* 507: 443–449

Thibault K, Carrel D, Bonnard D, Gallatz K, Simon A, Biard M, Pezet S, Palkovits M & Lenkei Z (2013) Activation-dependent subcellular distribution patterns of CB1 cannabinoid receptors in the rat forebrain. *Cereb Cortex* 23: 2581–2591

Thornton B & Basu C (2011) Real-time PCR (qPCR) primer design using free online software. *Biochem Mol Biol Educ* 39: 145–154

Todaro B (2012) Cannabinoids in the treatment of chemotherapy-induced nausea and vomiting. *JNCCN J Natl Compr Cancer Netw* 10: 487–492

Tsai YL, Zhang Y, Tseng CC, Stanciauskas R, Pinaud F & Lee AS (2015) Characterization and mechanism of stress-induced translocation of 78-kilodalton glucose-regulated protein (GRP78) to the cell surface. *J Biol Chem* 290: 8049–8064

Tsuboi K, Uyama T, Okamoto Y & Ueda N (2018) Endocannabinoids and related N-acylethanolamines: biological activities and metabolism. *Inflamm Regen* 38: 1–10

Ueda N, Liu Q & Yamanaka K (2001) Marked activation of the N-acylphosphatidylethanolamine-hydrolyzing phosphodiesterase by divalent cations. *Biochim Biophys Acta - Mol Cell Biol Lipids* 1532: 121–127

Viader A, Ogasawara D, Joslyn CM, Sanchez-Alavez M, Mori S, Nguyen W, Conti B & Cravatt BF (2016) A chemical proteomic atlas of brain serine hydrolases identifies cell type-specific pathways regulating neuroinflammation. *Elife* 5: e12345

Viñals X, Moreno E, Lanfumey L, Cordomí A, Pastor A, de La Torre R, Gasperini P, Navarro G, Howell LA, Pardo L, *et al* (2015) Cognitive impairment induced by delta9-tetrahydrocannabinol occurs through heteromers between cannabinoid CB1 and serotonin 5-HT2A Receptors. *PLoS Biol* 13: e1002194

Vogel JP, Misra LM & Rose MD (1990) Loss of BiP/GRP78 function blocks translocation of secretory proteins in yeast. *J Cell Biol* 110: 1885–1895

Wada T, Asahi T & Sawamura N (2016) Nuclear cereblon modulates transcriptional activity of Ikaros and regulates its downstream target, enkephalin, in human neuroblastoma cells. *Biochem Biophys Res Commun* 477: 388–394

Wade Harper J, Adami GR, Wei N, Keyomarsi K & Elledge SJ (1993) The p21 Cdk-interacting protein Cip1 is a potent inhibitor of G1 cyclin-dependent kinases. *Cell* 75: 805–816

Walf AA & Frye CA (2007) The use of the elevated plus maze as an assay of anxiety-related behavior in rodents. *Nat Protoc* 2: 322–328

Wang C, Xu H, Lin S, Deng W, Zhou J, Zhang Y, Shi Y, Peng D & Xue Y (2020) GPS 5.0: an update on the prediction of kinase-specific phosphorylation sites in proteins. *Genomics, Proteomics Bioinforma* 18: 72–80

Wang J, Lee J, Liem D & Ping P (2017) HSPA5 Gene encoding Hsp70 chaperone BiP in the endoplasmic reticulum. *Gene* 618: 14–23

Wang J, Okamoto Y, Morishita J, Tsuboi K, Miyatake A & Ueda N (2006a) Functional analysis of the purified anandamide-generating phospholipase D as a member of the metallo-β-lactamase family. *J Biol Chem* 281: 12325–12335

Wang J, Okamoto Y, Tsuboi K & Ueda N (2008) The stimulatory effect of phosphatidylethanolamine on N-acylphosphatidylethanolamine-hydrolyzing phospholipase D (NAPE-PLD). *Neuropharmacology* 54: 8–15

Wang W, Trieu BH, Palmer LC, Jia Y, Pham DT, Jung KM, Karsten CA, Merrill CB, Mackie K, Gall CM, *et al* (2016) A primary cortical input to hippocampus expresses a pathway-specific and endocannabinoid-dependent form of long-term potentiation. *eNeuro* 3: 10049–10053

Wang X, Venable J, LaPointe P, Hutt DM, Koulov A V., Coppinger J, Gurkan C, Kellner W, Matteson J, Plutner H, *et al* (2006b) Hsp90 Cochaperone Aha1 downregulation rescues misfolding of CFTR in cystic fibrosis. *Cell* 127: 803–815

Whistler JL, Enquist J, Marley A, Fong J, Gladher F, Tsuruda P, Murray SR & Von Zastrow M (2002) Modulation of postendocytic sorting of G protein-coupled receptors. *Science* 297: 615–620

Wieteska L, Shahidi S & Zhuravleva A (2017) Allosteric fine-tuning of the conformational equilibrium poises the chaperone BiP for post-translational regulation. *Elife* 6: 1–20

Wiley JL, Burston JJ, Leggett DC, Alekseeva OO, Razdan RK, Mahadevan A & Martin BR (2005) CB1 cannabinoid receptor-mediated modulation of food intake in mice. *Br J Pharmacol* 145: 293–300

Willis D, Ka WL, Zheng JQ, Chang JH, Smit A, Kelly T, Merianda TT, Sylvester J, Van Minnen J & Twiss JL (2005) Differential transport and local translation of cytoskeletal, injury-response, and neurodegeneration protein mRNAs in axons. *J Neurosci* 25: 778–791

Wilson RI & Nicoll RA (2002) Neuroscience: Endocannabinoid signaling in the brain. *Science* 296: 678–682

Wiśniewski JR, Nagaraj N, Zougman A, Gnad F & Mann M (2010) Brain phosphoproteome obtained by a fasp-based method reveals plasma membrane protein topology. *J Proteome Res* 9: 3280–3289

Xin W, Xiaohua N, Peilin C, Xin C, Yaqiong S & Qihan W (2008) Primary function analysis of human mental retardation related gene CRBN. *Mol Biol Rep* 35: 251–256

Xu G, Jiang X & Jaffrey SR (2013) A mental retardation-linked nonsense mutation in cereblon is rescued by proteasome inhibition. *J Biol Chem* 288: 29573–29585

Xu J, Antion MD, Nomura T, Kraniotis S, Zhu Y & Contractor A (2014) Hippocampal metaplasticity is required for the formation of temporal associative memories. *J Neurosci* 34: 16762–16773

Xu W, Filppula SA, Mercier R, Yaddanapudi S, Pavlopoulos S, Cai J, Pierce WM & Makriyannis A (2005) Purification and mass spectroscopic analysis of human CB1 cannabinoid receptor functionally expressed using the baculovirus system. *J Pept Res* 66: 138–150

Xu Y, Piston DW & Johnson CH (1999) A bioluminescence resonance energy transfer (BRET) system: Application to interacting circadian clock proteins. *Proc Natl Acad Sci U S A* 96: 151–156

Yamamoto J, Suwa T, Murase Y, Tateno S, Mizutome H, Asatsuma-Okumura T, Shimizu N, Kishi T, Momose S, Kizaki M, *et al* (2020) ARID2 is a pomalidomide-dependent CRL4CRBN substrate in multiple myeloma cells. *Nat Chem Biol* 16: 1208–1217

Yang J, Nune M, Zong Y, Zhou L & Liu Q (2015) Close and allosteric opening of the polypeptide-binding site in a human Hsp70 chaperone BiP. *Structure* 23: 2191–2203

Yang J, Zong Y, Su J, Li H, Zhu H, Columbus L, Zhou L & Liu Q (2017) Conformation transitions of the polypeptide-binding pocket support an active substrate release from Hsp70s. *Nat Commun* 8

Yao C, Guo X, Yao WX & Zhang C (2018) Cereblon (CRBN) deletion reverses streptozotocin induced

diabetic osteoporosis in mice. *Biochem Biophys Res Commun* 496: 967–974

Yoon YR, Lee TG, Choi MH, Shin SW, Ko YG, Rhyu IJ, Kim DH, Seong JK & Baik JH (2018) Glucose-regulated protein 78 binds to and regulates the melanocortin-4 receptor. *Exp Mol Med* 50: 1–14

Yoshida T, Fukaya M, Uchigashima M, Miura E, Kamiya H, Kano M & Watanabe M (2006) Localization of diacylglycerol lipase-α around postsynaptic spine suggests close proximity between production site of an endocannabinoid, 2-arachidonoyl-glycerol, and presynaptic cannabinoid CB1 receptor. *J Neurosci* 26: 4740–4751

Zhang P-W, Ishiguro H, Ohtsuki T, Hess J, Carillo F, Walther D, Onaivi ES, Arinami T & Uhl GR (2004) Human cannabinoid receptor 1: 5' exons, candidate regulatory regions, polymorphisms, haplotypes and association with polysubstance abuse. *Mol Psychiatry* 9: 916–931

Zhang T, Dong K, Liang W, Xu D, Xia H, Geng J, Najafov A, Liu M, Li Y, Han X, *et al* (2015) G-protein coupled receptors regulate autophagy by ZBTB16-mediated ubiquitination and proteasomal degradation of adaptor protein Atg14L. *Elife* 2015

Zhou S, Wang F, Hsieh T-C, Wu J & Wu E (2013) Thalidomide–A notorious sedative to a wonder anticancer drug. *Curr Med Chem* 20: 4102–4108

Zhuang H & Matsunami H (2008) Evaluating cell-surface expression and measuring activation of mammalian odorant receptors in heterologous cells. *Nat Protoc* 3: 1402–1413

Zou S, Somvanshi RK & Kumar U (2017) Somatostatin receptor 5 is a prominent regulator of signaling pathways in cells with coexpression of Cannabinoid receptors 1. *Neuroscience* 340: 218–231

Zygmunt PM, Petersson J, Andersson DA, Chuang HH, Sørgård M, Di Marzo V, Julius D & Högestätt ED (1999) Vanilloid receptors on sensory nerves mediate the vasodilator action of anandamide. *Nature* 400: 452–457